HALOGEN CHEMISTRY: BROMINATION AND FLUORINATION VIA C-H FUNCTIONALIZATION AND THEORETICAL INVESTIGATION OF HALOGEN BONDING IN CATALYSIS

KEE CHOON WEE

(B. Sci. (Hons.),NUS)

A THESIS SUBMITTED

FOR THE DEGREE OF DOCTOR OF PHILOSOPHY

DEPARTMENT OF CHEMISTRY

NATIONAL UNIVERSITY OF SINGAPORE

2014

Declaration

I hereby declare that this thesis is my original work and it has been written by me in its entirety, under the supervision of Associate Professor Tan Choon-Hong, Chemistry Department, National University of Singapore, and Division of Division of Chemistry & Biological Chemistry School of Physical & Mathematical Sciences College of Science between Jan 2010 and Jan 2014 and under the supervision of Professor Richard Wong Ming Wah, Chemistry Department, National University of Singapore, between January 2012 and January 2014.

I have duly acknowledged all the sources of information which have been used in the thesis.

This thesis has also not been submitted for any degree in any university previously.

The content of the thesis has been partly published in:

1. H. Liu, W. Feng, C. W. Kee, D. Leow, W.-T. Loh, C.-H. Tan, *Adv. Synth. Catal.* **2010**, *352*, 3373-3379.

2. Y. Pan, C. W. Kee, L. Chen, C.-H. Tan, *Green Chem.* **2011**, *13*, 2682-2685.

3. Y. Pan, C. W. Kee, *et al*, *Chem. - Eur. J.* **2011**, *17*, 8363-8370.

4. Y. Zhang, C. W. Kee, *et al*, *Chem. Commun.* **2011**, *47*, 3897-3899.

5. J. Wang, J. Chen, C. W. Kee, C.-H. Tan, *Angew. Chem. Int. Ed.* **2012**, *51*, 2382-2386.

6. C. W. Kee, K. M. Chan, M. W. Wong, C.-H. Tan, *Asian J. Org. Chem.* **2014**, *3*, 535-544.

7. C. W. Kee, K. F. Chin, M. W. Wong, C. –H. Tan, *Chem. Commun.* **2014**, *50*, 8211-8214.

8. L. Zong, X. Ban, C. W. Kee, C.-H. Tan, *Angew. Chem. Int. Ed.* **2014**, DOI: 10.1002/anie.201407512

Kee Choon Wee		29 August 2014
Name	Signature	Date

Acknowledgement

Table of Contents

Summary

Chapter 1 introduces the audience to C-H functionalization through selected examples and strategies to achieve selectivity. Photoredox chemistry is then introduced as chapter 2 involves the development of bromination *via* C-H functionalization with visible light photoredox chemistry. Finally, non-covalent interactions are introduced to set the stage for chapter 4.

Chapter 2 discusses the photoredox bromination that was development by our group. A detailed discussion on mechanism is provided based on our interpretation of experimental and theoretical evidences.

Chapter 3 discusses the development of a selective fluorination *via* photochemistry and C-H functionalization. Evidences to support the involvement of cationic *N*-radical are provided together with a discussion on plausible mechanisms.

Chapter 4 discusses our theoretical studies on guanidine catalyzed asymmetric reactions and halogen bonds in asymmetric phase transfer reaction catalyzed by pentanidium.

List of Abbreviations

AQN   Anthraquinone (Anthracene-9,10-dione)

BDE   Bond Dissociation Energy (Bond Dissociation Enthalpy)

BSSE   Basis Set Superposition Error

CP   Counterpoise

DA   Diels-Alder

DCM   Dichloromethane

DEPT   Distortionless Enhancement by Polarization

DFT   Density Functional Theory

EDA   Energy Decomposition Analysis

EWG   Electron Withdrawing Group

GC   Gas Chromatography

HOMO   Highest Occupied Molecular Orbitals

ISC   Intersystem Crossing

KIE   Kinetic Isotope Effect

LMOEDA   Localized Molecular Orbitals Energy Decomposition Analysis

LUMO   Lowest Unoccupied Molecular Orbitals

MAHT   Malonic Acid Half Thioester

MeCN   Acetonitrile

MM	Molecular Mechanics
MO	Molecular Orbitals
NBO	Natural Bond Orbital
NEDA	Natural Energy Decomposition Analysis
NLMO	Natural Localized Molecular Orbitals
NMR	Nuclear Magnetic Resonance
PT	Phase Transfer
PTC	Phase Transfer Catalysis/Catalyst
SCE	Saturated Calomel Electrode
SCF	Self Consistent Field
THF	Tetrahydrofuran
TS	Transition State
UV	Ultraviolet
ZPE	Zero Point Energy

Chapter 1

Introduction

1 Introduction

1.1 General introduction

Halogen (Group 17 of the periodic table) comprises of Fluorine, Chlorine, Bromine and Iodine. They are fundamental to modern chemistry. This thesis focuses on the chemistry of halogen – construction of C-F and C-Br bonds *via* C-H functionalization and the application of halogen bonding in catalysis and the study of non-covalent interaction in asymmetric catalysis.

Halogenated organic molecules are highly valuable compounds with diverse applications. On one hand, fluorinated compounds are invaluable in drugs,[1-5] molecular imaging,[6] agrochemicals,[7] and functional materials.[8] On the other hand, chloro-, bromo- and iodo-compounds are instrumental in organic synthesis.[9-14]

In addition, the participation of halogen in non-covalent interactions which is known as halogen bond is invaluable to supramolecular chemistry[15-18] and biology.[19-21]

1.2 C-H functionalization
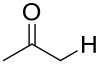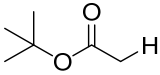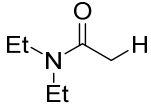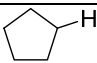
Selective functionalization of unactivated C-H bond under mild condition is of paramount importance to synthetic chemistry. Numerous reviews and books have been published on this topic.[22-46]

Selective C-H functionalization is highly attractive due to the ubiquity of alkyl C-H bonds and avoidance of the need to pre-functionalize the substrate. This has the potential to reduce the number of steps required in a particular synthesis, and thus achieved step economy which contributes to the "ideality" of the route.[47] However, the prevalence of C-H bonds in organic molecules poses a significant challenge in term of selectivity to the exploitation of C-H in synthesis. The need to overcome the selectivity problem was recognized by visionary chemists such as Breslow[22] and Barton.[23]

C-H bonds could be classified into three main classes based on hybridization of the carbon center which they are attached to. The three classes are (1) sp^3 C-H bonds which include alkyl, allylic and benzylic C-H bonds; (2) sp^2 C-H bonds which include aryl and alkenyl C-H bonds; (3) sp C-H bond.

The α-proton of carbonyl compounds falls under (1) as it is attached to a sp^3 carbon center. This class of C-H bonds typically has pK_a that is less than 35 (in DMSO).[48, 49] Therefore, they are considered acidic and could be activated by moderate base. The enolate formed is nucleophilic and could attack a variety of electrophile. This is a very powerful strategy in organic synthesis. Similarly, sp C-H or alkynyl C-H (e.g. Ph-C≡C-H ,pK_a = 28.7 in DMSO[49]) could be activated by a base to generate a nucleophile. Generally, alkyl C-H bonds that are not adjacent to the carbonyl group have a higher pK_a and are difficult to activate selectively with base, especially in the presence of more acidic C-H bonds, therefore different strategies must be employed to achieve selective functionalization.

Table 1.1 pK_a of selected compounds in DMSO[40, 41]

Entry	Compounds	pK_a in DMSO
1		26.5
2		30.3
3		35
4	CH_4	≈56
5		≈59

1.2.1 Strategies for selective C-H functionalization

Baran and co-workers classified the strategies to selectively activate C-H bond as either innate or guided.[50] Although the terms are defined through examples, but not stated explicitly, we inferred from their examples that the main difference between these two modes lies in whether the hydrogen abstracting species is tendered to the substrate covalently.

1.2.2 Selected examples of guided C-H functionalization

Classic examples of guided C-H functionalization include the Barton reaction, Hofmann–Löffler–Freytag reaction and related variations.[51-53] In the Hofmann–Löffler–Freytag reaction, cationic N-radical is generated from protonated N-chloro amine (**Scheme 1.1**). Initiation could be achieved through thermal activation (60-140°C), chemical reagents (Fe^{2+}, H_2O_2, and $K_2S_2O_8$) or ultraviolent radiation (263nm).[51] The cationic N-radical is highly reactive and could perform a 1,5 hydrogen abstraction to form a C radical. Subsequently, the C-radical attacks the protonated N-chloro amine to regenerate the cationic N-radical. Besides protonated N-chloro amine, protonated N-bromo amine also exhibit similar reactivity.
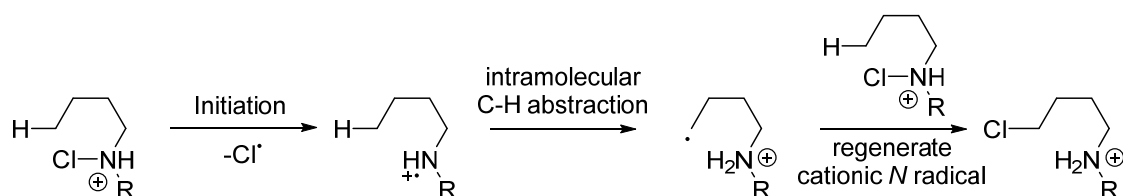
Scheme 1.1 Initiation and C-H abstraction step of the Hofmann–Löffler–Freytag reaction.

The classic Hofmann–Löffler–Freytag reaction is carried out in strongly acidic medium. The use of N-chloro or N-bromo amide circumvents the need for such solvent.[52] For a recent example, Baran and co-workers developed a variation based on N-bromo carboxamide to selectively brominate C-H *via* guided C-H functionalization (**Scheme 1.2**).[54] They then demonstrated that based on this methodology, synthesis of rengyol and isorengyol could be achieved with much better step economy and yield relative to previously reported routes.

3
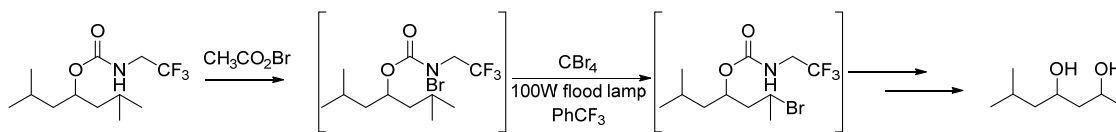
Scheme 1.2 Baran and co-workers variation based on *N*-Bromo carboxamide.

Strategies to generate *N*-radical directly (without going through N-Cl or N-Br intermediates) have also been developed. One of the earliest examples was reported by Nikishin and co-workers, they generated *N*-radical from sulfonamide group *via* stoichiometric amount of CuCl$_2$ and Na$_2$S$_2$O$_8$.[55] A recent extension based on amidine functional group was reported by Chiba and co-workers (**Scheme 1.3**).[56] They proposed a mechanism in which Cu^{2+} (from CuBr·SMe$_2$) oxidizes the amidine functional group, followed by deprotonation to generate a neutral *N*-radical which performs an intramolecular hydrogen abstraction. The *C*-radical formed traps dioxygen to form a peroxo- intermediate. The peroxo intermediate undergoes a Fenton type fragmentation and eventually regenerate Cu^{2+} and a molecule NH$_3$ is formed, together with the product.
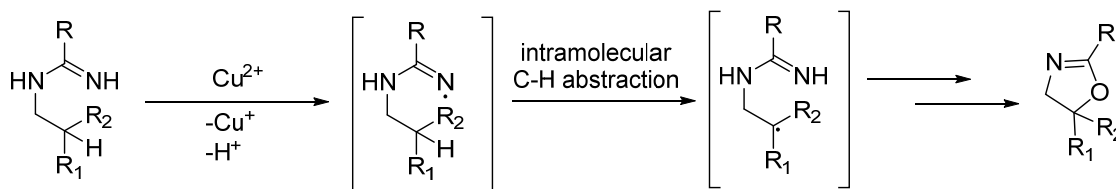
Scheme 1.3 Copper-Catalyzed Aerobic Aliphatic C−H Oxygenation Directed by an Amidine Moiety.

Besides nitrogen-based group discussed above, guided C-H functionalization based on *O*-radical is also possible. For instance, the Norrish-Yang type II reaction exploits the photo-chemically generated singlet and triplet excited state of ketone to effect intramolecular hydrogen abstraction (**Scheme 1.4**).[57-60] The product for the type II reaction is a cyclobutanol derivative, however, completing type I reaction which results in cleavage could also occur.
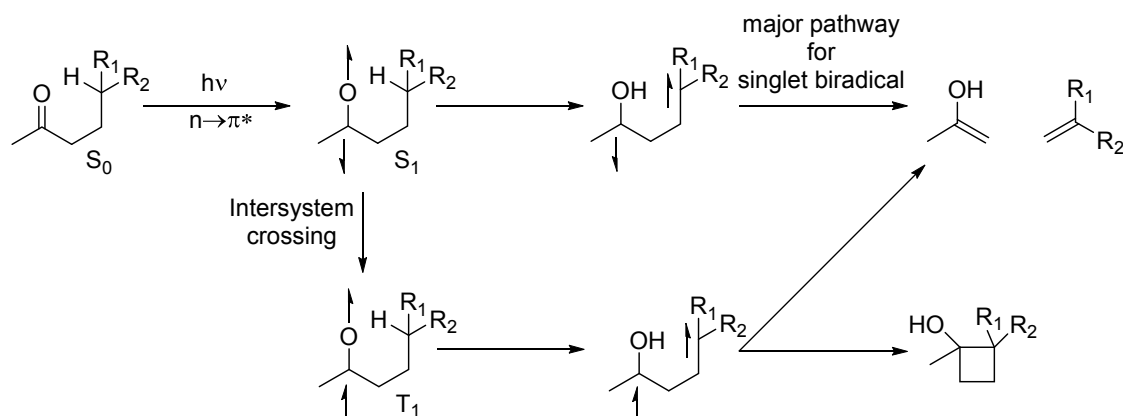
Scheme 1.4 Simplified mechanism for Norrish-Yang reaction.

Other classic examples of guided C-H functionalization that utilize *O*-radical are summarized in **Scheme 1.5**.[53] *O*-radical could be generated by hypochlorite (R-OCl) through thermolysis or photolysis, however, the need to isolate the unstable hypochlorite intermediate is a severe drawback of this methodology. The photolysis of nitrile ester (X=NO, Barton reaction) to generate *O*-radical was reported by Barton and co-workers in 1961.[61] The Barton reaction has been employed as key step in the total synthesis of azadiradione and (+)-perhydrohistrionicotoxin by Corey and co-workers, although the yield of the Barton reaction is rather low in these examples (28% for azadiradione and 20% for perhydrohistrionicotoxin).[62, 63] Hypoiodite could also be used to generate *O*-radical. Hypoiodite could be generated *in situ* by reacting alcohols with reagents such as N-iodosuccinimide (NIS), acyl hypoiodites or iodobenzene diacetate (IBD). Variations of the hypoiodite reactions include the use of $Pb(OAc)_4/I_2$ and HgO/I_2.
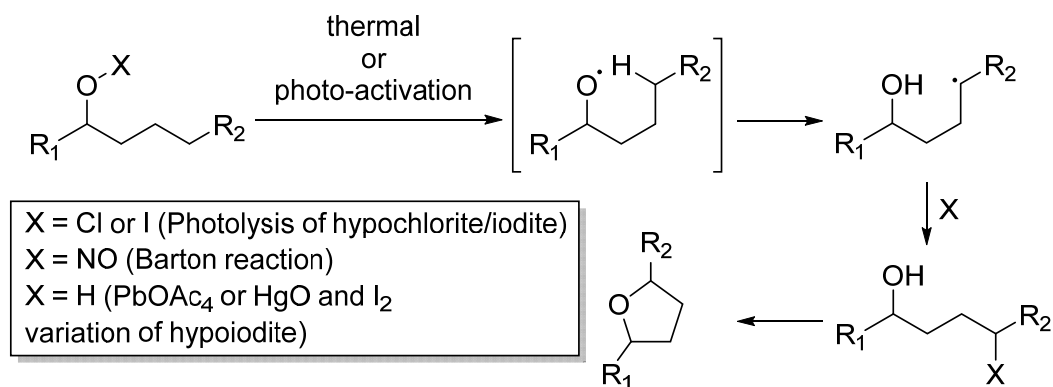
Scheme 1.5 Summary of classical guided C-H functionalization reactions which utilize *O*-radical.

Guided C-H functionalization *via O*-radical was demonstrated to be a useful strategy in the desaturation of alkane. Exemplary examples include the work of Breslow and co-workers which exploited the excited state of ketone to achieve alkane desaturation *via* guided C-H functionalization (**Scheme 1.6**, Equation 1)[64] and the work of Čekovió's group which used hydroperoxo- functional group (**Scheme 1.6**, Equation 2).[65]
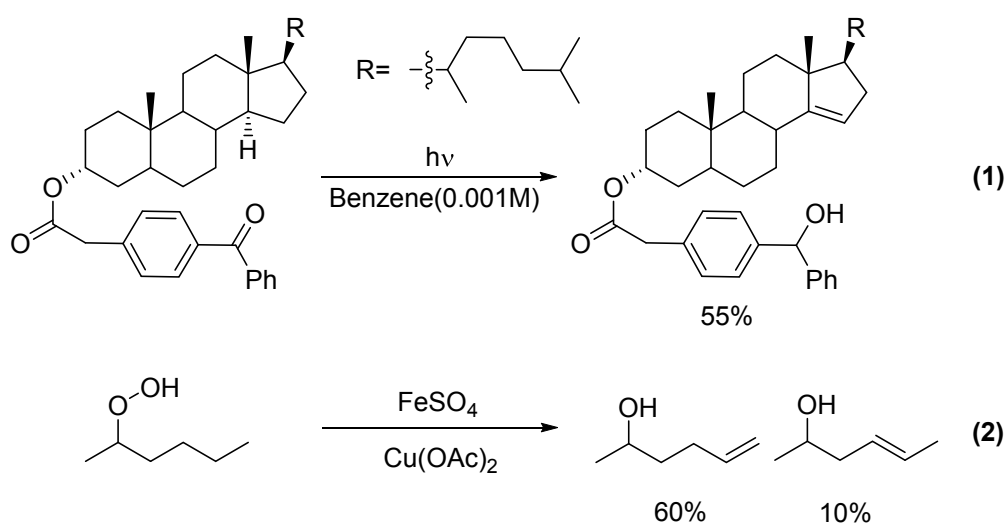
Scheme 1.6 Breslow's group and Čekovió's group guided alkane desaturation *via* photochemistry.

A recent breakthrough in desaturation of alkane *via* guided C-H functionalization was reported by Baran and co-workers (**Scheme 1.7**).[66] They design a "portable desaturase" which is

currently commercially available. The reaction tolerates a variety of functional group and could be used in the desaturation of complex molecules.
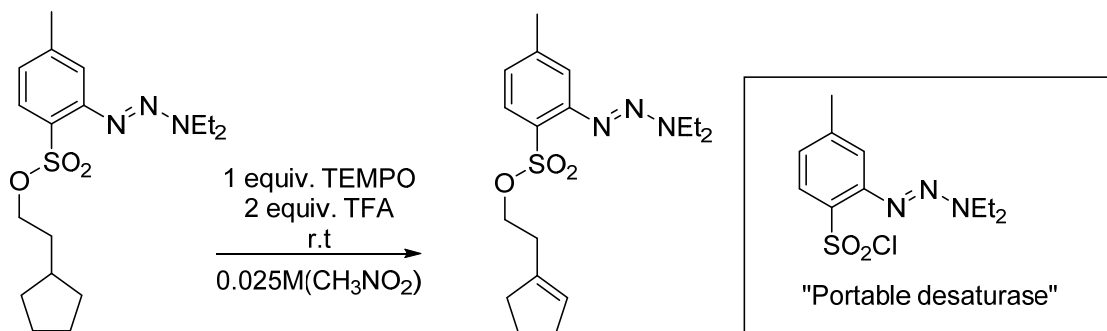
Scheme 1.7 Guided desaturated by Baran and co-workers.

In a recent report by Ball and co-workers,[67] *O*-radicals are generated by the decomposition of hydroperoxide group (R-OOH) which is catalyzed by copper(I) chloride. This methodology allows chlorination of unactivated C-H bonds that is δ to the –OOH group (**Scheme 1.8**).
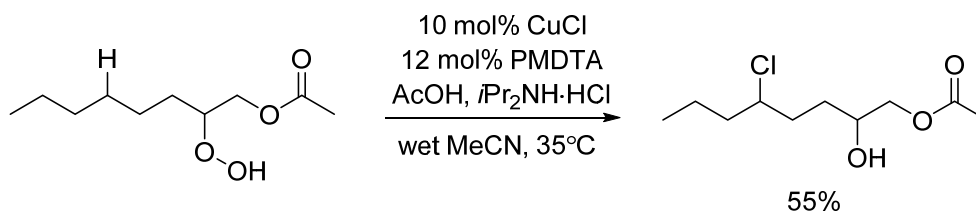
Scheme 1.8 Copper catalyzed guided C-H functionalization by Ball.

The examples given above generally involved the generation of reactive radical species on groups that are tethered to the substrate, these radicals are the hydrogen abstracting species. In another class of guided C-H functionalization, the C-H functionalization is performed by transition metals which bind to specific group that is present on the substrate coordinates to the transition metal and direct it towards certain C-H of the substrate. Selected examples will be presented below.

Du Bois and co-workers used the sulfamate functional group to serve as directing group for rhodium-catalyzed guided C-H functionalization.[68, 69] They observed that the C-H functionalization is stereospecific.[69] They proposed that a nitrene species was involved, which differs from the *N*-radical examples given in preceding paragraph. The product could be transformed into valuable β amino acids (**Scheme 1.9**). A diastereoselective version of this methodology was subsequently reported by Du Bois and Wehn and it was applied to the total synthesis of Manzacidin A and C.[70]
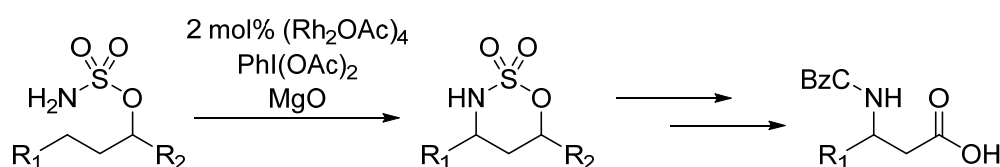
Scheme 1.9 Rhodium catalyst guided C-H functionalization *via* insertion between C-H bond.

Oxazoline was reported to be an effective directing group for palladium catalyzed desaturation of alkane and iodination of alkyl C-H bonds by Yu and co-workers.[71, 72]
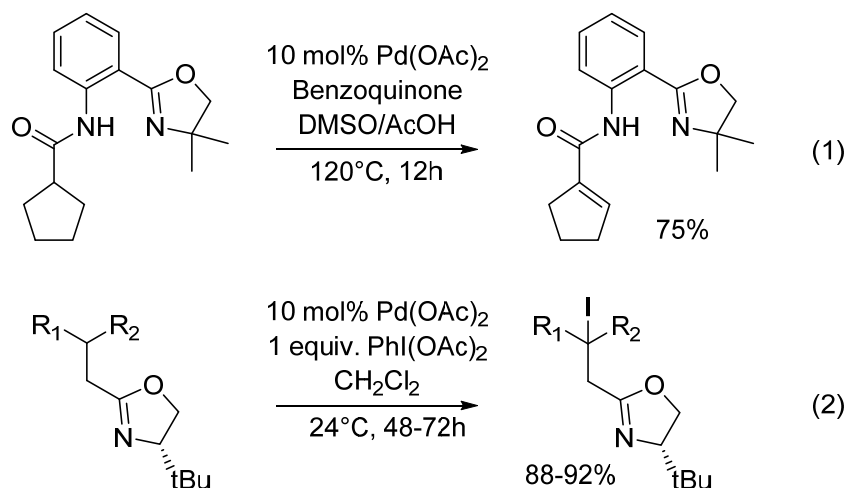
Scheme 1.10 Yu and co-workers Pd catalyzed guided C-H functionalization *via* oxazoline directing group.

Few methods allow for selective functionalization of methyl C-H bond, Simmons and Hartwig developed an Iridium catalyzed guided C-H silylation that could achieve this feat in good yield (**Scheme 1.11**).[73] The reaction is able to selectively functionalize the thermodynamically more stable C-H bond, even in the presence of benzylic C-H bond. This is presumably due to steric reason. Earlier examples of selective functionalization of methyl C-H bond *via* guided C-H functionalization includes Pt-catalyzed guided oxygenation in water by Sames and co-workers,[74] Pd-catalyzed guided oxygenation by Sanford and co-workers,[75] and Pd-catalyzed coupling by Yu and co-workers,[76, 77]
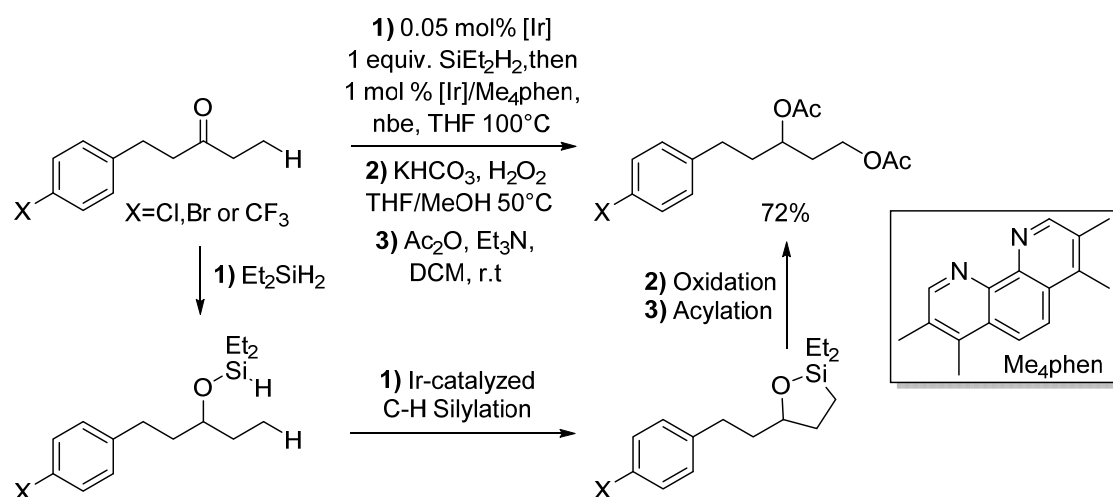
Scheme 1.11 Simmons and Hartwig methyl C-H selectivity guided C-H functionalization. [Ir] = [Ir(cod)OMe]$_2$; nbe = norbornene .

Zhao and Yeung reported a novel guided oxidation of aliphatic C-H bond to C=O (**Scheme 1.12**).[78] They proposed that coordination of the ester to the hypervalent iodine is important, as *n*-octane gave no observable product. A possible coordinate mode of the ester to iodine is shown in **Scheme 1.12**. Subsequent work by Maruoka and co-workers extended this methodology to innate C-H functionalization.[79]
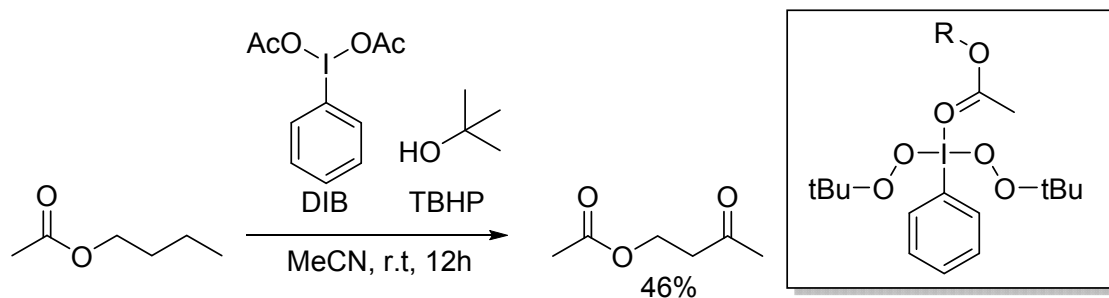
Scheme 1.12 Remote oxidation of C-H bond by hypervalent iodine species.

Due to the vast amount of works that have been done in guided C-H functionalization, an exhaustive review is beyond the scope of this thesis. Interested readers are encouraged to refer to the reviews of Sanford, [32] Wolff,[51] Majetich,[53] and Bergman and Ellman.[80]

1.2.3 Strategies in innate C-H functionalization

In guided C-H functionalization, the selectivity is primarily governed by geometrical constraint imposed by the directing group, however, for innate C-H functionalization, such constraint is not available. Therefore, selectivity could only be achieved *via* the interplay of stabilizing and destabilizing factors between the hydrogen abstracting species and the substrate bearing the C-H bond. These factors would be highlighted in this section.

The literature of radical chemistry indicates that selective abstraction of unactivated C-H bond could be achieved *via* the use of electrophilic/nucleophilic radicals (**Scheme 1.13**).[81, 82] In particular, the use of cationic *N*-radicals as electrophilic radicals to selectively chlorinate/brominate electron rich C-H bond has been well documented in literature.[83] This is known as the polar effect as illustrated in **Scheme 1.13**.

$$A^{\bullet} \; + \; H{-}R \longrightarrow \left[A\text{-}\text{-}H\text{-}\text{-}R\right]^{\ddagger} \longrightarrow AH \; + \; {}^{\bullet}R$$

Resonance structure in TS   Polar TS

$$\left[A^{\bullet}\,H{-}R\right]^{\ddagger} \longleftrightarrow \left[A{-}H\,{}^{\bullet}R\right]^{\ddagger} \longleftrightarrow \left[\overset{\bullet\bullet}{A}{}^{\ominus}H\overset{\oplus}{\overset{\bullet}{R}}\right]^{\ddagger} \longleftrightarrow \left[A^{\oplus}H\overset{\bullet}{\overset{\bullet\bullet}{R}}{}^{\ominus}\right]^{\ddagger}$$

A : electrophilic   A : nucleophilic
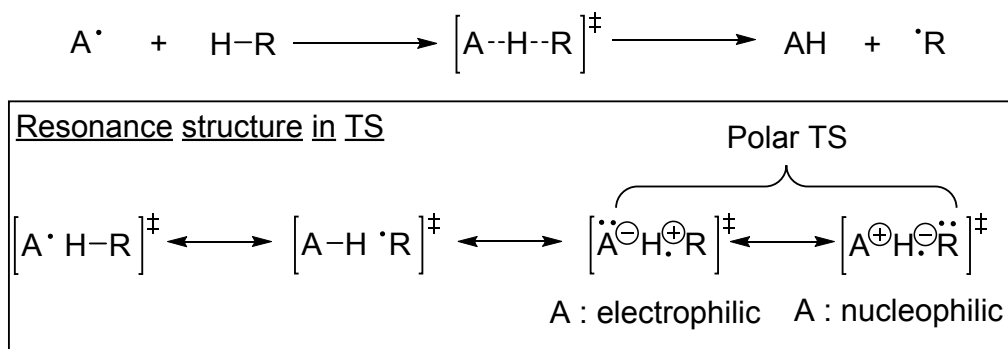
Scheme 1.13 Theory of the origin of polar effect in radical hydrogen abstraction reaction

Bond strength which is measured by the C-H bond dissociation energies could influence the selectivity of a C-H functionalization reaction. The rationale was first pointed out by Evan and Polanyi which suggested that factors which stabilize the radical also stabilize the TS in a hydrogen atom transfer reaction.[84] Therefore, bond dissociation energies which measure the stability of *C* radical in term of enthalpy would also be reflected in the relative stability of the C-H functionalization TS. This is because the TS structure is expected to possess a certain degree of *C* radical character.

Steric factors are important in controlling selectivity in C-H functionalization. Tedder classified steric factors into three categories: (1) steric hindrance (2) steric compression (3) steric inhibition of resonance.[81] All three categories are different manifestations of a more general concept which is termed steric repulsion, or electronic steric repulsions. This was first expressed by Weisskopf in terms of "kinetic energy pressure" and is based on Pauli exchange asymmetry.[85] In steric hindrance, selectivity is achieved *via* steric repulsions that destabilize the approach of an H abstracting species towards one C-H bond over another. In steric compression, strain that is present in the hydrocarbon substrate is partly relieved during the process of forming the *C* radical. In steric inhibition of resonance, steric repulsion prevents the radical to adopt conformation that favors electron delocalization.

Solvent could potentially have profound effect on the selectivity of innate C-H functionalization reaction. A classic example would be the abstraction of alkyl C-H bond by chlorine radical (**Table 1.2**). Russell and co-workers reported that the increase in selectivity when chlorination was performed in the presence of benzene and CS_2.[86] Breslow and co-workers reported that pyridine forms a complex with chlorine radical and this species exhibits a higher selectivity than chlorine radical itself.[87]

Table 1.2 The effect of solvent on the selectivity of primary and tertiary C-H bond abstraction by chlorine radical
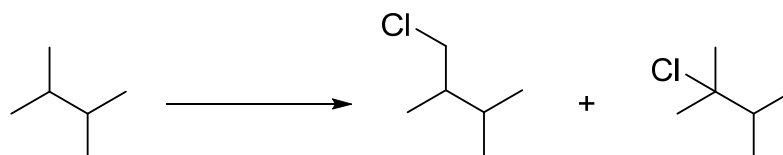
Solvent	Radical	Primary site	Tertiary site
CCl_4	Cl	1	4
4M Benzene/CCl_4	Benzene-Cl	1	50
8M Benzene/CCl_4	Benzene-Cl	1	59
8M CS_2/CCl_4	CS_2-Cl	1	106
4M pyridine/	Pyridine-Cl	1	200

1.2.4 Selected examples of innate C-H functionalization

The intermolecular version of the Hofmann–Löffler–Freytag reaction was reported by Minisci and co-workers.[88] Aliphatic esters could be selectively chlorinated at the secondary C-H bonds most distal to the methyl ester functional group. Cationic *N*-radicals are generated in and stabilized by the strongly acidic medium. Cationic *N*-radicals are able to differentiate C-H bonds based on their electron density, as indicated in the ESP map in **Scheme 1.14**. The preferred

secondary C-H bond has the least positive potential (the lightest blue amongst all secondary C-H bonds). We exploit this polar effect in the development of a photo-fluorination of unactivated C-H bond (see **Chapter 3**).
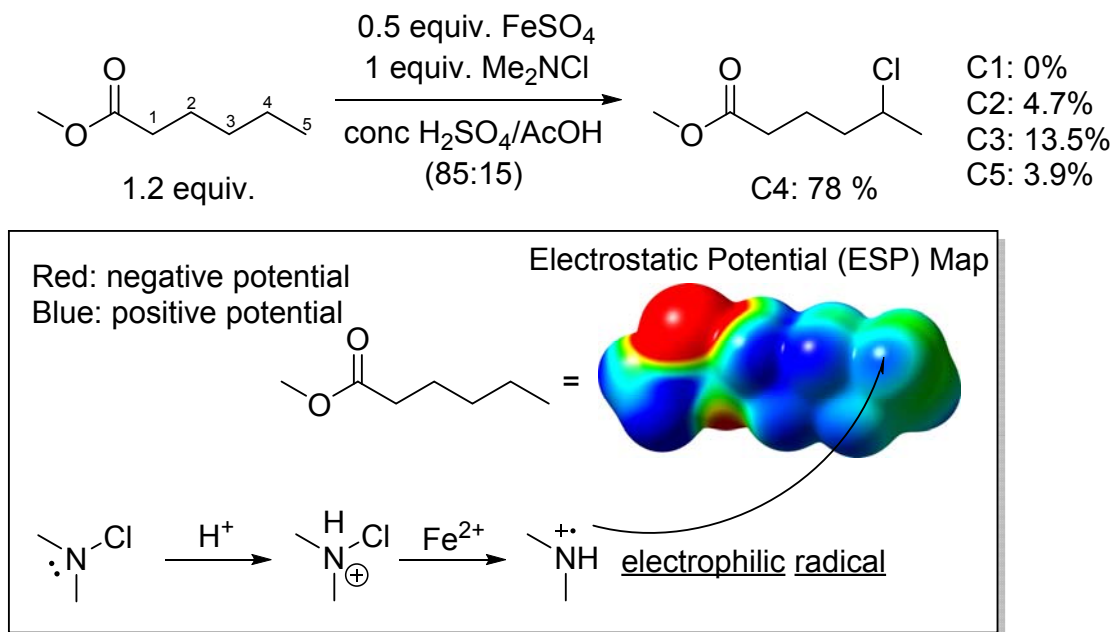
Scheme 1.14 Minisci and co-workers selectivity innate C-H functionalization *via* cationic *N*-radical. ESP map generated at MP2/ACCD//SMD(MeCN)wB97xD/6-311+G(d,p). ESP map generated at 0.001 a.u (isovalue of density). Red is electron deficient and blue is electron rich.

Chen and White reported the use of Fe complex in selective oxidation of sp^3 C-H bonds.[89-91] Selectivity of this method was shown to depend on both polar effect (with all being equal, electron rich C-H bond is preferred) and steric. (+)-Artemisinin, a drug for malaria, could be selectively hydroxylated at the most electron rich tertiary C-H bond (as quantified by NBO charge, see **Scheme 1.15**).
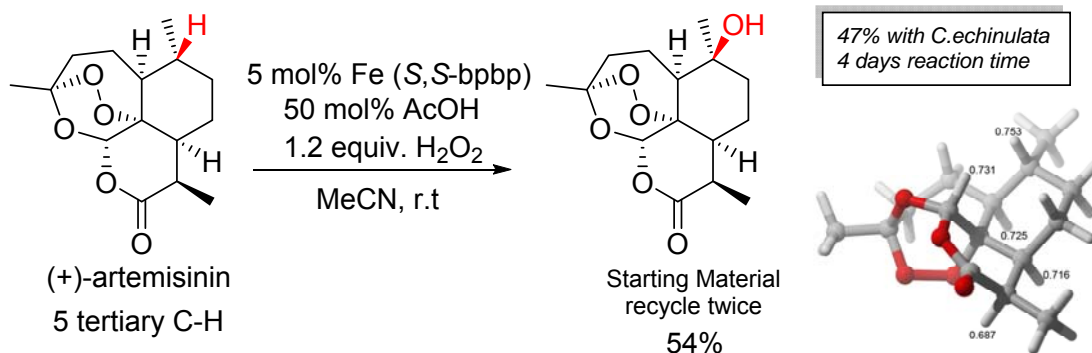
Scheme 1.15 Hydroxylation of artemisinin by Chen and White. NBO charge of artemisinin at RB3LYP/6-31+G(d,p)//RB3LYP/6-31G(d) is shown on the 3D molecular structure of artemisinin on the right. Red is oxygen, grey is carbon and white is hydrogen. For structure of (*S,S*)-bpbp, see Scheme 1.16 below.

Ribas and Costas reported a study to further optimize the catalyst developed by Chen and White catalyst.[92] The bulky pinene substituent in (*S,S,R*)-mcpp (see **Scheme 1.16**) was shown to both improve the stability and efficiency of the catalyst.
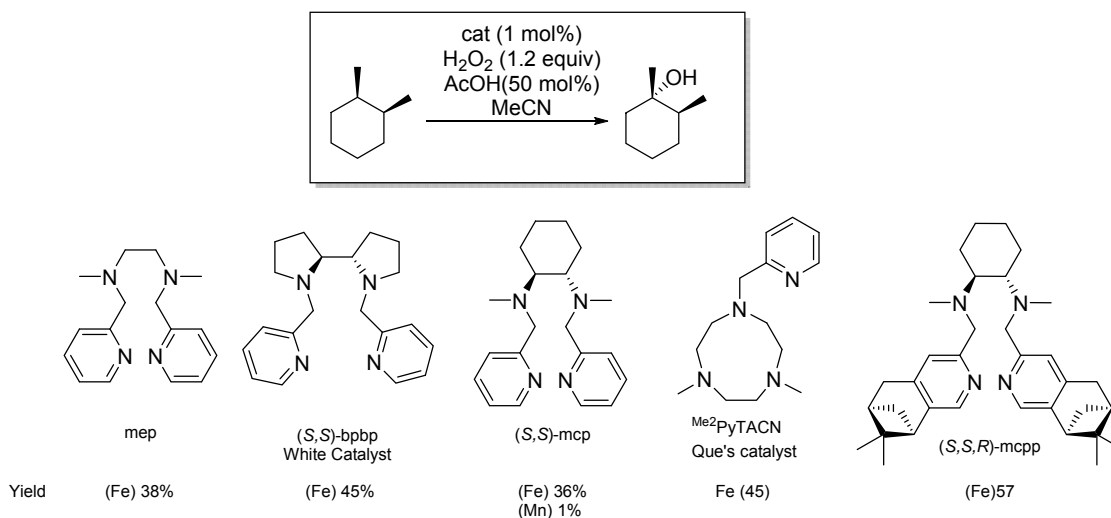
Scheme 1.16 Performance, in terms of GC yield, of selected ligands for Fe catalyzed hydroxylation of *cis*-1,2-dimethylcyclohexane. White catalyst. [89, 90] Que's catatlyst.[93]

Hartwig and co-workers reported a Rh catalyzed borylation which is highly selective for methyl C-H bond.[94] Subsequent detailed study of the mechanism *via* a combination of DFT and

experimental techniques by Hartwig, Balls and co-workers revealed that the selectivity is a result of selective C-H bond cleavage and selective C-B bond formation (reductive elimination has a lower $\Delta G^{\ddagger}$ for primary product than secondary product, see **Scheme 1.17**).[95]
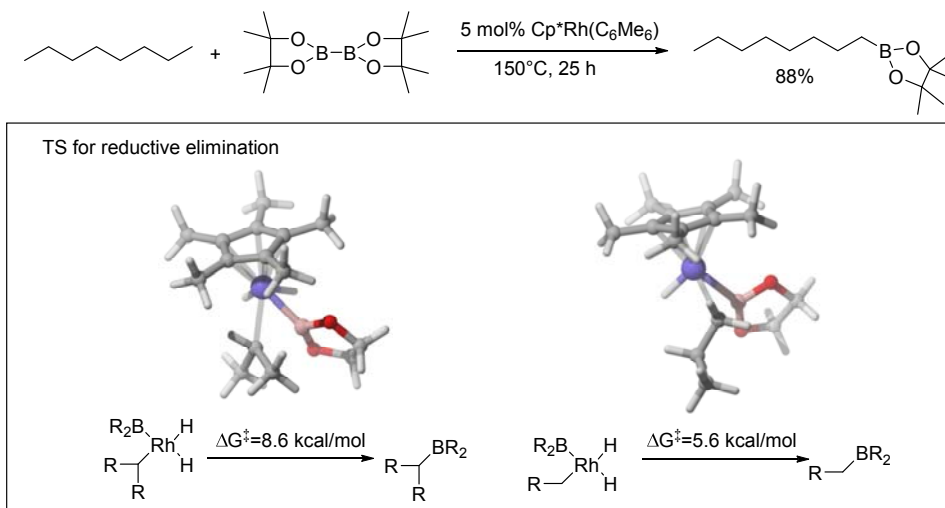
Scheme 1.17 Hartwig and co-workers Rh-catalyzed selective borylation of methyl C-H bond. The TS for reductive eliminations leading to secondary product (left) and primary product (right. Purple sphere = Rh, Pink = B, Red = O, Grey=C and Light grey = H.

Pertinent to the use of steric repulsion to control selectivity of innate C-H functionalization, Mizuno and co-workers reported the use of bulky polyoxomelate to achieve selective hydroxylation of alkyl C-H bonds.[96]
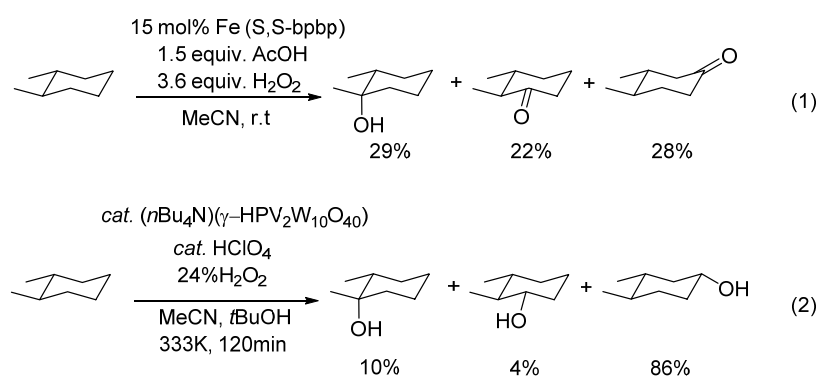
Scheme 1.18 (1) Chen and White report of Fe-catalyzed oxidation of alkyl C-H bonds.[90] (2) Mizuno and co-workers report of polyoxomelate-catalyzed hydroxylation of alkyl C-H bonds.[96]

1.2.5 Bromination *via* C-H functionalization

As this thesis focuses on bromination of alkyl C-H bond *via* C-H functionalization, a review on this topic would be presented in this section.

Bromination of alkanes *via* free radical substitution is a classic reaction in organic chemistry. In 1911，Bodroux and Taboury reported the acceleration of cyclohexane bromination with Br_2 in the presence of sunlight.[97] Bromine radical is a highly selective and its selectivity follows the bond dissociation of the C-H bond to be abstracted (**Table 1.3**).[98]

Table 1.3 Relative selectivity of Br radical for different types of alkyl C-H bond[98]

Radical	Conditions	CH_4	$R\text{-}CH_3$	R_2CH_2	R_3CH
Br	150°C, gas	0.002	1	80	1700

Br_2 is one of the most common reagents for the bromination of alkyl C-H bonds. Besides visible light, various means to activate Br_2 exists. For instance MnO_2,[99] sodium *tert*-butoxide,[100] $CBr_4\cdot2AlBr_3$,[101] and Li_2MnO_3.[102]

N-bromosuccinimide (NBS) is the reagent of choice for the bromination of allylic/benzylic C-H bond; this is known as the Wohl-Ziegler reaction.[103-105] The Wohl-Ziegler could be initialized by sub-stoichiometric amount of radical initiators such as benzoyl peroxide or azobisisobutyronitrile (AIBN). Photo-initialization is also possible and the heat emitted from the bulb is used to reflux the reaction mixture. Although the Wohl-Ziegler reaction is an excellent choice for bromination of allylic or benzylic C-H bond, it is particularly sluggish when applied to aliphatic substrate such as cyclohexane and *n*-hexane (reactivity of toluene: *n*-hexane: cyclohexane=86: 2.2: 1).[106] From a studies of Walling's and Russell's groups,[106, 107] the H abstracting species in the Wohl-Zielger reaction is currently believed to be the bromine radical.

CCl$_3$Br is an effective reagent for benzylic bromination.[108] It has the advantage of being a more selective reagent than Br$_2$ and NBS.[109] In addition, it is useful for substrates which are sensitive to acid (HBr which could be formed with Wohl-Zielger reaction) or completing electrophilic substitution that could occur with Br$_2$ and NBS. This reagent could be activated with chemical initiators such as butyronitrile/peroxides or with photoinitiation. Reports on the use of CCl$_3$Br for non-benzylic/allylic alkyl C-H are limited.[110, 111]

CBr$_4$ could also function as a reagent for the conversion of C-H to C-Br. It could be activated with copper catalysis at high temperature (150 to 180°C),[112] with 50% NaOH under phase transfer condition,[113-115] and recently with only visible light.[116]

Oxidative bromination of alkyl C-H bond could be achieved through the use of bromide salt and oxidant. Pioneering work of Schardt and Hill demonstrated the use of stoichiometric manganese bromide salt as bromine source for bromination of alkane under inert and anhydrous condition with iodosylbenzene as oxidant.[117] Subsequently, inorganic salt such as NaBr and LiBr was reported to serve as bromine source under Fe-catalyzed oxidative bromination.[118] This is related to the gjf chemistry developed mainly by Barton's group.[23] More recently, oxidative bromination was reported with HBr and H$_2$O$_2$ under a combination of thermal- and photo-activation.[119] A Mn-catalyzed oxidative bromination of alkane was reported by Liu and Groves, NaBr and bleach were used as the reagent to brominate cyclohexane.[120] The use of "green" oxidants such as O$_2$ and H$_2$O$_2$ for oxidative halogenation was reviewed by Iskra and co-workers.[12]

With cationic *N* radical that is generated from Me$_2$NBr, selective bromination of electron rich aliphatic C-H could be achieved. For instance, the selective bromination of 1-chloropentane and pentyl acetate was reported by Minisci and co-workers (Scheme 1.19).[121]

C2=0%
C3=2.5%
C4=7.5%
C5=19.7%
C7=2.7%

67.6%

C3=0%
C4=0.41%
C5=5.9%
C7=6.88%

87%
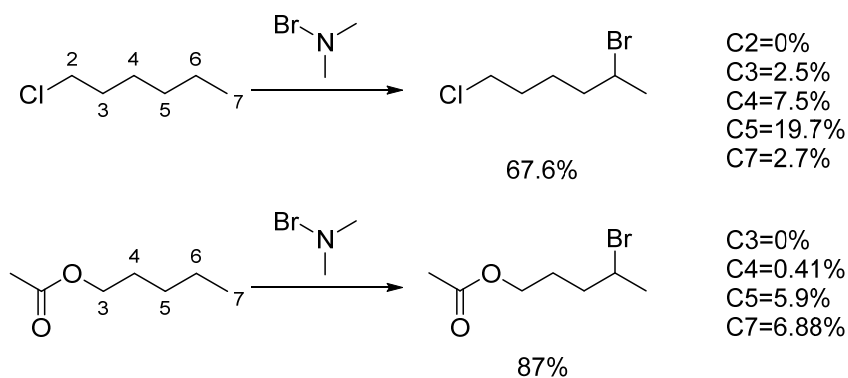
Scheme 1.19 Selective bromination of aliphatic C-H by polar effect

1.2.6 Fluorination *via* C-H functionalization

Fluorination of alkane *via* free radical substitution in the gas phase is highly exothermic and unselective.[122] Due to the high reactivity of fluorine radical, low selectivity between different types of alkyl C-H bond was observed (**Table 1.4**).[123, 124]

Table 1.4 Relative selectivity of F radical for different types of alkyl C-H bond[98]

Radical	Conditions	CH_4	$R\text{-}CH_3$	R_2CH_2	R_3CH
F	25°C, gas	0.5	1	1.2	1.4

Contrary to the low selectivity of fluorine radical in the gas phase, Chambers and Sandford demonstrated that useful fluorination of alkyl C-H bonds could be achieved with F_2 in MeCN at 0°C (**Scheme 1.20**).[125-127]

F_2(10% v/v/ mixture in N_2)

MeCN, 0°C

F

63%
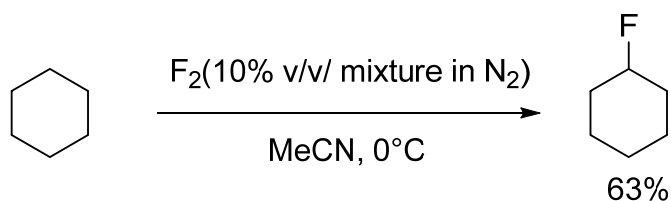
Scheme 1.20 Fluorination of cyclohexane with F_2.

Selective fluorination *via* alkyl C-H functionalization is highly attractive due to the ubiquity of alkyl C-H bonds and avoidance of the need to pre-functionalize substrate, therefore development of strategies to achieve this end is highly beneficial to the synthesis of fluorinated compounds.

Early examples of direct fluorination of alkyl C-H bonds include the work of Barton and co-workers which utilized CF_3OF to fluorinate adamantane and its derivative,[128] Feiring reported the benzylic fluorination of toluene and its derivatives with HF,[129, 130] Stavber and Zupan reported benzylic fluorination with Cesium Fluoroxysulfate $(CsSO_4F)$[131]and also trifluorination of benzylic C-H bond with XeF_2/CF_3COOH,[132] Wang and Mallock reported the selective photo-fluorination of benzylic C-H bond *via* TiO_2 and AgF,[133] the fluorination of carbonyl's alpha proton without bases was reported by Banks and co-workers,[134] and Zupan and co-workers.[135]

Recently, fluorination of aliphatic, allylic, and benzylic sp^3 C-H bonds has been demonstrated by Chen,[136] Dolye,[137] Groves,[138, 139] Lectka,[140, 141] Inuoe[142] and Sanford.[143]

1.2.7 Photochemistry and C-H functionalization

Photochemistry allows access to excited states and typically they have different reactivity from the ground state, therefore photochemistry is an important tool in organic synthesis.[144-151] Photochemistry has a long history in C-H functionalization.[145, 147] For instance, free radical halogenation (chlorination/bromination) could be initiated by visible or ultraviolet light,[152] and the use of polyoxomelate[153] as photocatalyst in C-H activation has been extensively studied.[145] In this thesis, we would focus on the development of C-H functionalization methodologies for bromination and fluorination *via* visible light photocatalysis.

1.3 Photoredox chemistry

Although photoredox catalysis with ruthenium poly-pyridine complexes has been known for a long time,[154] only during these few years has the use of visible light from low-powered

sources in organic synthesis experienced a renaissance. Numerous works on the use of photoredox chemistry in organic synthesis has been reported and this has culminated in numerous reviews.[155-163]

The basic principle of photoredox catalysis is the conversion of energy in photons to chemical energy which is used to drive a redox reaction. Photons in the visible light region (400nm to 700nm) have an energy range of 40.8 to 71.5 kcal/mol. This conversion is facilitated by a photoredox catalyst (PrC in **Figure 1.1**) which is promoted to its excited state (PrC* in **Figure 1.1**). In the oxidative quenching cycle, the excited state will transfer its excess energy together with an electron to an oxidative quencher ($S_2O_8^{2-}$, Ar-NO$_2$, and viologens, O$_2$) to form PrC$_{oxidized}$ which is an oxidant. In the reductive quenching cycle, the excited photoredox catalyst will accept an electron from a reductive quencher (e.g. triethylamine, oxalate, xanthane, ascorbate) to form PrC$_{reduced}$ which is a potent reducing agent. PrC$_{reduced}$ and PrC$_{oxidized}$ can further react with desired substrates *via* a redox reaction.
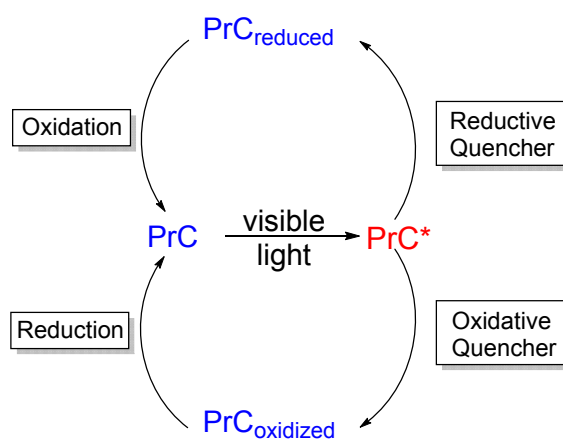
Figure 1.1 A general mechanism for visible light photoredox chemistry. PrC = Photoredox catalyst

Our group has been involved in the development of photoredox chemistry with organic dyes. Our initial work demonstrated that the excited state of rose bengal could serve as an oxidant

for 1,3-dicarbonyl and related compounds (**Scheme 1.21**).[164] The enol form of the substrate is

oxidized to a radical species which could be trapped by TEMPO to give the product.
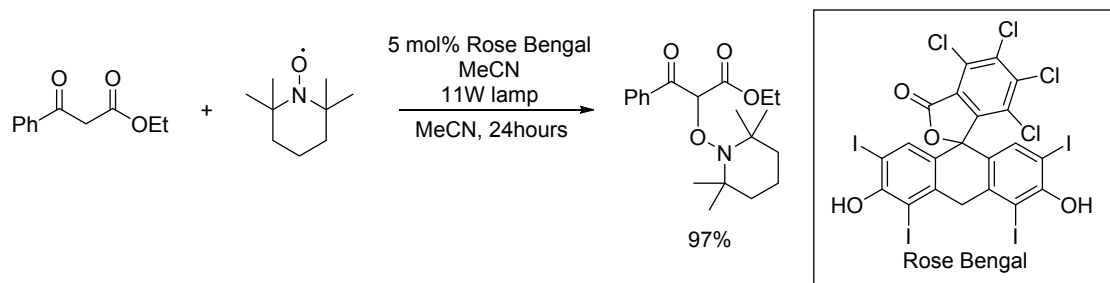
Scheme 1.21 Rose Bengal catalyzed photo-oxidation of 1,3-dicarbonyl compounds

Further investigation led us to propose a different mechanism from the one which we

reported earlier.[164] ^{1}H NMR in CD$_3$CN of the substrate reveals a significant amount of enol

tautomer. Together with precedent that the oxidation of enol related compounds by single

electron transfer is well known,[165] we proposed that the enol is oxidized by rose bengal. Two

possibilities exist, one of which is illustrated in **Scheme 1.22**. The photocatalyst's excited state is

quenched by dioxygen; the resulting PrC$_{oxidized}$ then oxidizes the enol. The other possibility

involves the excited PrC being quenched by the enol, and the enol is oxidized in the process. At

this stage, there is insufficient evidence to distinguish between the two possibilities. However, we

note that dioxygen is essential for the reaction, as when the experiment was conducted in a

glovebox (O$_2$<1ppm), rose bengal lost its bright red color overtime and no product formed.
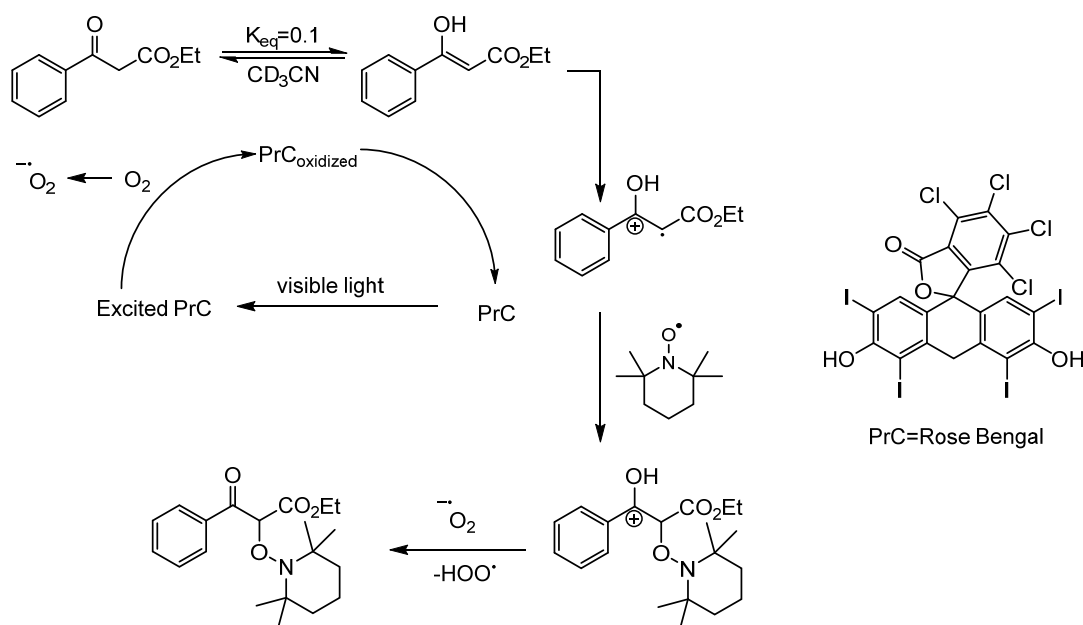
Scheme 1.22 Our proposed mechanism for the rose bengal catalyzed photoredox coupling of 1,3-dicarbonyl to TEMPO

Cross dehydrogenative coupling (CDC) reaction could be classified as a form of C-H functionalization reaction. It is a powerful strategy aimed to couple two C-H bonds to form a C-C bond (**Scheme 1.23**). In its ideal form, CDC has a very high atom economy[166] due to H_2 gas being the only by-product. However, this is rarely achieved. The early CDC reactions required a stoichiometric amount or more of an oxidant such as tBuOOH, in conjunction with a metal catalyst such as CuBr.[167]
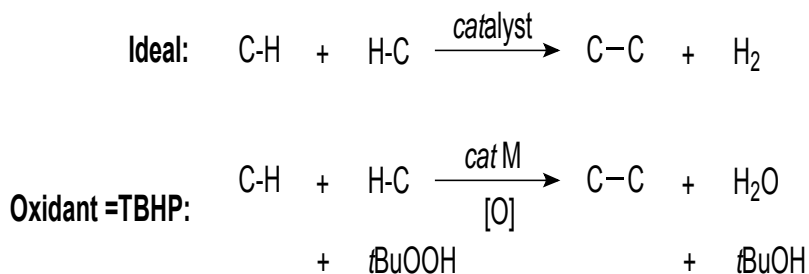
Scheme 1.23 CDC reactions.

The seminal work of Stephenson and co-workers demonstrated that with visible light photoredox catalysis, dioxygen could be used as the terminal oxidant.[168] A general mechanism for the photoredox CDC reaction is depicted in **Scheme 1.24**. Tertiary amine which is previously used in excess as sacrificial reductive quencher (see **Figure 1.1**) becomes the substrate. Reductive quenching of the excited photoredox catalyst by the substrate generates a cationic *N*-radical which could be deprotonated to form an electrophile (iminium). The iminium could be attacked by a variety of nucleophiles.[158]
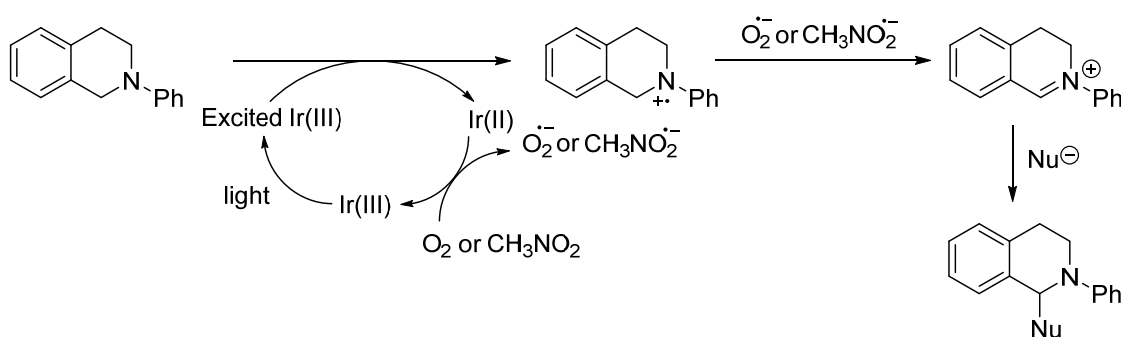
Scheme 1.24 General mechanism for photoredox CDC reactions

Pertinent to CDC reactions *via* visible light photoredox catalyst, we disclosed an organocatalytic version which utilizes rose bengal as the photoredox catalyst (**Scheme 1.25**).[169] Subsequently, we report that the addition of graphite oxide could enhance the reactivity of this reaction.[170]
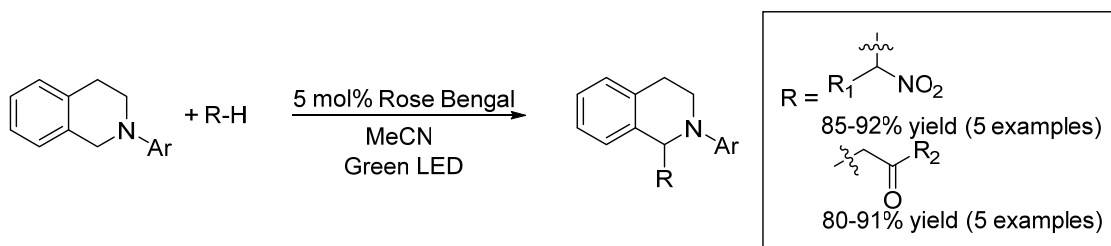
Scheme 1.25 organocatalytic visible light photoredox CDC reaction catalyzed by rose bengal

Preliminary mechanism investigation shows that the low reactivity of *N,N*-dimethylaniline **2a** relative to **1a** does not correlate to its oxidation potential, but instead the more favorable thermodynamics to the formation of iminium for **1c** to **2c** is consistent with the better reactivity for **1a**.
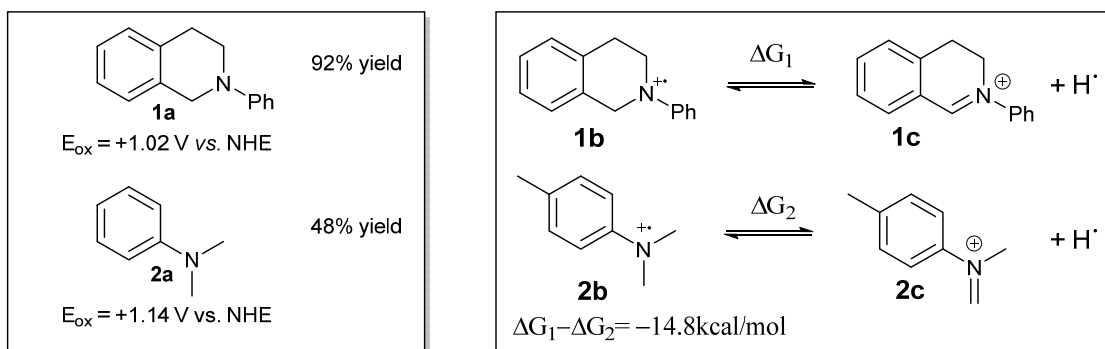
Scheme 1.26 Calculated thermodynamics data for rose bengal catalyzed CDC reaction

1.4 Non-covalent interactions

Non-covalent interactions or intermolecular interactions are central to chemistry. To the best of our knowledge, there is no standard definition of non-covalent interaction. It is often refer to as the force that drives the formation of molecular clusters. It is characterized by distance that is longer than the accepted ones for the corresponding covalent bond. In some cases, van der Waals interactions are sometime considered as a subset of non-covalent interactions.[171] The IUPAC definition of van der Waals forces is as follows: "The attractive or repulsive forces between molecular entities (or between groups within the same molecular entity) other than those due to bond formation or to the electrostatic interaction of ions or of ionic groups with one another or with neutral molecules.".[172]

1.4.1 Non-covalent interactions and supramolecular chemistry

Non-covalent interactions are fundamental to supramolecular chemistry. Supramolecular chemistry is defined by Lehn as the "chemistry of molecular assemblies and of the intermolecular

bond".[173, 174] The important non-covalent interactions in supramolecular chemistry are hydrogen bonding, stacking interactions, electrostatic interactions, hydrophobic interactions, charge-transfer interactions, and metal coordination.[171, 175] Recently, halogen bonding, which would be elaborated in the next subsection, has been recognized as an important class of non-covalent interactions in supramolecular chemistry. [15-18]

The impact of supramolecular chemistry in modern society is profound. Its applications span diverse but important fields such as medicinal chemistry: drug delivery systems,[176-184] catalysis,[185-190] and molecular devices such as light harvesting devices,[191] light conversion devices,[192] signaling devices,[193-196] and molecular electronics.[197-199] Given that non-covalent interactions are essential components of supramolecular chemistry, the ability to understand and describe these interactions accurately is of paramount importance. To this end, theoretical approaches *via* wave-function theory and density functional theory have become indispensable tools in modern chemistry.

Organocatalysts could be considered as a form of supramolecular catalyst (depend on the size of the catalyst). Similarly, non-covalent interactions are central to organocatalysis. In this thesis, we are interested in the use of computational methods to provide insights into organocatalytic system (refer **Chapter 4**).

1.4.2 Halogen bonding

In this thesis we are interested in the use of halogen bonding as a form of non-covalent interactions in catalysis.

According to the definition proposed by IUPAC, "A halogen bond occurs when there is evidence of a net attractive interaction between an electrophilic region associated with a halogen atom in a molecular entity and a nucleophilic region in another, or the same, molecular entity".[200]

Halogen bond is an attractive non-covalent intermolecular interaction, where the halogen functions as a Lewis acid and an electron-rich partner serves as the Lewis base (**Figure 1.2**). Some of the earliest reports of halogen bonded complexes include the complex of I_2 (Lewis acid) and NH_3 (Lewis base) reported by Guthrie in 1863,[201] and the complex of I_2 (Lewis acid) and benzene (Lewis base), which was characterized by ultraviolet-visible spectroscopy, by Benesi and Hildebrand in 1949.[202] The work of Hassel and co-workers presented experimental evidences of halogen bonding in several complexes *via* x-ray diffraction.[203] Legon and co-workers studied the gas-phase geometries and charge distribution of a diverse range of halogen bonded complexes. Their studies were conducted with a combination of microwave spectroscopy and supersonic expansion with a fast-mixing nozzle.[204]
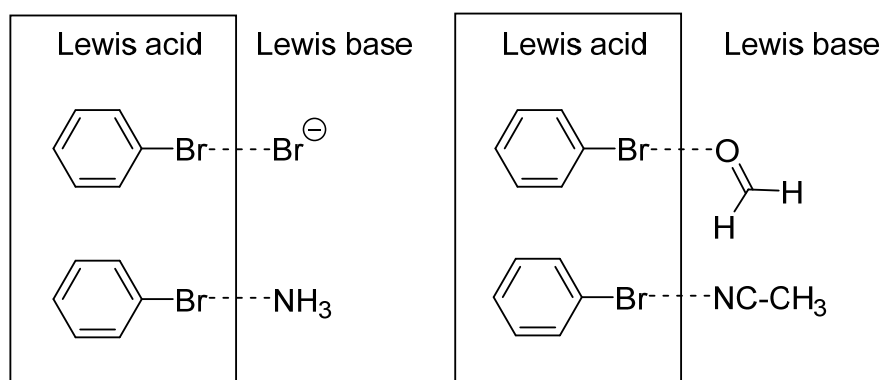
Figure 1.2 Examples of halogen bonded complexes

C-X bonds are generally thought to be polarized (the halogen which is more electronegative bears a partial negative charge), therefore it appears that interaction with a Lewis base (an electron-rich species) would be repulsive, at least from an electrostatic point of view. However, the preceding description is an over-simplification of the electron distribution of halogen in a compound. For instance, from the electrostatic potential map of bromobenzene derived from DFT calculation (**Figure 1.3**), it is evident that the electron distribution around the bromine atom is anisotropic (this appears to be a general phenomenon for many halogen presents

in organic molecules). A red ring of negative electrostatic potential could be observed perpendicular to the planes of bromobenzene. This peripheral red ring converges to a region of positive electrostatic potential, which is termed the "sigma hole".[205] The sigma hole is confined to a small region centered along the C-Br axis. The sigma hole model is consistent with both the high directionality and increasing halogen bond's strength with electron withdrawing substituents as advocated by Politzer and co-workers.
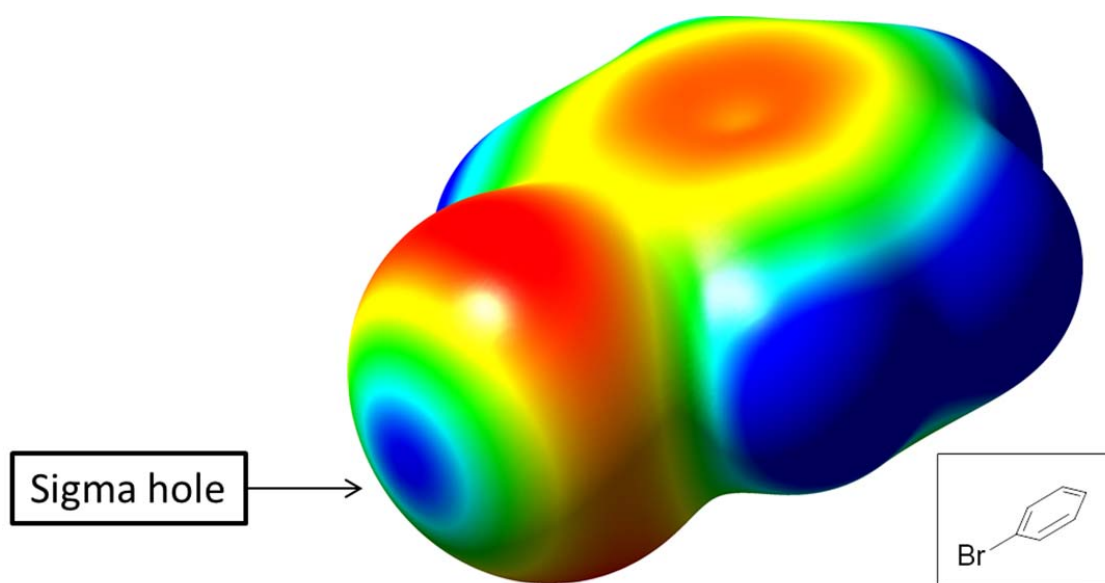
Figure 1.3 Electrostatic potential of bromobenzene. Blue region: repulsive interaction with respect(w.r.t) to a positive test charge. Red region: attractive interaction w.r.t a negative test charge. Isovalue of density = 0.001 a.u.

Currently, halogen bonding has been recognized as an important non-covalent interaction in supramolecular chemistry[15-18] and biology[19, 21]. The wide implication of halogen bonding in both chemistry and biology has motivated the development of various experimental techniques to study halogen bonding, both in gas phase[204] and also in solution[206]. Experimental techniques which allow the determination of the thermodynamics of halogen bonding in solution could be potentially helpful in the applying halogen bonding to supramolecular chemistry and biology.[207]

1.4.3 Halogen bonds in organic synthesis

The involvement of halogen bonding in reaction could be traced back to one of the classic reactions in organic chemistry - the addition of bromine to alkene. It was observed that upon mixing Br_2 with alkenes, a new, transient UV-vis absorption band at 270nm appeared.[208, 209] This is ascribed to the 1:1 bromine-alkene complex.[210] Subsequently, a 2:1 bromine-olefin π complex was reported which has an absorption band at 310nm.[209] The interaction between the π bond of alkene and Br_2 could be regard as a type of halogen bond in which the C=C acts as a Lewis base and Br_2 as the Lewis acid.[211] These halogen bonded complexes are regarded as key intermediates in the electrophilic addition of bromine alkene (**Scheme 1.27**).
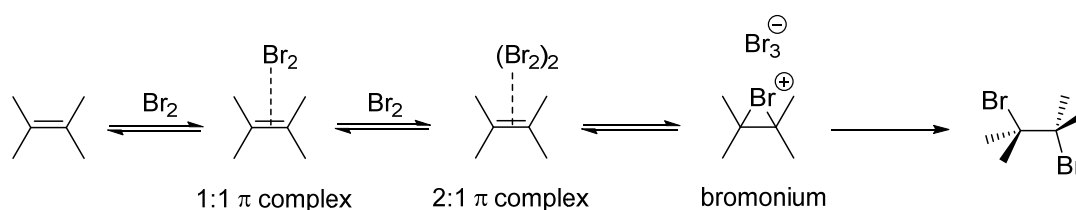
Scheme 1.27 Mechanism for the electrophilic addition of bromine to alkene.

Catalytic halofunctionalization reaction is an important class of organic reaction where halogen bonding could play an important role. Although it was not explicitly stated in the review of Denmark and co-workers on catalytic asymmetric halofunctionalization, halogen bonds between a Lewis base and halonium is classified as one of the important types of interaction to attain enantioselective halofunctionalization (**Scheme 1.28**).[212] Such interaction between a Lewis base and halonium (Lewis acid) fulfils the definition of a halogen bond. Halogen bonds between NBS and a Lewis basic component of the chiral catalyst has been proposed by Shi and coworkers,[213] Denmark and Burk,[214] and Yeung and co-workers.[215]
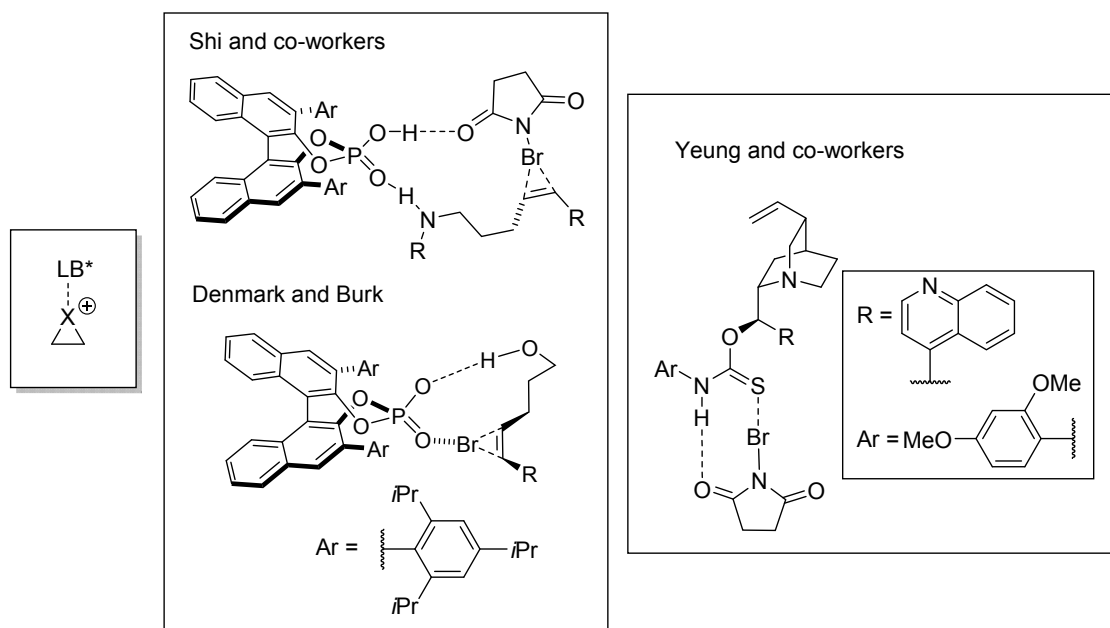
Scheme 1.28 Halogen bond between a Lewis base catalyst and halonium. Proposed TS from various groups.

Recently, Bolm and co-workers reported that iodoperfluoroalkane could promote the reduction of quinoline with Hantzsch ester as reducing agent and proposed that halogen bond is essential (**Scheme 1.29**).[216] However, attempt to characterize the proposed halogen bond between $CF_3(CF_2)_7I$ and the substrate was inconclusive from ^{13}C NMR (downfield shift of 0.01-0.06ppm was observed). ^{19}F NMR gave a 0.06 ppm downfield shift for CF_3 and CF_2 moiety. In our opinion, the chemical shifts are small and could be within experimental errors, therefore statistical tests should be applied before a conclusion is drawn. The authors note that $CF_3(CF_2)_7I$ decomposes in the presence of Hantzsch ester, when the substrate is not presence.
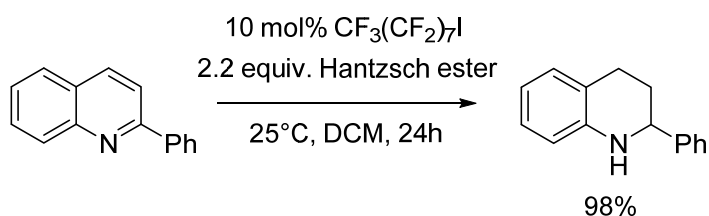
Scheme 1.29 Reduction of quinoline by Bolm and co-workers

Huber and co-workers reported that stoichiometric iodoimidazolium salt **4a** and **4b** is able to promote the Ritter reaction of benzyhydryl bromide with acetonitrile (**Scheme 1.30**).[217] The authors presented ^{13}C NMR study to support their proposal of halogen bonds being involved. They observed that after mixing **3** and **4b** the ^{13}C signal for the iodine-bearing carbon of **4b** shifted downfield in the presence of **3** (102ppm to 110ppm). However, this is contradictory to what would be expected if there is a bromine-iodine halogen bond. Iodine of **4b** acts as a Lewis acid in the halogen bond, therefore the electron density from bromine (the Lewis base) would be transfer to iodine and result in an increase in electron density which should culminate in an upfield shift. Our non-relativistic calculation of the ^{13}C NMR of **4b** in the presence of bromide supports our hypothesis. More recently, Huber's group disclosed a neutral halogen bond organocatalysis that is based on perfluorobenzene core.[218]
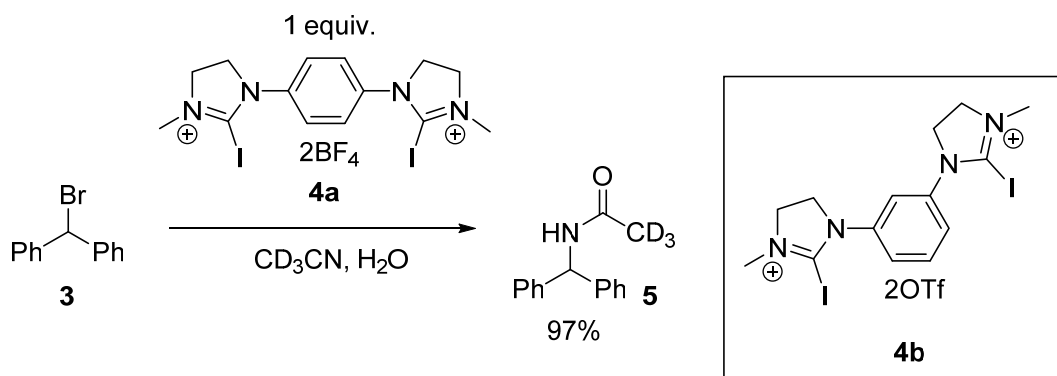
Scheme 1.30 Iodoimidazolium salt that promotes a variant of the Ritter reaction.

1.4.4 Theoretical methods to study non-covalent interactions in catalysis

We are interested to use theoretical methods such as wave-function theory (WFT) and density functional theory (DFT) to study the roles of non-covalent interactions in catalysis. Detailed information on the experimental and theoretical methods to study non-covalent interactions could be found in the reviews of Hobza and Zahradník,[219] Müller-Dethlefs and Hobza,[171] and Hobza and co-workers.[220] The reviews of Houk and co-workers present examples

and insights to the application of theoretical methods (mostly DFT) in the study of catalytic system.[221-223] Reviews on the treatment of large system using QM/MM methods by Shaik, Thiels and co-workers provides detailed information on this subject.[224, 225]

Chapter 2

Selective sp^3 C-H bond bromination *via* organo-photoredox catalysis

2 Selective sp^3 C-H bond bromination *via* organo-photoredox catalysis

2.1 Introduction

This work focuses on the bromination of sp^3 C-H bond (aliphatic and benzylic) with the objective of achieving a mild and regioselective synthetic procedure that has tolerance to common functional groups used in organic synthesis. The main motivation being that organic bromides are widely used as important building blocks in organic synthesis,[226-230] and the synthetic value of free-radical bromination is undermined by its low functional group tolerance; as a result most reactions based on the use of Br$_2$ are limited to hydrocarbons without functional groups.[99, 231, 232] Notably, bromination of allylic and benzylic C-H bond using the Wohl-Zielger reaction[103-105] displays tolerance to various functional and protecting groups,[233] but it is ineffective when applied to aliphatic C=H bonds.[106]

As a starting point for the development of bromination *via* visible light photochemistry, we noted that amines are frequently used as reductive quencher in visible light photoredox catalysis, and during the quenching process cationic *N*-radicals are generated. The potential of cationic *N*-radicals in C-H activation is evident from the classical Hoffman-Löffler-Freytag reaction, in which cationic *N*-radical served as directing group to intramolecularly functionalize C-H bond.[51] The intermolecular version was reported by Minisci and highly regioselective chlorination of aliphatic esters was observed.[88]

Preliminary exploration of the reactivity of these *N*-radicals with DFT calculations using the M06-2X functional[234-237] indicates that cationic *N*-radicals have reasonably low $\Delta G^{\ddagger}$ for the abstraction of H from cyclohexane, thus suggesting that these cationic *N*-radicals are, in theory, able to perform C-H activation (**Scheme 2.1**). However, given the strong electrostatic interaction between the reduced photocatalyst (PrC$_{reduced}$) and the cationic *N*-radical, it is unlikely that much separation of the ion-pair occurs, before unproductive charge recombination occurs,[238] thus

impeding the desired C-H activation. Therefore, it can be reasoned that generation of neutral radical could be a more viable strategy.
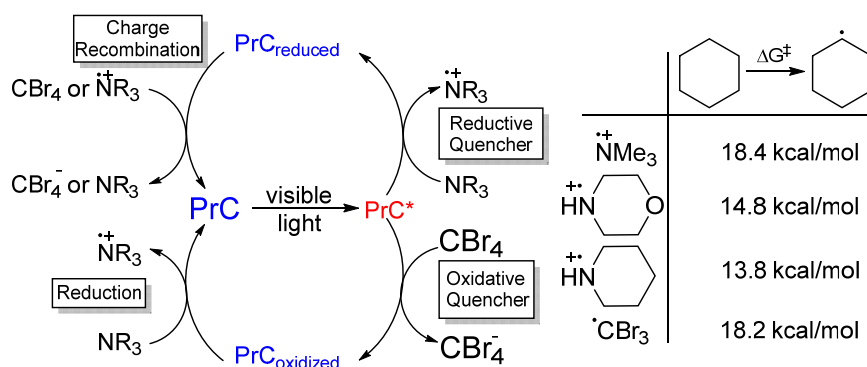
Scheme 2.1 PrC = Photoredox Catalyst. A general photoredox reductive and oxidative quenching cycle (Left). $\Delta G^{\ddagger}$ for abstraction of H from cyclohexane by various cationic N-radicals calculated at CPCM=DCM-M06-2X/BS1. (Right). BS1 denotes the use of 6-311++G(d,p) basis set on all non-Br atom and the use of LANL2DZ(d,p) on Br and also the LANL2DZ pseudopotential on Br. Frequency analysis at 298.15K and 1 atmosphere.

Inspiration for our initial exploration came from three different sources. Schreiner and co-workers demonstrated that reduction of CBr_4 could generate CBr_3 radical *via* dissociative single electron transfer (SET). The CBr_3 radical could abstract hydrogen from unactivated C-H bond. In addition, CBr_4 could serve as a source of Br for the alkyl radicals to form the desired alkyl bromide.[113, 115] We envisioned that a photoredox system could perform the reduction of CBr_4 as illustrated in **Scheme 2.1**. This hypothesis was corroborated by the work of Stephenson and co-workers, in which CBr_3 radical was proposed to be generated *via* the oxidative quenching cycle with Ru(bpy)$^{2+}$ as the photocatalyst (**Scheme 2.1**., oxidative quencher).[239]

Given our interest in the use of inexpensive organic dyes as photoredox catalyst[164, 169, 240] as well as inspiration from the works of König, Zeitler and co-workers, we begin our investigation using Eosin Y disodium salt and CBr_4 as partners for the bromination of sp^3 C-H bond.

2.2 Results and Discussion

2.2.1 Evaluation of reaction conditions

We began our investigation using cyclohexane as the model substrate. It was found that CBr_4 alone did not result in the formation of any product (**Table 2.1**, Entry 1). A series of amines were tested and morpholine was found to give the highest yield (**Table 2.1**, Entries 2–8). Stirring does not affect the product yield, thus implying that interfacial reaction is unimportant in this case (**Table 2.1**, Entry 8).The role of Eosin Y disodium salt as a photoredox catalyst is established by control experiments (**Table 2.1**, Entries 10 and 11).

The results in **Table 2.1** present some interesting trends. For instance, the use of structural similar cyclic amines such as piperidine (Entry 4), 4-methylmorpholine (Entry 6) and thio-morpholine (Entry 7) and morpholine (Entry 8) gave vastly different yield for the desired product. This would be discussed further in section **2.2.7**.

A related work was reported by Nishina and co-workers.[116] They reported that bromination of cyclohexane could be achieved with only CBr_4 and visible light. Yield of up to 150% could be obtained after 1 day.[116] We have repeated their work and found that their reported GC yields are largely inflated probably due to improper calibration on their part. Nevertheless, their results are interesting as they found that water inhibited the reaction which agrees with our control experiment (Entry 11). In addition, for their case, the $CHBr_3$ derived from CBr_4 could further promote the bromination of cyclohexane but this is not the case for our photoredox bromination (**Figure 2.10**).

Table 2.1 Screening of amines and control experiments
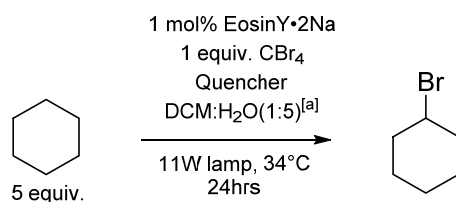
Entry	Cyclohexane: CBr$_4$:Quencher	Quencher	Yield (%)[b]
1	5:1:0	-	0
2		Et N—iPr iPr	4
3		Et N—Et Et	7
4		NH	13
5	5:1:2	HN NH	26
6		O N—	23
7		S NH	4
8		O NH	57
9(No stirring)			57
10(No light)			0.5
11(No PrC)[c]			2

[a] Volume of DCM used is 0.4 mL and water is 2mL [b] Yield of bromocyclohexane calculated based on 1 equivalent (0.3 mmol) of cyclohexane consumed (from GC-MS, an average of three runs). [c] PrC = photoredox catalyst.

The product yield was found to increase with increasing ratio of cyclohexane to CBr_4 (**Table 2.2**, Entries 7, 1 to 3). However, performing the reaction by replacing DCM with cyclohexane did not afford better yield (**Table 2.2**, Entry 4). Increasing concentration of cyclohexane is expected to increase the rate of hydrogen abstraction of cyclohexane. This is especially important when the rate determining step is the hydrogen abstraction step. The observation of a large kinetic isotope effect study indicates that the rate determining step is the hydrogen abstraction step (**section 2.2.7.2**).

Table 2.2 Effect of substrate is to CBr_4 ratio on product yield
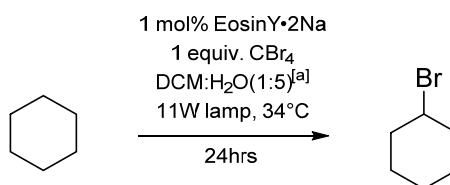
Entry	Cyclohexane: CBr_4:Morpholine	Yield (%)[b]
1	3:1:2	36
2	5:1:2	57
3	10:1:2	75
4	25:1:2[c]	8

[a] Volume of DCM used is 0.4 mL and water is 2mL [b] Yield of bromocyclohexane calculated based on 1 equivalent (0.3 mmol) of cyclohexane consumed (from GC-MS, an average of three runs). [c] DCM is replaced by cyclohexane as solvent and the amount of cyclohexane calculated based on its density at room temperature and volume added is 25 times CBr_4.

The biphasic condition is essential for the reaction, only 12% of bromocyclohexane was obtained in the absence of water (**Table 2.3**, Entry 1). Contrary to the inhibition of cyclohexane bromination observed by Nishina and co-workers,[116] we found that increasing the ratio of water to DCM resulted in better yield of bromocyclohexane (**Table 2.3**, 1 to 3). This indicates that a different mechanism is in operation although both methods utilized CBr_4 and visible light.

Table 2.3 Effect of DCM to water ratio on product yield
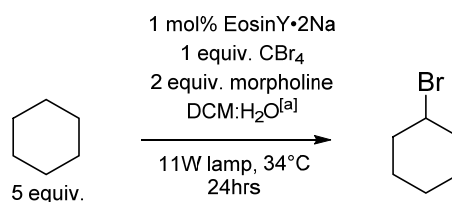
Entry	DCM:H$_2$O	Yield (%)[b]
1	1:0	12
2	1:1	35
3	1:5	57

[a] 1 equiv. of DCM is 0.4 mL and water [b] Yield of bromocyclohexane calculated based on 1 equivalent (0.3 mmol) of cyclohexane consumed (from GC-MS, an average of three runs).
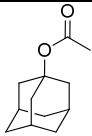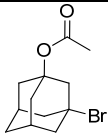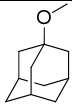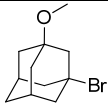
2.2.3 Application to simple substrates

2.2.3.1 Basic functional group tolerance

The photoredox C-H activation protocol was tested on several simple hydrocarbons. Tolerance for ketone, ester and ether functional group was demonstrated by bromination of adamantane derivatives (**Table 2.4**, Entries 2-4).

Table 2.4 Basic functional group tolerance[a]

Entry	Substrate	Product	Yield (%)
1			56[b] (51%[c])
2			74%[b] (57%[c])

38

3			55%[b]
4			56%[b]

[a] Reaction condition: substrate: CBr$_4$: morpholine = 3:1:1, room temperature. [b] Isolated yield based on remaining starting material (the hydrocarbon). [c] Isolated yield based on 1 equivalent (0.3mmol) of substrate consumed.

2.2.3.2 Yield and yield brsm

The products in **Table 2.4** are isolated by column chromatography. The difference between [b] isolated yield based on remaining starting material (the hydrocarbon) and [c] isolated yield based on 1 equivalent (0.3mmol) of substrate consumed is the denominator of the equation used in the calculation of yield.

$$isolated\ yield = \frac{amount\ of\ product\ isolated}{theoretical\ maximum\ amount\ of\ product\ that\ can\ be\ formed}$$

In [b], the theoretical maximum amount of product that can be formed is determined from the amount of hydrocarbon consumed. For instance, the hydrocarbon was recovered via column chromatography and from the amount of hydrocarbon recovered and the amount added to the reaction initially we could determine how much hydrocarbon is consumed. In summary for this definition of yield, we are interested in how much of the hydrocarbon is actually converted to the product.
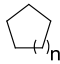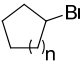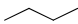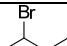
In [c], the theoretical maximum amount of product that can be formed is determined from the amount of CBr$_4$ added to the reaction initially. For this definition, we are interested to know how much of the product can be formed from the amount of CBr$_4$ we added to the reaction. Note: CBr$_4$ is virtually consumed at the end of the reaction.

[b] is higher than [c] because the hydrocarbon does not undergo much side reaction but CBr$_4$ undergoes more unproductive side reactions such as dimerization and decomposition.

3.2.3.3 Aliphatic and Alicyclic substrates

Homolog of cyclohexane, such as cycloheptane and cyclooctane could be mono-brominated with yield of more than 70% (Entry 1). Linear aliphatic hydrocarbon such as *n*-butane could also be brominated with a yield of 31% (Entry 2). However, our method is unlikely to be suitable for the synthesis of such compounds as the by-product: CHBr$_3$ has a very similar boiling point to the desired bromoalkane, therefore clean separation by distillation would be very difficult.

Table 2.5 Aliphatic and alicyclic substrate
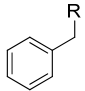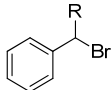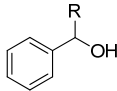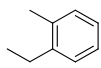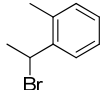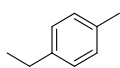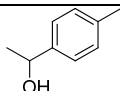
Entry	Substrate	Product	Yield (%)
1			n=1, 57%
			n=2, 57%
			n=3, 76%
			n=4, 74%
2			31%

Reaction condition: Substrate: CBr$_4$: morpholine = 5:1:2, 34°C. Yield determined from GC-MS with biphenyl as internal standard.

3.2.3.4 Benzylic substrates

Interestingly, insignificant amount of brominated product was detected when toluene was used as the substrate even after extended reaction time (**Table 2.6**, Entry 1), but ethylbenzene derivatives could be brominated at the benzylic position (**Table 2.6**, Entries 2 and 3). Thoroughly mixing the two phases converts the brominated product to hydroxylated product via a nucleophilic displacement (**Table 2.6**, Entry 4). This does not occur for other substrates, as they lack the stabilization provided by the benzyl group for nucleophilic displacement.

Table 2.6 Benylic substrates

Entry	Substrate	Product	Yield (%)
1			R=H, 2% R=CH$_3$, 50%[a]
2			R=H, 1%[b] R=CH$_3$, 33%[b]
3			38%
4			40%[b,c]
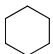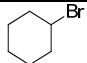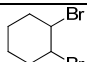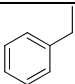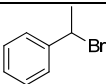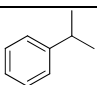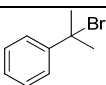
Condition: substrate:CBr$_4$:morpholine = 5:1:2, 34°C and GC yield unless otherwise stated. [a] 1 equivalent of morpholine instead. [b] Stirred the 2 phases thoroughly. [c] Condition: substrate:CBr$_4$:morpholine = 1:1:1, 34°C and isolated yield.

2.2.4 Comparative experiments

Comparative experiments were performed to benchmark the photoredox against established methods for bromination (**Table 2.7**). In the bromination of cyclohexane, the photoredox bromination produces exclusively the mono-brominated product (Table 4, entry 1) but bromination with Br$_2$ and visible light produced both the mono-brominated and di-brominated products in a ratio of 2.8:1 (**Table 2.7**, entry 1). The high selectivity for mono-brominated product reflects the mild condition of the photoredox bromination. Although it is possible to obtain high yield of mono-brominated product with Br$_2$ based reactions, these reactions generally require cyclohexane to be present in large excess (e.g. 74 equiv.[232] or 92 equiv.[99]), while this may not be a problem for inexpensive starting material such as cyclohexane, but it would not be equally feasible for more valuable starting material.

Cumene's tertiary benzylic C-H bond has higher reactivity than the secondary benzylic C-H bonds of ethylbenzene in free radical bromination.[107] However, when cumene was used as the substrates for the photoredox bromination; its reactivity was found to be much lower than ethylbenzene (**Table 2.7**, entry 2). Given the lower bond dissociation of cumene (BDE = 87.9 kcal/mol) compared to ethylbenzene (BDE = 88.6 kcal/mol), the origin of this lower reactivity should not be of bond strength; instead we ascribed it to the increased steric demand of the tertiary benzylic C-H bond. Nevertheless, it should be noted that synthesis of (2-bromopropan-2-yl)benzene (**Table 2.7**, Entry 3) is difficult in practice as it is found to be unstable even in the absence of light.

Table 2.7 Photoredox bromination *vs*. bromination *via* bromine radical

Entry	Substrate	Possible Product(s)	Yield/%	
			Eosin Y·2Na /morpholine /CBr$_4$	Bromination via Br radical
1		Br cyclohexyl	57[a]	44[a](33[b])
		Br,Br dibromocyclohexane	0	16[a](23[b])
2[d]	ethylbenzene	Br	50	(67[g])
3[d]	cumene	Br	10[c]	68[a,f](68[e])

[a] Performed with 5:1 (substrate: Br source) using Br$_2$/H$_2$O/light in the case of Br radical [b] From Shaw and co-workers.[231] [c] No (2-bromopropan-2-yl)benzene was detected from GC-MS, yield calculated from 2-phenylpropan-2-ol and α-methylstyrene. [d] Condition: substrate:CBr$_4$:morpholine = 3:1:1, room temperature [e] Wohl-Zielger reaction reported by Solomon and co-workers.[241] [f] Mixture of 4 products. [g] Reported by Megiel and co-workers.[242]

2.2.5 Methyl Ester of Ibuprofen: Qualitative prediction of regioselectivity based on charge and steric

It is well-established that bond-strength is an important parameter for free radical transfer reactions such as the abstraction of H by bromine radical and an Evans-Polanyi relation exists for such reactions.[81, 82] However, the influence of other factors such as steric, resonance, and polar effects[243-246] in the abstraction of H by radical is also well-documented in the literature. In a similar spirit, we attempt to qualitatively predict the regioselectivity of the photoredox bromination when applied to more complex molecules *via* quantification of steric and atomic charge on various hydrogens with natural bond order (NBO) analysis.[247]

Methyl ester of Ibuprofen, a non-steroidal anti-inflammatory drug (NSAID), was tested in the photoredox bromination. It was chosen as there are three possible sites where bromination could occur, after discounting the six methyl C-H bonds, thus presenting a good opportunity to study the effect of electronic and steric properties of these C-H bonds on their respective reactivity in the photoredox bromination.

46% isolated yield brsm
for photoredox bromination
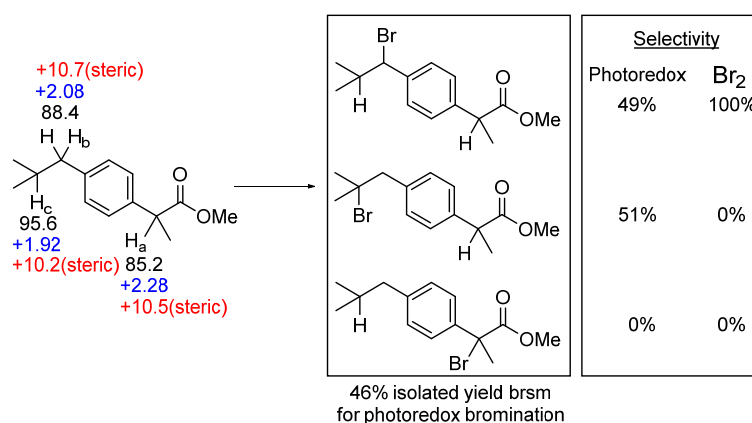
Scheme 2.2 Bond dissociation energy in black. Natural population analysis (NPA) charges in blue. Intermolecular pairwise-additive estimate of steric exchange interaction between relevant H and a He probe in red (refer to Figure 2.1) Isolated yield based on remaining starting material (brsm), combined yield of both identified isomers. Selectivity includes statistical correction for the number of benzylic C-H bonds vs. tertiary C-H bond.

The results in **Scheme 2.2** suggest that reactivity of C-H bonds does not solely depend on bond strength. In this case, the C-H bond with the lowest bond dissociation energy (**Scheme 2.2**, H_a) is not brominated; instead bromination occurs exclusively on the stronger H_b and H_c. This result suggests that electron deficient H is less reactive in the photoredox bromination; this phenomenon could also be seen in **Table 2.4** where the electron deficient *alpha* proton of carbonyl and ester functional group is not brominated. Electron density on H as quantified by NPA charges,[247] indicates that H_a is the most electron deficient and H_c is the most electron rich.

Despite H_c being about 7 kcal/mol stronger, in terms of bond dissociation energy, than H_b, the site selectivity between these two is almost equal in the case of methyl ester of ibuprofen. We ascribed this to both the higher electron density on H_c relative to H_b (NPA charge: +1.92 *vs*. +2.08) and higher steric demand as quantified *via* the pairwise-additive estimate ($E_{pw}^{(st)}$) of the steric exchange energy obtained from the NBO steric analysis[248, 249] (+10.2 kcal/mol *vs*. +10.7 kcal/mol). This example demonstrates the potential of selective C-H activation by exploiting the difference in electron density and steric environment of C-H bond.

2.2.5.1 NBO steric analysis of methyl ester of Ibuprofen

The fundamental origin of steric repulsions is the Pauli exclusion principle. The "exchange antisymmetry" guarantees that electron could not be distinguished and resists electrons from being crowded into small region of space. The NBO steric analysis allows the evaluation of steric exchange energy from anti-symmetrization of NLMOs and also the pairwise steric exchange energies for disjoint (no common atoms) interactions between NLMOs.

The four conformations of ibuprofen methyl ester with the lowest Gibbs free energy were chosen for NBO steric analysis with a He probe. A Helium atom was placed at 134pm, 144pm and 154pm from the relevant H where the C-H---He angle is 180° (See **Figure 2.1** for an example). A single point calculation at M06-2X/6-311++G(d,p) with int=ultrafine was then

performed to generate the archive file for GENNBO[247]. GENNBO was then used to perform the steric analysis. The Boltzmann distribution weighted results are presented in **Figure 2.1**.

He-H distance/pm	154	144	134
H	Relative steric exchange energy / kcal mol^{-1}		
12	10.5	15.1	21.4
14	10.6	15.2	21.6
15	10.7	15.4	21.9
17	10.2	14.8	21.2
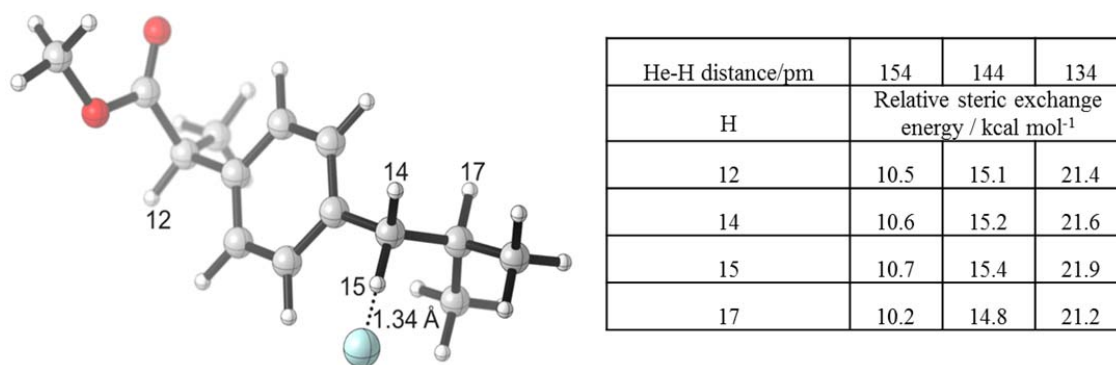
Figure 2.1 Use of Helium atom as probe for NBO steric analysis

2.2.6 Regioselective innate C-H functionalization of terpenoid and estrone derivative

The Barton reaction, Hofmann–Löffler–Freytag reaction and its variant[51, 54, 250] are amongst the most prominent strategies for guided radical-based C-H functionalization[50] of steroid and related compounds.[53] These reactions are powerful strategies and have been applied skillfully in synthesis.[53, 251-254] In the next two examples, we would demonstrate that the photoredox bromination is capable of performing regioselective innate C-H functionalization,[50] which would complement the well-established guided radical-based C-H functionalization.

(+)-Sclareolide, a plant-derived terpenoid with antifungal and cytotoxic activities, was chosen to further demonstrate the applicability of the photoredox bromination in the regioselective bromination of more complex substrate (**Scheme 2.3**). Bromination does not occur at the two tertiary C-H sites which are expected to have lower bond strength, instead the major product (about 76% selectivity) is found to be the C2 brominated sclareolide. The yield obtained was comparable to previous report on the oxidation of (+)-sclareolide by White[90] and chlorination by Grove.[120]

2.2.6.1 Brominated sclareolide product distribution analysis

From GC-MS analysis of the crude product in (+)-sclareolide bromination, 3 minor products containing Br is evident from MS spectra. From the GC-MS chromatogram of the crude product below, the selectivity for 2-position is 76.5% and the other positions are 23.5% (**Figure 2.2**). NMR analysis of the crude product gave 75.2% for the 2-position and 24.8% for other position (see crude ^{1}H NMR spectrum below).
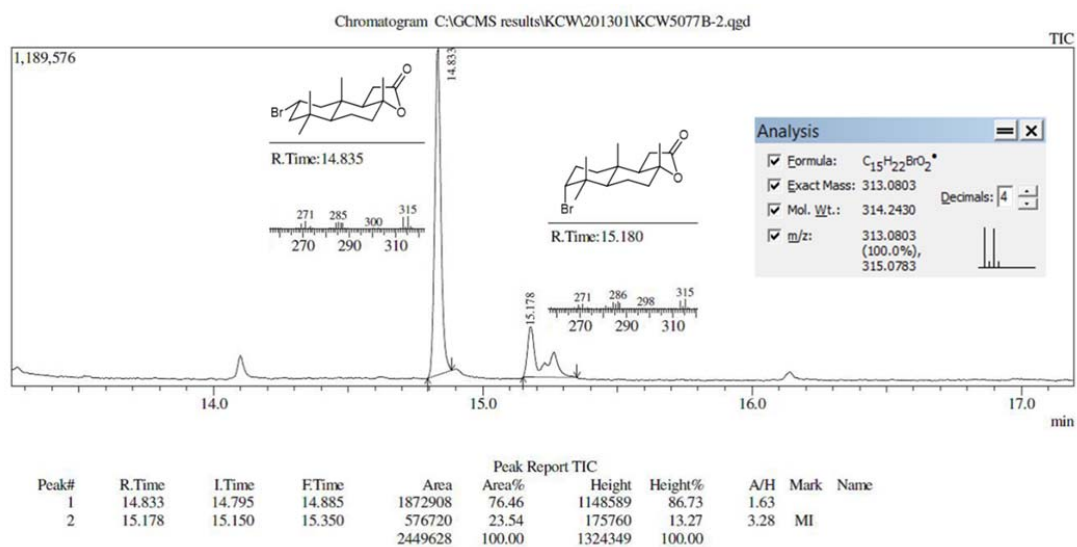
Figure 2.2 GC-MS analysis of crude mixture for (+)-Sclareolide bromination.

The main minor product (Retention time = 15.18 min, **Figure 2.2**) is assigned to the 3-Br product, which gives a triplet with $^3J_{HH}$=3.2Hz (**Figure 2.3**), thus suggesting that the Br is in the axial position. HMQC indicates that this H is attached to a carbon at 68.96ppm (**Figure 2.4**). HMBC and DEPT-135 (**Table 2.8**) is consistent with the 3-Br product.
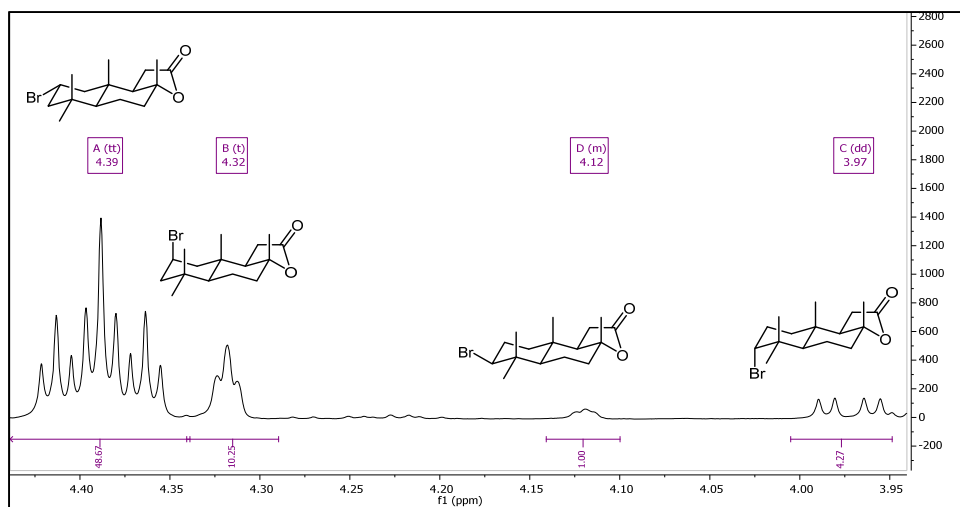
Figure 2.3 Crude ¹H NMR (500 MHz, Chloroform-*d*) of (+)-sclareolide bromination.
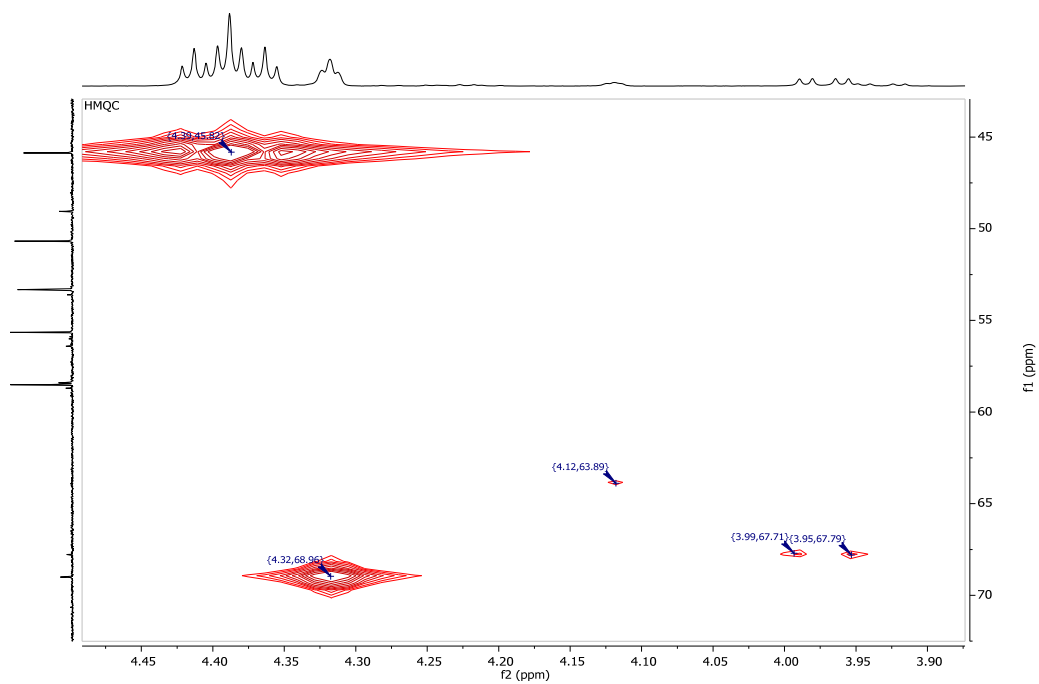
Figure 2.4 HMQC of crude mixture of (+)-sclareolide bromination.

Table 2.8 DEPT-135 results of crude mixture for (+)-sclareolide bromination

13C chemical shift /ppm	DEPT-135	Carbon type
21.41	+	1°
27.82	-	2°
33.76	-	2°
38.03	0	4°
48.99	+	1°

Quantification of steric demand of all hydrogens attached to 2° and 3° carbon center by NBO steric analysis with a He probe reveals that the equatorial C2 hydrogen has the lowest steric demand (**Scheme 2.3**), while the deeply entrenched tertiary C-Hs are sterically more demanding ($\Delta E_{pw}^{(st)} > +2$ kcal/mol, with respect to C2 hydrogen). Hydrogens on C7 and C11 are amongst the next sterically least hindered hydrogens after the equatorial H on C2, however insignificant bromination was found to occur on these hydrogens, we postulate that this is because of their proximity to the electron withdrawing ester group. Natural population analysis (NPA) indicates that the H on C11 has the highest positive NPA charge, which implies its electron-deficient character. H on C7 also has a slightly higher positive NPA charge relative to H on C2. Thus, a combination of electronic and steric complementarity results in a regioselective bromination of unactivated C-H bond in (+)-sclareolide.
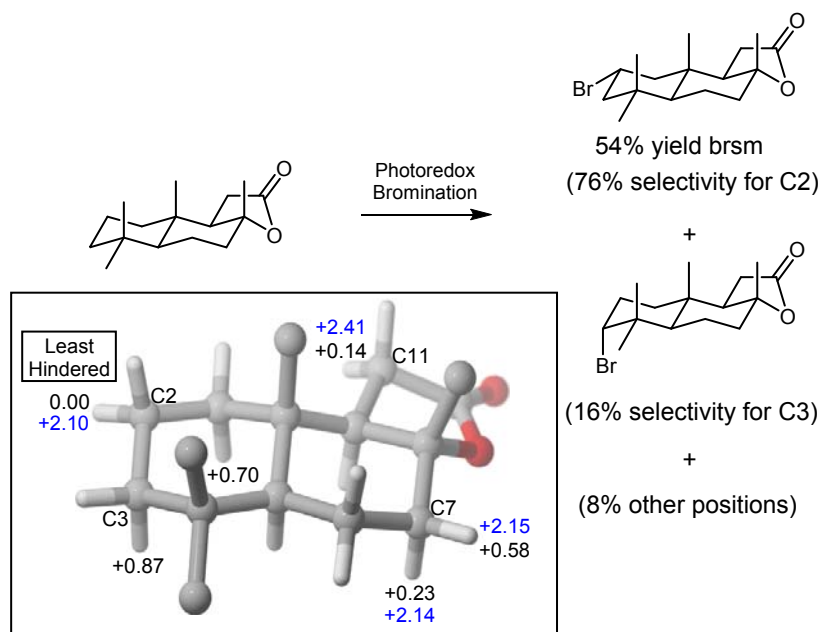
Scheme 2.3 Regioselective bromination of sclareolide. Relative pairwise-additive estimate ($\Delta E_{pw}^{(st)}$) of the steric exchange energy of H with a He probe in black. Hydrogens with $\Delta E_{pw}^{(st)} > 2$ kcal/mol are omitted. NPA charge in blue. 3D molecular image created with CYLview.[255] Yield of 2-Br sclareolide is calculated based on remaining starting material (brsm) from isolated product using column chromatography. Selectivity is estimated from crude ^{1}H NMR.

To further demonstrate the applicability of the photoredox bromination in the functionalization of biologically active molecules, we chose acetate-protected estrone **6** (**Table 2.9**). The choice is motivated by the high selectivity of the current methodology towards secondary benzylic C-H bond and the possibility of exploiting steric hindrance to override preference due to lower bond strength. Selective bromination of estrone **6**, a natural occurring human hormone, is challenging, as it possesses two 3° unactivated, one 3° benzylic C-H, two 2° benzylic C-H bond and two α-protons, all of which are potential sites for bromination. In addition, the highly labile acetate protecting group[256] poses a further challenge for the bromination of **6**.

The strongly basic 50% NaOH resulted in complete removal of acetyl group from **6** (**Table 2.9**, entry 1) to give **6c**. The Wohl-Zielger reaction gave a complex mixture, which could not be separated cleanly using column chromatographic purification. Bromination at the α-H

position to give **6b** and deprotection occurred when Br$_2$ was used (**Table 2.9**, Entry 3 and 4). Only the condition using Eosin Y as photoredox catalyst in the presence of morpholine resulted in a clean reaction giving a high yield of a single diastereoisomer **6a**, which was characterized by *X*-ray crystallographic analysis, thus demonstrating that the regioselectivity is not predominantly substrate-controlled, but is instead methodology-dependent.

Table 2.9 Methodology-controlled regioselective bromination.
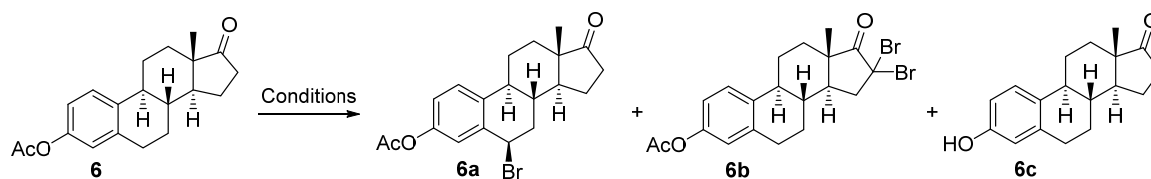
Entry	Procedure	Yield[a] of **6a** (%)	Yield[a] of **6b** (%)	Yield[a] of **6c** (%)
1	50% NaOH/CBr$_4$	Only loss of acetate was observed from crude 1H NMR		
2	Wohl-Zielger[b]	Complex mixture		
3	MnO$_2$/Br$_2$	0	21	27
4	Br$_2$/visible light[c]	0	7	16
5	Eosin Y·2Na /morpholine /CBr$_4$	76	0	0

[a] Yields are calculated based on the amount of **6** recovered by flash column chromatography. [b] NBS, 10 mol% benzoyl peroxide, CH$_3$CN 90 °C, 3 hrs. [c] Some mono α-bromo compound contaminated the recovered starting material, as seen from ^{1}H NMR.

2.2.7 Study of Mechanism

2.2.7.1 Probing H-abstracting radical *via* regioselectivity

Protocols which were suggested to rely on bromine radical (**Table 2.10**, Entries 1-3) gave a selectivity of 7-15 which differ considerably from the photoredox bromination. 7-15 refers to the selectivity of each reaction. Selectivity is defined in footnote [a] of **Table 2.10**.

Selectivity is measured by the yield of bromination at the primary C-H and secondary C-H bond of **7** through the relative yield of **7a** and **7b**.

The lower regioselectivity of the Wohl-Zielger reaction performed in $CHCl_3$ (Entry 1) relative to bromination with Br_2 with light or MnO_2 (Entry 2 and 3) is likely to be a solvent effect.[86] The protocol reported by Schreiner and co-workers, suggesting that CBr_3 radical might be the H-abstracting species also gave a different level of regioselectivity (Entry 4).[115]

Table 2.10 Probing C-H extraction species via regioselectivity in benzylic bromination.
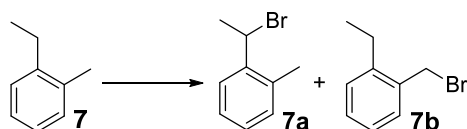
Entry	Procedure	Selectivity[a]
1	NBS/cat. (BzO)$_2$	7.3 (0.1)
2	MnO$_2$/Br$_2$	13.3 (0.6)
3	Br$_2$/visible light	15.3 (0.3)[b]

4	50% NaOH/CBr$_4$	7.0 (0.5)
5	Eosin Y /Morpholine /CBr$_4$	34.0 (1.2)

[a] Selectivity = Yield of **7a**/Yield of **7b**. [b] aromatic bromination was observed from GC-MS. [c] Average of 3 independent reactions, sample standard deviation in parentheses.

The results in **Table 2.10** suggest that the major radical species involved in the hydrogen abstraction is neither CBr$_3$ radical nor Br radical. However, at this point, we would like to highlight that a subsequent nucleophilic substitution between the benzyl bromide formed and morpholine was observed from GC-MS analysis of the crude reaction mixture (**Table 2.11**). This is likely to complicate or invalidate any deduction that is obtained from **Table 2.10** regarding selectivity.

Table 2.11 Detailed results of photoredox bromination of **7**
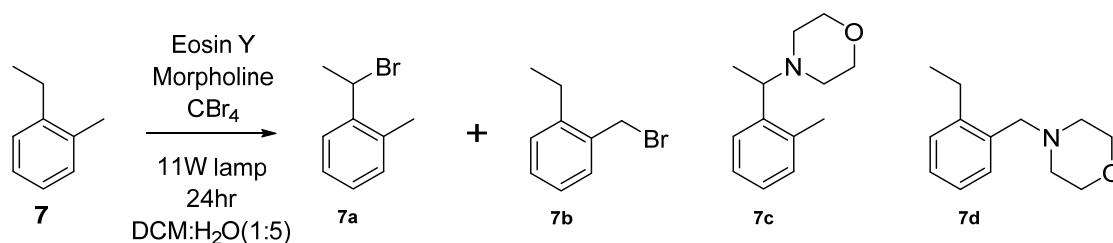
Entry	Morpholine: CBr$_4$	Yield of **7a**	Yield of **7b**	Selectivity	Area of **7c** /Area of **7d**
1	0.2:1	30.6(0.7)	7.3(0.04)	4.2(0.1)	0
2	0.5:1	41.3(0.8)	7.4(0.3)	5.6(0.3)	0
3	1:1	32.3(2.6)	3.7(0.6)	8.9(0.7)	0
4	2:1	33.8(0.6)	1.9(0.1)	17.4(0.7)	0.41
5	2.5:1	34.5(0.4)	1.0(0.04)	34.0(1.2)	0.53

6	3:1	33.1(0.2)	0.5(0.05)	73.5(7.7)	0.67
7	4:1	26.1(0.2)	0	N/A	1.1

Yields (average of 3 independent runs) are determined from GC-MS using internal standard calibration with authentic sample. Sample standard deviation in parentheses.

For steric reason, we would expect that the nucleophilic substitution on primary C-Br bond would be faster than on secondary C-Br bond. As a result, nucleophilic displacement of Br and hydrogen abstraction exhibit opposite site preference. When the ratio of morpholine: CBr$_4$ is more than 1:1, the amount of nucleophilic displacement products became significant. At the same time, the yield of **7b** decreases as it is being converted to **7d**. Thus, the selectivity which is defined as Yield of **7a**/ Yield of **7b** increases, because conversion of **7a** to **7c** is slower than **7b** to **7d**.

Therefore, the result in **Table 2.10** is unlikely to reflect the intrinsic selectivity of the hydrogen abstracting species in the photoredox bromination. The observed ratio of **7a** and **7b** is most probably the result of two tandem reactions which exhibit different rate on the same site as depicted in **Scheme 2.4**.
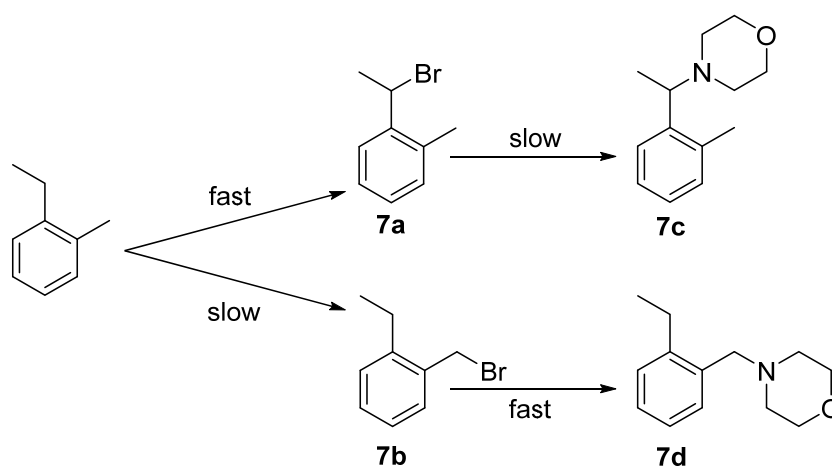
Scheme 2.4 Tandem bromination and nucleophilic displacement

2.2.7.2 Kinetic isotope effect

Experiments were performed to determine the kinetic isotope effect of the photoredox bromination. Two different methodologies were adopted to determine the kinetic isotope effect: Method 1: Independent measurement of the difference in rate between D_{12}-cyclohexane and H_{12}-cyclohexane. Method 2: Competitive bromination between D_{12}-cyclohexane and H_{12}-cyclohexane in the same reaction system.

Method 1 attempts to determine the difference in rate between D_{12} and H_{12} cyclohexane bromination during the initial state of the reaction (<500 minutes). The change in rate is assumed to be linear and systematic error is reduced with least-square linear regression. The kinetic isotope effect is determined from the gradients of the two linear equations (0.1025/0.0083). The value is 12.3±2.3 (**Figure 2.5**). This method is expected to be subjected to experimental errors as evident from the large standard deviation of 2.3 which is about 19% of the determined kinetic isotope effect of 12.3. For instance, it is difficult to weigh D_{12}-cyclohexane and H_{12}-cyclohexane accurately due to their volatile nature. In addition, it should be noted that in this method, we are measuring the rate and not rate constants thus the validity of kinetic isotope effect that is determined is questionable.
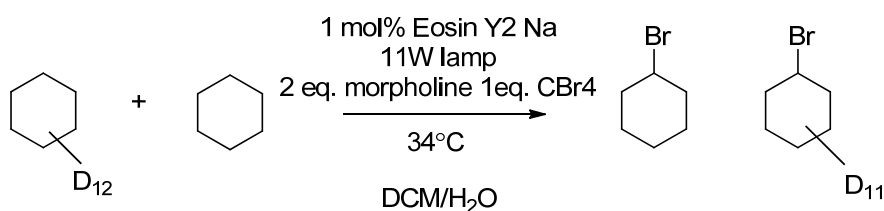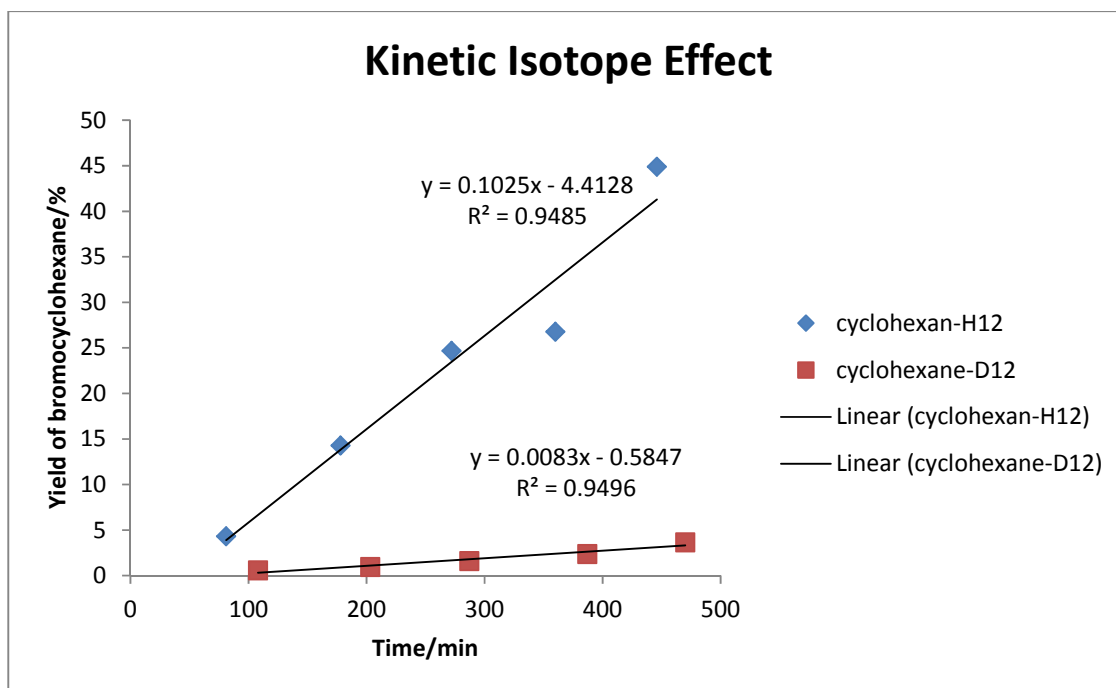
Figure 2.5 Kinetic isotope effect determined by method 1.

In method 2, equal amount of D_{12}-cyclohexane and H_{12}-cyclohexane was added to the reaction system. K_H/K_D could be determined from the y-intercept of the linear equation, as it is only at time = 0 minutes that the amount of D_{12}-cyclohexane and H_{12}-cyclohexane are equal (see justification at the end of this section). As the reaction progresses the ratio of [D_{12}-cyclohexane] to [H_{12}-cyclohexane] increases because H_{12}-cyclohexane is being consumed at a higher rate. This, in turn, will reduce the relative rate of H_{12}-cyclohexane bromination to D_{12}-cyclohexane bromination due to reduced [H_{12}-cyclohexane] to [D_{12}-cyclohexane]. The results in **Table 2.12** are consistent with the above explanation; a negative gradient was obtained from the plot of K_H/K_D *vs*. time. In general, method 2 gave more precise value for the kinetic isotope effect as evident from the much smaller standard deviation relative to method 1.
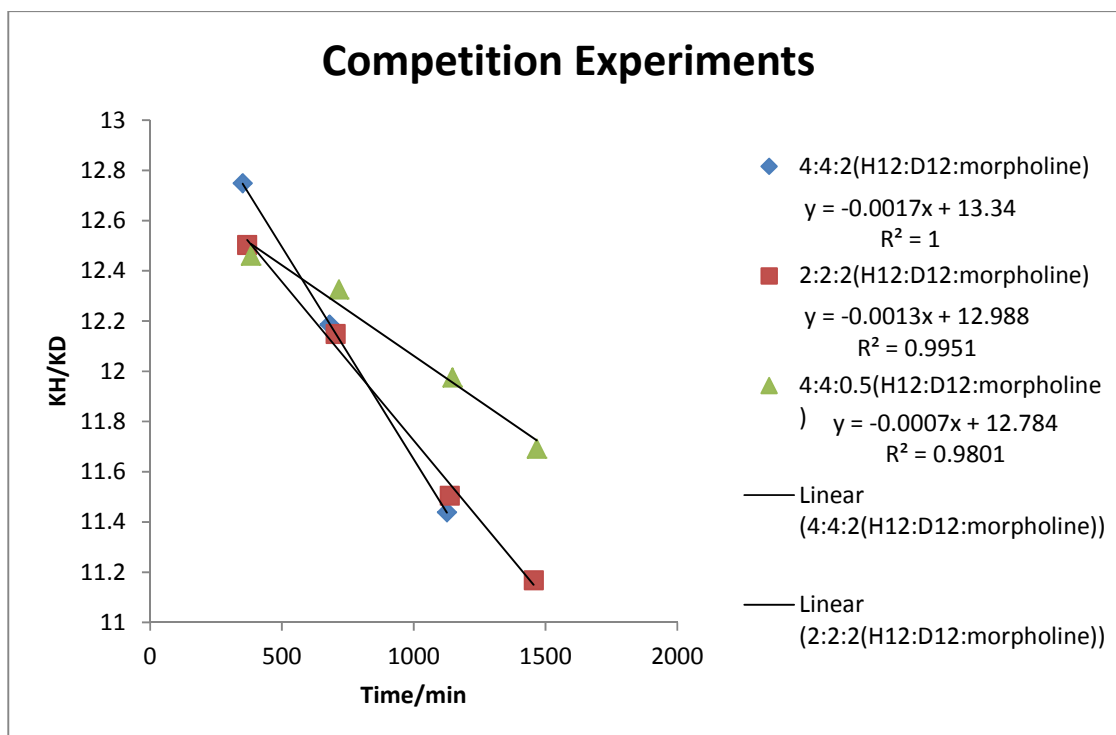
Figure 2.6 Kinetic isotope effect determined by method 2.

Table 2.12 Results of KIE measurement by methods 2

H$_{12}$-cyclohexane	D$_{12}$-cyclohexane	Morpholine	K_H/K_D(from intercept)
2	2	2	12.99(0.06)
4	4	2	13.34(0.005)
4	4	0.5	12.78(0.07)

The primary conclusion that can be drawn from this kinetic isotope effect study is that the rate determining step involves the breaking of the C-H bond. It should be noted that the kinetic isotope effect obtained is a sum of primary kinetic isotope effect and secondary kinetic isotope effect. The quasiclassical limit of primary KIE is generally in the range of 7-10,[256-258] thus if the measured primary KIE is more than 10, a plausible involvement of quantum mechanical tunneling effect in the reaction could be considered. As secondary kinetic isotope effect is

generally l.1-1.2 for a change of sp^3 to sp^2 hybridization in the TS,[259] and our measured KIE is about 13, the primary KIE should be about 12, therefore involvement of quantum mechanical tunneling in the rate determining step is suggested from our KIE study.

A justification on the validity of method 2 would be give here:

This is a general rate law for the photoredox bromination. The rate constant is given by k_H (k_D for D_{12}-cyclohexane). The order of reaction with respect to cyclohexane is m and CBr_4 is n. They are not known but this does not affect our conclusion. We assume that for D_{12}-cyclohexane the orders with respect to each reagent are the same.

$$k_H[H_{12} - cyclohexane]^m[CBr_4]^n = rate_H = \frac{d[H_{12} - bromocyclohexane]}{dt}$$

The integrated rate law is

$$k_H \int_0^t [H_{12} - cyclohexane]^m[CBr_4]^n = \int_0^t d[H_{12} - bromocyclohexane]$$

$$[H_{12} - bromocyclohexane] = \int_0^t [H_{12} - cyclohexane]^m[CBr_4]^n$$

In **Figure 2.6**, we measured [H_{12}-cyclohexane]/[D_{12}-cyclohexane] from GC-MS.

$$\frac{[H_{12} - bromocyclohexane]}{[D_{12} - bromocyclohexane]} = \frac{k_H \int_0^t [H_{12} - cyclohexane]^m[CBr_4]^n}{k_D \int_0^t [D_{12} - cyclohexane]^m[CBr_4]^n}$$

At t=0 the integrands are identical because the initial concentrations of H_{12}-cyclohexane, D_{12}-cyclohexane and CBr_4 are the same. Therefore,

$$\frac{[H_{12} - bromocyclohexane]}{[D_{12} - bromocyclohexane]} = \frac{k_H}{k_D}, at\ time = 0$$

2.2.7.3 Proposed mechanism
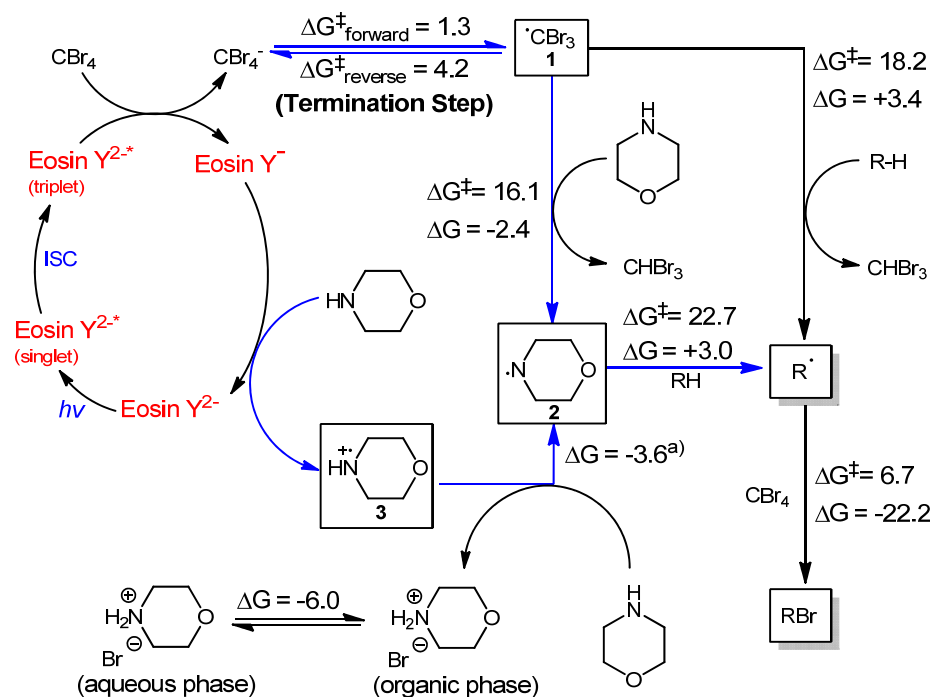
Figure 2.7 Proposed Mechanism. All $\Delta G^{\ddagger}$ and ΔG are given in kcal/mol calculated at $CPCM_{DCM}$-M06-2X/BS1. [a] Barrierless/low barrier implied

A tentative mechanism was proposed based on computational and experimental studies (**Figure 2.7**). Given the low solubility of the substrate and the presence of the photoredox catalyst in the organic phase, the reaction is assumed to predominantly occur in the organic phase. This is supported by observation. The organic phase remained strongly color after the reaction. As the red color is assumed to be due to the presence of the dye and the dye is essential for the reaction, therefore it is highly probable that the reaction occurs in the organic phase (**Figure 2.8**).

The reaction began with the absorption of light by the photoredox catalyst, followed by the reduction of CBr_4 by the excited photoredox catalyst. CBr_4 reduction results in significant lengthening of one of the C-Br bonds (**Figure 2.9**, **8a**). The dissociation of CBr_4^- in DCM has a low $\Delta G^{\ddagger}$ of 1.3 kcal/mol. The reverse reaction from CBr_3 radical and bromide to CBr_4 anion has a barrier of only 4.2 kcal/mol (**Figure 2.9**), which is much lower than $\Delta G^{\ddagger}$ for C-H or N-H

abstraction (**Figure 2.7**). This calculation could be related to an observation: Light was found to be essential throughout the reaction and removal of light at any point of time during the reaction effectively quenches the reaction. This could be explained by the fast reverse reaction from CBr_3 radical and bromide to CBr_4 anion which provides a termination step to remove excess CBr_3 radical, thus the light source is required at all time.
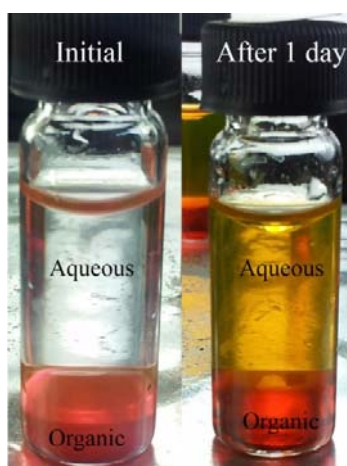
Figure 2.8 Snapshot of reaction before and after

The C-Br bond is about 1.9Å as could be seen from 8a. For the dotted line the Br is 3.4Å, which is 1.5Å longer than other C-Br distances. In addition, the sum of covalent radius of C and Br is (0.76+1.20) = 1.96Å, therefore in our opinion the bromide in **8a** should be non-covalently bonded to CBr_3.
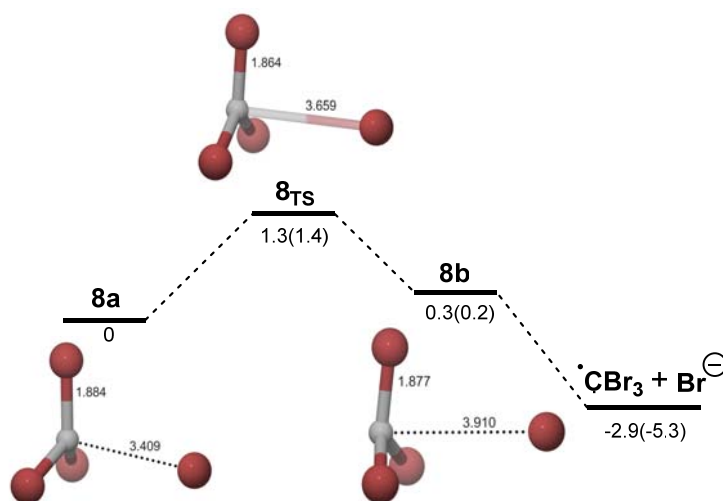
Figure 2.9 CBr$_4$ anion dissociation free energy profile. All values given are relative Gibbs free energy in kcal/mol calculated at CPCM=DCM-M06-2X/BS1. Number in brackets are CPCM$_{DCM}$-CCSD(T)/6-311++G(3df,3pd)//CPCM$_{DCM}$-M06-2X/BS1 Frequency analysis at 298.15K and 1 atm. 3D molecular image created with CYLview.

2.2.7.4 Radical Relay to morpholine *N*-radical
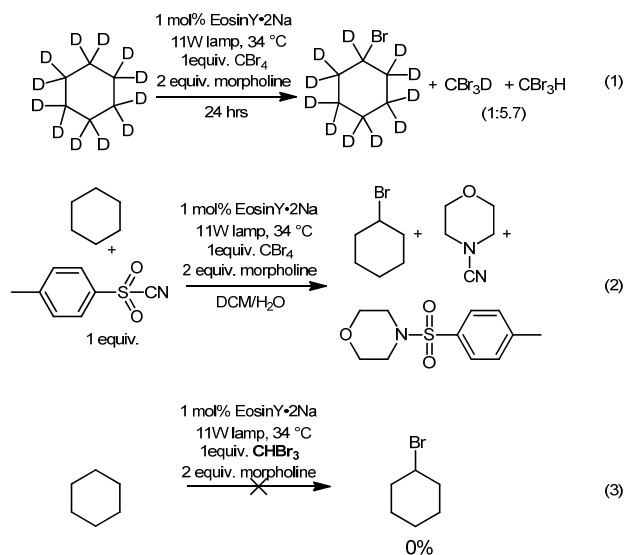
Figure 2.10 Preliminary Study of the Mechanism.

Experiment in which H$_{12}$-cyclohexane was replaced with D$_{12}$-cyclohexane suggested that CBr$_3$ radical might not be the main hydrogen-abstracting species (**Figure 2.10**, Eqn. 1). When

D_{12}-cyclohexane was used, it was found that $CDBr_3$ constituted only about 15% of the bromoform formed. DFT calculations demonstrated that for CBr_3 radical, the $\Delta G^{\ddagger}$ for abstracting hydrogen from cyclohexane is higher than morpholine (**Figure 2.7**). In addition, the abstraction of H from morpholine by CBr_3 radical is exergonic as opposed to the endergonic abstraction of H from cyclohexane by CBr_3 radical (**Figure 2.7**). This led us to propose that hydrogen abstraction from morpholine generate a neutral *N*-radical and this is the main role of the CBr_3 radical. This is a radical relay, which generates a longer live radical (morpholine radical) from one that is transient (CBr_3 radical) *via* a thermodynamically favorable reaction. Additional evidence for the existence of such *N*-radical was obtained from a radical trapping experiment with 4-methylbenzenesulfonyl cyanide (**Figure 2.10**, Eqn. 2).[261] Bromoform formed from CBr_4 constitutes a dead end to the reaction and does not contribute productively to the formation of brominated product (**Figure 2.10**, Eqn. 3); this justifies our calculation of yield base on initial amount of CBr_4 when substrate is present in excess.

2.2.7.5 Role of water

Water is essential for this reaction. We postulated that the role of the water phase is to remove excess bromides, which is required for the termination step (**Figure 2.7** and **Figure 2.9**), via protonated morpholine. The relatively more exergonic solvation of protonated-morpholine bromide complex by water *vs*. DCM ensures that the amount of bromide in the organic phase is low at all times, thus making the formation of the brominated product competitive to the termination step (**Figure 2.7**: $\Delta G^{\ddagger}_{reverse}$ *vs*. $\Delta G^{\ddagger}$ for H-abstraction). Electrospray Ionization mass spectroscopy measurement of the aqueous phase revealed a species related to the proposed morpholine bromide complex (**Figure 2.11**).
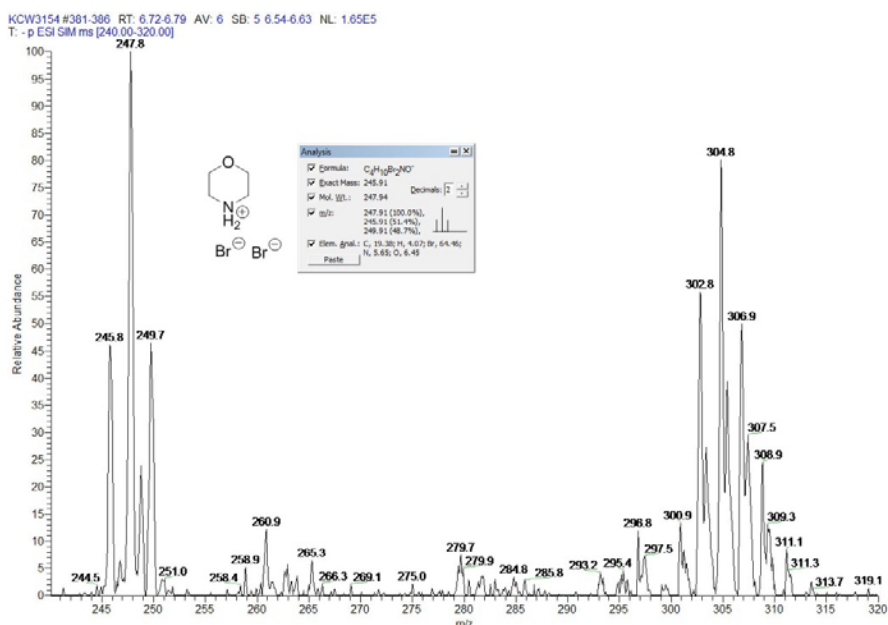
Figure 2.11 Electrospray Ionization Spectrum for aqueous phase after reaction

The dissociation of CBr_4^- in DCM has a low $\Delta G^\ddagger$ of 1.3 kcal/mol and leads to **8b** (a complex in which CBr_3 and Br are loosely associated). The reverse reaction from **8b** to **8a** has only a barrier of 1.0 kcal/mol (or 4.2 kcal/mol from $CBr_3 + Br^-$) (**Figure 2.9**). This reverse reaction results in the formation of **8a** which can undergo unproductive reduction of the oxidized photocatalyst. The fast reverse reaction from **8b** to **8a** provides a termination step to remove excess CBr_3 radical, thus we proposed that if the light source is removed at any point of time, this termination step would remove all the CBr_3 radical and effectively quenches the photoredox bromination. Consistent with this termination mechanism, when 1 equivalent of KI was added to the reaction, significant formation of iodocyclohexane and $CHBr_2I$ was observed from GC-MS (**Scheme 2.5**). One plausible mechanism to account for this is given in **Scheme 2.5**, the highly nucleophilic iodide attacks CBr_3 radical, which eventually leads to CBr_3I.

a

1 mol% EosinY•2Na
10 mol% NEt$_4$Br
11W lamp, 34°C
1eq. CBr$_4$
2 eq. Morpholine
24hours

KI + (cyclohexane) → (bromocyclohexane) Br 8% + (iodocyclohexane) I 28% + CHBr$_3$/CHBr$_2$I

(1 eq)

b

CBr$_4^{\ominus}$ ⇌ (±Br$^{\ominus}$) $^\bullet$CBr$_3$ ⇌ (±I$^{\ominus}$) CBr$_3$I$^{\ominus}$ → (Eosin Y$^-$ → Eosin Y^{2-}) CBr$_3$I → (R$^\bullet$, -CHBr$_3$) RI

CBr$_3$I$^{\ominus}$ ⇌ (±Br$^{\ominus}$) $^\bullet$CBr$_2$I ⇌ (±I$^{\ominus}$) CBr$_2$I$_2^{\ominus}$ → (Eosin Y$^-$ → Eosin Y^{2-}) CBr$_2$I$_2$ → (R$^\bullet$, -CHBr$_2$I)

c

(bromocyclohexane) Br

1 mol% EosinY2Na
CBr$_4$, morpholine
1 eq. TBAI
DCM/H$_2$O
11W lamp, 34°C
24 hours

→ (iodocyclohexane) I 0%

(bromocyclohexane) Br

1 eq. TBAI
DCM/H$_2$O
11W lamp, 34°C
24 hours

→ (iodocyclohexane) I 0%

Scheme 2.5 Experimental evidences of proposed mechanism (a) Experiment to demonstrate the attack of bromide/iodide on CBr$_3$ radical, iodocyclohexane and CHBr$_2$I were observed from GC-MS (b) Mechanism to account for the formation of iodocychexane (c) control experiment to demonstrate that nucleophilic displacement of Br in bromocyclohexane by iodide does not occur.

2.2.7.6 Further discussion on proposed mechanism

The first inadequacy of our current proposed mechanism is that it is not clear why structurally similar cyclic amines exhibit such diverse reactivity (**Table 2.1**). It is evident that morpholine plays a pivotal role in the photoredox bromination, as the use of known aliphatic amines (DIPEA and TEA), and (piperidine and piperazine) resulted in low yields of brominated products. DFT calculations suggested that the origin of this does not lie in the C-H activation step as *N*-radicals of piperidine and morpholine have similar $\Delta G^{\ddagger}$ and $\Delta H^{\ddagger}$ for C-H activation (Table 2.13).

Table 2.13: Activation energies and thermodynamics for abstraction of H from cyclohexane

R$^\bullet$ + (cyclohexane) → (cyclohexyl radical) + RH
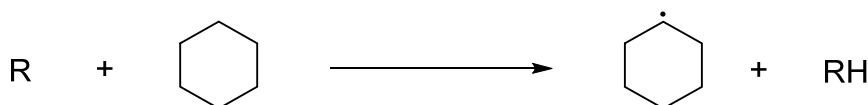
H abstracting species(**R**)	$\Delta G^{\ddagger}(\Delta H^{\ddagger})$ / kcal mol^{-1}	$\Delta G(\Delta H)$ / kcal mol^{-1}	Yield (Standard Deviation)/%
piperidine N-radical	+24.0(+13.3)	+3.3(+3.6)	12.8(0.4)
morpholine N-radical	+23.6(+13.2)	+3.4(+3.6)	57.3(3.6)
thiomorpholine N-radical	+22.4(+12.1)	+1.8(+2.1)	4.1(0.04)

Level of theory: SMD(DCM)-M06-2X/6-311+G(d,p). Default convergence criteria and integration grid
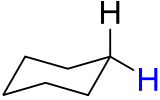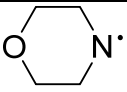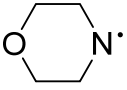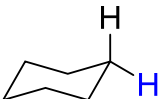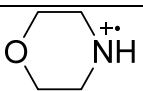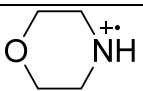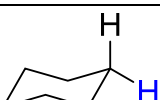
The second inadequacy of the mechanism which is based on neutral morpholine *N*-radical as hydrogen abstractor is the inability to account for the lack of dichloromethane bromination. C-H bonds of DCM possess lower bond dissociation energy (BDE) relative to that of cyclohexane (BDE of DCM = 400.6kJ/mol[262] *vs.* BDE of cyclohexane = 416.3kJ/mol[262]), and despite being present in excess, abstraction of H from DCM is not competitive with abstraction of H from cyclohexane. The calculated $\Delta G^{\ddagger}$ for H-abstraction suggests that DCM abstraction is more favorable than cyclohexane abstraction (**Table 2.4**), which does not agree with experimental observation. One plausible explanation to reconcile the disagreement between theory and experiment is the difference in tunneling correction to the rate constant between DCM abstraction and cyclohexane abstraction.

For the photoredox bromination, we observed a large kinetic isotope effect of 13, which could suggest the involvement of H-tunneling. Estimation of tunneling contribution indicates a larger correction for cyclohexane abstraction than DCM abstraction (28 for cyclohexane *vs.* 16 for DCM). However, even with the inclusion of tunneling correction the rate constant for the abstraction of H from DCM is still slightly higher than that of abstraction of H from cyclohexane

(k_{DCM}=9.5×10^{-23} *vs.* $k_{cyclohexane}$ =2.4×10^{-23}). As the rate constant has an exponential relationship with $\Delta G^{\ddagger}$, an error of 1 kcal/mol between k_{DCM} and $k_{cyclohexane}$ will result in an overestimate of their relative rate constants by 5 times (i.e. . k_{DCM} = 5$k_{cyclohexane}$ or vice versa). Therefore, it is possible the disagreement between calculated rate constants and experimental observation resides in the inability to predict the rate constants accurately.

As evidence to preclude CBr_3 radical as the dominant hydrogen abstracting species is presented in **Figure 2.10**, an alternative explanation for the disagreement between calculated results and experimental observation could be that the dominant species for abstraction of hydrogen is a cationic *N*-radical instead of the neutral *N*-radical proposed in **Figure 2.7**. From **Table 2.14**, the selectivity of cationic *N*-radical of morpholine for the hydrogen of cyclohexane over that of DCM is overwhelming. This agrees qualitatively with the experimental results that DCM is brominated only to a very small extent when compared to cyclohexane.

Table 2.14 Calculated kinetic parameters for abstraction H from DCM and cyclohexane.

$$R \quad + \quad CH_2Cl_2 \quad \longrightarrow \quad {}^{\bullet}CHCl_2 \quad + \quad RH$$

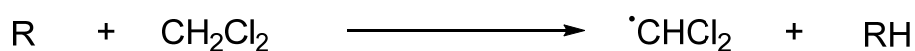| H abstracting species	Substrate	$\Delta G^{\ddagger}(\Delta H^{\ddagger})$ / kcal mol^{-1}	Rate constant at 300K	Tunneling corrected rate constant[a]	Tunneling correction factor[a]
$^{\bullet}CBr_3$	HCHCl$_2$	21.2(11.1)	3.1×10^{-23}	5.4×10^{-22}	17.4
$^{\bullet}CBr_3$	H / H (cyclohexane)	18.6(7.6)	3.3×10^{-21}	2.5×10^{-20}	7.4
O N$^{\bullet}$ (morpholine radical)	HCHCl$_2$	22.4(11.6)	5.4×10^{-24}	9.5×10^{-23}	17.5
O N$^{\bullet}$ (morpholine radical)	H / H (cyclohexane)	23.6(13.0)	7.5×10^{-25}	2.4×10^{-23}	32.2
O NH$^{+\bullet}$	HCHCl$_2$	24.7(13.0)	1.4×10^{-25}	9.1×10^{-24}	64.3
O NH$^{+\bullet}$	H / H (cyclohexane)	16.0(5.3)	2.5×10^{-19}	3.8×10^{-19}	1.5

Level of theory: SMD(DCM)-M06-2X/6-311+G(d,p). Tight convergence criteria and ultrafine integration grid [a] calculated with by using an asymmetric Eckart potential[263] with Gaussian Post Processor[264].

From **Table 2.1**, the use of structural cyclic amines such as piperidine (Entry 4), 4-methylmorpholine (Entry 6) and thio-morpholine (Entry 7) and morpholine (Entry 8) gave vastly different yield for the desired product. A plausible explanation is the consumption of CBr$_4$ probably *via* polymerization, which is observed by Schreiner and co-workers.[113]

Tertiary amines such as NEt_3 and iPr$_2$NEt could not prevent polymerization which consumed CBr_4. This result in precipitation and/or a very dark brown organic phase after one day (**Figure 2.12**) the same is observed from piperidine (**Table 2.1**, Entry 4). It is known that amine such as NEt_3 and piperidine could promote polymerization of certain compounds.[265] For 4-methylmorpholine, significant precipitation could be observed after 24 hours of reaction.
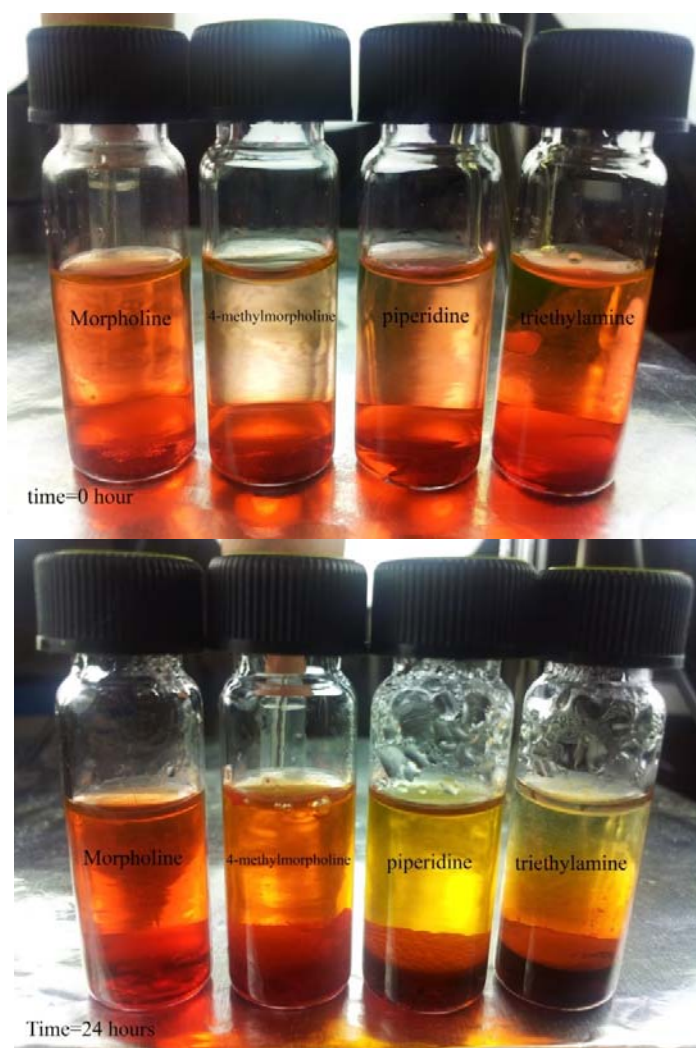
Figure 2.12 Photos of reaction with different amines at time=0 and time =24 hours.

From the GC-MS chromatograms, there is considerable consumption of CBr_4 in the case of NEt_3 and piperidine but the amount of bromocyclohexane formed is relatively lesser than 4-methylmorpholine.

In the case of morpholine and 4-methylmorpholine the organic phase remained bright red after 1 day, although considerable amount of precipitate could be observed in the case of 4-methylmorpholine. Nevertheless, the consumption of CBr_4 in the case of 4-methylmorpholine is relatively lower than NEt_3 and piperidine.

Both H abstraction and Br abstraction are essential to the formation of bromoalkanes. Due to the labile nature of CBr_4, fast CBr_4 consumption (possibly *via* polymerization) in the case of piperidine results in a lower yield relative to 4-methylmorpholine. While it is not possible for tertiary amine to form the *N*-radical as shown in our proposed mechanism, generation of other H abstracting species such as cationic *N*-radical (**Scheme 2.1**) and CBr_3 radical could explain the formation of product in the case of tertiary amine.

2.4 Conclusion

In summary, we have extended the synthetic application of visible light photoredox catalysis to bromination of sp^3 C-H bond (aliphatic and benzylic). A novel, mild and regioselective photoredox bromination procedure is reported in this work. Reaction can be conveniently performed without the need to exclude water and dioxygen, inexpensive Eosin Y disodium salt could be used with low catalyst loading of 1 mol%, easy-to-handle CBr_4 serve as Br source and low-power household lamp could be used. A mechanism based on visible light photoredox catalysis and radical relay to produce neutral *N*-radical of morpholine as hydrogen abstractor is proposed based on experimental and computational study. Synthetic applications of the photoredox bromination *via* innate C-H functionalization were demonstrated through the regioselective bromination of (+)-sclareolide and acetate-protected estrone.

Chapter 3

Selective sp^3 C-H bond fluorination *via* organo-

photocatalysis

3 Selective sp³ C-H bond fluorination *via* organo-photocatalysis

3.1 Introduction

Fluorinated compounds are of paramount importance in medicinal chemistry.[1-5] Access to diverse fluorinated building blocks has the potential to broaden our existing library of fluorinated drugs. Significant progress has been made in the introduction of fluorine to arenes[266-273] and asymmetric fluorination *via* electrophilic and nucleophilic fluorine source.[267, 274, 275] Recently, radical-based approach to introduce fluorine into sp³ carbon centers has received increased attention.[276] C-F bond formation through the generation of *C*-radical *via* functionalized substrates was demonstrated by Li[277] and Sammis.[272] These studies utilized Selectfluor® and *N*-fluorobenzenesulfonimde (NFSI) as radical fluorine source, respectively.

Two strategies for selective functionalization of unactivated C-H bonds have been coined by Baran and co-workers: Innate and guided[66, 73, 278] C-H activation.[50] Pertinent to innate C-H functionalization, the literature of radical chemistry indicates that selective abstraction of unactivated C-H bond could be achieved *via* the use of electrophilic/nucleophilic radicals.[81, 82] In particular, the use of cationic *N*-radicals as electrophilic radicals to selectively chlorinate/brominate electron rich C-H bond has been well documented in literature.[83] However, to the best of our knowledge, analogous fluorination reaction which exploits the selectivity of cationic *N*-radical to achieve selective fluorination *via* C-H functionalization has not been developed.

The stable and commercially available Selectfluor® is a well-established electrophilic fluorine source[279, 280] and is amenable to structural modification.[281, 282] It possesses a di-cationic core and could act as an oxidant *via* single electron transfer. This is evident from its oxidizing potential[267, 280] and calculated ΔG of reduction (**Scheme 3.1**). From cyclic voltammetry studies, the reduction of Selectfluor® dication is essentially an irreversible process.[283] Although the

dissociation of reduced Selectfluor® dication is thermodynamically unfavorable (+7.6 kcal/mol), additional stabilization such as electrostatic interaction of the fluoride with cationic species could render the dissociation favorable.
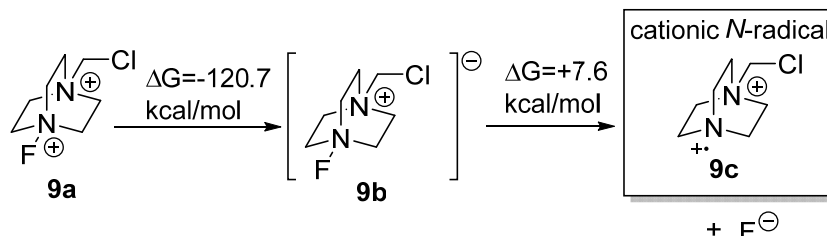
Scheme 3.1 Working Hypothesis: Thermodynamics of dissociative single-electron reduction of Selectfluor®

3.2 Results and Discussion

3.2.1 Survey of reaction condition

We found that site selective fluorination of secondary C-H bond most distal to electron withdrawing group (EWG) can be achieved with Selectfluor® and catalytic amount of anthraquinone (AQN). Benzoyl ester **10** was chosen as the model substrate to study the effects of various factors on the fluorination reaction. Control experiments (**Table 3.1**, Entry 1 and 2) established that both AQN and light are essential to the reaction. Triplet dioxygen, which is able to quench the triplet state of AQN *via* energy transfer, was found to be detrimental to the reaction (Entry 3). Commercially available photoredox catalyst such as Rose Bengal and Ru(bpy)$_3$Cl$_2$ are inept when they are tested as replacement for AQN (**Table 3.1**, Entry 4-6). The reaction was found to be rather insensitive to substrate and Selectfluor® ratio (**Table 3.1**, Entry 4 and 7-8). As fluorescence bulbs emit near ultraviolet (UVA: 315nm-400nm), we performed an experiment with an LED bulb, which does not emit light in the ultraviolet region. This provides evidence that this reaction can be driven by absorption of visible light. Preparative experiment (**Table 3.1**, Entry 10) demonstrates the scalability of the photo-fluorination.

Table 3.1 Survey of reaction conditions

Entry	PC[a]	Light source	Substrate:	Yield	Yield Brsm[b]	rsm
1	AQN	No Light	1.5:1	0	0	85
2	-	OSRAM 11W fluorescence	1.5:1	0	0	88
3	AQN(1 atm of O_2)		1.5:1	0	0	83
4	AQN		1.5:1	65	71	9
5	Ru(bpy)$_3$Cl$_2$		1.5:1	0	0	77
6	Rose Bengal		1.5:1	0	0	-
7	AQN		1:1	56	73	23
8	AQN		1:1.5	61	73	16
9[d]	AQN	Philip 10W LED	1.5:1	54	70	23
10[e]	AQN	OSRAM 11W fluorescence	1.5:1	54	62	14

Entries 1-9: 0.1 mmol scale. [a] PC = photocatalyst, [b] Yield based on remaining starting material (GC-MS yield based on internal standard calibration – biphenyl - for entry 1-9), [c] Remaining starting material (rsm), [d] 10W Philips LED was used, [e] 2.0 mmol scale, isolated yield.

3.2.1.1 Definition and Calculation of yield and yield brsm.

The products are isolated by column chromatography. This has been discussed in Section 2.3, but we would elaborate more in this section. Further details and definition of yield based on remaining starting material would be discussed below.

$$yield = \frac{amount\ of\ product\ formed}{maximum\ amount\ of\ product\ that\ can\ be\ formed}$$

This is a working definition of yield used in our work. The amount of product formed is unambiguous, although it could be determined *via* several means such as GC yield, HPLC yield, NMR yield. For GC, HPLC and NMR yield, the product is not isolated instead a calibration curve is usually employed to relate the amount of product to the responses (area or height of peaks) that were obtained using these methods. This type of yield is useful for optimization and screening of condition, but from a synthetic perspective only isolated yields are usefully. For isolated yield, the amount of product formed is determined by purification process which allows the separation of product from other components in the reaction mixture. The purified product is then weighted on a balance and the amount formed in g or mg is determined and can be converted to mole.

The "maximum amount of product that can be formed" can be obtained may not be uniquely defined and to the best of our knowledge there is no standardization in its definition. However, we note that in most reported reaction; the authors would use the limiting reagent that is added to the reaction for "the maximum amount of product that can be formed".

For yield based on remaining starting material (brsm), the "the maximum amount of product that can be formed" is determined from the amount of hydrocarbon substrate (which C-H bond would be replace with a C-F bond) that is consumed. In most of the examples, the hydrocarbon is used in excess (*e.g.* 1.5 equiv. w.r.t Selectfluor) and in most cases the amount of hydrocarbon consumed is less than the amount of Selectfluor added to the reaction despite the fact the hydrocarbon is present in excess. This is because Selectfluor undergoes an unproductive decomposition pathway (this was verified by control experiments without the substrate from ^{1}H NMR).

For yield, the "the maximum amount of product that can be formed" is determined from the amount of Selectfluor added.

The fact that the amount of hydrocarbon consumed is less than the amount of Selectfluor added implies that yield brsm would be higher than yield. They would be equal if the amount of hydrocarbon consumed is equal to the amount of Selectfluor added.

An example would be provided:
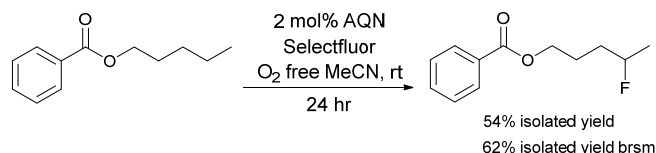
Scheme 3.2 An example to demonstrate calculation of yield and yield brsm.

In this reaction (**Scheme 3.2**) the amount of hydrocarbon added was 3.01mmol or 580mg and the amount of Selectfluor added was 718mg or 2.03mmol. The amount of pentyl benzoate recovered by column chromatography is 244.2mg and the amount of total 4-fluoropentyl benzoate obtained was 228.8mg or 1.09mmol.

The amount of starting material consumed is (580-244.2)335.8mg or 1.75mmol.

The isolated yield (based on limiting reagent) = 1.09/2.03(amount of Selectfluor added) X100 = 54%.

The isolated yield brsm = 1.09/1.75 (the amount of hydrocarbon consumed) = 62%.

The isolated yield brsm is lower than 100% is partly due to the formation of isomeric side products. The total amount of isomeric fluorinated product is about 85% of the hydrocarbon consumed (**Scheme 3.3**).
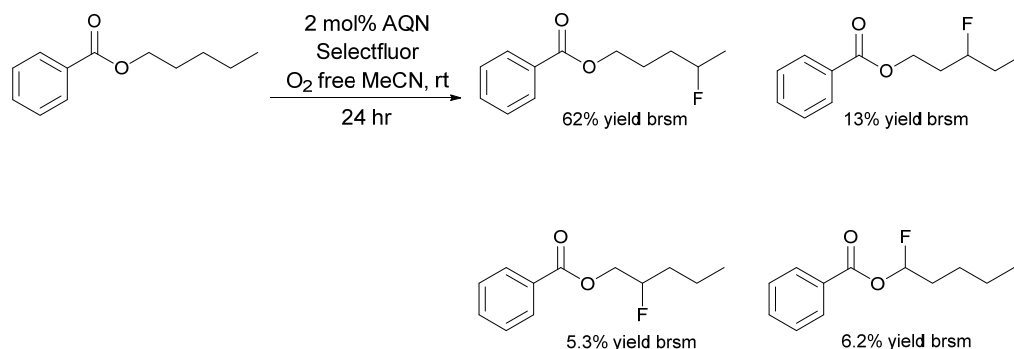
Scheme 3.3 yield brsm of various isomeric products

3.2.1.2 Other fluorine source

We have screened through a series of other commercially available fluorine sources such as NFSI, *N*-fluoropyridinium salts and DAST. This reaction only works with Selectfluor and related compounds. This is consistent with our hypothesis on the role of Selectfluor is more than a fluorine source (we proposed that its cationic component is the hydrogen abstractor).

3.2.2 Scopes of reaction and functional group tolerance

A diverse variety of functional groups ranging from esters, amides, ketone, carbonate, sulfonate, bromo, tertiary alcohol, carboxylic acid and nitrile can be tolerated with the photo-fluorination (**Figure 3.1**). For all the aliphatic linear substrates, the secondary C-H bond most distal to the EWG was fluorinated with the highest selectivity. Benzoyl esters of aliphatic alcohols are fluorinated at the secondary C-H bond most distal to the OBz group (**Figure 3.1**, **11-14**). For **14**, the tertiary C-H bond is disfavored due to its proximity to the OBz group; hence selective fluorination of secondary C-H over the thermodynamically weaker tertiary C-H bond could be achieved. Sulfonate compound **15** gave similar result to Bz protected compounds.

Currently, few methods allow the direct β-functionalization of carbonyl compounds.[284-289] The direct β-fluorination of carbonyl groups such as ester, carboxylic acid, ketone and amide is unknown and can be achieved with this methodology. Methyl ester of adipic acid **16**, adipic acid

17 and 1-phenylbutan-1-one **18** were fluorinated at the β-position and were obtained in good yield. For **18**, slight dehydrofluorination occurred during flash chromatography, leading to lower than expected yields. Primary, secondary and tertiary amides functional groups are tolerated, although their yields are generally lower. Butyramide could be fluorinated at the β-position on 5.0 mmol scale; recrystallization yielded 3-fluorobutanamide **19** of high purity. Free amine groups are not tolerated by the photo-fluorination; however, fluorination became viable when the amine is protected with the trifluoroacetyl group. Selectivity of protected amines is similar to that of protected alcohols. Secondary amide of 1-pentylamine was fluorinated at the C-H most distal leading to the amide group. Similar result was observed for tertiary amide of dibutylamine **21**. Aldehyde functional group is not tolerated; an acid fluoride was formed instead through the fluorination of aldehydes' C-H bond.

Alkyl bromides are generally less reactive. The electron withdrawing effect exerted by bromo group is weaker and thus also resulted in lower selectivity. For example, when 1,8-dibromooctane was used mixture of 4- and 3-fluorinated compounds were obtained in a ratio of 3.4:1(**22a: 22b**) respectively. Nitriles exhibit similar reactivity and selectivity as the alkyl bromides. Decanedinitrile could be fluorinated to give 5-fluoronitrile **23a** and 4-fluoronitrile **23b** in a ratio of 4.1:1.

The adamantane core is present in several biologically active molecules such as amantadine and rimantadine (antiviral drugs) and saxagliptin (Type II diabetes therapeutic). Fluorinated methyl ketone adamantane **24**, -*N*Boc protected adamantane **25** and tertiary alcohol adamantane **26** are obtained through fluorination at the tertiary position on the adamantyl group. Due to the high reactivity of the tertiary C-H bond on the adamantane core,[290] some difluorination was observed. It was largely prevented when the substrate is used in excess (1.5 equiv.) relative to Selectfluor®.

11 39% (49%)   **12** 54% (62%)   **13** 47% (54%)   **14** 51% (62%)[a]

15 60% (60%)   **16** 53% (69%)   **17** 55% (55%)[b]   **18** 68% (83%)

19 47% (47%)[c]   **20** 40% (46%)   **21** 37% (41%)[a,e,f]   **24** 60% (65%)

22a

22b
44% (62%)
(**16a:16b** = 3.4:1)

23a

23b
41% (60%)[d]
(**17a:17b** = 4.1:1)

25 R=NHBoc 44% (54%)

26 R=OH 68% (68%)
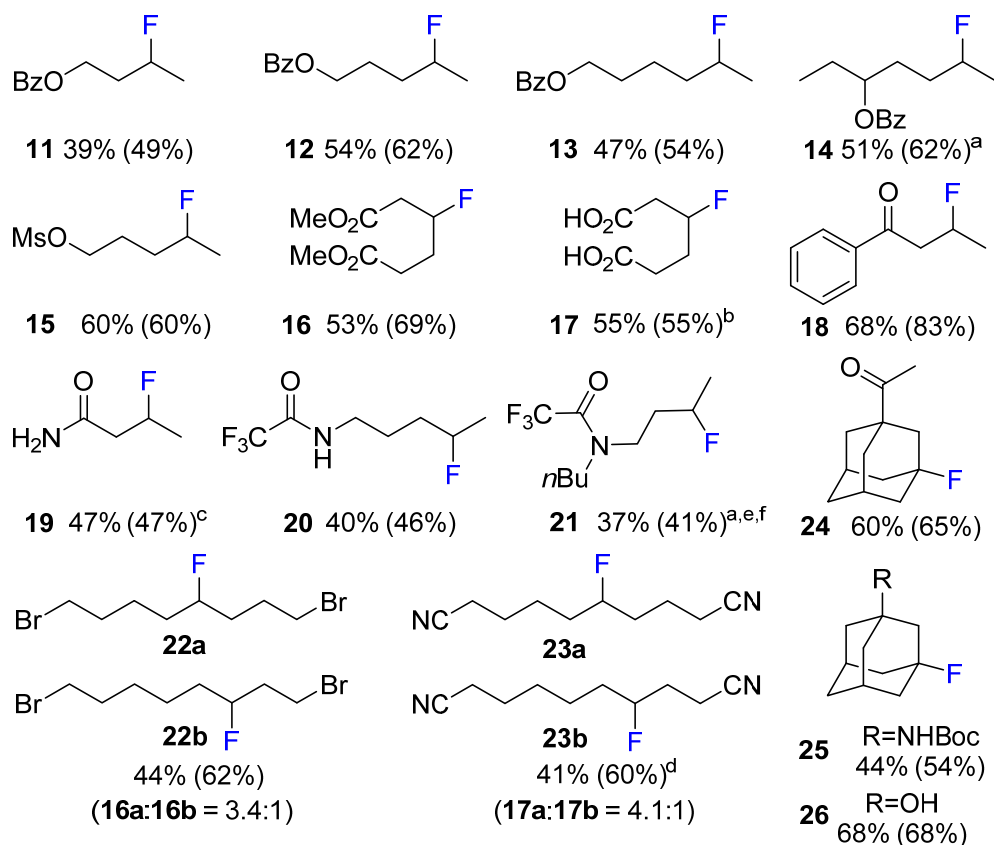
Figure 3.1 Scope of the photo-fluorination reaction; Protocol: 2 mol% of AQN, Substrate: Selectfluor = 1.5:1 (2 mmol), 8 mL of anhydrous and O_2 free MeCN, under Ar and irradiation from an 11W fluorescent bulb, unless otherwise stated; Isolated yield brsm (rsm). [a] Inseparable diastereomers/isomers. [b] Converted to ester to facilitate separation. [c] 5 mmol of substrate [d] 1.5 equiv. of Selectfluor. [e] 2 equiv. of substrate [f] 2-Cl-AQN (2-chloroanthracene-9,10-dione) was used as photocatalyst, R_f of AQN and product is the same on TLC.

It should be noted that we have not attempted the fluorination of aliphatic alkane as selectivity is expected to be low due to similar electronic properties of secondary C-H bonds in aliphatic alkane.

Pertinent to cyclic alkane, adamantane could be fluorinated under our condition; the yield is about 50-60%. We believe that cyclohexane and related homologs could be fluorinated under our condition, this is based on our experience from the bromination study (Chapter 2). Cyclic alkanes that is symmetrical (cyclohexane, cycloheptane, cyclooctane, *etc.*) are more reactive than aliphatic type. Therefore if aliphatic hydrocarbons such as those discussed in section 3.2.1, 3.2.2

and 3.2.3 could be fluorinated, there is a high chance that symmetrical cyclic alkanes could be fluorinated as well.

In this work, we tried to avoid hydrocarbons that do not have pre-existing functional group. The reason being that C-F bonds are highly stable (one of the reasons why fluorinated compounds are useful in drugs) and effective methods to convert C-F to other functional groups are scarce, therefore fluorinated *n*-hexane, cyclohexane and related homologs are not potential usefully for the synthesis of more complex compounds.

Relevant to aliphatic alkane, we believe that it could be fluorinate but with lower selectivity relative to those which possess an electron-withdrawing group to, because the electron density is very similar for the secondary C-H bonds of *n*-hexane and its homologs.

3.2.3 Applications

Fluorinated compounds are of exceptional value in medicinal chemistry; introduction of fluorine has the potential to confer favorable properties to biologically active molecules (**Scheme 3.4)**. This forms the impetus to apply the newly developed photo-fluorination to selected examples of useful biologically active compounds. (+)-Sclareolide **27**, a terpenoid from plant with antifungal and cytotoxic properties,[291] was subjected to the photo-fluorination condition. Amongst its 26 sets of C-H bonds, C2 and C3 was selectively fluorinated to give combined high yield of 81% and a selectivity of 10:3 (**27a**: **27b**, **Scheme 3.4**, Eqn. 1). *N*Boc-derivative of Rimantadine **28**, an anti-viral drug,[292] was fluorinated at the tertiary position on the adamantyl group (**Scheme 3.4**, Eqn. 2). The fluorination did not occur at the electron deficient tertiary C-H adjacent to the NHBoc group, which is consistent with the involvement of cationic *N*-radical. Derivative of *L*-Leucine **29** was fluorinated selectively at the tertiary C-H bond furthest from its electron-withdrawing groups (**Scheme 3.4**, Eqn. 3). Analogous hydroxylation has been achieved by White and co-worker with a Fe catalyst.[89] Hydroxyl carboxylic acids (AHAs) are widely used

in the cosmetic industrial to treat dermatological disorders.[293] Ester derivative of 2-hydroxyhexanoic acid **30**, an alpha hydroxyl carboxylic acid, could be fluorinated predictably at the secondary C-H bond most distal from its electron-withdrawing groups (**Scheme 3.4**, Eqn. 4).
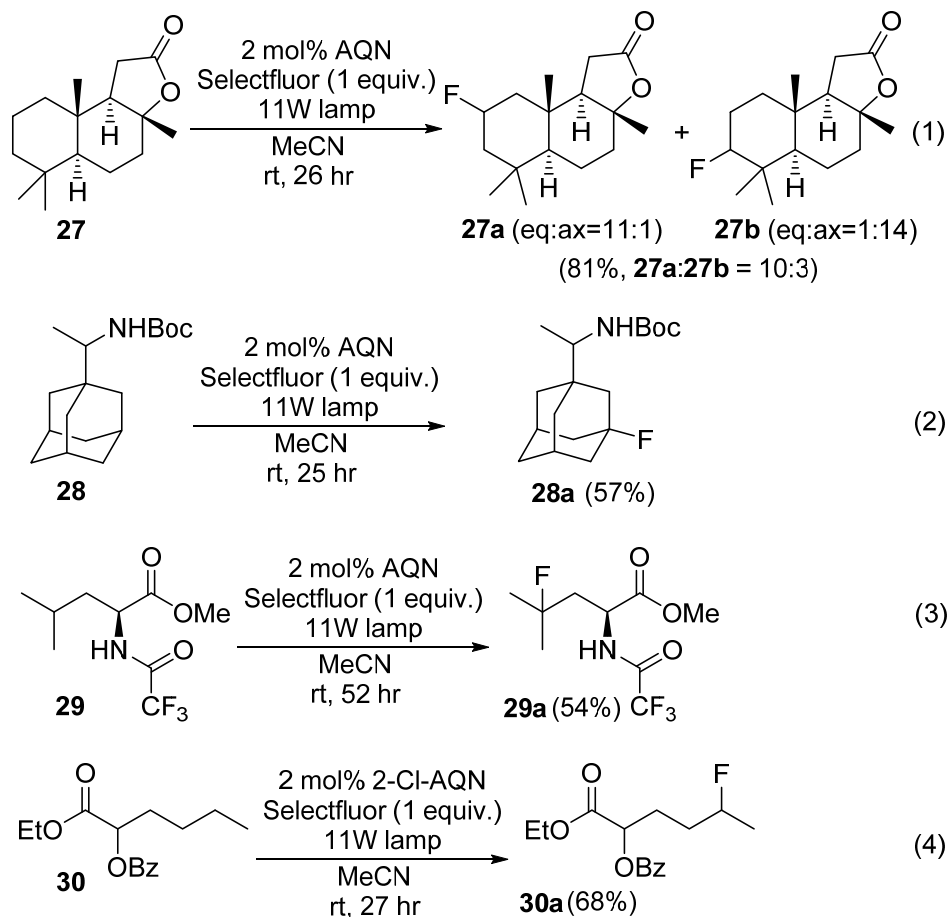
Scheme 3.4 Application of photoredox fluorination

The scalability of the photo-fluorination was tested by fluorinating butyramide on a 25 mmol scale (**Scheme 3.5**). One gram of 3-fluorobutanamide **19** was obtained. Relative to the 5 mmol scale, no significant decrease in product yield was observed. Purification of crude **19** was achieved by direct recrystallization from isopropyl alcohol and *n*-hexane.
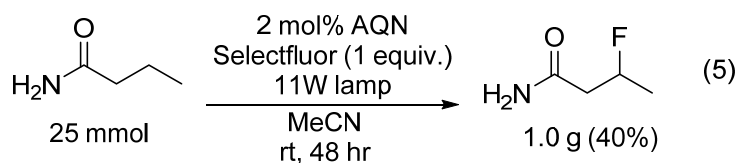
Scheme 3.5 Gram scale synthesis of fluorinated butyramide

3.2.4 Further Characterization of Selected Compounds *via* DFT calculations

The position of fluorine for aliphatic substrate with a terminal methyl group could be easily discerned from ^{1}H NMR (for an example see **Figure 3.2** and **Figure 3.3**). The $^3J_{FH}$ coupling constant is 23.9Hz and the $^3J_{HH}$ coupling constant is 6.2Hz, therefore the signal of the terminal methyl group would appear as a doublet of doublet. The H that is on the same carbon as the F would have a large geminal coupling constant, $^2J_{FH,}$ which is about 48.8Hz. However, in the case of products without a terminal methyl group such as **10**, **16**, and **17**. Evidence for the position of F could only be obtained through a combination of 2D NMR techniques such as COSY, HMQC and HMBC.
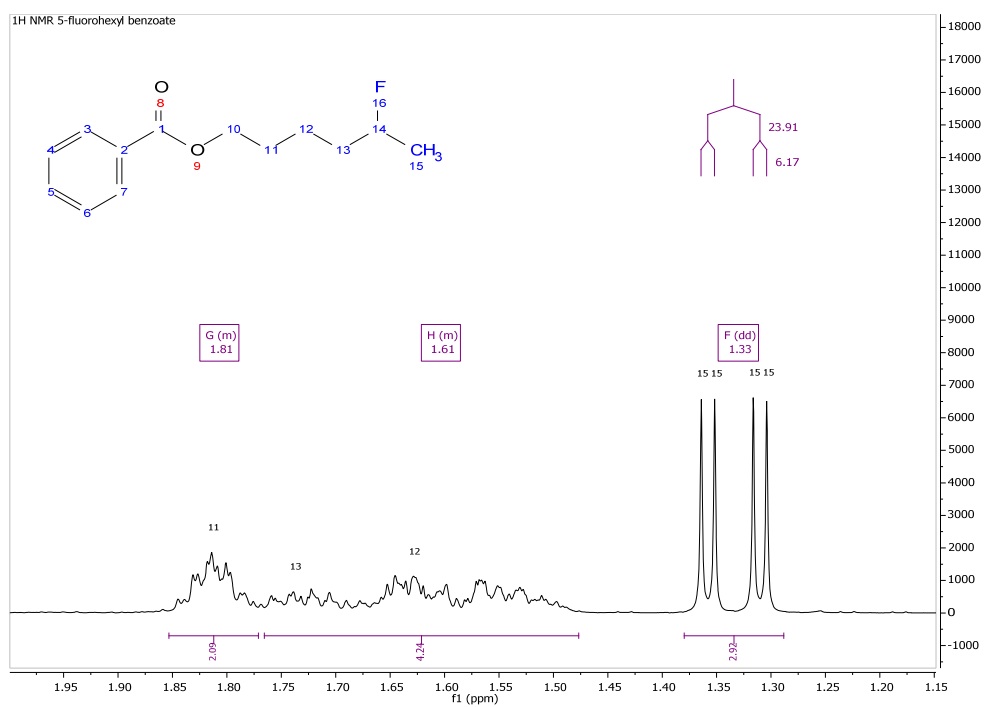
Figure 3.2 Selected region of ^{1}H NMR (500MHz, CDCl$_3$) of 5-fluorohexybenzoate.
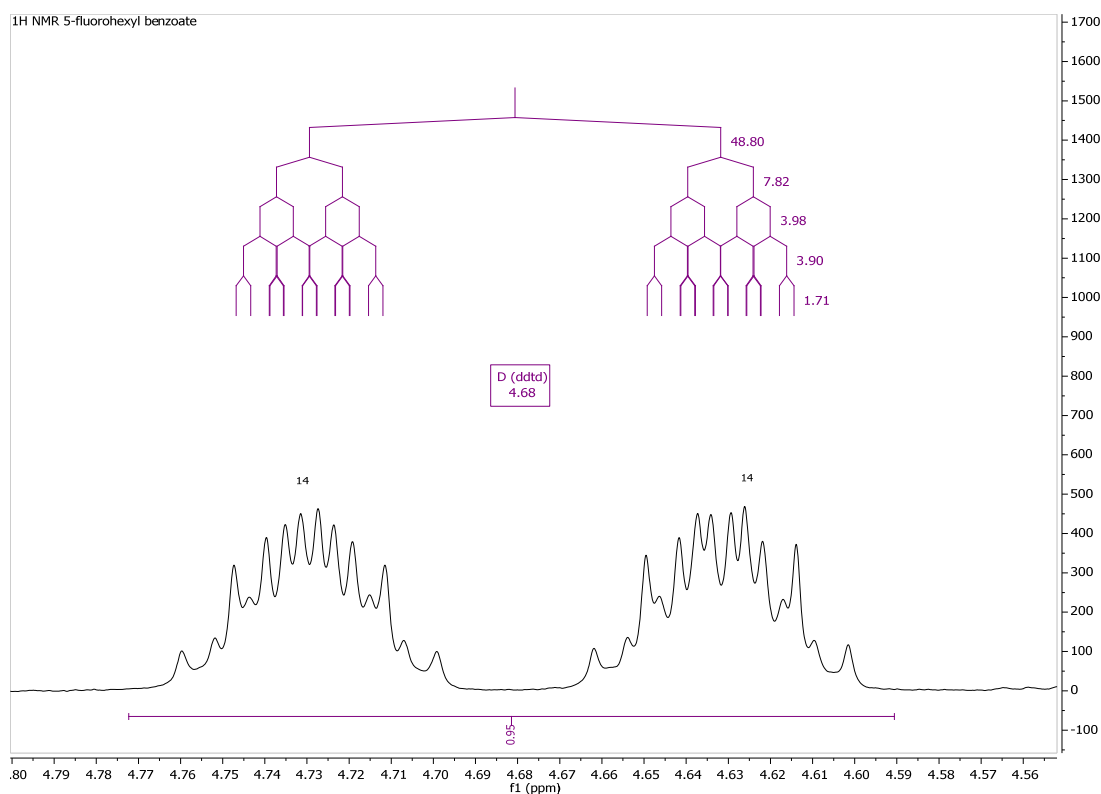
Figure 3.3 Selected region of ^{1}H NMR (500MHz, CDCl$_3$) of 5-fluorohexybenzoate.

In order to provide further evidences to support our proposed structure, DFT calculations were performed to predict the ^{19}F chemical shifts of compounds given in **Figure 3.1** and sclareolide. For most of the compounds, multiple conformations exist, therefore conformation samplings were performed. A maximum of 12 conformations were included in geometry optimization *via* DFT. Geometry optimizations were performed at wB97xD/6-311+G(d,p) and solvent effect was included *via* the SMD[294] implicit solvation model by Truhlar and coworkers. NMR calculations were then performed on the optimized geometries at wB97xD/6-311+G(2df,2pd). The effect of solvent on NMR shielding tensors was not modeled in the DFT calculation, as we assumed that the solvent effect would be similar for all compounds of interest. Therefore, we expect that the subsequent least square linear regression would be sufficient to correct for it. The linear model which expresses the experimental chemical shifts as a function of

the calculated NMR shielding Tensor is given in **Figure 3.4**. A very good correlation coefficient of 0.9953 was obtained.

NMR2 wB97xD 6-311+G(2df,2pd) CDCl₃ Data

$y = -0.9516x + 175.54$
$R^2 = 0.9953$

Experimental ¹⁹F chemical shift /ppm

calculated NMR shielding tensor
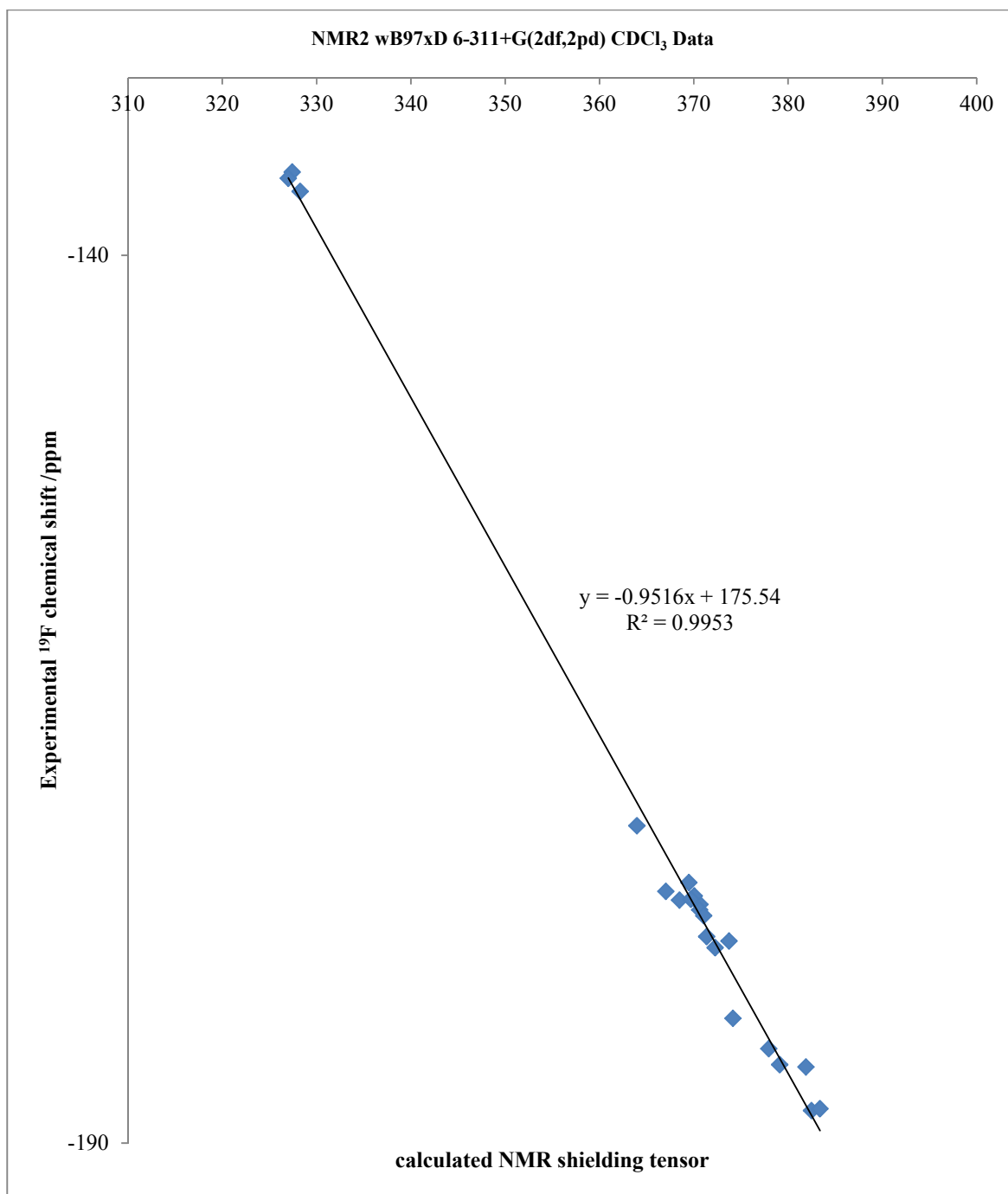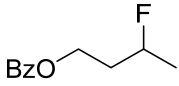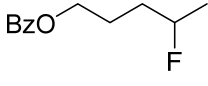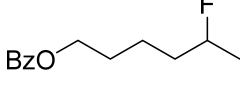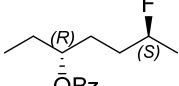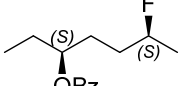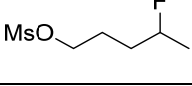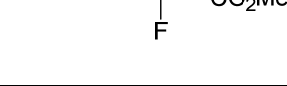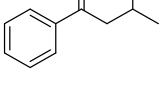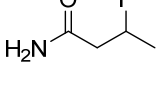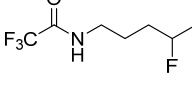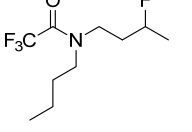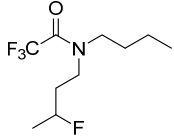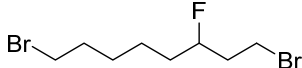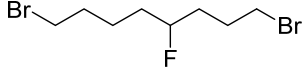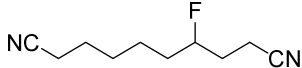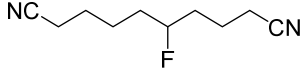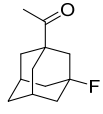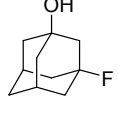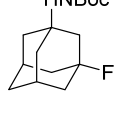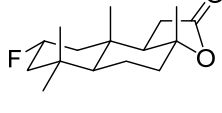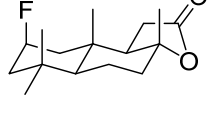
Figure 3.4 Result of least square linear regression

Table 3.2 Calculated ¹⁹F NMR shielding tensor, Predicted ¹⁹F chemical shift from **Figure 3.4** and experimental ¹⁹F chemical shifts.

Entry	Compounds	Calculated NMR shielding Tensor	Predicted from regression model/ppm	Experimental (reference to C_6F_6 at -164.90)/ppm
1	BzO— ... F	373.7307	-180.10	-178.62
2	BzO— ... F	370.6451	-177.17	-176.56
3	BzO— ... F	370.0535	-176.60	-176.08
4	(R) OBz ... (S) F	370.6228	-177.14	-176.87
5	(S) OBz ... (S) F	368.4722	-175.10	-176.31
6	MsO— ... F	371.0508	-177.55	-177.19
7	MeO_2C ... CO_2Me, F	381.8872	-187.86	-185.71
8	O ... F (phenyl)	367.0430	-173.74	-175.82
9	H_2N O ... F	369.4833	-176.06	-175.33
10	F_3C O N H ... F	369.6864	-176.25	-176.26
11	F_3C O N ... F	372.2576	-178.70	-178.99

12	F_3C–C(O)–N(butyl)(CH$_2$CH$_2$CHFCH$_3$)	371.3615	-177.85	-178.37
13	Br–(CH$_2$)$_6$–CHF–CH$_2$–Br	382.4705	-188.42	-188.17
14	Br–(CH$_2$)$_4$–CHF–(CH$_2$)$_2$–Br	377.9543	-184.12	-184.68
15	NC–(CH$_2$)$_5$–CHF–CH$_2$–CN	383.3830	-189.29	-188.06
16	NC–(CH$_2$)$_4$–CHF–(CH$_2$)$_2$–CN	379.1003	-185.21	-185.58
17	acetyl-fluoroadamantane	327.4145	-136.03	-135.31
18	OH-fluoroadamantane	326.2822	-134.95	-136.4
19	HNBoc-fluoroadamantane	327.0042	-135.64	-135.66
20	fluoro terpenoid lactone	374.1440	-180.50	-182.97
21	fluoro terpenoid lactone	363.9657	-170.81	-172.13

3.2.4.1 Sclareolide Selectivity determination

Two major products were observed from the fluorination of (+)-sclareolide **27** (**Scheme 3.6**. They are the 2-F (**27a**) and 3-F (**27b**) products. Separation of these two isomers by silica gel column chromatography is difficult. **27a** could be obtained in good purity but not **27b**. Therefore, detail characterization by 1D and 2D NMR is not available for **27b**. In addition, the equatorial and axial isomers could be not separated by us. Nevertheless, preliminary assignment of ^{19}F peaks to the various isomers could still be achieved with the aid of DFT calculations.
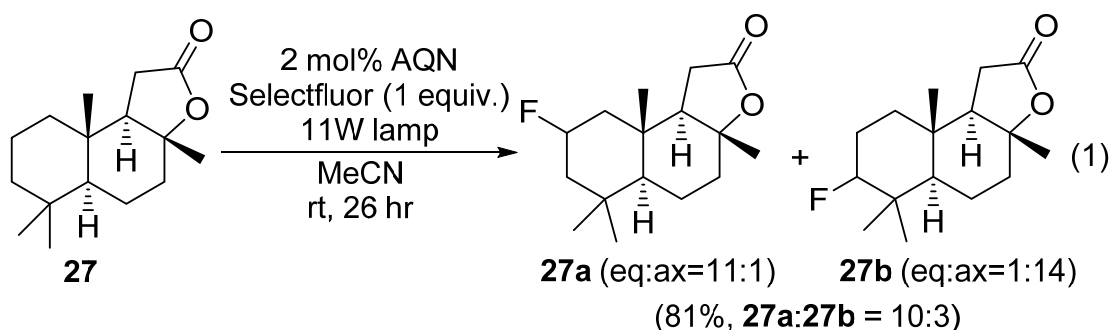
Scheme 3.6 Sclareolide fluorination

The ^{19}F NMR of crude mixture gave 5 peaks (**Figure 3.5**). Four of which is believed to be due the four products given in **Scheme 3.6**. The shielding tensor of **27a** and **27b** were calculated by DFT calculations (same level of theory as described in **section 3.2.4**). From these shielding tensors, the ^{19}F NMR chemical shifts were predicted by using the linear model that is given in **Figure 3.4**. The results are tabulated in **Table 3.3**. The predicted ^{19}F NMR chemical shifts for the various isomers are in good agreement with the corresponding experimental results. Thus, allowing confident assignment of the ^{19}F NMR chemical shifts to the various isomers of sclareolide fluorination. The root mean-square error between calculated results and experimental results is 0.76.
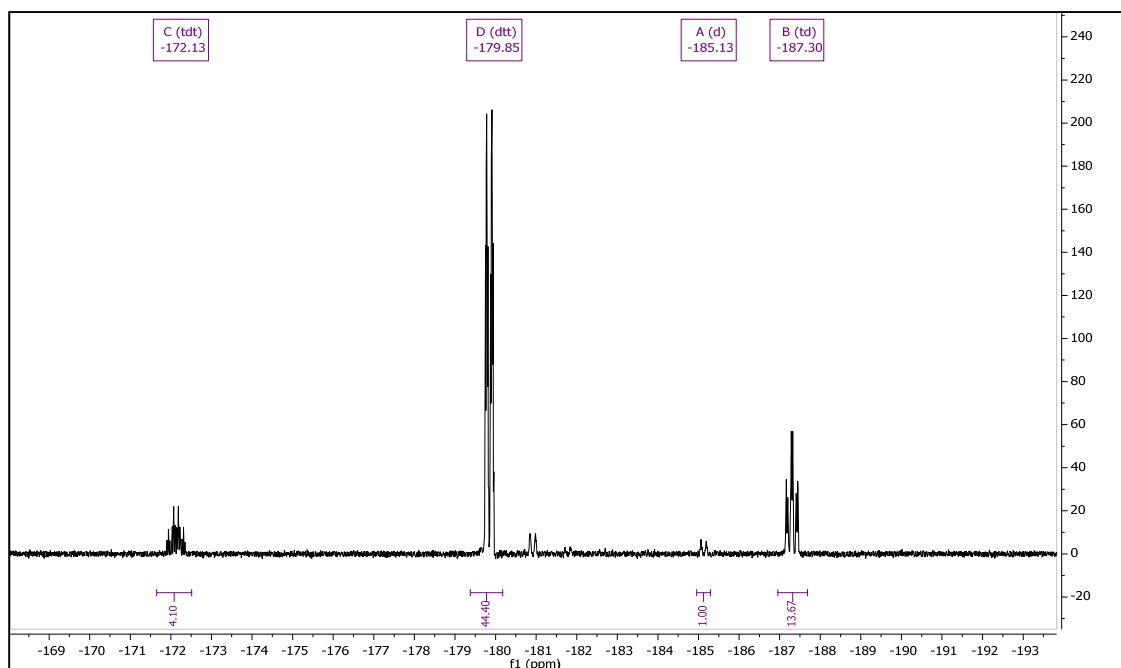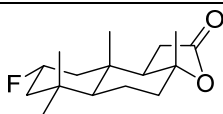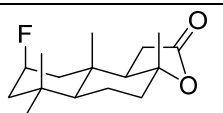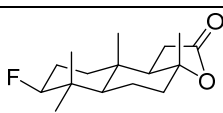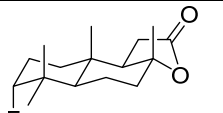
Figure 3.5 Crude ^{19}F NMR of (+)-sclareolide fluorination mixture after work-up .

Table 3.3 Calculated ^{19}F shielding tensor, predicted and experimental ^{19}F chemical shift for (+)-sclareolide fluorination

	Calculated ^{19}F NMR shielding tensor	Predicted ^{19}F NMR chemical shift	Experimental ^{19}F chemical shift/ppm
	374.144	-180.65	-179.85
	363.9657	-170.98	-172.13
	379.0884	-185.35	-185.13
	382.9581	-189.03	-187.30

3.2.4.2 Determination of diastereomer for 6-fluoroheptan-3-yl benzoate

The *cis*- and *trans*- (*cis* is defined as both the chiral center having the same absolute configuration, i.e. *R,R* or *S,S*) isomers formed from the fluorination of heptan-3-yl benzoate could also be assigned to their respective ^{19}F chemical shifts through DFT calculations. The assignments are made based on results in **Table 3.2**, entry 4 and 5. The error for the *trans*- isomer is 0.27ppm which is smaller than the *cis*- isomer (1.21ppm). As only a portions of the total number of conformations generated by Macromodel® are included (for *cis*- 12 out of 49 conformations and *trans*- 12 out of 54 conformations), further refinement of the predicted results could be made by increasing the number of conformations used in the calculation.
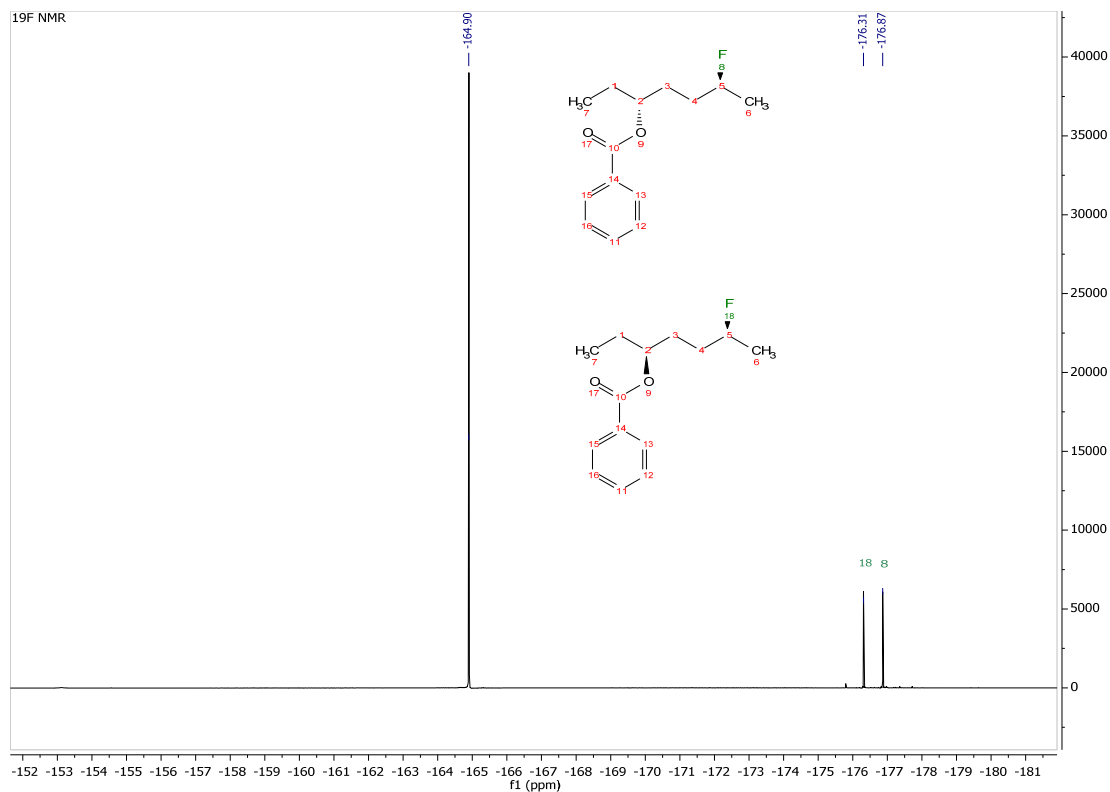
Figure 3.6 ^{19}F NMR of 6-fluoroheptan-3-yl benzoate.-164.90ppm is the internal standard: perfluorobenzene

3.2.4.3 Determination of conformation isomers for *N*-butyl-2,2,2-trifluoro-N-(3-fluorobutyl)acetamide

Rotation about the amide partial double bond is restricted and could be observed from NMR. The fluorination of *N,N*-dibutyl-2,2,2-trifluoroacetamide gave a mixture of *cis*- and *trans*-fluorinated amide. The predicted ^{19}F NMR chemical shifts of both isomers are in good agreement with the experimentally measured chemical shifts (**Table 3.2**, entry 11 and 12). Thus, allowing reliable assignment of the corresponding isomer to their respective ^{19}F NMR chemical shift (**Figure 3.7**).
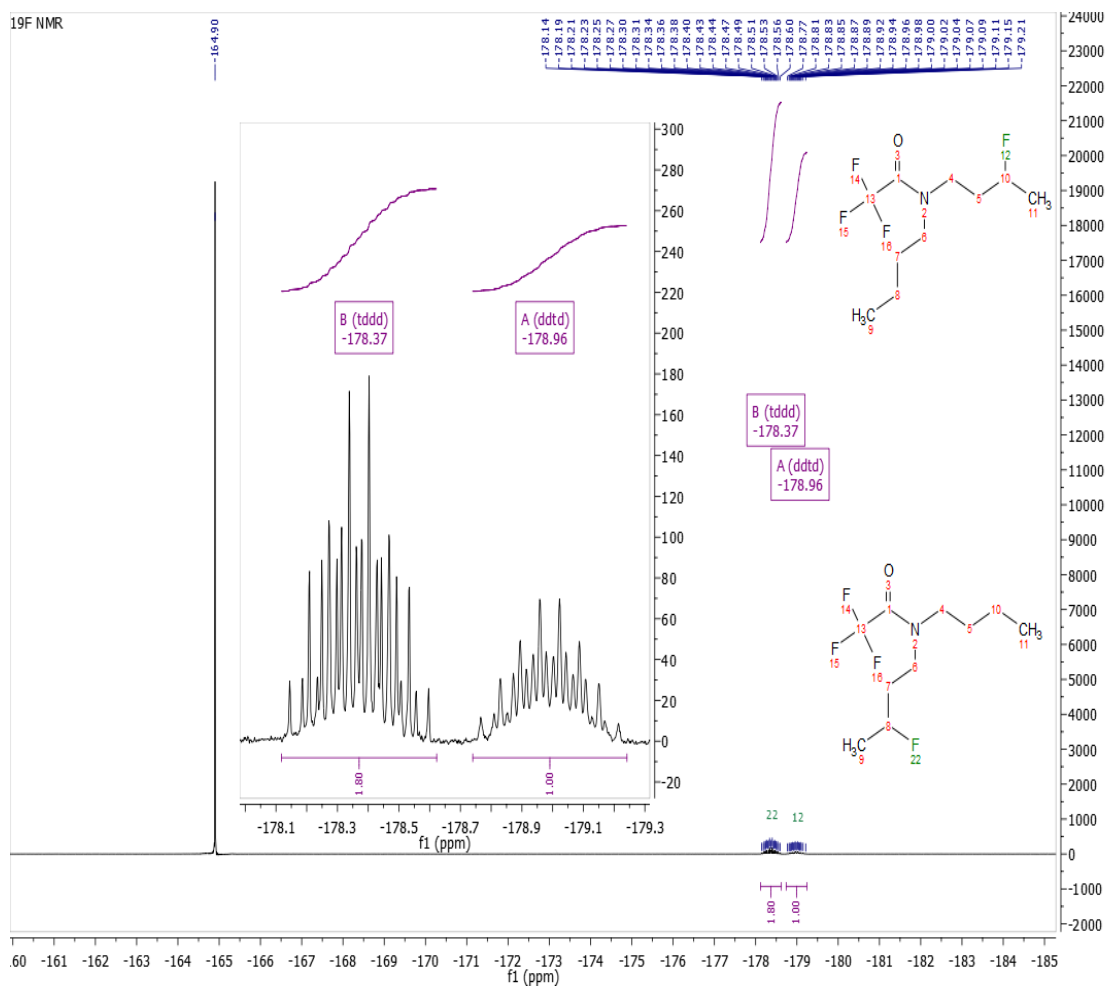
Figure 3.7 ^{19}F NMR of N-butyl-2,2,2-trifluoro-N-(3-fluorobutyl)acetamide. -164.90ppm is the internal standard: perfluorobenzene

3.2.5 Mechanism Study

Two main questions could be conceived regarding the mechanism of this reaction:

1) What is the role of the photocatalyst? Is this a photoredox reaction or an energy transfer reaction or is the triplet excited state of AQN the hydrogen abstractor?

2) Evidences for the proposal that the hydrogen abstractor is the cationic *N*-radical derived from Selectfluor®.

3.2.5.1 The role of the photocatalyst

S_0 Ground State   **S_1 Singlet Excited State**   **T_1 Triplet Excited State**
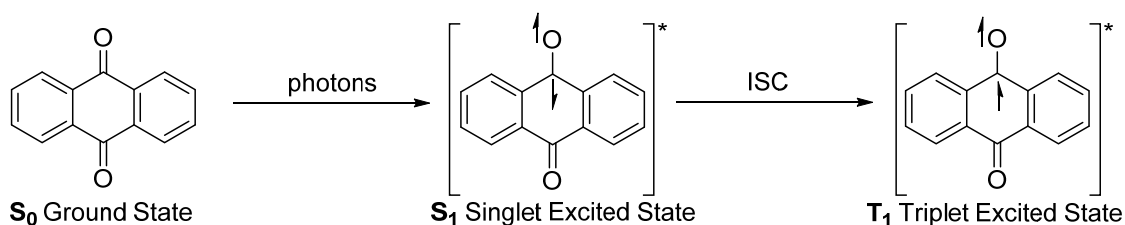
Scheme 3.7 Absorption of light by AQN and its photochemical pathway

The photochemical pathway of AQN is depicted in **Scheme 3.7**. Upon absorption of a photon, AQN in its ground state **S_0** is promoted to its first singlet excited state **S_1**. **S_1** undergoes very efficient intersystem crossing (ISC) to the triplet state **T_1** with a quantum yield for ISC of 90% (in benzene).[295] The triplet state of AQN has a lifetime of about 10μs in O_2 free acetonitrile.[296] Given the high quantum yield for ISC, we would assume that the **T_1** is the key form of AQN involved in the photo-fluorination.

Three roles of **T_1** are possible. It could transfer its excess energy to Selectfluor® *via* energy transfer mechanism or it could reduce **9a**: the dicationic component of Selectfluor® (**Scheme 3.8**). The redox pathway requires triplet AQN to act as an electron donor. However, from literature the use of **³AQN** as an electron acceptor is more common[147] than as a donor, but there is a report on the oxidation of AQN in MeCN.[297] The $E_{1/2}$ of AQN (ground state) was found

to be $+1.21V^{297}$ vs. SCE in MeCN while that of Selectfluor® was found to be $+0.30V^{298}$ vs. SCE

in MeCN. Due to the irreversible redox process of Selectfluor®,[283] the half wave potential $E_{1/2}$ is

unlikely to be equal to the standard potential.[299] Therefore, it would be inappropriate to drawn

thermodynamic related conclusion from these half wave potentials.[300] However, the $E_{1/2}$ of

Selectfluor® suggests that it could act as a single electron oxidation which is consistent with our

calculation (refer to **Scheme 3.1**), but whether this is important for the photo-fluorination requires

further study. The third role of the triplet excited state of AQN is to serve as the hydrogen

abstractor, which is reported for triplet benzophenone and derivatives.[147]
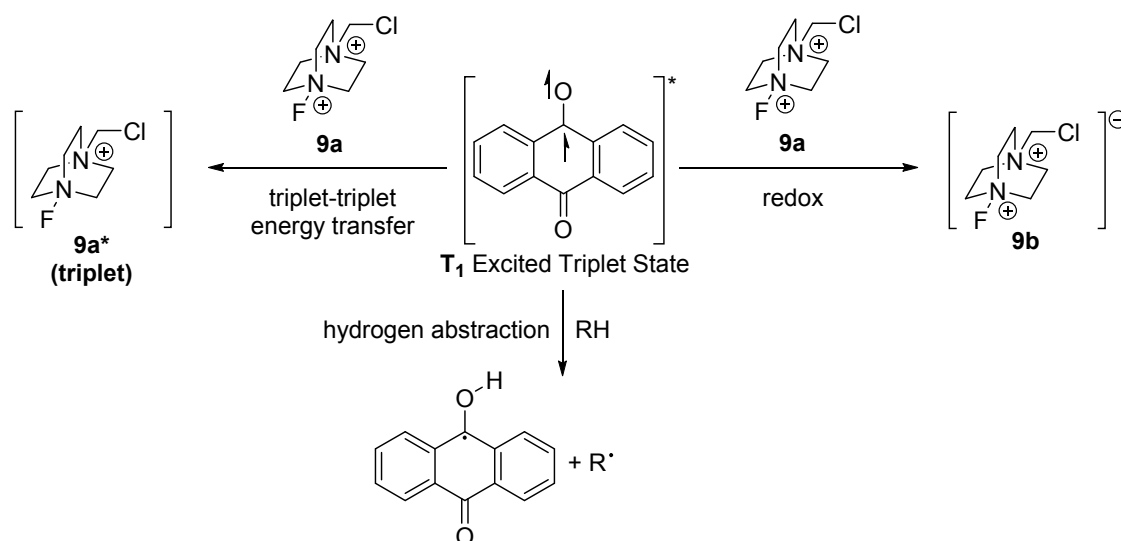
Scheme 3.8 Possible pathways for interaction between T_1 of AQN and Cationic component of Selectfluor® **9a**

Experimentally, fluorenone and alizarin red S sodium salt do not produce significant

amount of fluorinated product (**Scheme 3.9**). Chen and co-workers reported that fluorenone is

able to catalyze the photo-fluorination of benzylic substrates (with Selectfluor® as the fluorine

source, and visible light, which is essentially identical to our condition, except for the

photocatalyst) and they proposed that the triplet excited state of fluorenone functions as the

hydrogen abstractor. Therefore if we assume that their hypothesis is valid, then the lack of

reactivity when the substrate is changed suggests that a different mechanism is at work, most probably the hydrogen abstractor is different (not the triplet excited state of the photocatalyst). We would provide further evidence that the hydrogen abstractor is the cationic *N*-radical of Selectfluor® in section **3.2.5.4.** Nevertheless, how the cationic *N*-radical of Selectfluor® is generated remained to be discussed.
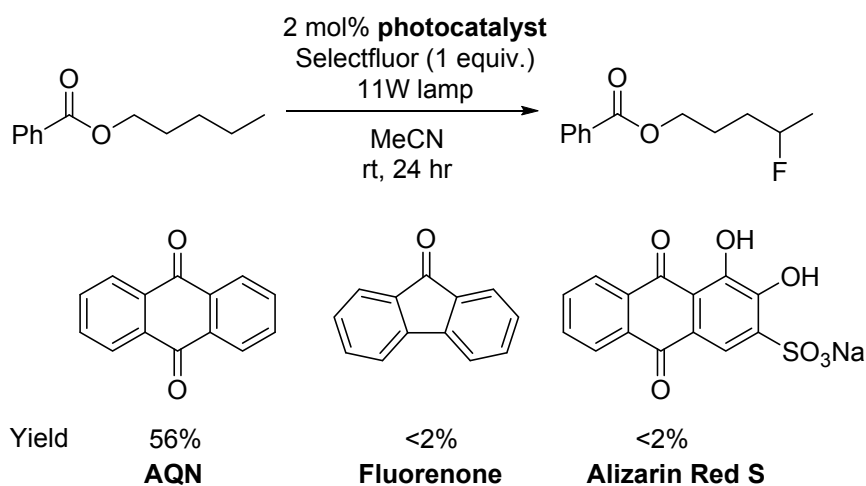
Scheme 3.9 Variation of photocatalysts

3.2.5.2 Energy transfer pathway

At first slight it appears that the energy transfer pathway is feasible as AQN possesses the highest triplet energy E_T among the three photocatalysts used in **Scheme 3.10**. Therefore, it could be argued that there is a minimal E_T requirement to catalyze the photo-fluorination. A triplet-triplet energy transfer would result in the formation of the triplet state of the **9c** (the dicationic component of Selectfluor®). DFT calculation indicates that the unpaired electrons which are of the same spin reside in the N-F bond, and the result of a triplet excitation is to elongate the N-F bond of **9a** (**Figure 3.8)**. The calculated singlet-triplet gap of **9a** is 61.4 kcal/mol (SCF energy +ZPE) which is equivalent to the E_T of AQN, thus effective energy transfer is possible.

E_T(kcal/mol) +62(+61)   +54.3(+55)   (+34)
AQN   **Fluorenone**   **Alizarin Red S**

Decreasing triplet energy
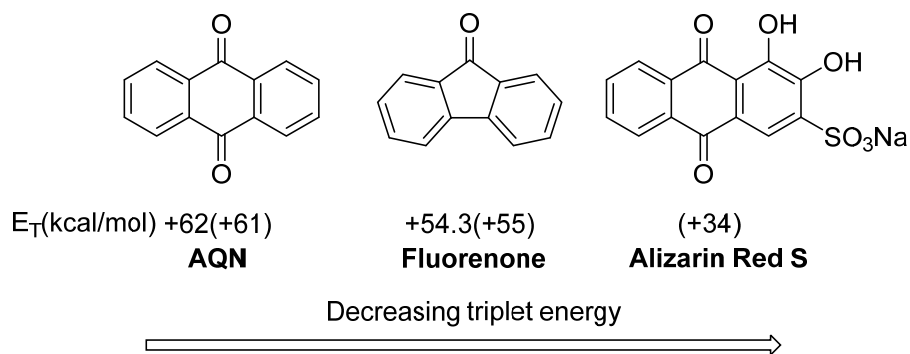
Scheme 3.10 Inability of Fluorenone and Alizarin Red S sodium salt to catalyst the photo-fluorination. The triplet energy (E_T) of each photocatalyst is given. E_T for AQN and Fluorenone are taken from work of Zalesskaya.[300] Calculated E_T based on SCF energy + ZPE is in parentheses.
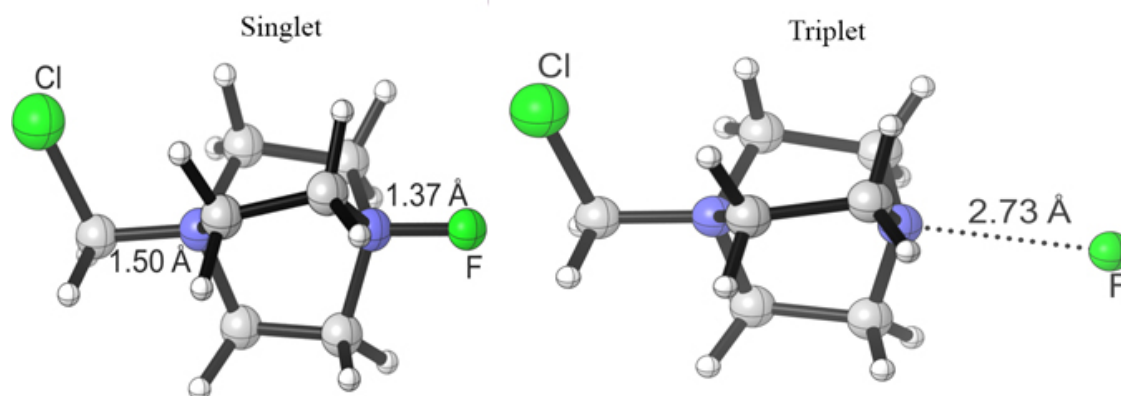
Figure 3.8 Equilibrium geometry of **9a** (the dicationic component of Selectfluor®). Left: Singlet state. Right: Triplet state. Calculated at M06-2X/6-311+G(d,p) with SMD solvation model and acetonitrile as solvent. Stability of wavefunction was tested.

The triplet-triplet energy transfer pathway appears to be feasible. In addition, a non-radiative decay of the triplet excited state by transfer of energy to the vibration modes of **9a** could also be viable.[301] The transfer of excess energy of triplet AQN to the vibrational mode of **9a** is sufficient to break the N-F bond of **9a** to form the desired cationic *N*-radical **9c** (**Scheme 3.11**). The lack of reactivity for Alizarin Red S salt (**Scheme 3.9**, E_T =34kcal/mol) and Rose Bengal (**Table 3.1**, Entry 6, E_T = 44 kcal/mol) could also be explained by this hypothesis. Some issues
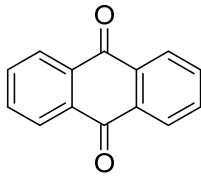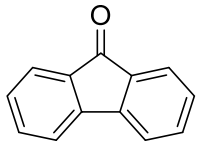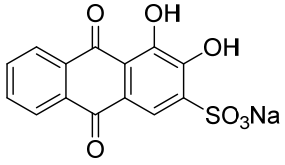
such as whether it is physically viable to transfer all the E_T into the N-F vibration mode of **9a** and

the fate of the fluorine radical formed remained to be investigated and answered.
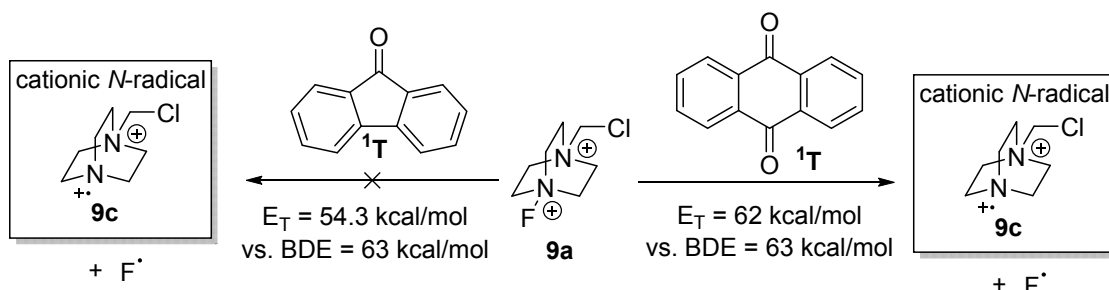
Scheme 3.11 Nonradiative decay energy transfer pathway. E_T for AQN and Fluorenone are taken from work of Zalesskaya.[300] BDE calculated from enthalpy Calculated at M06-2X/6-311+G(d,p) with SMD solvation model and acetonitrile as solvent at 298.15K and 1atm. Stability of wavefunction was tested.

3.2.5.3 Redox Pathway

Table 3.4 Redox properties of AQN, Fluorenone and Alizarin Red S

Entry	Properties			
1	Ionization potential/eV	+9.25[302]	+8.34[303]	-
2	Ionization - E_T /eV	+6.56	+5.99	-
3	Calculated ΔG/eV	+4.6	+4.0	+5.1

E_T is for AQN and Fluorenone are +62 kcal/mol and +54.3kcal/mol from Zalesskaya.[300] $\Delta G = G$ of cation – G of triplet state. Calculated at M06-2X/6-311+G(d,p) with SMD solvation model and acetonitrile as solvent. Stability of wavefunction was tested.

The redox pathway in **Scheme 3.8** does not explain the results in **Scheme 3.9**. Based on

ionization potential, oxidation of fluorenone is more favorable than AQN (**Table 3.4**, Entry 1).

The inclusion of E_T does not change the conclusion (**Table 3.4**, Entry 2). Solvation could affect

the thermodynamics of charged species significantly; however, DFT calculated $\Delta G_{oxidation}$ for the oxidation of the triplet state for each photocatalyst gave the same conclusion as that derived from the ionization potential and E_T (**Table 3.4**, Entry 3), although Alizarin Red S salt does have a much higher $\Delta G_{oxidation}$ than the other two photocatalysts.

A caveat of the above analysis of the redox pathway is that we have not considered the kinetic of electron transfer. The kinetic of electron transfer could be model by Marcus-Hush Theory.[304, 305] The Marcus equation is given below. k_{et} is the rate constant for electron transfer, λ is the solvent reorganization energy, $H_{A,B}$ describes the overlap between the wavefunction of A and B during the electron transfer (A and B are the redox partners), and $\Delta G°$ is the thermodynamics of the electron transfer, and $\Delta G^{\ddagger}$ is the Gibbs energy of activation.

$$k_{et} = \frac{2\pi}{\hbar} |H_{A,B}|^2 \frac{1}{\sqrt{4\pi\lambda k_b T}} e^{-\frac{\Delta G^{\ddagger}}{k_b T}}, \Delta G^{\ddagger} = \frac{(\lambda + \Delta G°)^2}{4\lambda}$$

According to Marcus equation, for a given solvent reorganization energy, the reaction rate will not increase indefinitely as $\Delta G°$ becomes more negative (or the electron transfer becomes thermodynamically more favorable). When $\Delta G° = -\lambda$, the barrier for electron transfer $\Delta G^{\ddagger}$ becomes zero, making $\Delta G°$ more negative than $-\lambda$ will increase the barrier for electron transfer and slow down the transfer (The contribution from wavefunction overlap is ignored at this point). This is known as the Marcus inverted region.[306]

Pertinent to the oxidation of photocatalyst by **9a**, the oxidation of fluorenone (triplet) by **9a** has a much more negative ΔG_{T1} than the oxidation of AQN (triplet) by **9a**, as predicted by DFT calculations (**Scheme 3.12**). If the conditions of the Marcus inverted region is satisfied then the oxidation of triplet fluorenone by **9a** would be much slower than that for the oxidation of triplet AQN. Therefore, there is sufficient time for the triplet state of fluorenone to revert to its ground state. The oxidation of AQN and fluorenone in their ground by **9a** is highly favorable

(ΔG_{S0} in **Scheme 3.12**). Further evidences of whether the electron transfer process is in the Marcus inverted region is required to support this hypothesis and consequently the redox pathway for the photo-fluorination.
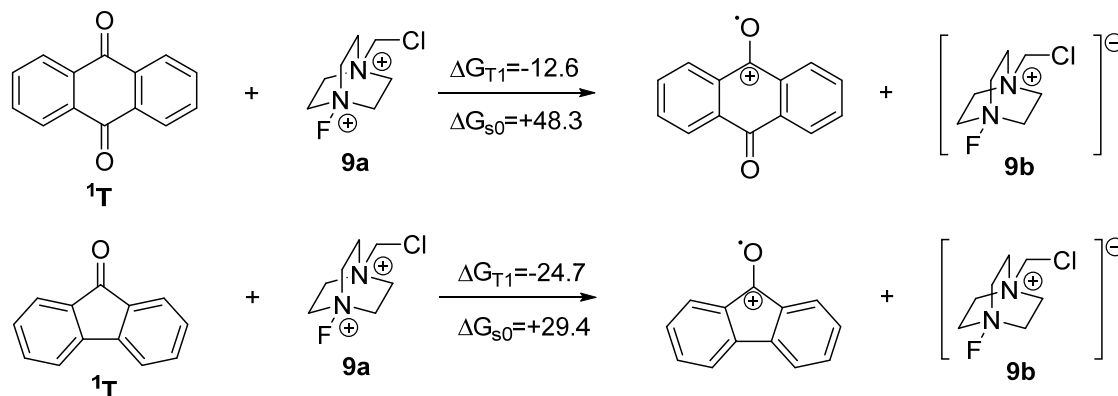
Scheme 3.12 Thermodynamics for the oxidation of triplet states of AQN and fluorenone by **9a**. ΔG_{T1} applies to the triplet state (^{1}**T**) of AQN and fluorenone and ΔG_{S0} applies to the ground state of AQN and fluorenone, both are in kcal/mol, Calculated at M06-2X/6-311+G(d,p) with SMD solvation model and acetonitrile as solvent at 298.15K and 1atm.

3.2.5.4 Selectivity *via* DFT calculations

There are two possible species that can play the role of hydrogen abstractor: cationic *N*-radical and triplet AQN. Triplet benzophenone and derivatives are well known as hydrogen abstractor,[147] while there are less reports on AQN.[307, 308] However, triplet benzophenone[309] and AQN[307] are reported to be nucleophilic radical and preferentially abstract from electron poor C-H bond. Therefore, they exhibit opposite reactivity observed for the photo-fluorination. Sammis and co-workers had demonstrated that NFSI can be an effective radical fluorine source.[272] The lack of fluorinated products when Selectfluor® was replaced with NFSI shows that Selectfluor® is more than a fluorine source. The selectivity observed for this photo-fluorination resembles that of other reactions using cationic *N*-radicals.[83]

Table 3.5 Probing the hydrogen abstracting species using DFT

31
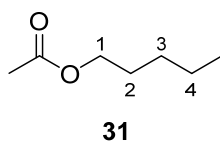
H-abstractor	Calculated $\Delta\Delta G^{\ddagger}$ for H abstraction (kcal/mol)			
	1	2	3	4
^{3}AQN	+0.5	+0.2	+0.0	+0.9
9d	+2.3	+2.4	+1.2	+0.0
Experimental result[a]	+1.4	+1.4	+0.9	+0.0

SMD(MeCN)-wB97xD/6-31+G(d,p).[235] [a] Determined from crude ^{19}F NMR.

DFT calculation was used to predict the selectivity of hydrogen abstraction for triplet AQN and cationic *N*-radical derived from Selectfluor II® (**9d**), which was chosen to simplify calculation as multiple conformations exist for **9c** (**Table 3.5**). Experimentally, similar selectivity was observed for Selectfluor® and Selectfluor II®. The calculated result shows that cationic *N*-radical derived from **9d** has selectivity that is consistent with the experimentally observed results. In the case of triplet AQN, the hydrogen abstraction is predicted to proceed with poor selectivity, with a majority of C2 and C3-fluorinated products predicted.

3.2.5.5 Assignment of ^{19}F NMR signal to various isomer of 29 in Table 3.5

Assignment of ^{19}F NMR to various regioisomers of fluoropentyl acetate was performed by DFT calculations. Macromodel® was used to generate structures of 1-,2-,3-, and 4-fluoropentyl acetate. 10 conformations for each regioisomer were optimized at SMD(MeCN)-wB97xD/6-

311+G(d,p) using default convergence criteria and integration grid as implemented in Gaussian 09 A2. Frequency calculations were performed to ensure that there is no imaginary frequency for all the conformers. NMR calculations were performed on all the optimized conformers at wB97xD/6-311+G(2df,2pd). A Boltzmann distribution was used to calculate the contribution of each conformer to the final ^{19}F NMR shielding tensor (i.e. the ^{19}F NMR shielding tensor is a weighted average and the weights are derived for the Boltzmann distribution using the relative Gibbs free energy of each conformer). A least square linear regression was performed to correct for systematic error (**Figure 3.9**). The predicted and experimentally measured ^{19}F NMR chemicals are tabulated in **Table 3.6**. Excellent agreement between the predicted and measured chemical shifts was obtained. The root mean-square error is 0.46.
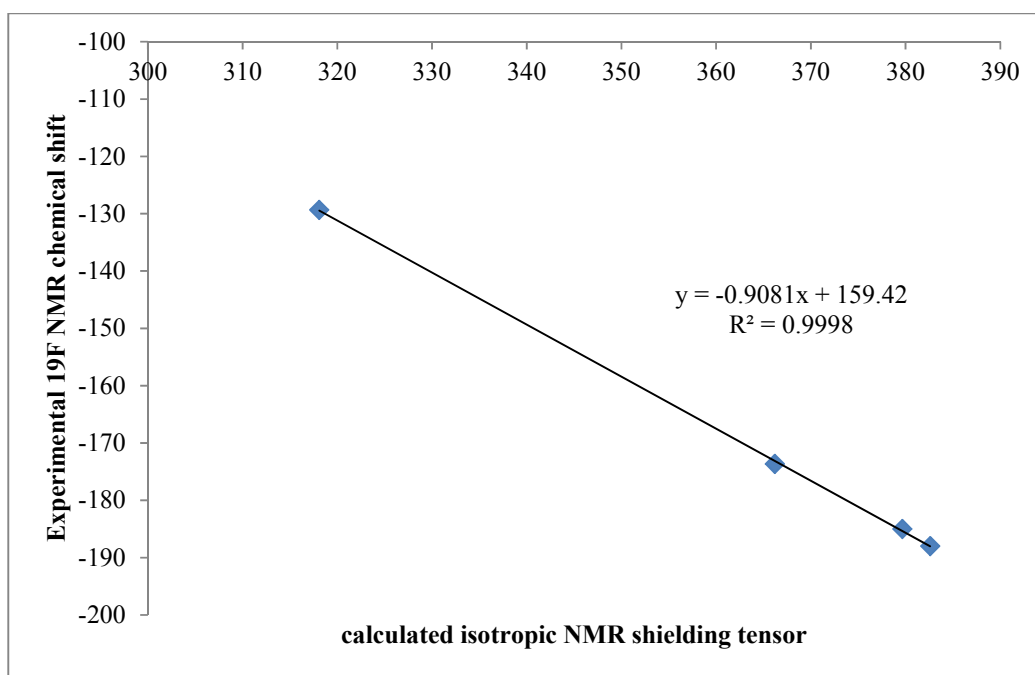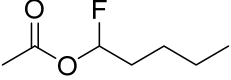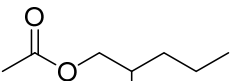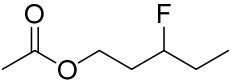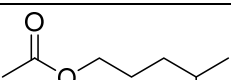
Figure 3.9 Linear regression result for various isomer of fluoropentyl acetate.

Table 3.6 Calculated ^{19}F shielding tensor, predicted and experimental ^{19}F chemical shift for fluorination of pentyl acetate

	Calculated isotropic NMR shielding tensor	Experimental chemical shift/ppm	Predicted chemical shift using linear regression model/ppm
	318.093	-129.33	-129.44
	382.5983	-187.99	-188.02
	379.667	-184.99	-185.36
	366.192	-173.64	-173.12

3.2.5.6 Proposed mechanism

As it is unclear whether the energy transfer pathway or redox pathway is in operation (the possibility of a combination of both but to a different extent could not be excluded), we would proposed two different cycles tentatively. The redox pathway cycle is shown in **Figure 3.10** and the nonradiative decay energy transfer pathway is depicted in **Figure 3.11**.

Regardless of which pathway, we proposed that the reaction begins with the excitation of AQN by absorption of light. At the concentration used in the reaction, AQN exhibits significant absorption in the visible region (400-460nm, **Figure 3.12**), thus absorption of visible light is possible AQN is promoted to its singlet excited state, which undergoes facile intersystem crossing (ISC) to its triplet excited state. In the redox pathway (**Figure 3.10**), the triplet excited state of AQN is oxidized by **9a**, which eventually will undergo a dissociative SET to form **9c** (the

hydrogen abstractor). For the energy transfer pathway (**Figure 3.11**), transfer of excess energy into the N-F vibration mode of **9a** will result in the formation of **9c**.
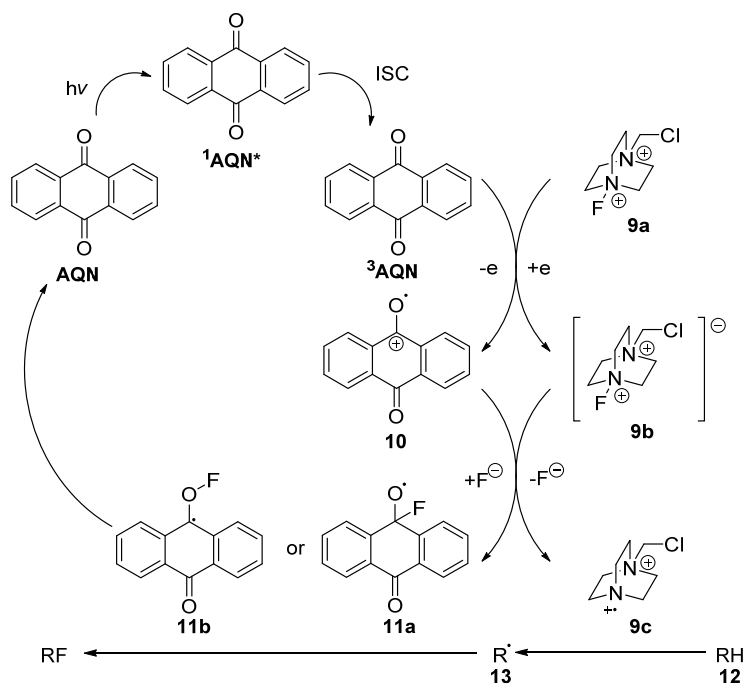
Figure 3.10 Proposed mechanism (Redox Pathway)
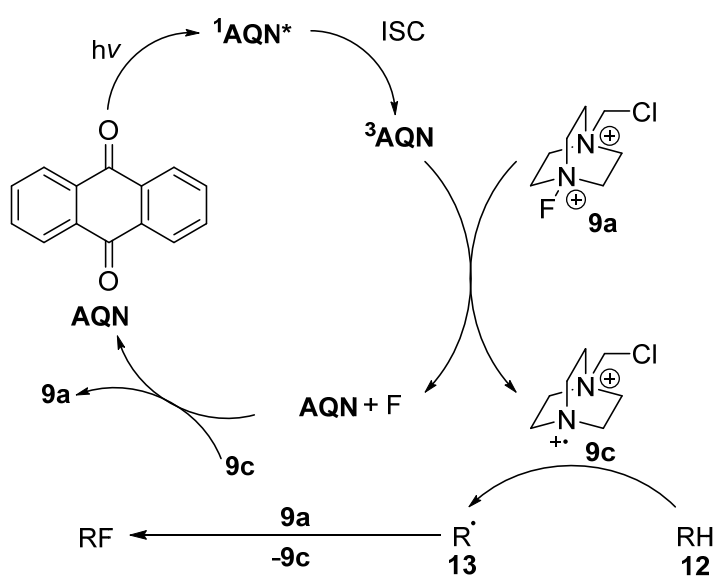
Figure 3.11 Proposed mechanism (Nonradiative decay pathway)
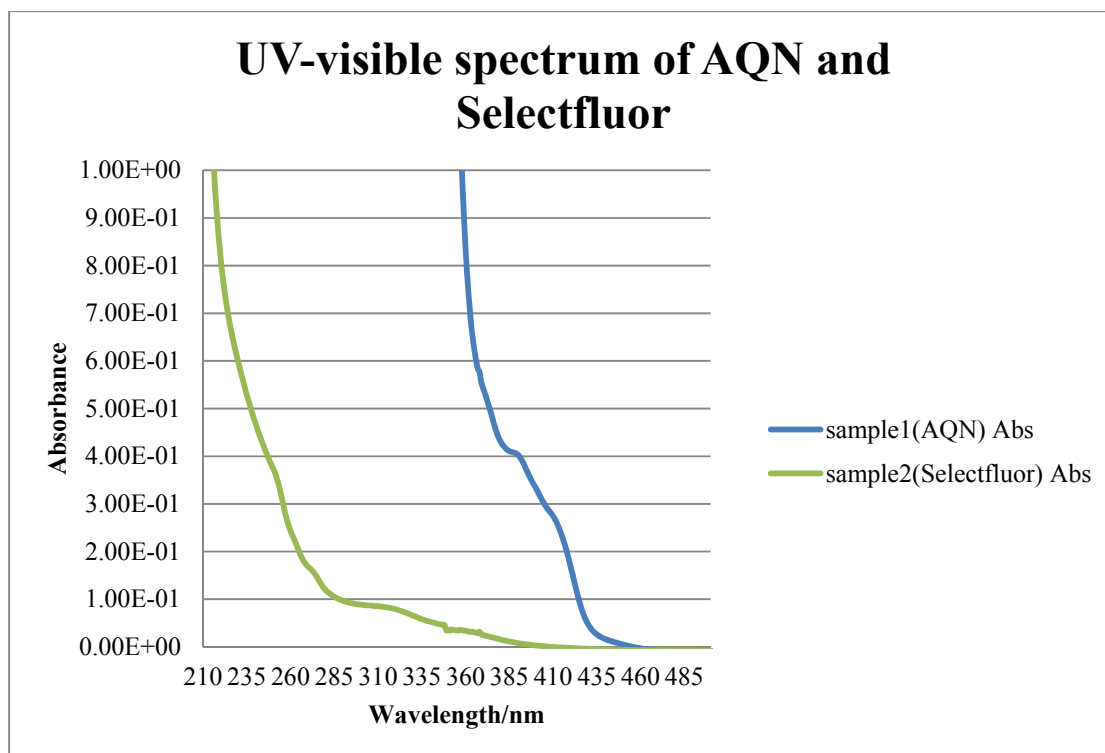
Figure 3.12 UV-visible spectroscopy spectrum of AQN and selectfluor in acetonitrile

At this point, the fate of the dissociated fluoride (**Figure 3.10**) or fluorine (**Figure 3.11**) is unclear. In the redox pathway, we proposed that the dissociated fluoride reacts with the cation of AQN **10** to form novel species **11a/11b,** which are tentatively proposed to be the radical fluorine source for the alkyl radical **13**. This is to reconcile with the experimental fact that continuous irradiation is essential throughout the reaction – removal of light at any point of quenches the reaction. An alternative explanation of the need for continuous irradiation is that there exists a termination pathway in which fluoride could react with **9c** to form **9a**, which is depicted in **Figure 3.11**. In the nonradiative decay pathway we proposed that the fluorine source is **9a**, theoretically this is also possible for the redox pathway, but for the sake of clarity of the cycle only one possibility is shown for each pathway.

3.2.5.7 Novel species 11a and 14a to explain the result in Scheme 3.9

For AQN, **11a** is more stable than **11b** (**Figure 3.10**) by 22.4 kcal/mol of Gibbs free energy, thus in the absence of a substantial kinetic barrier, **11b** should be converted spontaneously to **11a**. For fluorenone, **14a** (**Scheme 3.13**) is more stable than **14b** (the analogous to **11b**) by a similar amount of Gibbs free energy (21.1 kcal/mol). The formation of **11a** and **14a** from **9a** and the triplet state of AQN and fluorenone are highly thermodynamically favorable (**Scheme 3.13**). Thus, the hydrogen abstracting species **9a** could be formed from the triplet state of both AQN and fluorenone. Therefore this does not provide an explanation for the experimental results in **Scheme 3.9** (the lack of reactivity for fluorenone).
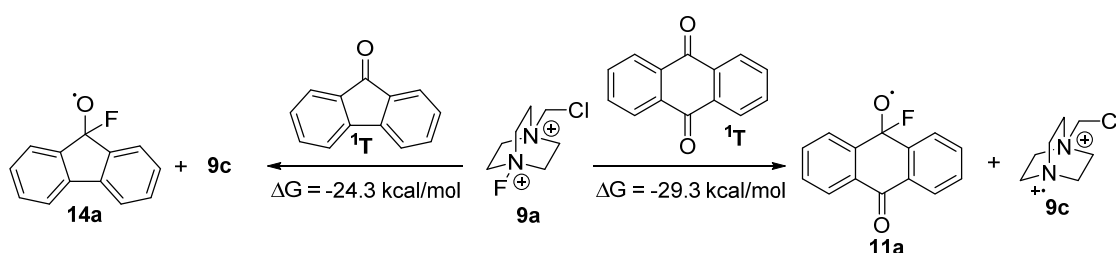
Scheme 3.13 Thermodynamics of the formation of **11a** and **14a** from the triplet state of AQN and Fluorenone, with **9a**. Calculated at M06-2X/6-311+G(d,p) with SMD solvation model and acetonitrile as solvent at 298.15K and 1atm.

Next, the thermodynamics for the formation of **11a** and **14a** from the oxidized AQN and fluorenone and **9b** are presented (**Scheme 3.14**). For oxidized fluorenone, the change in Gibbs free energy is +0.5 kcal/mol which is thermodynamically unfavorable. For oxidized AQN **10**, the reaction is highly thermodynamically favorable (ΔG = -16.7 kcal/mol). Thus, the formation of the hydrogen abstractor **9c** is unfavorable in terms of thermodynamics for fluorenone. This could potentially explain the lack of reactivity for fluorenone in the photo-fluorination: Even though fluorenone could be oxidized by **9a** (see section **3.2.5.3**), it is unable to generate the hydrogen abstractor **9c** before the back electron transfer to **9b** occurs to regenerate ground state fluorenone and **9a**.
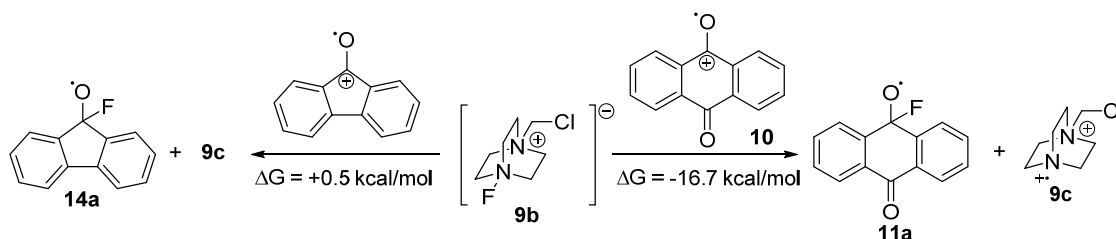
Scheme 3.14 Thermodynamics of the formation of **11a** and **14a** from the oxidized AQN and Fluorenone, with **9b**. Calculated at M06-2X/6-311+G(d,p) with SMD solvation model and acetonitrile as solvent at 298.15K and 1atm.

The equilibrium geometry of **11a** is shown in **Figure 3.13**. Most of **11a** spin density resides on the O on the sp^3 carbon center. As for the electron distribution, ESP map indicates that the most negative potential (highest electron density) resides on the O of the C=O. From the spin density, it appears that the F does not have much radical character, as most of the spin density is on the O. Despite this, preliminary calculations indicate that **11a** is unstable in the presence of CH_3 radical, and will readily transfer a fluorine atom to form AQN and CH_3F without a barrier. Nevertheless, it is premature to overemphasize the role of **11a** in the photo-fluorination without more concrete evidences (spectroscopic evidences on its existence, etc.).
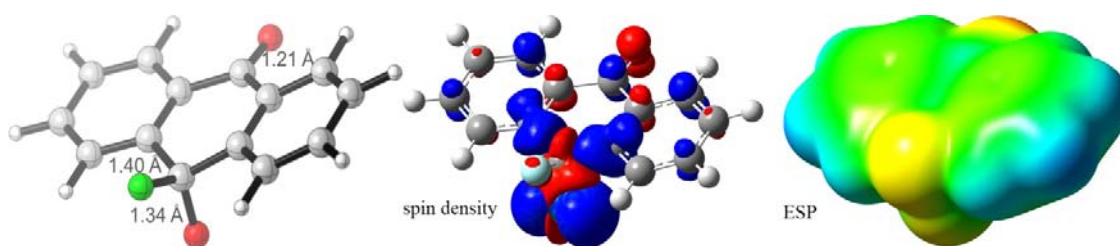
Figure 3.13 3D structure of **11a** follow by its spin density then ESP map. Spin density and ESP map calculated from SMD-HF/6-311+G(d,p)//SMD-M06-2X/6-311+G(d,p). Solvent is acetonitrile for SMD solvation model. Isovalue for density = 0.001 a.u.

11b is structurally similar to highly reactive hypofluorites, which are known to fluorinate C-H bond.[128] Its equilibrium structure is shown in **Figure 3.14**. Contrary to **11a**, the F of **11b** has

significant spin density which might suggests that it could act as a radical fluorine source. As with **11a**, more evidence is required before more definite conclusion on its role is made.
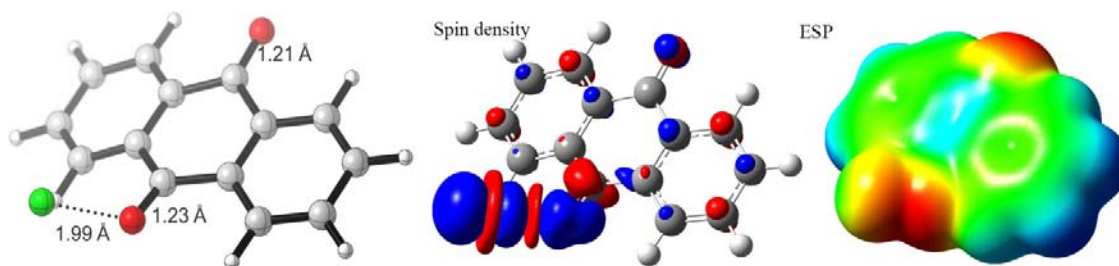
Figure 3.14 3D structure of **11b** follow by its spin density then ESP map. Spin density and ESP map calculated from SMD-HF/6-311+G(d,p)//SMD-M06-2X/6-311+G(d,p). Solvent is acetonitrile for SMD solvation model. Isovalue for density = 0.001 a.u.

3.2.5.8 Trend of C-H chlorinating process using AQN or related catalysis.

Pertinent to the use of cationic *N*-radical, chlorination exhibits similar selectivity.[83] Because the selective fluorination of secondary C-H bond is not known in the literature as Minisci and co-works focus only on chlorination and bromination with cationic *N*-radical, there is no basis of comparison.

Nevertheless we believe that the selectivity would not be affected significantly by changing to chlorination or bromination for AQN photocatalysis. This is because selectivity should be determined in the H abstracting step. Therefore, the subsequent halogenating step should not have much impact on the selectivity of the C-H functionalization.

3.4 Conclusion

In conclusion, we have developed a photo-fluorination reaction catalyzed by an organo-photocatalyst. The reaction can be performed with common low power household lamps. The reaction is selective for electron rich sp^3 C-H bonds due to the involvement of cationic *N*-radical in hydrogen abstraction. This work presents a novel method to generate cationic *N*-radical without the need of strongly acidic medium and extend the scope of innate C-H functionalization

of cationic *N*-radicals to include fluorination. A diverse variety of functional groups can be tolerated by the reaction and it is scalable without significant loss in yield. It can be applied to the fluorination of biologically active molecules *via* direct C-H functionalization. Further experimental and/or theoretical study would be required to further elucidate the mechanism.

Chapter 4

Theoretical studies

4 Theoretical studies

4.1 Introduction

Non-covalent interactions are fundamental to asymmetric catalysis, as these interactions bring the substrates to close proximity with the chiral catalyst in the transition state. As a result, differences in energy between diastereomeric transition states that lead to opposite enantiomers of the product exist, this enables enantioselective reaction to occur.

Non-covalent interactions that are important in asymmetric catalysis include hydrogen bonds and aromatic interactions. The importance of aromatic interactions in controlling stereoselectivity has been highlighted by Houk and Krenske.[223] Hydrogen bonds are widely exploited as non-covalent interactions in asymmetric catalysis.[310, 311] Halogen bonding has often been regarded as parallel to hydrogen bonding, in terms of directionality and strength,[312] and has been extensively utilized in supramolecular chemistry[17] and biology[19, 21]. However, the use of halogen bonding in asymmetric catalysis is more scarcely documented relative to hydrogen bonding.

This chapter begins with our theoretical investigation of chiral guanidine catalyzed asymmetric reactions; follow by other studies of halogen bonds with focus on the role of halogen bonds in catalysis.

4.2 Theoretical studies on guanidine as organocatalysis

4.2.1 Guanidine-catalyzed enantioselective desymmetrization of meso-aziridines

We reported an enantioselective desymmetrization of aziridine catalyzed by amino-indanol derived chiral guanidines (**Scheme 4.1**).[313] The catalyst bearing the TBDPS (*tert*-Butyl diphenyl silyl) substituent was found to give the best enantioselectivity
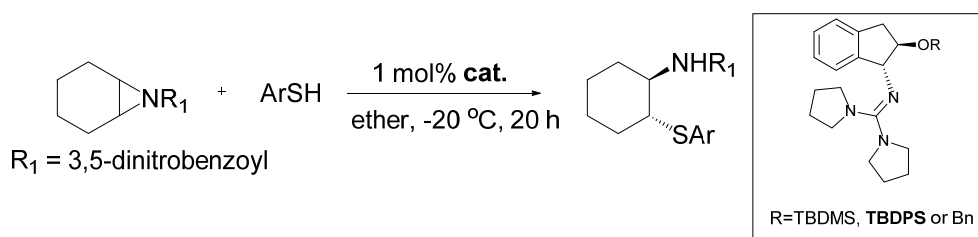
Scheme 4.1 General reaction scheme for Guanidine-catalyzed enantioselective desymmetrization of meso-aziridines. The catalysts that were investigated were given in the box.

The mechanism is proposed to involve the deprotonation of thiol follow by nucleophilic ring opening of the *meso* aziridine. Two plausible pathways could be envisaged: In the first mechanism, the thiol is not fully deprotonated, instead it is hydrogen bonded to the catalyst and the nucleophile-catalyst complex attacks the aziridine. (Mechanism 1 in **Figure 4.1**). In the second mechanism, the nucleophile is replaced with the aziridine which is hydrogen bonded to the catalyst, the thiolate attacks the aziridine-catalyst complex. (Mechanism 2 in **Figure 4.1**)
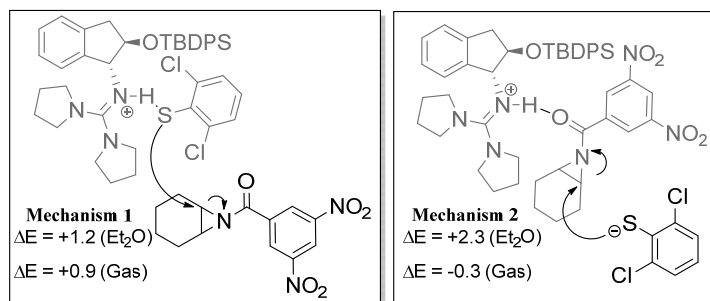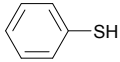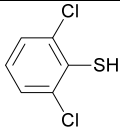
Figure 4.1 Possible mechanisms for aziridine-opening reaction. $\Delta E = E_{SS} - E_{RR}$ (kcal/mol), where E is the electronic energy at M06-2X/6-311+G(2df,2p)//B3LYP/6-31G(d,p)

Theoretically, in order to determine the dominant mechanism that is operating, one would have to calculate all relevant stationary points along both mechanisms that lead to the product. However, the large size of this system renders a detailed computational study infeasible within a reasonable period of time. Therefore, we decided to predict the dominant mechanism based on the ability of each mechanism to predict trend in experimental enantioselectivity with different thiols.

The calculated results show that Mechanism 2 is able to reproduce qualitatively the observed trend in enantioselectivity with variation of substituent on the aryl group of the thiols, but Mechanism 1 could not (**Table 4.1**). Therefore, it is likely that the desymmetrization goes through Mechanism 2.

Table 4.1 Calculated results of Mechanism 1 and 2 for different thiols and experimental $\Delta G^{\ddagger}$ and enantiomeric ratio.

ArSH	Mechanism 1 ΔE /kcal mol^{-1}	Mechanism 2 ΔE /kcal mol^{-1}	Experimental $\Delta G^{\ddagger}$	Experimental *e.r*
(phenyl)—SH	+2.4	0.0	+0.48	72:28
Br—(phenyl)—SH	+2.6	+0.7	+0.68	79.5:20.5
Cl—(phenyl,2,6-diCl)—SH	+1.2	+2.3	+1.60	96:4

$\Delta E = E_{SS} - E_{RR}$ (kcal mol^{-1}), where E is the electronic energy at M06-2X/6-311+G(2df,2p)//B3LYP/6-31G(d,p).

The TS structure of mechanism 2 in **Figure 4.2** provides a basis for rationalizing the enantioselectivity observed. Despite the much shorter hydrogen bond in TS$_{SS}$ (1.859 Å), it is less stable than TS$_{RR}$ (2.141 Å). This is ascribed to larger steric repulsion which arises from bringing the aziridine and thiol closer to the catalyst. The large increase in enantioselectivity when the

phenyl group of the thiol is substituted with chlorine at the 2- and 6- positions can be attributed to an increase in steric repulsion between the two chloro-substituents and neighboring atoms of the catalyst–aziridine complex. The number of neighboring atoms within 5 Å to both chloro-substituents is 29 in TS_{SS} (average: 4.1 Å) and 25 in TS_{RR} (average: 4.3 Å).11 As chlorine (1.75 Å) has a larger van der Waals radius relative to hydrogen (1.20 Å), destabilization of TS_{SS} relative to TS_{RR} will be more significant in Ar = 2,6-$Cl_2C_6H_3$ than Ar = Ph and contributes to the observed increase in enantioselectivity.
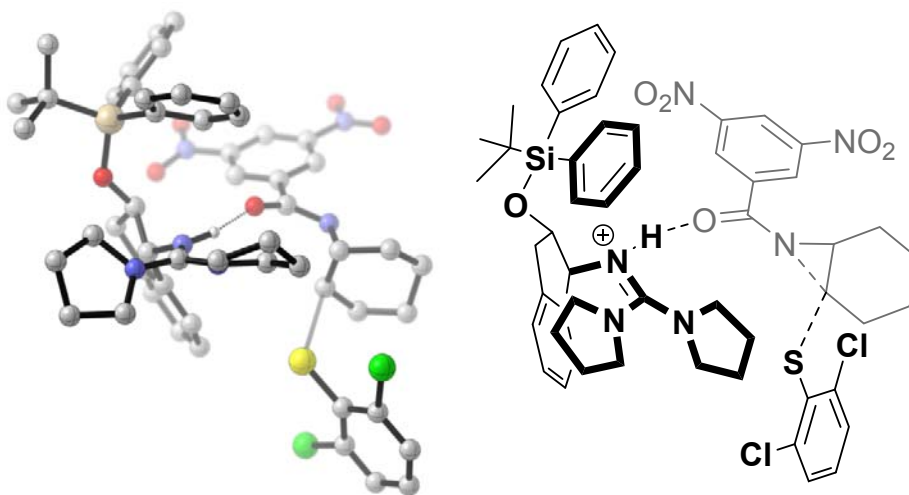
Figure 4.2 Lowest energy TS structure for (*R,R*) product for mechanism 2 optimized at RB3LYP/6-31G(d,p). On the right is the ChemDraw representation of TS_{RR}

4.2.2 Brønsted Base-Catalyzed Tandem Isomerization–Michael Reactions of Alkynes: Synthesis of Oxacycles and Azacycles

We reported an efficient synthesis of oxacycles and azacycles using Brønsted-base catalyzed tandem alkyne isomerization-Michael reaction,[314] which is an extension of a work by our group.[315] Amide **15** was used to test the possibility of obtaining atropisomeric lactam directly from chiral Brønsted base-catalyzed asymmetric tandem isomerization-cyclization. The chiral guanidine-catalyze reaction and subsequent purification led to axially chiral lactams **17** (Table 3). High enantioselectivities of lactam **17** were observed when THF was used as the solvent in this reaction (89% ee).
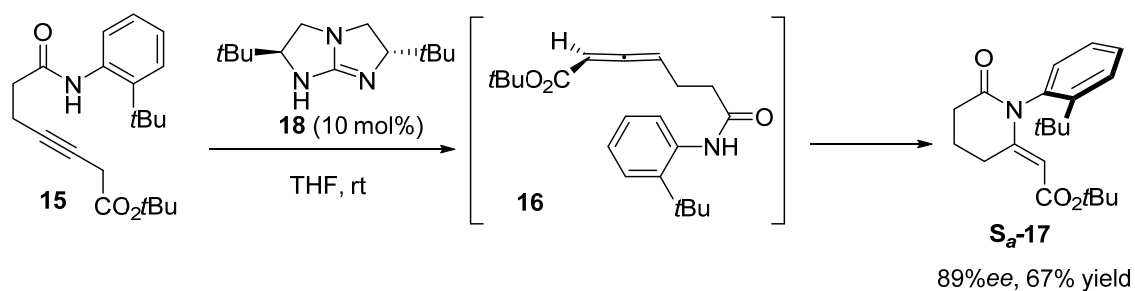
Scheme 4.2 Chiral guanidine-catalyzed tandem isomerization-Michael reaction for the synthesis of axially chiral lactams.

Difficulty in obtaining single crystals for **17**, together with the lack of heavy atoms, which could impede absolute configuration determination *via* single crystal X-ray diffraction[316] motivated us to derive the absolute configuration *via* theoretical approach. Reliable specific optical rotation can be calculated from density functional theory (DFT) by considering thermally accessible conformations and with judicious choice of basis set and functional coupled with solvation model to account for solvent effects.[317] The specific optical rotation for S_a-**17** configuration calculated is -57.8, which agrees well with the -64.1 obtained experimentally. For the methodology to assign S_a and R_a to their respective enantiomer, please refer to **Figure 4.3**.
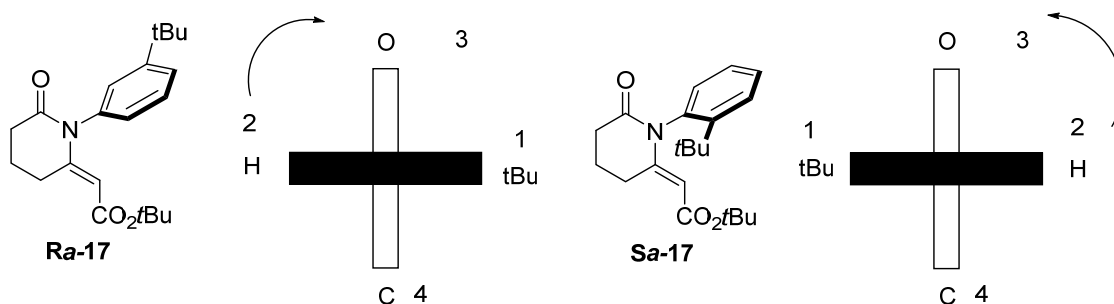
Figure 4.3 Methodology to assign axial chirality. 1 – 4 indicates priority. Arrows indicate whether the sequence 1 to 4 is clockwise which gives R*a* or anti-clockwise which gives S*a*.

In our study of the reaction pathway, geometries (both TS structures and equilibrium structures) were optimized at CPCM/RB3LYP/6-31+G(d,p). The CPCM implicit solvation model was used to simulate the effect of THF. Gibbs free energy and enthalpy were derived from the sum of SCF energy at CPCM/RM06-2X/6-311+G(2df.2p) and the required corrections derived from frequency calculation at CPCM/RB3LYP/6-31+G(d,p). The tight convergence criteria and ultrafine integration grid was used. For thermochemistry calculation, temperature used was 298.15K and pressure is 1 atm.

The pathway leading to the product **17** comprised of three equilibrium structures (the reactant **16**, the product **17** and an intermediate **Enol-Ra/Sa**) and two TS structures (**Figure 4.4** and **Figure 4.5**). Two distinct steps are required to form the product **17**, the first step is the intramolecular cyclization of the allene **16**, and the second is the intramolecular proton transfer of the enol intermediate to the product.

The first step (intramolecular cyclization of the allene) is the key step which determines the enantiomeric purity of the product **17**. If we assume the validity of Curtin-Hammett kinetics,[318-320] only the relative Gibbs free energy/enthalpy of the diastereomeric TS structures needs to be considered to determine the enantioselectivity of the cyclization step. **TS1-S*a*** which leads to the major enantiomer experimentally is more favourable in terms of Gibbs energy than

TS1-R*a* by 3.7 kcal/mol. The same conclusion is obtained if we consider the enthalpy (**TS1-S***a* is more favourable than **TS1-S***a* by 2.2kcal/mol). Therefore, the *e.r* predicted by DFT is 477:1 (**S**$_a$-**17**: **R**$_a$-**17**, if we consider Gibbs free energy at 298.15K). This implies that the cyclization should proceed with virtually absolute retention of enantiomeric purity of the allene **16** and the enantiomeric purity is only limited by the allene formation step (**15** to **16**).
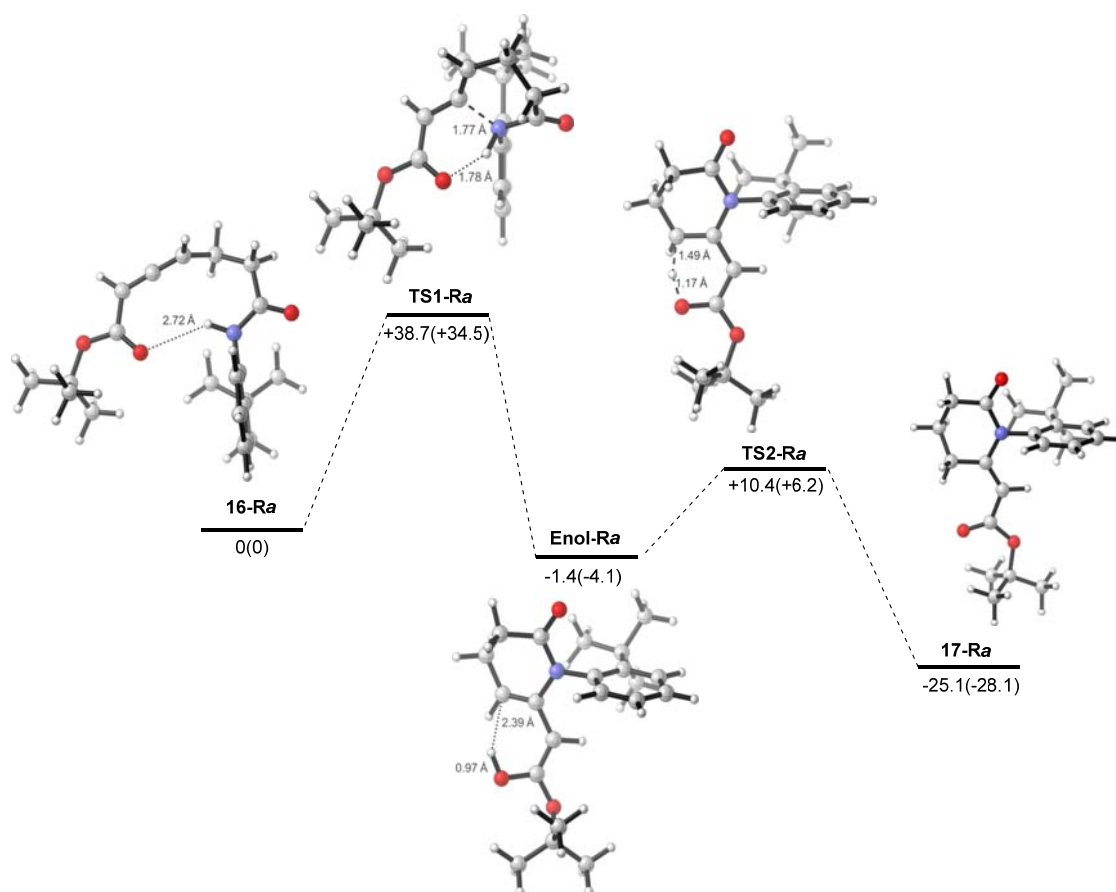
Figure 4.4 Reaction path leading to R$_a$ product. Relative Gibbs free energy and enthalpy are given in kcal/mol. Enthalpy is in parentheses and Gibbs free energy is not.

The Gibbs free energy/enthalpy profile for the tautomerization state is similar for both enantiomers. The barrier for proton transfer is about 12kcal/mol which is lower than the cyclization step. Thus, the cyclization step is rate determining.
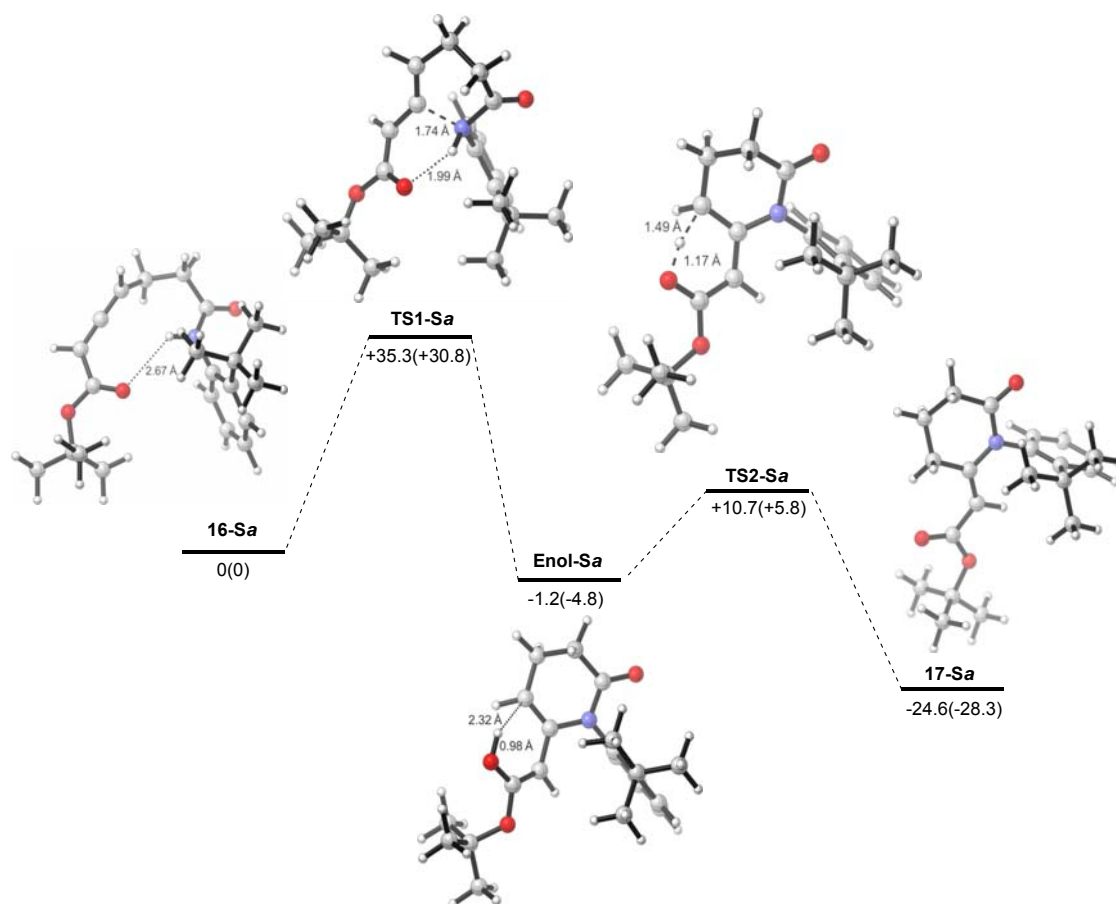
Figure 4.5 Reaction path leading to S$_a$ product. Relative Gibbs free energy and enthalpy are given in kcal/mol. Enthalpy is in parentheses and Gibbs free energy is not.

In conclusion, we have demonstrated the feasibility of using DFT calculation to assign absolute configuration and according to DFT calculation the cyclization of allene **16** proceed in an enantiospecific manner.

4.2.3 Biomimetic Enantioselective Decarboxylative Reactions

We reported the generation of thio-ester enolate *via* the decarboxylation of malonic acid half thioester (MAHT).[321] Computational study was conducted, in conjunction with experimental study, to provide evidences for whether decarboxylation precedes nucleophilic addition or *vice versa*.
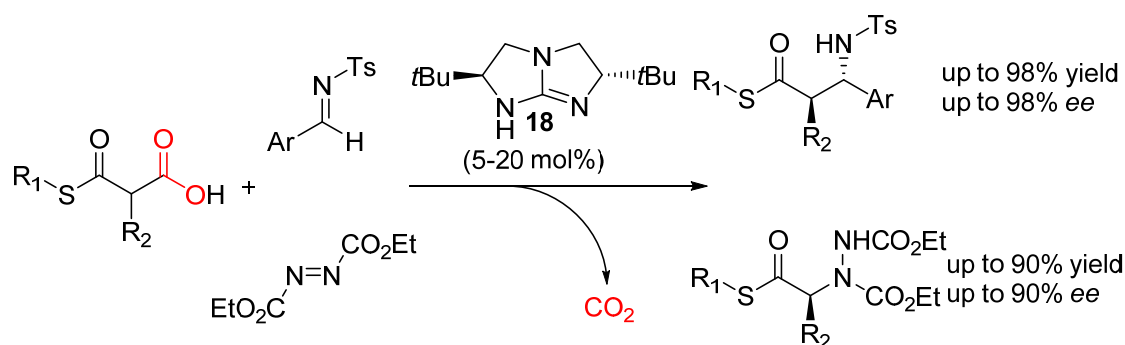
Scheme 4.3 Summary of the decarboxylative Mannich reaction

Two possible reaction pathways could be envisaged: a decarboxylation/nucleophilic addition pathway in which MAHT undergoes decarboxylation first to form a thioester enolate and a nucleophilic addition/decarboxylation mechanism in which nucleophilic addition precedes decarboxylation. The latter is supported by previous studies.[322, 323]

The calculations were performed at CPCM/M06-2X/6-31(d) for geometry optimization. The solvent THF for used for the CPCM implicit solvent model. The Gibbs free energies reported were obtained as a sum of single point calculation at CPCM/M06-2X/6-311++G(2df,2p) on the CPCM/M06-2X/6-31G(d) geometries and thermal correction to Gibbs free energy from the frequency calculation at CPCM/M06-2X/6-31(d). The tight convergence criteria and ultrafine integration grid as implemented in Gaussian 09 was used.
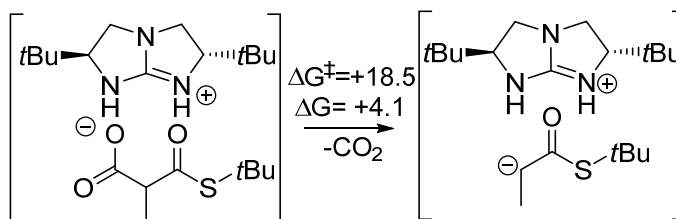
Scheme 4.4 Kinetic barrier and thermodynamics for the decarboxylation of MAHT-catalyst complex

In this study, we chose a TS structure in which the *tert*-Butyl guanidine catalyst **18** binds to the imine and enol of MAHT through hydrogen bonds (**Scheme 4.5**) because we have previously showed that such a side-on TS structure (dual mono-dentate hydrogen bonding to substrates) is more favorable than the corresponding face-on TS structure (single bidentate hydrogen bonding, for geometrical description of side-on and face-on, see **Figure 4.7**).[324]

In this case, several conformations can be conceived for the side-on TS structure due to the presence of multiple hydrogen-bond acceptor sites on the enol of the MAHT (i.e., the O atoms in the thioester functional group, tosyl protecting group, and carboxylate group). We assumed that the highly negatively charged carboxylate group will form a stronger hydrogen-bonding interaction with protonated guanidine catalyst **18**; therefore we restricted our present computational study to the side-on conformation as shown in **Scheme 4.5**.

Configuration	$\Delta G_{Mannich}^{\ddagger}$(kcal/mol)
1*R*,2*S*	**+3.95**
1*S*,2*R*	+8.90
1*S*,2*S*	+7.85
1*R*,2*R*	+13.6

*Bold configuration gave the absolute configuration determined by *X*-ray after decarboxylation
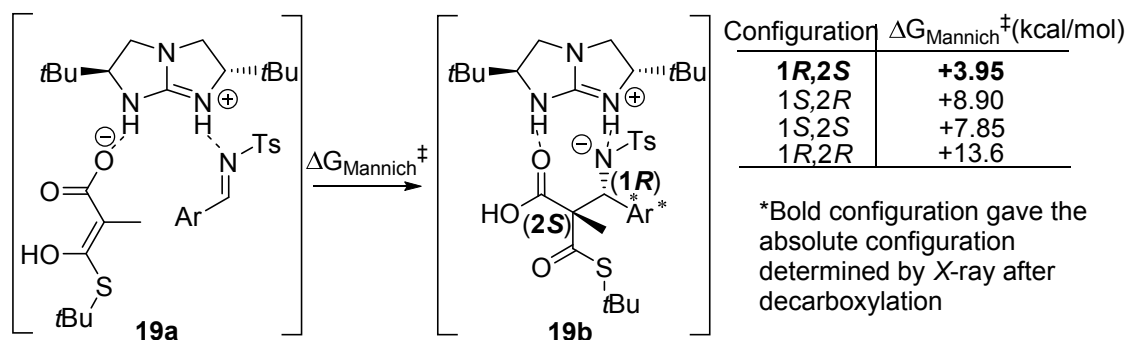
Scheme 4.5 Enantioselective Mannich step

On the basis of $\Delta G^{\ddagger}$ values, DFT calculations indicated that nucleophilic addition precedes decarboxylation. Decarboxylation of MAHT has a barrier of 18.5 kcal mol^{-1} (**Scheme 4.4**), which is substantially higher than both the barriers for the Mannich reaction (**Scheme 4.5**) and tautomerization (**Scheme 4.6**). In addition, under the reaction conditions, the anion that is relevant to **19d** was characterized by using electrospray ionization (ESI) mass-spectrometric analysis. The mass-to-charge ratio (m/z) and isotopic patterns are consistent with the proposed anionic species **20a/20b** (**Figure 4.6**). Our results strongly support a mechanism in which nucleophilic addition precedes decarboxylation. Rouden and co-workers reported a similar observation in triethylamine- catalyzed decarboxylative Mannich reactions.[325]
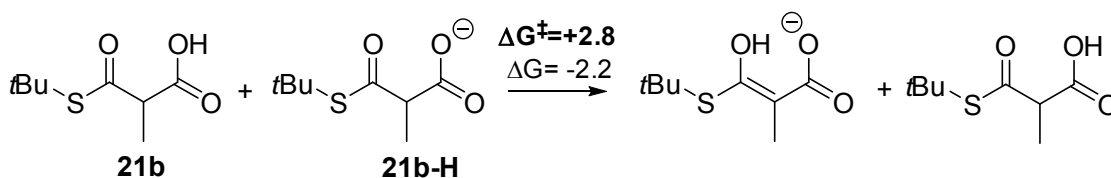
Scheme 4.6 Tautomerization of **21b**.
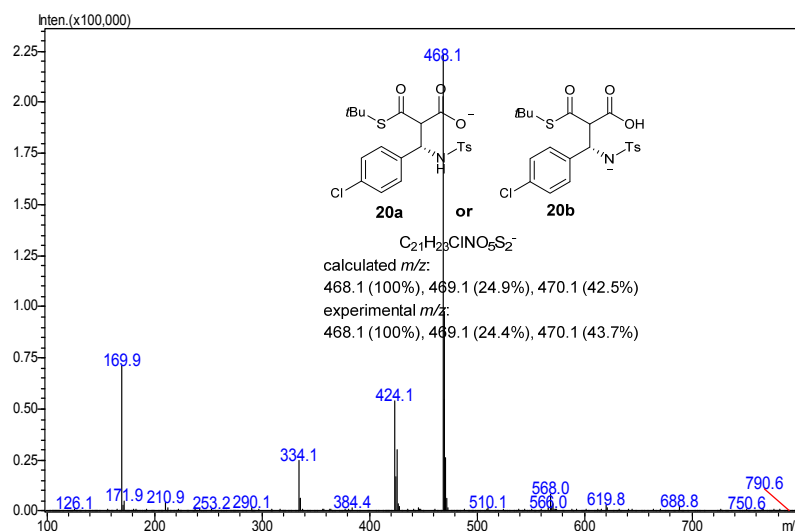
Figure 4.6 Detection of anion **20a** or **20b** by direct injection ESI-MS.

4.2.2.1 Further study on decarboxylation

DFT calculations suggest that the barrier to decarboxylation is fairly independent of the chemical environment of the TS structure. The $\Delta G^{\ddagger}$ value for the decarboxylation of **19d** is only 0.2 kcal mol^{-1} lower than that for MAHT (**Scheme 4.7**). On the basis of the relevant $\Delta G^{\ddagger}$, the rate-determining step is the decarboxylation, thus future attempts to increase the reaction rate should focus on tuning properties that can lower the $\Delta G^{\ddagger}$ value of decarboxylation.
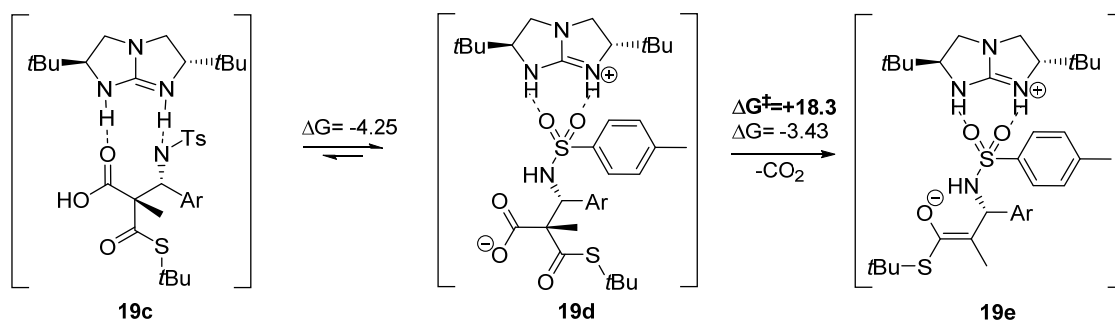
Scheme 4.7 Decarboxylation after Mannich Reaction. Ar = 4-ClC$_6$H$_5$. $\Delta G^{\ddagger}$ is the difference in Gibbs free energy between the transition states and the reactants. All units are given in kcal/mol. $\Delta G^{\ddagger}$ for the step linking **19b** and **19c** is +0.39 kcal/mol.

As a comparative study, we calculated the barrier of decarboxylation for the ester derivative of MAHT, **21a**. The results are tabulated in **Table 3.7** (A larger basis set was used for geometry optimized when compared to **Scheme 4.4**).

In all cases, **21a** has a higher barrier for decarboxylation relative to **21b**. As the reaction requires a low temperature of -10°C (65% *ee* at 0° vs. 92% *ee* at -10°C) to obtain good enantioselectivity, the increased barrier for substrate **21a** relative to **21b** renders it unsuitable for the enantioselective decarboxylation catalyzed by **18**.

From **Table 3.7**, the gas phase barriers are lower than those calculated with implicit solvation model. The choice of solvation model does not affect the calculated barrier significantly. The SMD model which includes non-electrostatic term predicts a higher barrier than CPCM and

PCM implicit solvation model. The Gibbs free energy of activation is lower than the enthalpy of activation as in the TS, there is an increased in entropy contribution from the CO_2 which is being dissociated from the catalyst.

Table 3.7 The barriers of decarboxylation of **21a** and **21b**
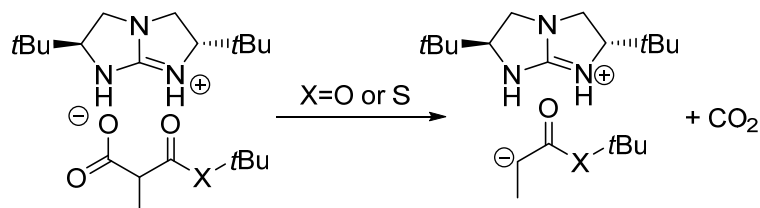
Level of theory	OH O $\overset{}{\bigvee}$ O $\overset{}{\bigvee}$ O-*t*Bu **21a**		OH O $\overset{}{\bigvee}$ O $\overset{}{\bigvee}$ S-*t*Bu **21b**	
	$\Delta G^{\ddagger}$	$\Delta H^{\ddagger}$	$\Delta G^{\ddagger}$	$\Delta H^{\ddagger}$
RM06-2X/6-311++G(d,p)//RM06-2X/6-31+G(d,p)	+22.1	+25.1	+17.7	+19.5
SMD-RM06-2X/6-311++G(d,p)//RM06-2X/6-31+G(d,p)	+24.1	+27.1	+18.3	+20.1
CPCM-RM06-2X/6-311++G(d,p)//RM06-2X/6-31+G(d,p)	+23.4	+26.4	+17.5	+19.3
PCM-RM06-2X/6-311++G(d,p)//RM06-2X/6-31+G(d,p)	+23.5	+26.5	+17.7	+19.5

$\Delta G^{\ddagger}$ and $\Delta H^{\ddagger}$ are barriers in kcal/mol calculated from the pre TS complex to the TS. Default convergence criteria and integration grid as implemented in Gaussian 09 A2 was used. Solvent used in implicit solvation model (PCM, CPCM and SMD) is THF.

4.2.4 Enantiodivergent and γ-Selective Asymmetric Allylic Amination

We disclosed an enantiodivergent and γ-selective asymmetric allylic amination catalyzed by bicyclic guanidine **18**.[326] This reaction presents two interesting features for theoretical study. Firstly, the reaction could proceed *via* a hetereo- DA (Diels-Alder) mechanism or it could be a sequence of two stepwise reactions. Secondly, the C=C configuration of the starting material has pronounce influence on which enantiomer is obtained.
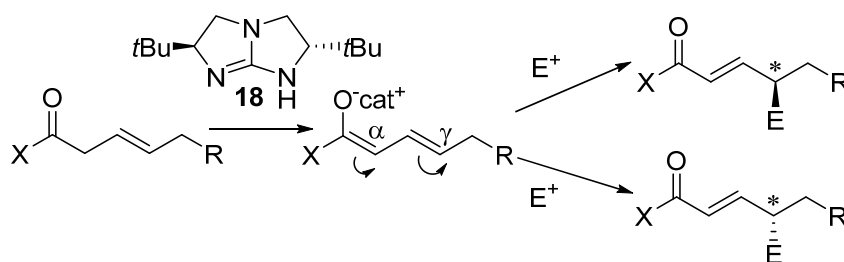
Scheme 4.8 Brønsted base catalyzed allylic addition.

To gain insight into the reaction, DFT calculations with the M06 functional[236] were performed. TS structures based on a side-on model[324] previously reported by our group and a hetero-DA mechanism proposed by Jøgensen[327] were located. Amongst the 58 conformations located for the TS structures of both mechanisms (**Figure 4.7**), those based on the DA-mechanism (face-on model) were higher in energy (9.5-32.4 kcal mol^{-1} relative to lowest-energy side-on TS) than those based on the side-on model. The DA TS structures are disfavored because of the weaker intermolecular interactions between dienolate and catalyst, and the 1,3-allylic strain in the *s-cis* dienolates. Side-on TSs are stabilized by stronger intermolecular interactions, in particular the interaction between the lone pair of electrons on the N atom of the diazocarboxylate with the σ* of the NH of the catalyst is especially strong. Side-on TSs based *s-cis* dienolates are generally higher in energy (5.3– 26.3 kcal mol^{-1} relative to lowest-energy side-on TS) compared to those based on *s-trans* dienolates; this is expected because of the unfavorable 1,3-allylic interaction in the *s-cis* enolates.
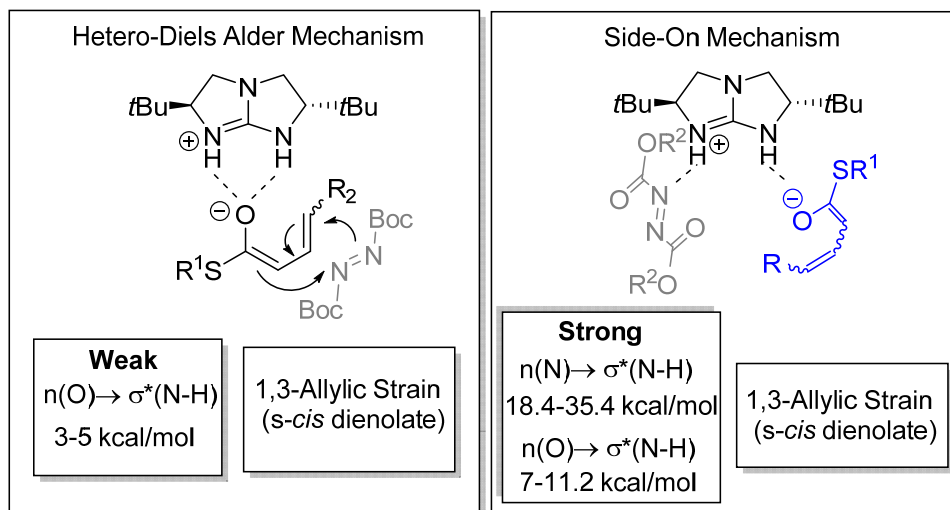
Figure 4.7 Plausible mechanisms. n(O) refers to the lone pair on O of dienolate, n(N) refers to the lone pair on N of diazocarboxylate. n(O)/n(N)→σ*(n-H) interaction energies are obtained from NBO analysis. Right: face-on model. Left: side-on model.
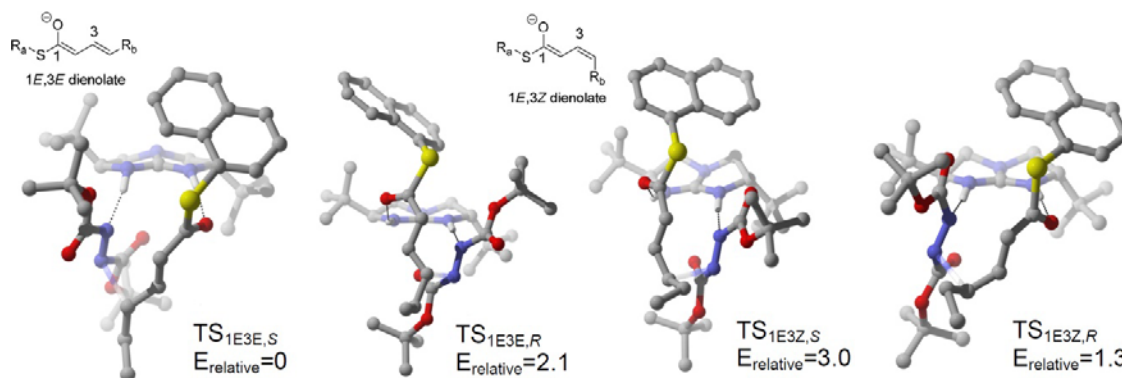
Figure 4.8 Most stable TS structures for side-on mechanism based on s-trans dienolate at SMD-RM06/6-311++G(2df,2p)//RM06/6-31G(d).

The side-on mechanism based on *s-trans* dienolates was tested against the experimental results. The trend in change of enantioselectivity with solvent and substituents correlates well to $\Delta\Delta E$ (**Table 4.2**), thus validating the calculations. Analysis of the TS structures (**Figure 4.8**) revealed that the energetically less favorable TS in both the *E* and *Z* unsaturated thioester have the naphthyl substituent of the thioester in the same quadrant as the *tert*-butyl substituent of the catalyst **18**, thus indicating that destabilizing interaction between these two groups plays a major

role in determining the relative energy of the transitions states leading to either *R* or *S* configurations. In contrast, the substituent on the C=C of the thioester is pointing away from the catalyst, and thus does not interact significantly with the catalyst. Its effect on the *ee* value should be minimal, and is consistent with experimental result that a variety of substituent on C=C could be used without significant change to the enantioselectivity. The inversion of the absolute configuration with the use of (*Z*)-β-unsaturated thioesters is also predicted by the side-on mechanism with the *s-trans* dienolate, $\Delta\Delta E^{\ddagger}$=-1.7 kcal mol^{-1}. It is consistent with both the inversion of the configuration and the lower *ee* value relative to the case in which the (*E*)-unsaturated thioesters were used (see **Table 4.2**).

Table 4.2 Comparison between DFT calculations and experimental results.
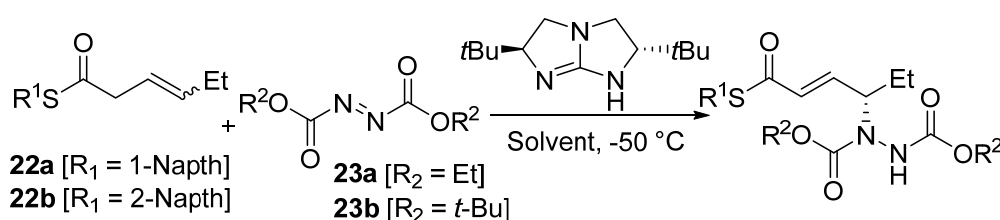
22a or 22b	23	Solvent[a]	Expt. %ee	Expt. $\Delta\Delta G^{\ddagger}$	Calculated $\Delta\Delta E^{\ddagger}$
22a(E)	23a	DCM	50	+0.5	+1.5
22a(E)	23b	DCM	73	+0.8	+1.7
22a(E)	23b	iPr$_2$O	90	+1.3	+2.1
22b(Z)	23b	MTBE[c]	74	-0.8	-1.7

[a] Solvent effects were modelled with IEFPCM calculation using radii and non-electrostatic terms for Truhlar and co-workers' SMD solvation model [b] $\Delta\Delta E^{\ddagger}$ (in kcal/mol) = $E_{TS,R}$-$E_{TS,S}$, E refers to the electronic energy of the TS structure at SMD-RM06/6-311++G(2df,2p)//RM06/6-31G(d) [c] Single-Point calculation was performed with iPr$_2$O instead of MTBE.

Inversion of the absolute configuration is intuitively explained by the more stable TS having the 1-naphthyl substituent pointing away from the *tert*-Butyl substituent of the catalyst.

The TS for the *S* configuration satisfied this condition for the *E* thioester. As the *Z* thioester has the opposite configuration at the carbon at which the chiral center is formed, the TS with the 1-naphthyl pointing away from *tert*-Butyl substituent of the catalyst became the TS with the *R* configuration, and hence inversion of the absolute configuration occurs (see **Figure 4.9**).
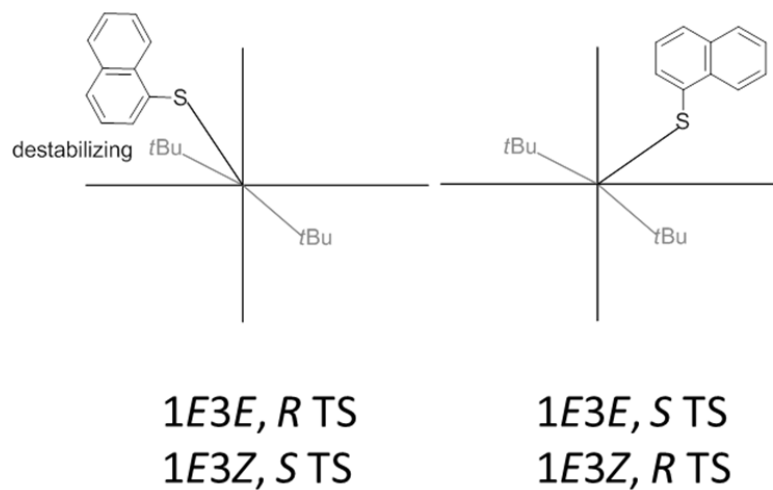
Figure 4.9 Illustrating the inversion of absolute configuration in product with C=C geometry.
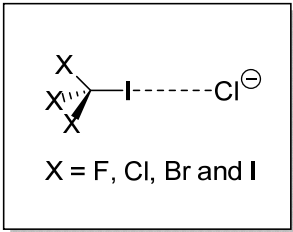
4.3 Theoretical studies on halogen bonding in catalysis

4.3.1 Sigma Hole and Halogen bond

The sigma hole model was proposed by Politzer and co-workers to explain the apparently contradictory nature of halogen bonding.[205] Politzer and co-workers attributed sigma hole to a depletion of electronic charge, and according to them, halogen bonding is an electrostatically driven attractive interaction between a positive sigma hole on a covalently-bonded halogen atom and a negative site.[328] Positive correlation between $V_{S,max}$ (the most positive surface potential on the sigma hole)[329] and the binding energies of halogen bonded complex is reported mainly by Politzer groups.[330-333] An exception to the correlation between $V_{S,max}$ and binding energies was reported by Huber and co-workers. [334]

An unexpected trend in halogen bonding: electron withdrawing groups weaken halogen bonding, more specifically C-I and chloride halogen bond (**Figure 4.10**) was reported by a computational study of Huber and co-workers. As the sigma hole $V_{S,max}$ generally increases with the electronegativity of the substituent (X in **Figure 4.10**), Huber and co-workers claimed that the trend for the halogen bond between iodine and chloride is unexpected.

X	$V_{s,max}$	ΔE_{int}	I-Cl distance
F	+28.5	-29.3	2.77
Cl	+27.4	-33.5	2.69
Br	+26.6	-35.6	2.67
I	+25.5	-37.0	2.65

X
X⁴⁴—I - - - - - Cl⁻
X
X = F, Cl, Br and I

Figure 4.10 Halogen bonded complexes of interest in this study. Huber and co-workers results are given. $V_{S,max}$ and E_{int} are in kcal/mol. E_{int} is calculated at MP2/TZ2P. I-Cl distance is in Å. I-Cl is calculated with DFT (PBE/TZ2P).[334]

We have repeated the calculation with a different DFT functional and basis sets, namely the M06/aug-cc-pVTZ[335-338] level of theory as implemented in Gaussian 09 A2 for geometry optimization. For Br and I, the SDB pseudopotential was used.[339] At M06/aug-cc-pVTZ, the halogen bond lengths are longer than those reported by Huber and co-workers. For X=Cl, Br and I, the difference in bond length is +0.03Å, but for X=F a difference of +0.07 Å was observed.

Table 4.3 Bond length and LMOEDA results for relevant halogen bonded complexes
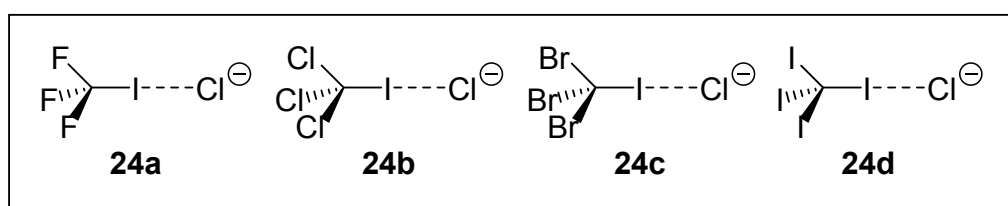
CX$_3$I-Chloride	24a	24b	24c	24d
[a]Distance of I-Cl/Å (Huber *et al*)	2.77	2.69	2.67	2.65
[b]Distance of I-Cl/Å	2.84	2.72	2.70	2.68
[c]$\Delta E_{interaction}$/kcal mol^{-1}	-23.7(-25.2)	-28.4(-30.3)	-27.7(-30.5)	-29.5(-31.5)
Electrostatic energy/kcal mol^{-1}	-26.0(-26.0)	-28.2(-28.1)	-28.1(-28.7)	-27.4(-27.3)
Polarization energy/kcal mol^{-1}	-31.5(-31.5)	-47.8(-48.0)	-51.1(-50.4)	-55.7(-55.9)
Exchange energy/kcal mol^{-1}	-55.0(-54.9)	-74.3(-74.2)	-78.3(-78.3)	-83.2(-83.2)
Repulsion energy/kcal mol^{-1}	+93.1(+93.0)	+127.8(+127.7)	+135.2(+135.0)	+144.0(+144.0)
MP2 dispersion/kcal mol^{-1}	-4.3(-5.8)	-5.9(-7.7)	-5.3(-8.0)	-7.0(-9.0)
HF Interaction energy/ kcal mol^{-1}	-19.4(-19.5)	-22.5(-22.6)	-22.4(-22.5)	-22.4(-22.5)

For Br and I the SDB pseudopotential was used. Number without parentheses includes CP)correction for BSSE, number in parentheses excludes CP correction [a] from Huber and co-workers[334] [b] Calculated at M06/aug-cc-pVTZ as implemented in Gaussian 09 A2 [c] $\Delta I_{interaction}$ is obtained from the LMOEDA analysis at SCS-MP2/aug-cc-pVTZ as implemented in GAMESS[340, 341].

The trend of increasing interaction energy from F to I could be observed when counterpoise (CP) correction[342] for basis set superposition error (BSSE) is not included (**Table**

4.3), however the difference between **24b** and **24c** is much smaller than that calculated by Huber and co-workers. CP correction breaks the trend; **24b** becomes more stable than **24c**. However, the reliability of CP correction, which typically overestimate BSSE,[343] with a triple zeta basis set is questionable. From our calculations, the interaction energies are much smaller in magnitude when compared to those reported by Huber and co-workers.

Localized Molecular Orbital energy decomposition analysis (LMOEDA)[344] as implemented in GAMESS was applied to the four halogen bonded complexes (**24a-24d**), the results are tabulated in **Table 4.3**. In LMOEDA, the interaction energy is decomposed into five terms, namely electrostatic, exchange, polarization, repulsion, and dispersion energy. The only term that is significantly affected by CP correction for BSSE is the dispersion energy. This may be due to the overestimate of BSSE by the CP method. It should be noted that arguments against energy decomposition analysis (EDA) are advanced by some in the literature. For instance, Politzer and co-workers claim that only the total binding energy is a physical observable, but not its components whatever they maybe.[345] In addition, they argued that electrostatic and polarization terms cannot be totally decoupled from each other. Detailed arguments on the physical meaningfulness of EDA are beyond the scope of this thesis. We would attempt to use LMOEDA and chemical intuition to provide insight into the nature of halogen bonds in the four complexes being considered in this section.

Assuming the validity of the LMOEDA scheme, one immediate conclusion that can be drawn from **Table 4.3** is dispersion interaction is the key energetic term that renders **24d** more stable than **24b** and **24c** in terms of interaction energy (compare the HF interaction energies which exclude dispersion interactions).

Regarding the electrostatic energy, the smaller value of **24a** relative to the rest of the complexes (**Table 4.3**) appears to be counter-intuitive due to the high electronegativity of fluorine.

However, one should take into consideration that the interaction energy of **24a** is smaller than the rest of the complexes (**24b-d**) in the first place; therefore comparison of the absolute value may not be meaningful. Instead, we proposed that dividing each individual term with the interaction energy should reveal more meaningful trend. The results for electrostatic and polarization energy are presented in **Figure 4.11**. After normalization, it could be seen that electrostatic energy (expressed in percentage of interaction energy) is now the largest for **24a** (X=F) which is consistent with the highest electronegativity of fluorine and also the largest $V_{S,max}$, while **24d** (X=I) has the smallest percentage. The polarization energy as a percentage of the interaction energy increases with increasing polarizability of the halogen bond donor component (from CF_3I of **24a** to CI_4 of **24d**).
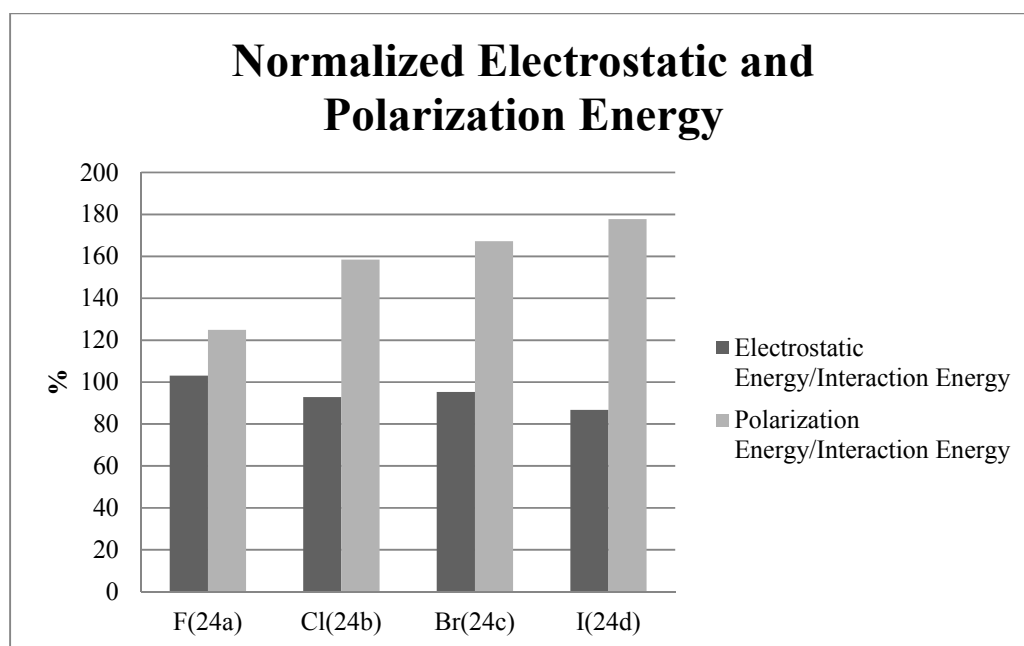
Figure 4.11 Electrostatic and polarization energy are expressed in percentage of interaction energy (e.g. electrostatic energy/interaction energy × 100%)

Next, we study the effect of lengthening the iodine-chloride halogen bond on the various terms in the LMOEDA calculation. Relaxed potential energy surface scans were performed on **24a** and **24d**. LMOEDA was then performed on **24a** and **24d** at various iodine-chloride distances.

The results for the repulsion and exchange energies are shown in **Figure 4.12**. The repulsion and exchange energy (which is considered as a single term in the Kitaura-Morokuma EDA[346]) decreases exponentially with increasing halogen bond length from their respective equilibrium distance. At about 1.8 times the equilibrium distance, contributions from the exchange and repulsion terms are negligible. Consistent with the short range nature of exchange and repulsion, this is expected.
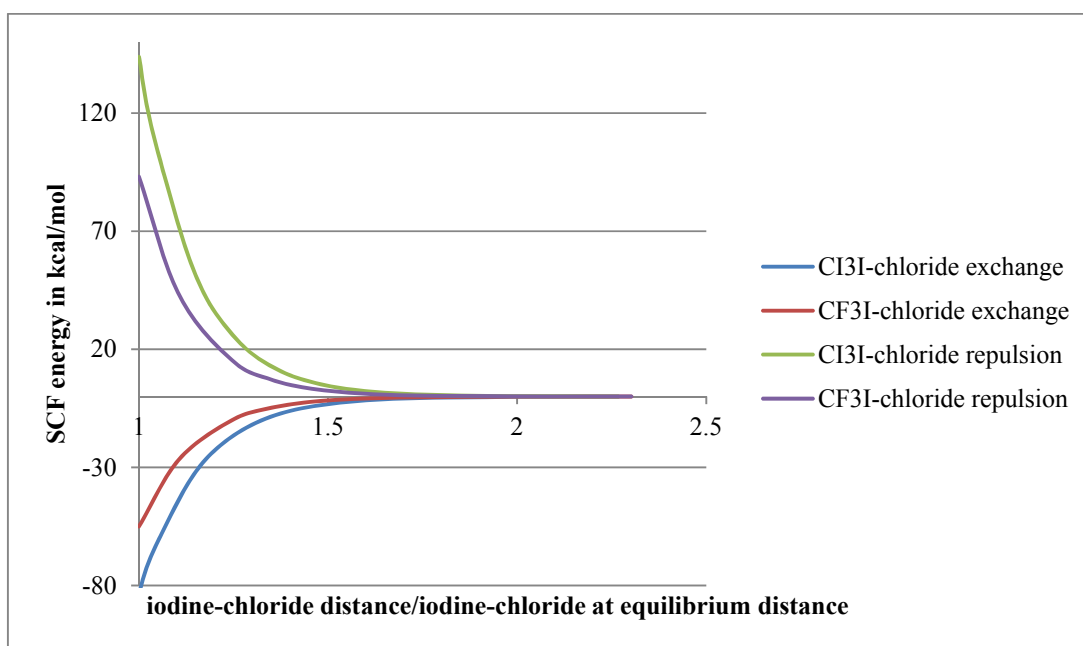
Figure 4.12 Electrostatic energy of LMOEDA for **24a** (CF$_3$I-chlroide) and **24d** (CI$_3$I-chloride) as a function of fraction of iodine-chlorine distance from its equilibrium distance.

Figure 4.13 summarized the results for the electrostatic energy. The electrostatic energy persists even beyond 2 times the equilibrium distance, thus indicating the importance of electrostatic interaction in guiding the anionic halogen bond acceptor (chloride in this case) to the halogen bond donor (the Lewis acid, CF$_3$I and CI$_4$). The high electronegativity of fluorine is likely to result in the crossover of electrostatic energy as observed in **Figure 4.13** at extended iodine-chloride distance. The V$_{s,max}$ of the sigma hole in **24a** is larger than **24d**, which correlates to the larger electrostatic energy of **24a** over **24d** at about 1.1 times the equilibrium distance. One

possible conclusion that can be drawn is that sigma hole is important in guiding the halogen bond acceptor toward the donor, at least in this case. This may be related to the dynamics of halogen bond formation. However, given that this study is not exhaustive, the above hypothesis remains largely speculative in nature.
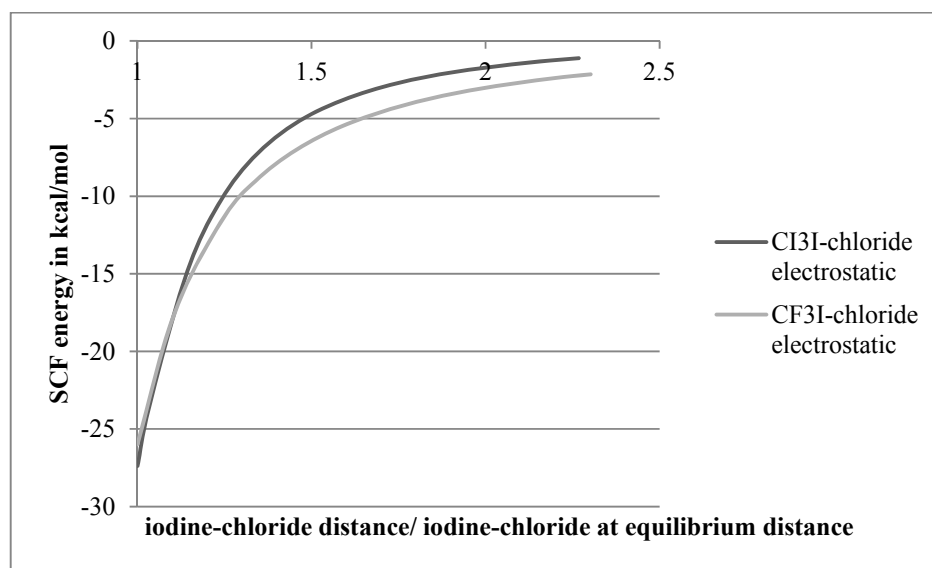
Figure 4.13 Electrostatic energy of LMOEDA for **24a** (CF$_3$I-chlroide) and **24d** (CI$_3$I-chloride) as a function of fraction of iodine-chlorine distance from its equilibrium distance.

The result for polarization energy is shown in **Figure 4.14**. The polarization energy for **24d** is larger than **24a** at all distance considered here. Similar to the electrostatic energy, the polarization energy has influence at a larger distance than exchange-repulsion. It is important for **24a** and **24d** at distance that is about 2 times the equilibrium distance.
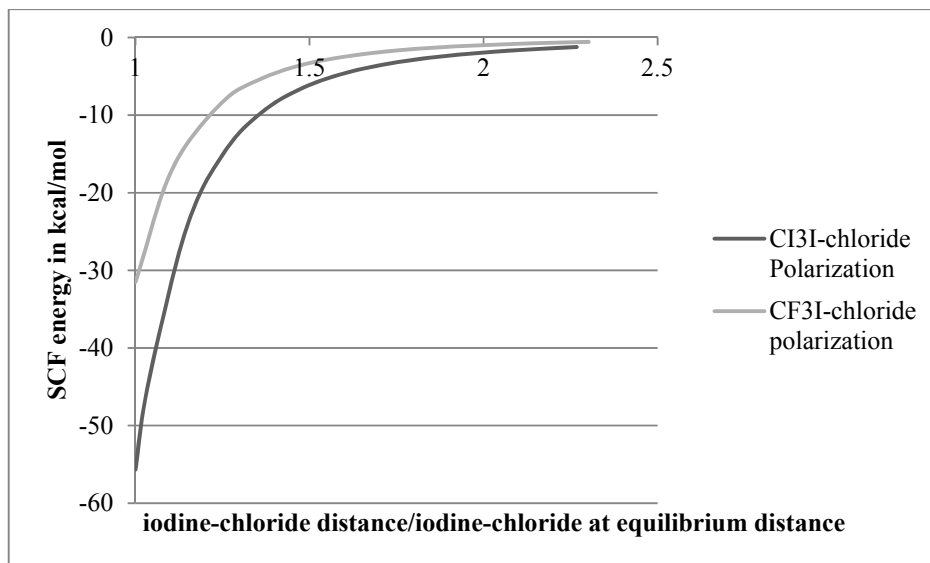
Figure 4.14 Polarization energy of LMOEDA for **24a** (CF$_3$I-chlroide) and **24d** (CI$_3$I-chloride) as a function of fraction of iodine-chlorine distance from its equilibrium distance.

In conclusion, a combination of polarization and electrostatic energy are important attractive interactions for the halogen bonded complex **24a** and **24d** at long distance (about 2 times from equilibrium distance). The sigma hole may be important in bringing the halogen bond partners together at long distance.

To end this section, we note that the "unexpected" trend observed by Huber and co-workers does have precedent in the literature. For instance, the Lewis acidity of BX$_3$ (X=F, Cl, Br and I) increases from F to I, *i.e.* BI$_3$ is the strongest Lewis acid. One can refer to the Gutmann–Beckett method to verify this.[347, 348] As halogen bond is a subset of Lewis acidic interaction, a similar trend should be expected.

4.3.2 Halogen Bonding in pentanidium catalyzed sulfenate

4.3.2.1 Introduction

Various groups have demonstrated the feasibility of halogen bonding in catalyzing/promoting chemical reactions. For instance, Bolm and co-workers reported the use of 1-haloperfluoroalkane as catalysts for reduction of 2-substituted quinolones with Hantzsch esters as the reducing agent.[216] The group of Huber has been active in the development of organocatalysts which exploit halogen bond as a form of Lewis acid.[217, 218, 349, 350] However, the use of halogen bonding in asymmetric catalysis is more scarcely documented relative to hydrogen bonding.

Recently, our group developed structurally novel pentanidiums[351, 352] based on quaternized sp^2-hybridized N-atoms[353-356] as phase-transfer catalysts (PTC). The R groups of pentanidiums are highly amenable to variation. As an extension of our previous work, we introduced halogenated aryl as R groups (**25b** and **25c**) to explore the potential of halogen bonding in asymmetric synthesis of sulfoxides under phase transfer conditions catalyzed by this new class of pentanidiums (**Figure 4.15**).
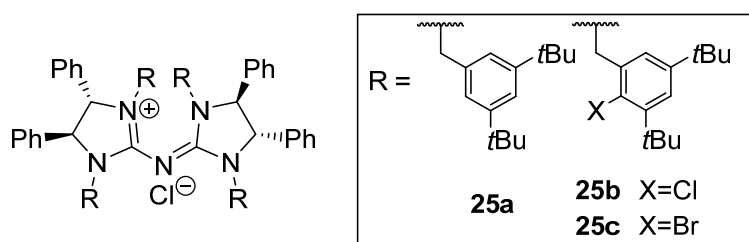
Figure 4.15 Novel pentanidium based phase-transfer catalysts

In this theoretical study, we investigate the possibilities of halogen bonding as controlling elements in asymmetric phase transfer catalysis. In particular, a reaction in which optically active sulfoxides is synthesized through the nucleophilic displacement of bromide with sulfenate.

Optically active sulfoxides are extensively used as chiral auxiliaries, chiral ligands for metal complexes and organocatalyst.[357-361] They are also invaluable in the pharmaceutical industry.[362]

Currently, two main strategies for the synthesis of enantioenriched sulfoxides exist – nucleophilic substitution of nonracemic sulfenates (e.g. Andersen method) and oxidation of prochiral sulfides. In 1984, Kagan's and Moderna's groups independently reported the asymmetric sulfide oxidation *via* modified Sharpless epoxidation.[363-365] Following the success of these Titanium-based catalysts, many practical and efficient metal-based variations for asymmetric sulfide oxidation methods have been reported.[360] Recently, a highly enantioselective organocatalytic sulfoxidation with aqueous H_2O_2 as oxidant has been achieved by the List's group.[366]

In the classical Andersen method and its variants, the reactive sulfur center is electrophilic. Complementary to these methodologies, the reactive sulfur center could be rendered nucleophilic through the generation of sulfenates[367-370] which has the structure [R-S-O]-. The use of sulfenates has emerged as a viable method for the synthesis of sulfoxides.[371-374] Pertinent to the synthesis of non-racemic sulfoxides *via* sulfenates, diastereoselective methodology has shown significant advancement.[375-381] However, reports which exploit sulfenates in catalytic asymmetric synthesis of sulfoxides remain scant.[382-384]

Thiophene derivatives are important heteroaromatic compounds in the pharmaceutical industry.[385-389] This coupled with the fact that the synthesis of optically active sulfoxides containing thiophene group has not been well developed motivated us to investigate enantioselective synthesis of such compounds.

Our strategy was to generate the nucleophile – sulfenate – *via* a retro-Michael reaction of **26 (Scheme 4.9)** under basic condition. The anionic sulfenate is expected to interact strongly with

the cationic catalyst, especially in a solvent of low polarity. Subsequently, the sulfenate reacts with the electrophile – benzyl bromide – *via* a nucleophilic substitution. In the nucleophilic substitution transition state (TS), the negative charge of the sulfenate is partially transferred to the Br leaving group. This renders the Br a potential Lewis base, in the TS, and therefore it could be stabilized by interaction with a Lewis acid (LA), for instance by halogen bonding with the bromobenzene moiety in catalyst **25c**. The ionic halogen bonding between bromide and bromobenzene could amount to 4.1 kcal/mol of interaction energy. Related activation of C-Cl and C-Br bonds *via* halogen bonding has been reported by Huber and co-workers.[217, 218]
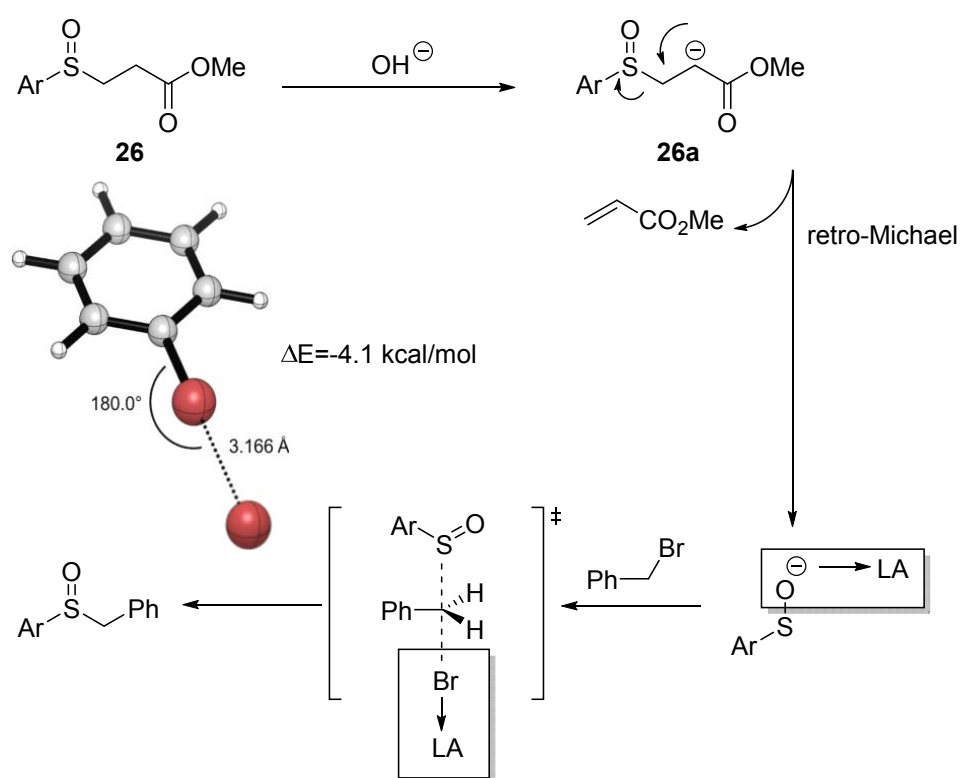
Scheme 4.9 Hypothesized pathway. LA denotes Lewis acid. Δ E is determined at MP2/aug-cc-pVTZ (CP corrected for BSSE)

4.3.2.2 Benchmark studies

The large number of atoms in the pentanidiums renders computational study based solely on DFT infeasible. Fortunately, the study of large system could be made viable through the Our own N-layered Integrated molecular Orbital and molecular Mechanics (ONIOM) technique[390] implemented in Gaussian 09. This computational technique models large molecules by defining two or three layers within the structure that are treated at different levels of accuracy, for instance a DFT high layer where the bond formation/dissociation is occurring and a semi-empirical/molecular mechanics low layer.

The use of the ONIOM technique in the computational study of asymmetric organo-catalysis was reported by Houk,[391] and Simón and Goodman.[392] The former used a DFT/AM1 hybrid and the latter used a DFT/Molecular Mechanics hybrid.

In the ideal case, the low level partition in ONIOM should be as large as possible, however this is subjected to the constraint that the low level method employed (molecular mechanics or semi-empirical) is able to provide a sufficiently accurate model for important interactions that are of interest. In this case, we are interested in two particular halogen bonds that could be formed between the bromobenzene derivative present in the catalyst and the sulfenate and the bromide that is generated in the S_N2 displacement (**Figure 4.16**) and also that is generated *via* retro-Michael (**Figure 4.17**).

Calculations of the halogen bonded complex between bromobenzene and bromide (see **Figure 4.16** for structure) at various level theories were performed. The purpose of this study is to benchmark DFT methods (M06 and M06-2X) with small basis set and semi-empirical methods (AM1, PM6 and PM7) against DFT with large basis set (aug-cc-pVTZ) and MP2.
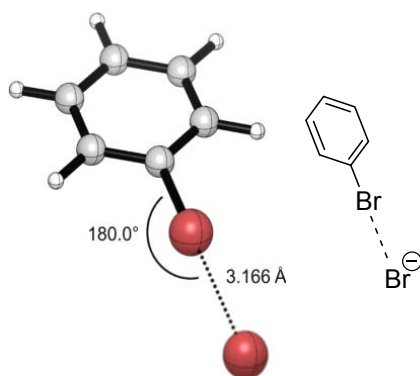
Figure 4.16 Optimized geometry of halogen bonded complex between bromobenzene and bromide at MP2/aug-cc-pVTZ

Table 4.4 Benchmark result for bromobenzene-Br halogen bond

Entry	Level of theory	Bond length/Å	Interaction energy/ kcal mol^{-1}		
			M06/6-31+G(d,p)	M06/aug-cc-pVDZ	MP2/aug-cc-pVDZ
1	MP2/aug-cc-pVDZ	3.237	-6.41	-7.08	-4.75
2	MP2/aug-cc-pVTZ	3.166	-5.97	-6.66	-4.17
3	M06/aug-cc-pVDZ	3.296	-5.99	-6.63	-4.53
4	M06-2X/ aug-cc-p-VDZ	3.296	-5.99	-6.63	-4.53
5	M06/aug-ccpVTZ	3.199	-6.02	-6.68	-4.28
6	M06/6-31+G(d,p)	3.149	-6.09	-6.79	-4.20
7	M06/6-31G(d,p)	3.067	-5.98	-6.71	-3.84
8	M06/6-31G(d,p) Br:LANL2DZ(d,p)	3.271	-6.19	-6.84	-4.61
9	AM1	2.346	+24.33	+22.62	+30.55
10	PM6	2.647	+2.65	+1.63	+6.38
11	PM7	3.122	-5.53	-6.24	-3.59

Interaction energy = SCF energy of complex - SCF energy of bromobenzene – SCF energy of bromide + CP correction for BSSE. Calculated with Gaussian 09 A2.

From **Table 4.4**, the reference for this benchmark study is taken to be the result at MP2/aug-cc-pVTZ which gave a Br-Br distance of 3.166Å. The effect of increasing the basis set size is shortening of the Br-Br halogen bond (Entry 1 and 2, Entry 3 and 5). The Br-Br halogen bond length is significantly underestimated by semi-empirical methods such as AM1 and PM6 (Entry 9 and 10). However, the latest semi-empirical method by Stewart: PM7,[393, 394] gave superior result (Entry 11).

With the results from the benchmark study for bromobenzene and bromide halogen bonded complex. We restricted the level of theory to a smaller subset relative to those used in **Table 4.4** in a subsequent study on the bromobenzene-sulfenate complex. The negative charge of the sulfenate anion is delocalized - mainly between the S and O of the S=O group. Therefore, two different halogen bonds could be formed between bromobenzene and the sulfenate anion – an S-Br and an O-Br halogen bond.

Table 4.5 *cis*- and *trans*- conformation of sulfenate and relevant thermodynamics
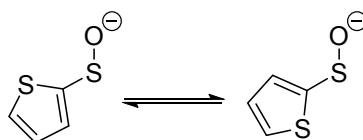
	ΔH	ΔG
M06/aug-cc-pVDZ	+0.43	+0.14
SMD(Et$_2$O)-M06/aug-cc-pVDZ	+0.64	+0.40
M06/aug-cc-pVTZ	+0.29	+0.05
SMD(Et$_2$O)-M06/aug-cc-pVTZ	+0.44	+0.32

$\Delta G = G_{trans\ isomer} - G_{cis\ isomer}$. $\Delta H = H_{trans\ isomer} - H_{cis\ isomer}$.

The sulfenate anion could adopt two possible conformations as depicted in **Table 4.5**. DFT calculations indicate that the *cis*- conformation (S of thiophene and O are on the same side) is more stable in all cases (gas phase and condensed phase), although the difference in Gibbs energy is not very large, both conformations should exist at equilibrium. For instance, from the Boltzmann distribution at 298.15K, the ratio of *cis*- and *trans*- is 1.7:1 with a ΔG of 0.32 kcal/mol.

In the benchmark of the sulfenate-bromobenzene halogen bond, we began with the M06/6-31+G(d,p) which perform very well in term of halogen bond length for the bromobenzene-bromide halogen bond benchmark (**Table 4.4**, compare Entry 2 and 6). Three conformations were located (**Figure 4.17**). O-Br halogen bond complex **27a** was found to be more stable than the S-halogen bond complex **27c**. When the complex **27b** is optimized with a different basis set, it converges to **27a**.Therefore the conformation **27b** is only unique to M06/6-31+G(d,p).

27a (0)   **27b** (2.6)   **27c** (3.9)
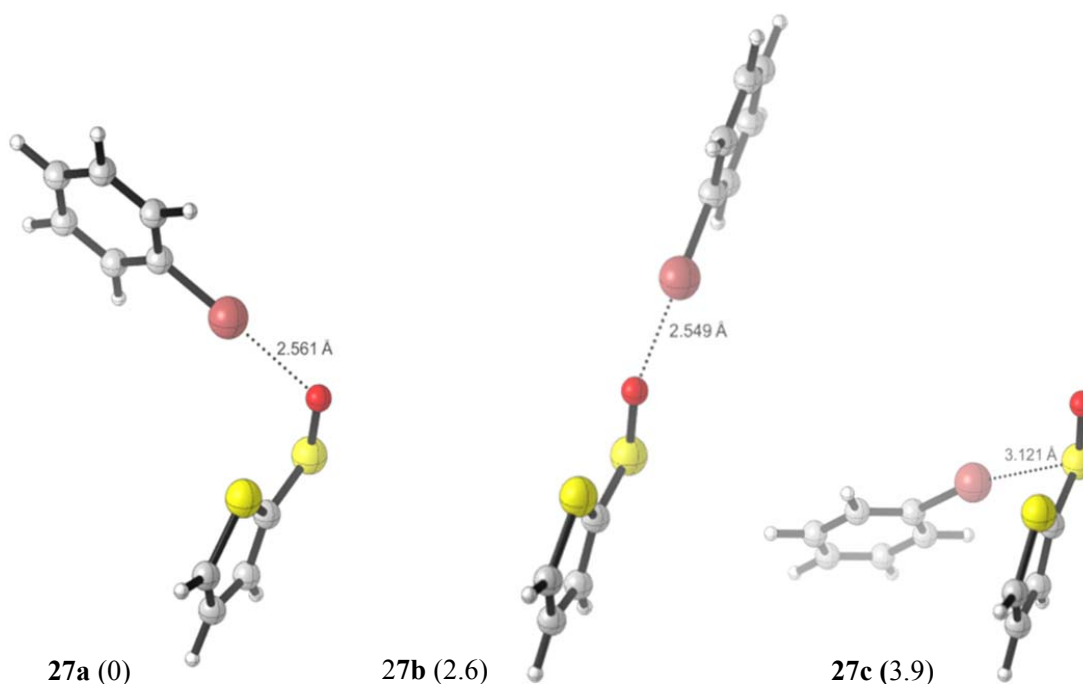
Figure 4.17 Optimized geometry of halogen bonded complex between bromobenzene and sulfenate at M06/6-31+G(d,p). Relative enthalpy in kcal/mol calculated at the M06/6-31+G(d,p) is given in parenthesis.

Table 4.6 Benchmark result for Sulfenate-Br halogen bond

Entry	Level of theory	27a		27b		27c	
		Bond length	ΔH	Bond length	ΔH	Bond length	ΔH
1	M06/aug-cc-pVDZ	2.597	0	-	-	3.185	+3.4
2	M06/6-31+G(d,p)	2.561	0	2.549	+2.6	3.121	+2.9
3	M06/6-31G(d,p)	2.516	0	-	-	3.089	+4.5
4	M06/6-31G(d,p) Br:LANL2DZ(d,p)	2.515	0	-	-	3.112	+5.7
5	AM1	2.041	+4.4	-	-	2.408	0
6	PM6	1.983	0	-	-	2.299	+7.5
7	PM7	2.314	0[a]	-	-	3.090	+3.3[a]

Entry 1 to 6 is calculated is Gaussian 09 A2. Entry 7 is calculated with MOPAC2012. ΔH is obtained at the same level of theory as the geometry optimization. [a] ΔH is obtained from the heat of formation as calculated with MOPAC2012

From **Table 4.4** and **Table 4.6**, it is apparent that semi-empirical methods such as PM6 and AM1 are unsuitable for the halogen bonds of interest. PM6 and AM1 both gave halogen bond lengths that are too short. Although PM7 gave relatively better halogen bond length in both cases, it is not implemented in the current version of Gaussian 09; therefore it cannot be used in the ONIOM calculation.

4.3.2.3 ONIOM partitioning and experimental results

From the benchmark studies in section **4.3.2.2**, we concluded that semi-empirical methods such as AM1 and PM6 are unsuitable to model the halogen bonds that could be present in the TS structures of the S_N2 displacement of Br by sulfenate. Therefore, in the ONIOM calculation only the *tert*-Butyl groups and phenyl rings that do not contain a halogen are included in the low level layer (See **Scheme 4.10** for partitioning detail). The rest of the atoms in the TS structure are included in the high level layer which would be calculated at M06/6-31G(d,p).

25c
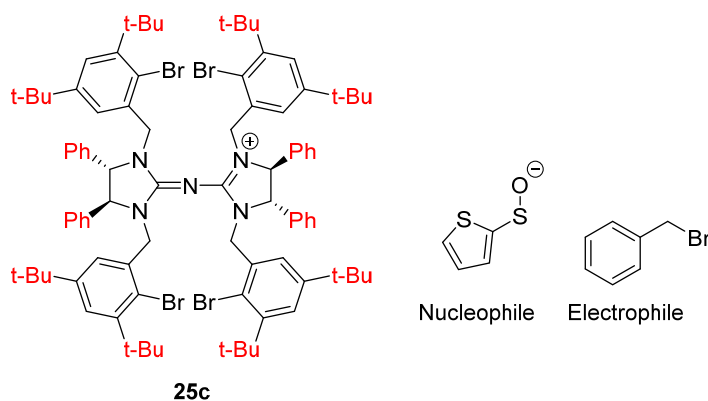
Scheme 4.10 Partitioning of the catalyst for ONIOM calculations. Groups in red are included in the low level layer. The rest is included in the high level layer

Two possible choices are available for the low level layer in the ONIOM calculation: semi-empirical or molecular mechanics. In this study, both choices will be explored. For semi-empirical method, PM6 was used. For molecular mechanics method, the UFF force field was used (force field parameters were derived by default setting in Gaussian 09 A2).

4.3.2.4 PM6 low level results

It is evident that multiple conformations exist for the TS structure. For the conformation sampling, we generated a series of conformations from an arbitrary TS structure which was located initially. While keeping the catalyst structure unchanged, the O-S-C-C dihedral was varied to locate another TS structure. Theoretically, 3 possible conformations for the "product" (more accurately, the TS of the sulfenate and benzyl bromide leading to the product) are possible (**Figure 4.18**), however, due to steric requirement of the catalyst not all 3 conformations of the "product" could be adopted in the TS structures.
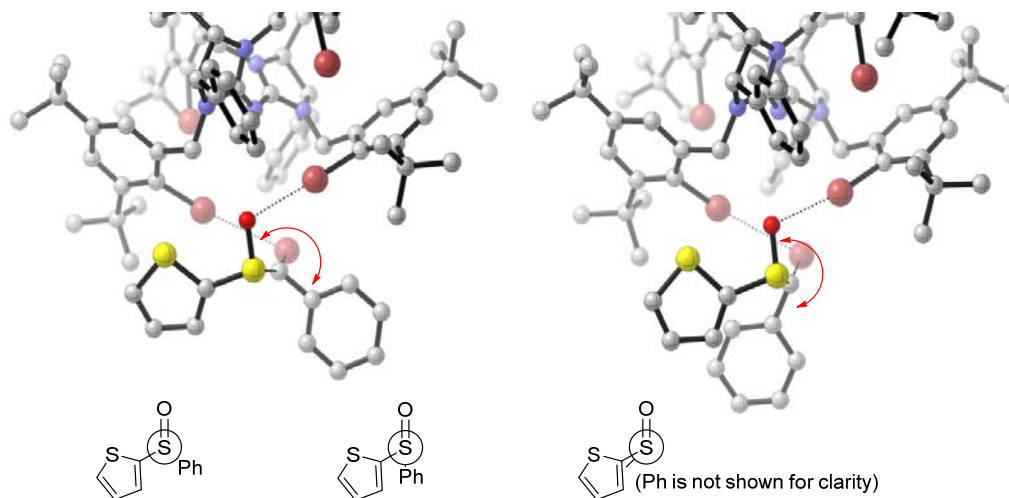
Figure 4.18 Selected examples of conformational sampling based on O-S-C-C dihedral angles. Red sphere = Br. Bright Red sphere of smaller size = O. Yellow sphere = S. Grey sphere = Carbon. Blue sphere = N.

Additional conformations of the TS structures are generated by rotating the dihedral angle of the bond that attached the pentanidium core to the benzyl side arms (see **Figure 4.19**). The effect of this resulted in very large changes to overall structure of the new TS structure.
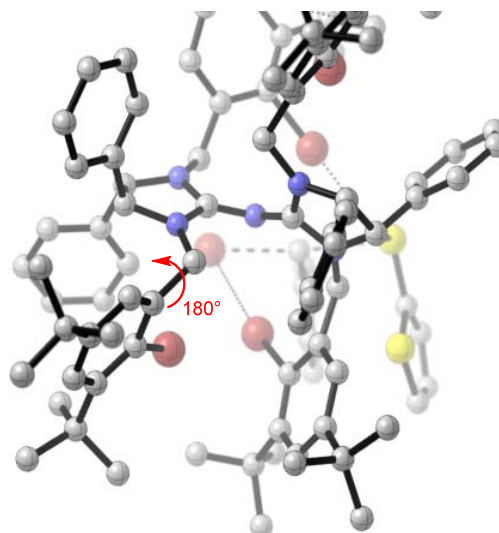
Figure 4.19 Generating new TS conformation by varying the N-C(sp^3)-C(sp^2)-C(sp^2) dihedral angles by 180°. Red sphere = Br. Bright Red sphere of smaller size = O. Yellow sphere = S. Grey sphere = Carbon. Blue sphere = N.

Besides the two means to generate TS conformation, new conformations could also be generated by using *cis-* and *trans-* conformation of the sulfenate (see **Table 4.5**). This would essentially increase the number of conformations by a multiple of two. Due to time constraint, we would only generate TS conformation based on *cis-* and *trans-* conformation of the sulfenate for the most stable TS structures from the *R* TS set and the *S* TS set.

A total of 22 TS conformations were located (8 for *R* product and 14 for *S* product). We would only consider enthalpy in this discussion as the large number of low frequency modes that are approximated as vibration is expected to introduce very large error to the entropy term in Gibbs free energy.

Three sets of results are tabulated in **Figure 4.20**. The enthalpies derived directly from M06:PM6 ONIOM calculations are given in blue. The results in red and green are derived from the sum of single point calculation at M06/6-31G(d,p) and enthalpy correction to the single point energy at M06:PM6. The difference between red and green is the SCF convergence criteria (red = 10^{-5} and green = 10^{-8}). The reason for performing single point calculation using different SCF convergence criteria is due to difficulty in SCF convergence when a larger basis set with diffuse function such as M06/6-31+G(d,p) was used later. It could be seen from **Figure 4.20** that loosen the SCF convergence criteria from the default in Gaussian 09 of 10^{-8} to 10^{-5} does not significantly affect the enthalpy, but it saved considerable amount of time due to faster convergence. The average difference in SCF energy between 10^{-5} and 10^{-8} is 0.0044 kcal/mol (standard deviation of 0.003 kcal/mol) which is inconsequential to predicting enantioselectivity that are of interest in this study.
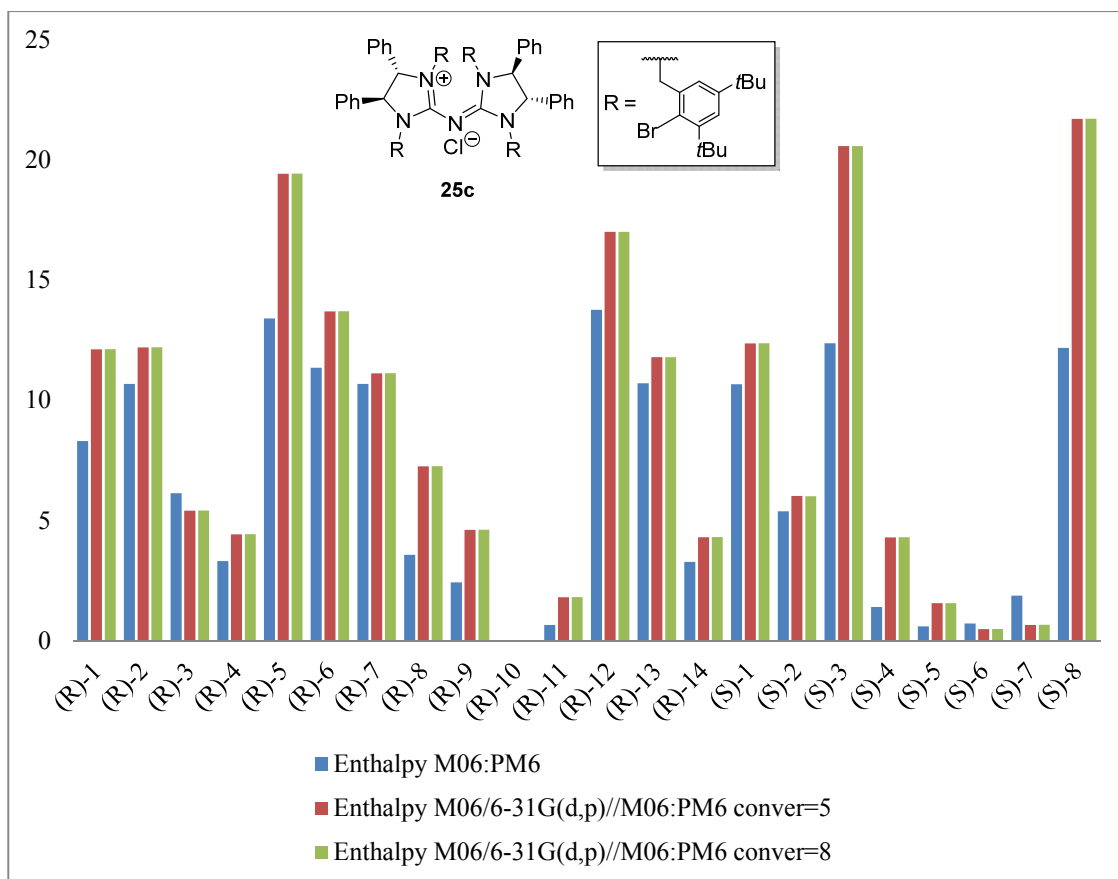
Figure 4.20 Relative enthalpy for TS structures optimized at M06/6-31G(d,p):PM6. Catalyst **25c**.

The correct enantiomer was predicted by the relative enthalpy of the most stable TS structure from the *R* and *S* sets of TS structures from M06:PM6 ONIOM calculations (see **Figure 4.22** for 3D structures). The $\Delta\Delta H^{\ddagger}$ for M06:PM6 is +0.59 kcal (the *R* TS is 0.59 kcal/mol more favorable in terms of enthalpy to the *S* TS). The $\Delta\Delta H^{\ddagger}$ for M06/6-31G(d,p)//M06:PM6 is +0.49 kcal/mol, the predicted enantiomer is also the *R* product. Experimentally, the absolute configuration of a related product is *R* as determined from X-ray diffraction (**Figure 4.21**); therefore we would assume that the absolute configuration is the same for the product that would be formed from the TS structures in our calculations. Therefore, the correct enantiomer is predicted in both cases.
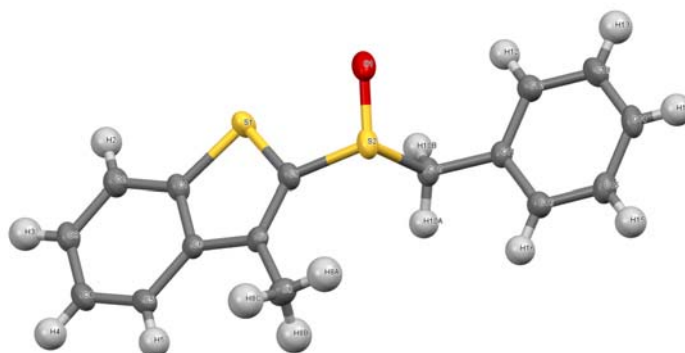
Figure 4.21 X-ray structure of (*R*)-2-(benzylsulfinyl)-3-methylbenzo[b]thiophene

In both TS structures, halogen bond between the Br of the catalyst's side chain and the leaving bromide in the S_N2 TS could be seen (**Figure 4.22**). In both bases, the Br-Br distance is less than the sum of the van der Waals radius of two Br (3.70 Å). The *(R)* TS has a relatively more linear and shorter Br-Br halogen bond than the *(S)* TS (which is 172° *vs.* 155° and 3.50Å *vs.* 3.55 Å). A O(sulfoxide)-Br halogen bond is present in the TS which lead to the minor enantiomer – *(S)* TS – but it is absence in the *(R)* TS.
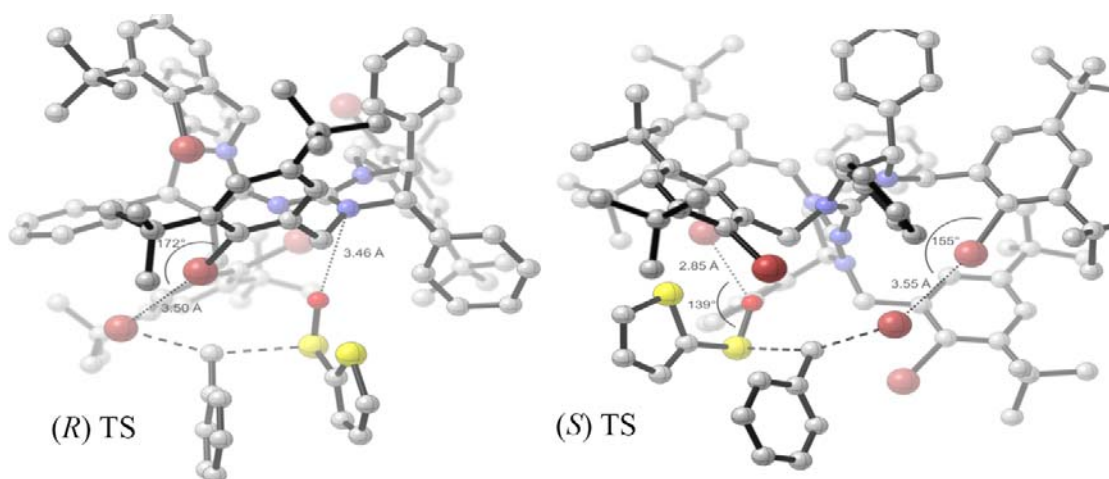
Figure 4.22 most stable (*R*) and (*S*) TS structures for catalyst **25c**, in terms of enthalpy, from M06:PM6 ONIOM calculations

Analysis of the electrostatic potential (ESP) map of catalyst **25c** in the (*R*) TS revealed that the O of sulfenate resides in a region of strongly positive ESP, which is expected to have strong electrostatic interaction with the partially anionic sulfenate in the TS (blue region in **Figure 4.23**). The leaving Br of benzyl bromide resides in another cationic pocket formed by the sigma hole of the upper right side chain's Br, electron-deficient benzylic H of the lower left side chain and the pentanidium core. Thus, the leaving group is stabilized by multi non-covalent interaction in the *R* TS.
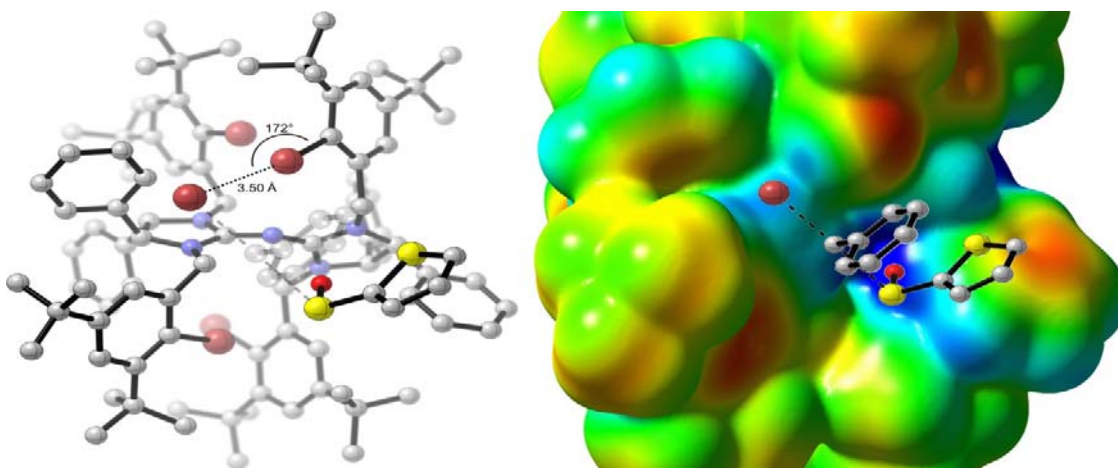
Figure 4.23 Left: 3D structures of (*R*) TS to illustrate the S=O interaction with the catalyst **25c**. Right: sulfenate and benzyl bromide in S_N2 TS superimpose onto ESP map of catalyst generated by removal of substrate in (*R*) TS

Next, we proceeded to locate TS structures for the catalyst without Br by removing the required Br from the TS structures of the catalyst with Br. The results are shown in **Figure 4.24**. An inversion of the absolute stereochemistry of the product was predicted from the calculations for gas phase results at all three different levels of theory. The $\Delta\Delta H^{\ddagger}$ for M06:PM6 is -0.76 kcal (the *S* TS is 0.76 kcal/mol more favorable in terms of enthalpy to the *R* TS). When the relative enthalpy is derived from single point calculation at M06/6-31G(d,p) (red bar in **Figure 4.24**) or M06/6-31+G(d,p) (green bar in **Figure 4.24**), the disagreement with experimental became larger.

The experimental *e.r* is 4:1 (*R*:*S*) which translates to +0.59 kcal/mol (in terms of Gibbs free energy at 215.15K).
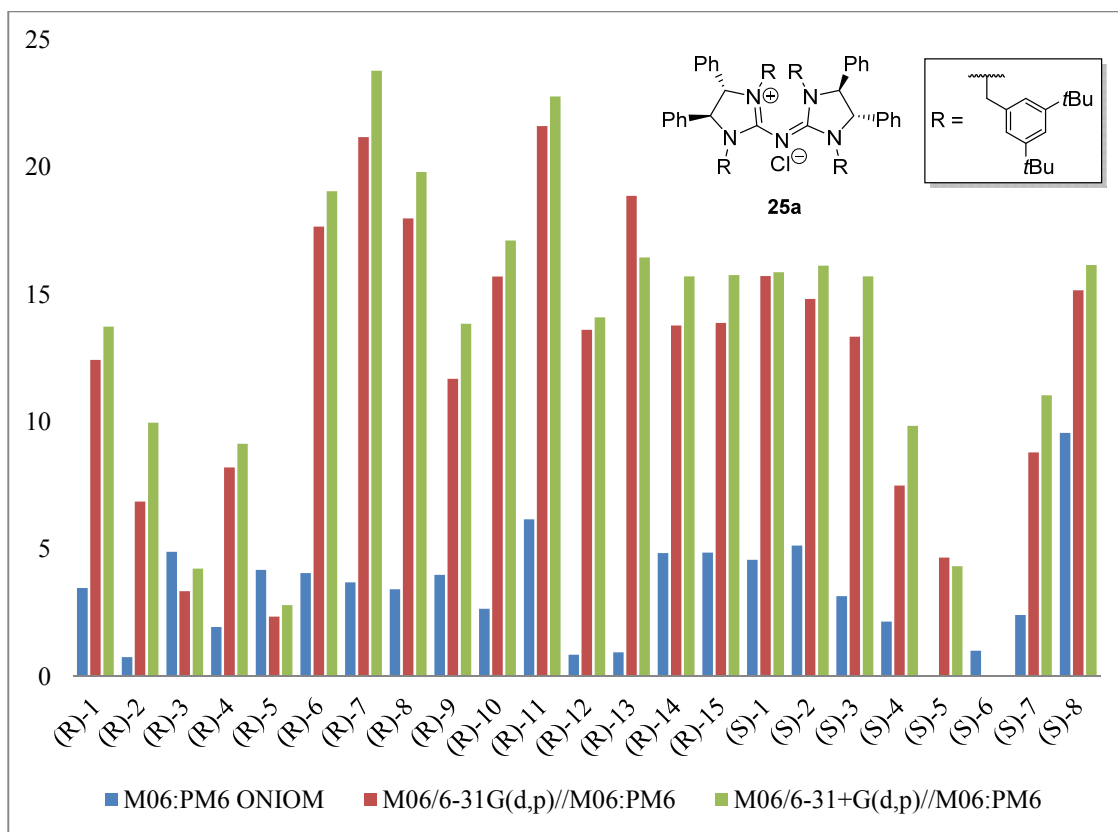
Figure 4.24 Relative enthalpy for TS structures optimized at M06/6-31G(d,p):PM6. Catalyst **25a**

As we are unable to predict the correct major enantiomer from the methods presented in **Figure 4.24**, we attempt to rectify this by modelling the effect of solvent (diethyl ether) *via* additional single point calculation using the CPCM[234] and SMD[294] implicit solvation model at M06/6-31+G(d,p). The results are shown in **Figure 4.25**. Neither implicit solvation models changed the gas phase result in the desired direction – towards the (*R*) TS. With the inclusion of solvent effect, the (*S*) TS became more stable than in the gas phase calculation ($\Delta\Delta H^{\ddagger}$ = -1.4 kcal/mol for SMD and $\Delta\Delta H^{\ddagger}$ = -2.2 kcal/mol). Therefore it appears that with the current set of TS

structures of catalyst **25a**, we are unable to predict the correct enantiomer with the M06:PM6

ONIOM geometries.
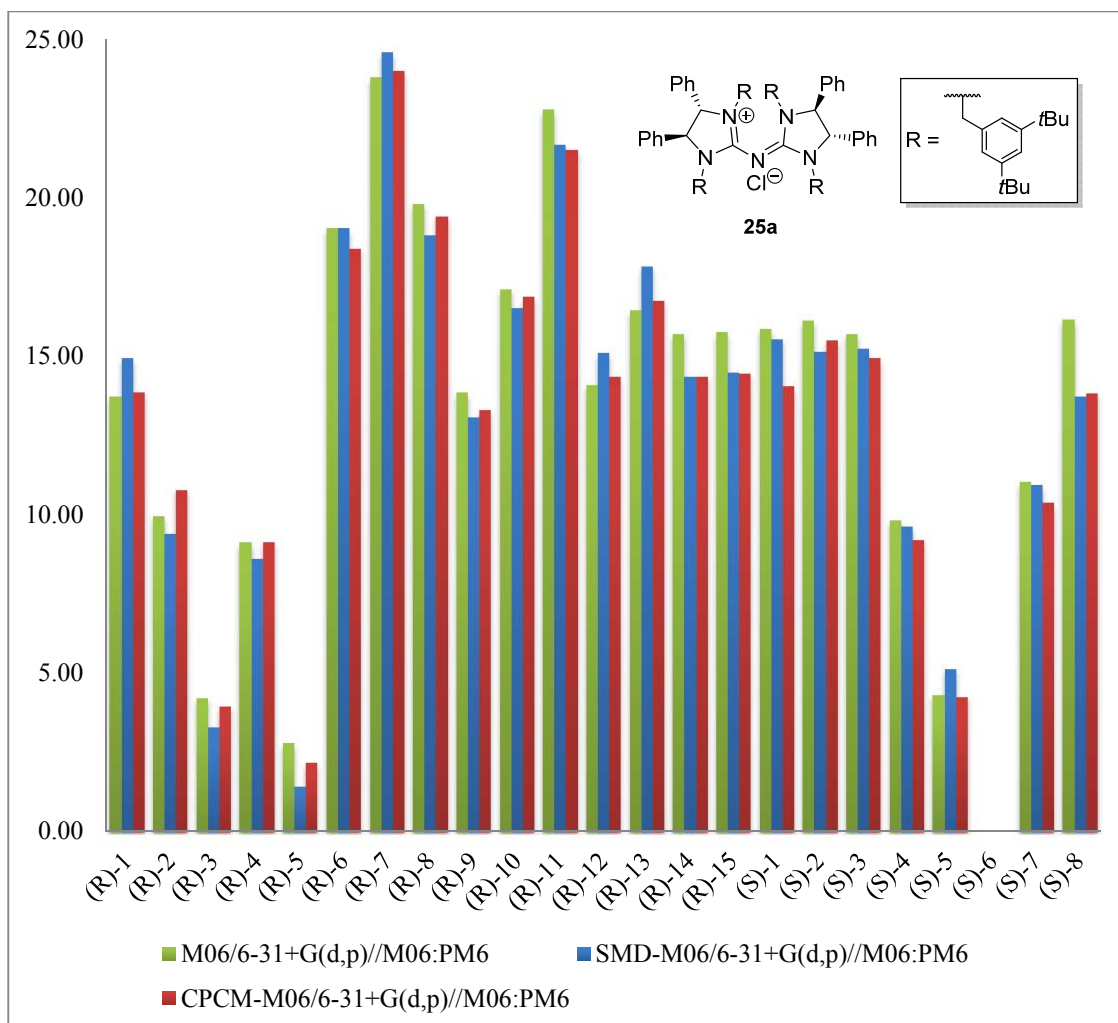
Figure 4.25 Relative enthalpy for TS structures optimized at M06/6-31G(d,p):PM6. Catalyst **25a**

4.3.2.5 UFF low level results

Due to the inability of M06:PM6 to predict the correct enantiomer for the non-halogenated

catalyst. We turn to UFF force field[395] as the low level in the ONIOM model. The UFF force field

was also utilized by Simón and Goodman in their computational study.[392] The M06:UFF TS

structures are derived from their respective M06:PM6 TS structures. The results are shown in

Figure 4.26. TS (*R*)-10 which is the most stable in the M06:PM6 ONIOM calculations is +4.5 kcal/mol less stable than TS (*S*)-6 which is the most stable (*S*) TS structures in the M06:PM6 ONIOM calculation. Thus, the wrong enantiomer was predicted to be overwhelming favored at M06:UFF. However, when enthalpies were derived from single point calculation at M06 with increasing basis set size from 6-31G(d,p) to 6-31+G(d,p), TS (*R*)-10 became increasing stable. At M06/6-31+G(d,p), TS (*R*)-10 is +0.84 kcal/mol less stable than TS (*S*)-6, It is possible that inclusion of solvent (Et$_2$O) effect *via* implicit solvation model could change the relative stability, therefore we performed additional single point calculation with SMD and CPCM solvation model at M06/6-31+G(d,p).
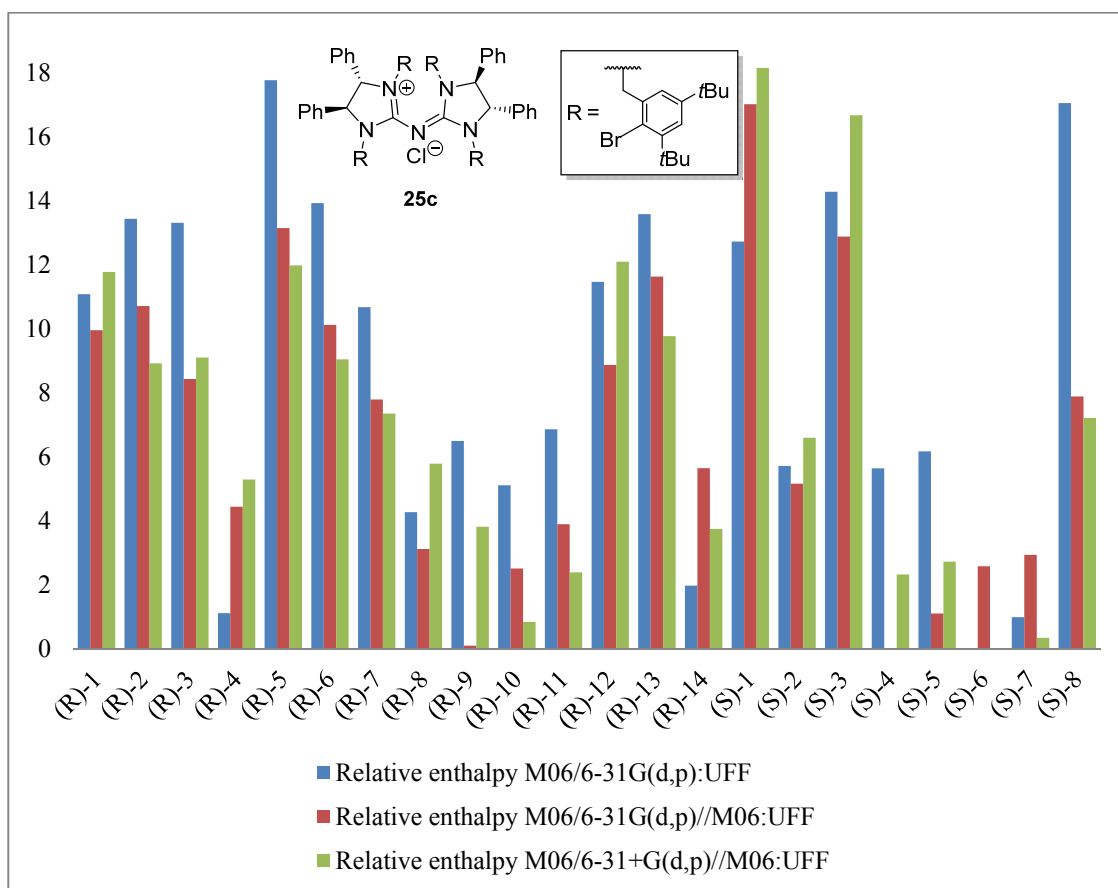
Figure 4.26 Relative enthalpy for TS structures optimized at M06/6-31G(d,p):UFF. Catalyst **25c**.

147

The results which include solvent effect *via* single point calculations are shown in **Figure 4.27** below. When the SMD solvation model was used, TS (*R*)-10 is 0.45 kcal/mol more stable than TS (*S*)-6 in terms of enthalpy; therefore the correct enantiomer is predicted by this level of theory. This difference is mainly due to the stronger non-electrostatic stabilization of the solvent as predicted by the SMD solvation model (-28.24 kcal/mol for TS (*R*)-10 and -27.12 for TS (*S*)-6). Therefore, implicit solvation model which does not include such non-electrostatic term does not favored TS (*R*)-10. For instance, with the CPCM solvation model TS (*S*)-6 is more stable than TS (*R*)-10 by 1.2 kcal/mol in term of enthalpy, which predicts the opposite enantiomer as the major product.
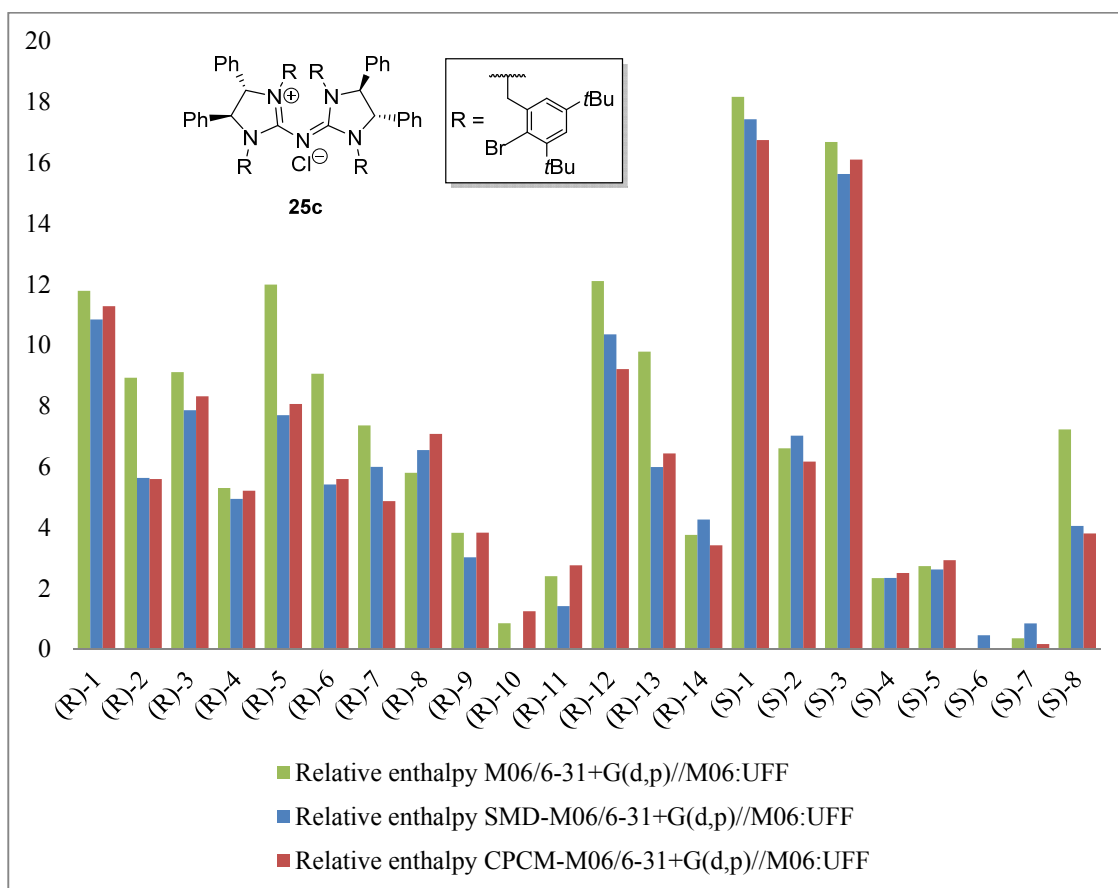
Figure 4.27 Relative enthalpy for TS structures optimized at M06/6-31G(d,p):UFF. Catalyst **25c**.

The 3D models of TS (*R*)-10 and TS (*S*)-6 optimized at M06:UFF are shown in in **Figure 4.28**. TS (*R*)-10 was more stable than TS (*S*)-6 by 0.5 kcal/mol, which is in good agreement with the experimental *e.r* of 94:6. Br-Br halogen bond between the leaving group Br and the bromobenzene derivative side chain of catalyst **1c** is evident in both (*R*) and (*S*) TS structures. The Br-Br distance in the (*R*) TS is 3.48Å and *S* TS is 3.42Å, they are shorter than the sum of Van der Waals radius of 2 Br (3.60Å) in both cases, which are characteristics of halogen bonding.[200] Both halogen bonds are fairly linear. A second halogen bond between O of sulfenate and Br in another side chain could be observed in the *S* TS, but not the *R* TS. This O-Br halogen bond at 2.67 Å is significant shorter than the sum of Van der Waals radius of O and Br (3.37Å). For the *R* TS, the partially anionic sulfenate group resides in a cationic pocket (**Figure 4.29**), which is similar to the M06:PM6 TS structures.
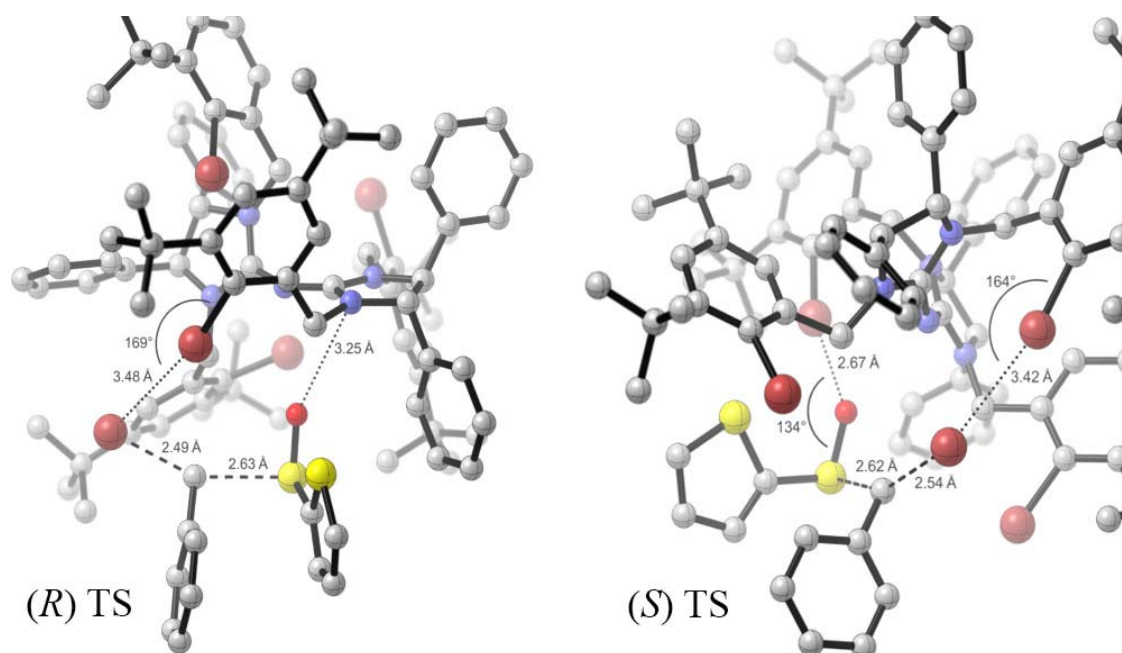
Figure 4.28 most stable (*R*) and (*S*) TS structures for catalyst **25c**, in terms of enthalpy at SMD(Et$_2$O)-M06/6-31+G(d,p)//PM6:UFF, from M06:UFF ONIOM calculations
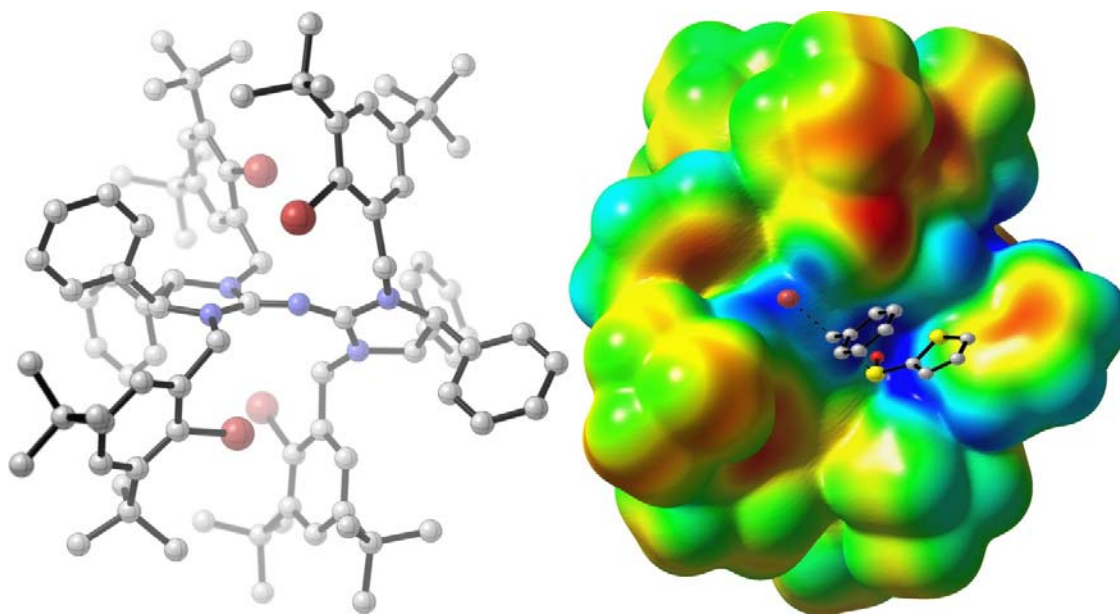
Figure 4.29 Left: 3D model of catalyst **25c** in TS (*R*)-10. Right: Corresponding ESP map generated at isovalue of density = 0.001. Blue region is more electron deficient than red.

The sets of (*R*) and (*S*) TS structures for catalyst **25a** were optimized at M06:UFF. The problem of some TS having 2 imaginary frequencies was encountered in some of the TS structures obtained at M06:UFF. Increasing the integration grid size alone does not solve the problem, and with tight convergence it is very difficult to get the TS structures to converge. Nevertheless, some TS structures were obtained. The current lowest (*R*) TS is more stable than the lowest (*S*) TS by 0.6 kcal/mol in term of enthalpy. This predicts the correct major enantiomer but incorrect trend as **25a** was found to give a lower level of enantioselectivity than **25c** (the *e.r* of **25**a is 1:4 while **25c** is 1:9). Nevertheless, the M06:UFF calculation is an improvement for catalyst **25a** when compared to M06:PM6.

The structures of the lowest (*R*) and (*S*) TS for catalyst **25a** are shown in **Figure 4.30**. In the absence of the halogen, hydrogen bonds were observed instead. For instance the leaving Br in (*R*) TS is stabilized by multiple halogen bonds at about 2.8Å. The oxygen of the sulfenate is also observed to be involved in multiple hydrogen bonds (not shown). The conformation of the

catalyst and substrates are similar to those of catalyst **25c** (compare to **Figure 4.28**). Similar to the TS for catalyst **25c**, the leaving Br and O of sulfenate resides in pockets of positive electro-potential (**Figure 4.31**)
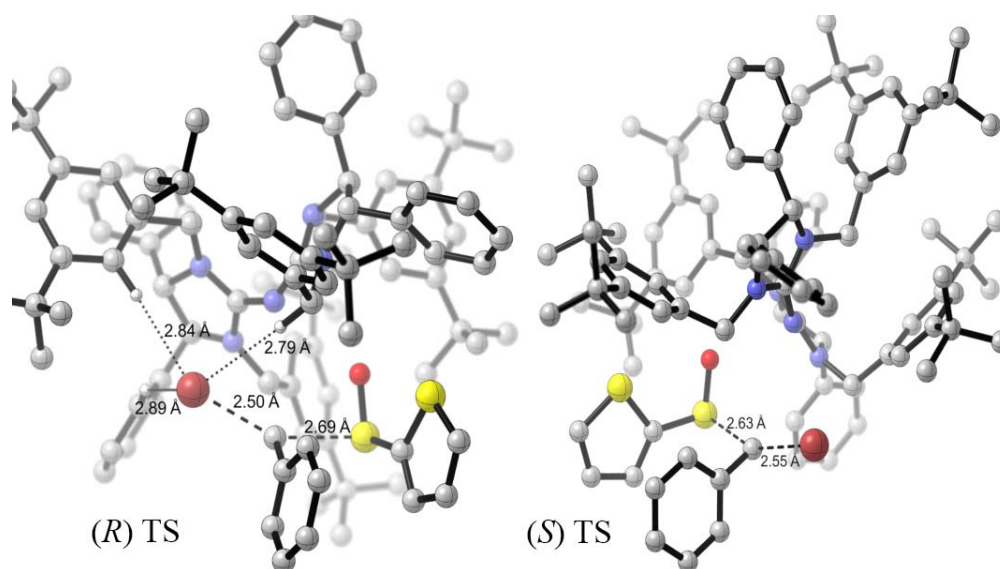
Figure 4.30 most stable (*R*) and (*S*) TS structures for catalyst **25a**, in terms of enthalpy at SMD(Et2O)-M06/6-31+G(d,p)//PM6:UFF, from M06:UFF ONIOM calculations
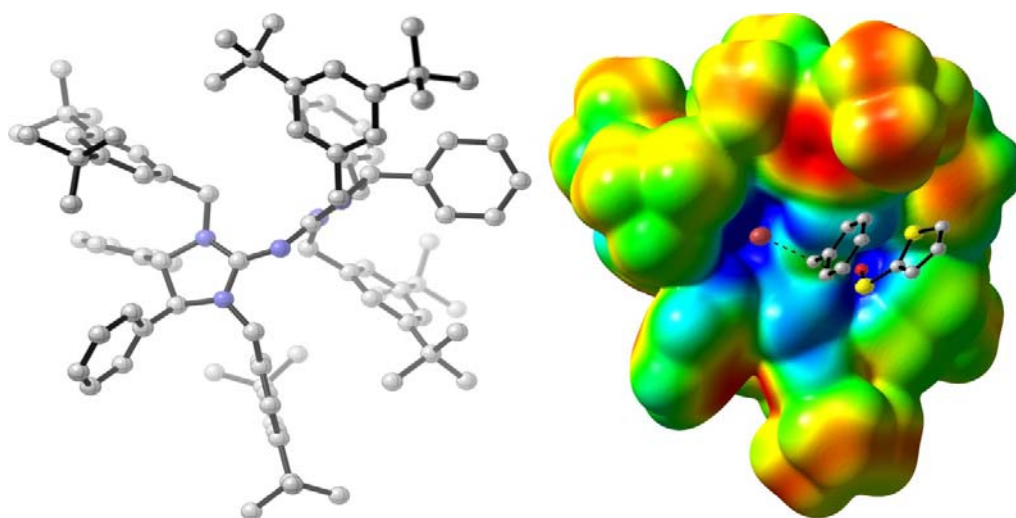
Figure 4.31 Left: 3D model of catalyst **25a** in (R) TS. Right: Corresponding ESP map generated at isovalue of density = 0.001. Blue region is more electron deficient than red.

Chapter 5

Summary and Outlook

5.1 Summary

This thesis presents our works on the bromination and fluorination of sp^3 C-H bond *via* photochemistry and our theoretical investigations on guanidine catalyzed asymmetric reactions and pentanidium catalyzed phase transfer synthesis of chiral sulfoxide. We have extended the synthetic application of visible light photoredox catalysis to bromination of sp^3 C-H bond (aliphatic and benzylic) with inexpensive Eosin Y disodium salt as photoredox catalyst and CBr$_4$ serve as Br source. We have also developed a photo-fluorination reaction catalyzed by an organo-photocatalyst. The reaction can be performed with common low power household lamps. The reaction is selective for electron rich sp^3 C-H bonds due to the involvement of cationic *N*-radical in hydrogen abstraction. In the theoretical section, we investigated guanidine catalyzed enantioselective desymmetrization of *meso*-aziridine, decarboxylative Mannich reaction and enantiodivergent and γ-Selective allylic amination. We have also studied the use of halogen bond in pentanidium catalyzed phase transfer synthesis of sulfoxide.

5.2 Outlook

One of the major drawbacks of the photobromination is the low reactivity of the protocol. Large excess (about 3-5 equivalent) of substrates has to be used in order to obtain a reasonable yield based on CBr$_4$ added. This problem was partly overcome by the photo-fluorination reaction with AQN.

Current evidences suggest that *N*-radicals are involved in both the photoredox bromination and photo-fluorination. Nevertheless, more evidences are required to support our proposal. Spectroscopic techniques such as electron spin resonance (ESR) and transient spectroscopic techniques would be helpful in providing more insights. Identifying the hydrogen abstracting species is important for tuning of selectivity. This would be discussed further below.

One of the major difficulties faced in both bromination and fluorination projects is purification of the halogenated products. Chlorinated and brominated compounds are difficult to separate from the starting material by silica gel based column chromatography. Distillation is viable for bromated compounds, but a reasonable scale is required even with microscale distillation (about 0.5mL of product or for *e.g.* 4mmol or 0.66g of bromocyclohexane). For fluorinated products, separation of products from starting material is feasible with column chromatography. However, the isomeric fluorinated products can only be separated from the major isomer after a few repeated column chromatographic attempts on the impure product. One possible mean to overcome this would be to increase the selectivity of C-H abstraction by tuning the electronic and steric properties of the hydrogen abstractor - according to our mechanistic study, the *N*-radicals. This could form the basis of future works on C-H functionalization *via N-radical*.

Currently, our most effective method involved the generation of cationic *N*-radical *via* photochemistry with AQN as the photocatalyst. The C-H abstracting ability of cationic *N*-radical should be general, in the sense that it should be able to be extended to any class of C-H functionalization (halogenation, hydroxylation, cyanation, *etc*.) as long as the alkyl radical generated from C-H abstraction could be trapped with a suitable radical trap. Further development could focus on expanding C-H functionalization with cationic *N*-radical to other class of C-H functionalization.

One of the problems with the generation of cationic *N*-radical from Selectfluor® is that it is not atom economical. This is evident from the small molecular weight of F relative to Selectfluor®. Thus, waste generation could be a major issue especially upon scaling up. If a means to convert the salt back to Selectfluor with fluoride salt, then Selectfluor could in principal be used in sub-stoichiometric amount (**Scheme 5.1**).
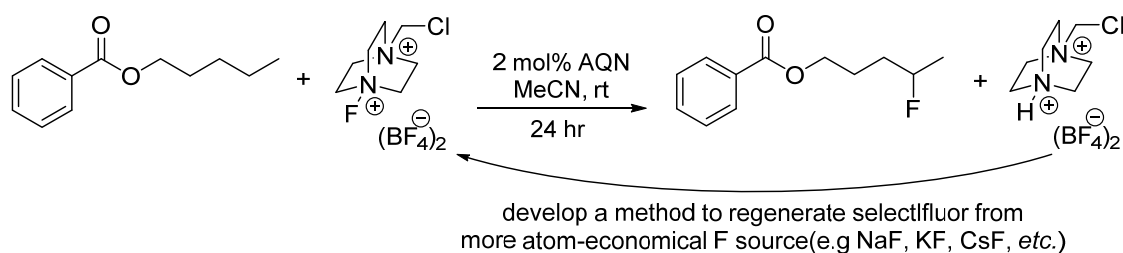
Scheme 5.1 Regeneration of Selectfluor® to minimize waste generation.

Theoretical methods such as DFT and ONIOM were employed to study the energetics and structural features of TS. Pertinent to catalysis, the objective of computational chemistry, from a practical point of view, is to provide a guide on how to improve the efficiency of a catalyst *via* structural modifications. One of the current methodologies in computational chemistry involves the location of TS structures. However, if the mechanism is unclear, finding TS structures may not be straightforward. In addition, for flexible systems, many conformation exists therefore extensive conformation sampling has to be performed. For large systems (>1000 basis functions), this may require a lot of time for calculations. Gibbs free energy is usually required to describe kinetic and thermodynamics of a reaction accurately. However, accurate calculations of Gibbs free energy especially in solution phase remain a challenge for theoretical methods currently. Therefore, we proposed the extension of common tools of biology such as molecular docking, statistical modeling to aid the design of small molecule catalysis.

References

1.   S. Purser, P. R. Moore, S. Swallow and V. Gouverneur, *Chem. Soc. Rev.*, 2008, 37, 320-330.
2.   C. Isanbor and D. O'Hagan, *J. Fluorine Chem.*, 2006, 127, 303-319.
3.   K. L. Kirk, *Curr. Top. Med. Chem.*, 2006, 6, 1447-1456.
4.   S. Sun and A. Adejare, *Curr. Top. Med. Chem.*, 2006, 6, 1457-1464.
5.   K. Müller, C. Faeh and F. Diederich, *Science*, 2007, 317, 1881-1886.
6.   S. M. Ametamey, M. Honer and P. A. Schubiger, *Chem. Rev.*, 2008, 108, 1501-1516.
7.   P. Jeschke, *ChemBioChem*, 2004, 5, 570-589.
8.   M. H. Hung, W. B. Farnham, A. E. Feiring and S. Rozen, in *Fluoropolymers: synthesis*, ed. G. Hougham, Kluwer Academic/Plenum, New York, 1999, vol. 1, pp. 51-66.
9.   E. Erdik, *Tetrahedron*, 1984, 40, 641-657.
10.   Y. Sasson, in *Industrial Chemistry Library*, eds. B. G. Jean-Roger Desmurs and J. G. Melvin, Elsevier, 1995, vol. Volume 7, pp. 1-3.
11.   D. P. Curran, *Synthesis*, 1988, 1988, 417-439.
12.   A. Podgoršek, M. Zupan and J. Iskra, *Angew. Chem. Int. Ed.*, 2009, 48, 8424-8450.
13.   A. Rudolph and M. Lautens, *Angew. Chem. Int. Ed.*, 2009, 48, 2656-2670.
14.   T. Ishiyama, S. Abe, N. Miyaura and A. Suzuki, *Chem. Lett.*, 1992, 21, 691-694.
15.   E. Corradi, S. V. Meille, M. T. Messina, P. Metrangolo and G. Resnati, *Angew. Chem. Int. Ed.*, 2000, 39, 1782-1786.
16.   C. B. Aakeröy, M. Fasulo, N. Schultheiss, J. Desper and C. Moore, *J. Am. Chem. Soc.*, 2007, 129, 13772-13773.
17.   P. Metrangolo, F. Meyer, T. Pilati, G. Resnati and G. Terraneo, *Angew. Chem. Int. Ed.*, 2008, 47, 6114-6127.
18.   A. Priimagi, G. Cavallo, P. Metrangolo and G. Resnati, *Acc. Chem. Res.*, 2013, 46, 2686-2695.
19.   P. Auffinger, F. A. Hays, E. Westhof and P. S. Ho, *Proc. Natl. Acad. Sci. U. S. A.*, 2004, 101, 16789-16794.
20.   Y. Lu, T. Shi, Y. Wang, H. Yang, X. Yan, X. Luo, H. Jiang and W. Zhu, *J. Med. Chem.*, 2009, 52, 2854-2862.
21.   M. R. Scholfield, C. M. V. Zanden, M. Carter and P. S. Ho, *Protein Sci.*, 2013, 22, 139-152.
22.   R. Breslow, *Acc. Chem. Res.*, 1980, 13, 170-177.
23.   D. H. R. Barton and D. Doller, *Acc. Chem. Res.*, 1992, 25, 504-512.
24.   A. E. Shilov and G. B. Shul'pin, *Chem. Rev.*, 1997, 97, 2879-2932.
25.   G. A. Olah and Á. Molnár, Wiley-Interscience,, Hoboken, N.J., 2nd edn., 2003, p. 871.
26.   A. A. Fokin and P. R. Schreiner, *Adv. Synth. Catal.*, 2003, 345, 1035-1052.
27.   K. Godula and D. Sames, *Science*, 2006, 312, 67-72.
28.   C. I. Herrerías, X. Yao, Z. Li and C.-J. Li, *Chem. Rev.*, 2007, 107, 2546-2562.
29.   H. M. L. Davies and J. R. Manning, *Nature*, 2008, 451, 417-424.
30.   R. Giri, B.-F. Shi, K. M. Engle, N. Maugel and J.-Q. Yu, *Chem. Soc. Rev.*, 2009, 38, 3242-3272.
31.   I. A. I. Mkhalid, J. H. Barnard, T. B. Marder, J. M. Murphy and J. F. Hartwig, *Chem. Rev.*, 2010, 110, 890-931.
32.   C.-H. Activation, in *Top. Curr. Chem.*, eds. J.-Q. Yu and Z. Shi, Springer GmbH, 2010, vol. 292, p. 384.
33.   R. H. Crabtree, *Chem. Rev.*, 2010, 110, 575-575.
34.   T. W. Lyons and M. S. Sanford, *Chem. Rev.*, 2010, 110, 1147-1169.
35.   T. Newhouse and P. S. Baran, *Angew. Chem. Int. Ed.*, 2011, 50, 3362-3374.

36. C.-H. F. i. o. synthesis, in *Chem. Soc. Rev.*, eds. H. M. L. Davies, J. Du Bois and J.-Q. Yu, The Royal Society of Chemistry, 2011, vol. 40, pp. 1845-2040.
37. L. McMurray, F. O'Hara and M. J. Gaunt, *Chem. Soc. Rev.*, 2011, 40, 1885-1898.
38. H. Lu and X. P. Zhang, *Chem. Soc. Rev.*, 2011, 40, 1899-1909.
39. C.-M. Che, V. K.-Y. Lo, C.-Y. Zhou and J.-S. Huang, *Chem. Soc. Rev.*, 2011, 40, 1950-1975.
40. W. R. Gutekunst and P. S. Baran, *Chem. Soc. Rev.*, 2011, 40, 1976-1991.
41. J. F. Hartwig, *Chem. Soc. Rev.*, 2011, 40, 1992-2002.
42. C.-L. Sun, B.-J. Li and Z.-J. Shi, *Chem. Rev.*, 2011, 111, 1293-1314.
43. K. M. Engle, T.-S. Mei, M. Wasa and J.-Q. Yu, *Acc. Chem. Res.*, 2011, 45, 788-802.
44. J. Pan, M. Su and S. L. Buchwald, *Angew. Chem. Int. Ed.*, 2011, 50, 8647-8651.
45. M. Wasa, K. S. L. Chan, X.-G. Zhang, J. He, M. Miura and J.-Q. Yu, *J. Am. Chem. Soc.*, 2012, 134, 18570-18572.
46. C. H. Functionalization, in *Acc. Chem. Res.*, eds. M. P. Doyle and K. I. Goldberg, American Chemical Society, 2012, vol. 45(6), pp. 777-958.
47. T. Gaich and P. S. Baran, *J. Org. Chem.*, 2010, 75, 4657-4673.
48. F. G. Bordwell, Bordwell pKa Table (Acidity in DMSO), http://www.chem.wisc.edu/areas/reich/pkatable/, Accessed 19 December, 2013.
49. F. G. Bordwell, *Acc. Chem. Res.*, 1988, 21, 456-463.
50. T. Brückl, R. D. Baxter, Y. Ishihara and P. S. Baran, *Acc. Chem. Res.*, 2012, 45, 826-839.
51. M. E. Wolff, *Chem. Rev.*, 1963, 63, 55-64.
52. R. S. Neale, *Synthesis*, 1971, 1971, 1-15.
53. G. Majetich and K. Wheless, *Tetrahedron*, 1995, 51, 7095-7129.
54. K. Chen, J. M. Richter and P. S. Baran, *J. Am. Chem. Soc.*, 2008, 130, 7247-7249.
55. G. I. Nikishin, E. I. Troyansky and M. I. Lazareva, *Tetrahedron Lett.*, 1985, 26, 1877-1878.
56. Y.-F. Wang, H. Chen, X. Zhu and S. Chiba, *J. Am. Chem. Soc.*, 2012, 134, 11980-11983.
57. P. J. Wagner, *Acc. Chem. Res.*, 1971, 4, 168-177.
58. T. Laue and A. Plagens, in *Named Organic Reactions*, John Wiley & Sons, Ltd, 2005, ch13, pp. 207-217.
59. J. W. Peter, in *Synthetic Organic Photochemistry*, eds. G. G. Axel and M. Jochen, CRC Press, 2004, ch. 2, pp. 11-40.
60. W. Pablo and M. Olaf, in *Synthetic Organic Photochemistry*, eds. G. G. Axel and M. Jochen, CRC Press, 2004, ch. 3, pp. 41-88.
61. D. H. R. Barton, J. M. Beaton, L. E. Geller and M. M. Pechet, *J. Am. Chem. Soc.*, 1961, 83, 4076-4083.
62. E. J. Corey and R. W. Hahl, *Tetrahedron Lett.*, 1989, 30, 3023-3026.
63. E. J. Corey, J. F. Arnett and G. N. Widiger, *J. Am. Chem. Soc.*, 1975, 97, 430-431.
64. R. Breslow, S. Baldwin, T. Flechtner, P. Kalicky, S. Liu and W. Washburn, *J. Am. Chem. Soc.*, 1973, 95, 3251-3262.
65. Ž. Čeković, L. Dimttruević, G. Djokić and T. Srnić, *Tetrahedron*, 1979, 35, 2021-2026.
66. A.-F. Voica, A. Mendoza, W. R. Gutekunst, J. O. Fraga and P. S. Baran, *Nature Chem*, 2012, 4, 629-635.
67. R. Kundu and Z. T. Ball, *Org. Lett.*, 2010, 12, 2460-2463.
68. C. G. Espino, P. M. Wehn, J. Chow and J. Du Bois, *J. Am. Chem. Soc.*, 2001, 123, 6935-6936.
69. C. G. Espino and J. Du Bois, *Angew. Chem. Int. Ed.*, 2001, 40, 598-600.
70. P. M. Wehn and J. Du Bois, *J. Am. Chem. Soc.*, 2002, 124, 12950-12951.
71. R. Giri, N. Maugel, B. M. Foxman and J.-Q. Yu, *Organometallics*, 2008, 27, 1667-1670.
72. R. Giri, X. Chen and J.-Q. Yu, *Angew. Chem. Int. Ed.*, 2005, 44, 2112-2115.
73. E. M. Simmons and J. F. Hartwig, *Nature*, 2012, 483, 70-73.

74.   B. D. Dangel, J. A. Johnson and D. Sames, *J. Am. Chem. Soc.*, 2001, 123, 8149-8150.
75.   L. V. Desai, K. L. Hull and M. S. Sanford, *J. Am. Chem. Soc.*, 2004, 126, 9542-9543.
76.   R. Giri, N. Maugel, J.-J. Li, D.-H. Wang, S. P. Breazzano, L. B. Saunders and J.-Q. Yu, *J. Am. Chem. Soc.*, 2007, 129, 3510-3511.
77.   D.-H. Wang, M. Wasa, R. Giri and J.-Q. Yu, *J. Am. Chem. Soc.*, 2008, 130, 7190-7191.
78.   Y. Zhao, W.-L. Yim, C. K. Tan and Y.-Y. Yeung, *Org. Lett.*, 2011, 13, 4308-4311.
79.   S. A. Moteki, A. Usui, T. Zhang, C. R. Solorio Alvarado and K. Maruoka, *Angew. Chem. Int. Ed.*, 2013, 52, 8657-8660.
80.   D. A. Colby, R. G. Bergman and J. A. Ellman, *Chem. Rev.*, 2010, 110, 624-655.
81.   J. M. Tedder, *Angew. Chem. Int. Ed.*, 1982, 21, 401-410.
82.   B. P. Roberts, *Chem. Soc. Rev.*, 1999, 28, 25-35.
83.   F. Minisci, *Synthesis*, 1973, 1973, 1-24.
84.   M. G. Evans and M. Polanyi, *Trans. Faraday Soc.*, 1938, 34, 11-24.
85.   V. F. Weisskopf, *Science*, 1975, 187, 605-612.
86.   G. A. Russell, *J. Am. Chem. Soc.*, 1958, 80, 4997-5001.
87.   R. Breslow, M. Brandl, J. Hunger, N. Turro, K. Cassidy, K. Krogh-Jespersen and J. D. Westbrook, *J. Am. Chem. Soc.*, 1987, 109, 7204-7206.
88.   F. Minisci, R. Galli, A. Galli and R. Bernardi, *Tetrahedron Lett.*, 1967, 8, 2207-2209.
89.   M. S. Chen and M. C. White, *Science*, 2007, 318, 783-787.
90.   M. S. Chen and M. C. White, *Science*, 2010, 327, 566-571.
91.   P. E. Gormisky and M. C. White, *J. Am. Chem. Soc.*, 2013, 135, 14052-14055.
92.   L. Gómez, I. Garcia-Bosch, A. Company, J. Benet-Buchholz, A. Polo, X. Sala, X. Ribas and M. Costas, *Angew. Chem. Int. Ed.*, 2009, 48, 5720-5723.
93.   A. Company, L. Gómez, M. Güell, X. Ribas, J. M. Luis, L. Que and M. Costas, *J. Am. Chem. Soc.*, 2007, 129, 15766-15767.
94.   H. Chen, S. Schlecht, T. C. Semple and J. F. Hartwig, *Science*, 2000, 287, 1995-1997.
95.   C. S. Wei, C. A. Jiménez-Hoyos, M. F. Videa, J. F. Hartwig and M. B. Hall, *J. Am. Chem. Soc.*, 2010, 132, 3078-3091.
96.   K. Kamata, K. Yonehara, Y. Nakagawa, K. Uehara and N. Mizuno, *Nature Chem*, 2010, 2, 478-483.
97.   F. Bodroux and F. Taboury, *Bull. Soc. Chim. Fr.*, 1911, 9, 592-594.
98.   G. A. Russell, in *Reactive intermediates in organic chemistry*, ed. J. K. Kochi, New York, 1973, vol. 1, ch. 7, pp. 275-332.
99.   X. Jiang, M. Shen, Y. Tang and C. Li, *Tetrahedron Lett.*, 2005, 46, 487-489.
100.   R. Montoro and T. Wirth, *Synthesis*, 2005, 1473-1478.
101.   I. S. Akhrem, A. V. Orlinkov, L. V. Afanas'eva, E. L. Mysov and M. E. Vol'pin, *Tetrahedron Lett.*, 1995, 36, 9365-9368.
102.   Y. Nishina, J. Morita and B. Ohtani, *RSC Advances*, 2013, 3, 2158-2162.
103.   C. Djerassi, *Chem. Rev.*, 1948, 43, 271-317.
104.   L. Horner and E. H. Winkelmann, *Angew. Chem.*, 1959, 71, 349-365.
105.   Z. Wang, in *Comprehensive Organic Name Reactions and Reagents*, John Wiley & Sons, Inc., 2010, ch. 680, p. 3067.
106.   C. Walling, A. L. Rieger and D. D. Tanner, *J. Am. Chem. Soc.*, 1963, 85, 3129-3134.
107.   G. A. Russell, C. DeBoer and K. M. Desmond, *J. Am. Chem. Soc.*, 1963, 85, 365-366.
108.   E. S. Huyser, *J. Am. Chem. Soc.*, 1960, 82, 391-393.
109.   G. A. Russell and C. DeBoer, *J. Am. Chem. Soc.*, 1963, 85, 3136-3139.
110.   R. Vanni, S. J. Garden, J. T. Banks and K. U. Ingold, *Tetrahedron Lett.*, 1995, 36, 7999-8002.
111.   D. H. R. Barton, É. Csuhai and D. Doller, *Tetrahedron*, 1992, 48, 9195-9206.
112.   V. V. Smirnov, V. M. Zelikman, I. P. Beletskaya, E. N. Golubeva, D. S. Tsvetkov, M. M. Levitskii and M. A. Kazankova, *Russ. J. Org. Chem.*, 2002, 38, 962-966.

113. P. R. Schreiner, O. Lauenstein, I. V. Kolomitsyn, S. Nadi and A. A. Fokin, *Angew. Chem. Int. Ed.*, 1998, 37, 1895-1897.
114. O. Lauenstein, A. A. Fokin and P. R. Schreiner, *Org. Lett.*, 2000, 2, 2201-2204.
115. P. R. Schreiner, O. Lauenstein, E. D. Butova, P. A. Gunchenko, I. V. Kolomitsin, A. Wittkopp, G. Feder and A. A. Fokin, *Chem. Eur. J.*, 2001, 7, 4996-5003.
116. Y. Nishina, B. Ohtani and K. Kikushima, *Beilstein J. Org. Chem.*, 2013, 9, 1663-1667.
117. C. L. Hill and B. C. Schardt, *J. Am. Chem. Soc.*, 1980, 102, 6374-6375.
118. D. H. R. Barton, S. D. Bévière, W. Chavasiri, D. Doller and B. Hu, *Tetrahedron Lett.*, 1993, 34, 1871-1874.
119. Y. Li, J. Ju, J. Jia, W. Sheng, L. Han and J. Gao, *Chin. J. Chem* . 2010, 28, 2428-2432.
120. W. Liu and J. T. Groves, *J. Am. Chem. Soc.*, 2010, 132, 12847-12849.
121. F. Minisci, R. Galli and R. Bernardi, *Chem. Commun.*, 1967, 903-904.
122. M. L. Poutsma, in *Reactive intermediates in organic chemistry*, ed. J. K. Kochi, New York, 1973, vol. 2, ch. 15, pp. 159-229.
123. P. C. Anson, P. S. Fredricks and J. M. Tedder, *J. Chem. Soc.*, 1959, 918-922.
124. G. C. Fettis, J. H. Knox and A. F. Trotman-Dickenson, *J. Chem. Soc.*, 1960, 1064-1071.
125. R. D. Chambers, M. Parsons, G. Sandford and R. Bowden, *Chem. Commun.*, 2000, 959-960.
126. R. D. Chambers, A. M. Kenwright, M. Parsons, G. Sandford and J. S. Moilliet, *J. Chem. Soc., Perkin Trans. 1*, 2002, 2190-2197.
127. R. D. Chambers, M. Parsons, G. Sandford, E. Thomas, J. Trmcic and J. S. Moilliet, *Tetrahedron*, 2006, 62, 7162-7167.
128. D. H. R. Barton, R. H. Hesse, R. E. Markwell, M. M. Pechet and H. T. Toh, *J. Am. Chem. Soc.*, 1976, 98, 3034-3035.
129. A. E. Feiring, *J. Org. Chem.*, 1979, 44, 1252-1254.
130. A. E. Feiring, *J. Fluorine Chem.*, 1977, 10, 375-386.
131. S. Stavber and M. Zupan, *J. Org. Chem.*, 1991, 56, 7347-7350.
132. S. Stavber and M. Zupan, *J. Org. Chem.*, 1983, 48, 2223-2226.
133. C. M. Wang and T. E. Mallouk, *J. Am. Chem. Soc.*, 1990, 112, 2016-2018.
134. R. E. Banks, M. K. Besheesh, S. N. Mohialdin-Khaffaf and I. Sharif, *J. Fluorine Chem.*, 1997, 81, 157-161.
135. G. Stavber, M. Zupan and S. Stavber, *Tetrahedron Lett.*, 2007, 48, 2671-2673.
136. J.-B. Xia, C. Zhu and C. Chen, *J. Am. Chem. Soc.*, 2013, 135, 17494-17500.
137. M.-G. Braun and A. G. Doyle, *J. Am. Chem. Soc.*, 2013, 135, 12990-12993.
138. W. Liu, X. Huang, M.-J. Cheng, R. J. Nielsen, W. A. Goddard and J. T. Groves, *Science*, 2012, 337, 1322-1325.
139. W. Liu and J. T. Groves, *Angew. Chem. Int. Ed.*, 2013, 52, 6024-6027.
140. S. Bloom, C. R. Pitts, D. C. Miller, N. Haselton, M. G. Holl, E. Urheim and T. Lectka, *Angew. Chem. Int. Ed.*, 2012, 51, 10580-10583.
141. S. Bloom, C. R. Pitts, R. Woltornist, A. Griswold, M. G. Holl and T. Lectka, *Org. Lett.*, 2013, 15, 1722-1724.
142. Y. Amaoka, M. Nagatomo and M. Inoue, *Org. Lett.*, 2013, 15, 2160-2163.
143. K. B. McMurtrey, J. M. Racowski and M. S. Sanford, *Org. Lett.*, 2012, 14, 4094-4097.
144. P. Esser, B. Pohlmann and H.-D. Scharf, *Angew. Chem. Int. Ed.*, 1994, 33, 2009-2023.
145. C. L. Hill, *Synlett*, 1995, 1995, 127-132.
146. A. G. Griesbeck and J. Mattay, in *Synthetic organic photochemistry*, Marcel Dekker,, New York, 2005, vol. 12, pp. 1 online resource (x, 629 p.) ill.
147. M. Fagnoni, D. Dondi, D. Ravelli and A. Albini, *Chem. Rev.*, 2007, 107, 2725-2756.
148. J. Iriondo-Alberdi and M. F. Greaney, *Eur. J. Org. Chem.*, 2007, 2007, 4801-4815.
149. N. Hoffmann, *Chem. Rev.*, 2008, 108, 1052-1103.
150. T. Bach and J. P. Hehn, *Angew. Chem. Int. Ed.*, 2011, 50, 1000-1045.

151. S. Fukuzumi and K. Ohkubo, *Chem. Sci.*, 2013, 4, 561-574.
152. E. S. Huyser, in *The Carbon—Halogen Bond (1973)*, John Wiley & Sons, Ltd., 2010, ch8 , pp. 549-607.
153. M. D. Tzirakis, I. N. Lykakis and M. Orfanopoulos, *Chem. Soc. Rev.*, 2009, 38, 2609-2621.
154. A. Juris, V. Balzani, F. Barigelletti, S. Campagna, P. Belser and A. von Zelewsky, *Coord. Chem. Rev.*, 1988, 84, 85-277.
155. J. M. R. Narayanam and C. R. J. Stephenson, *Chem. Soc. Rev.*, 2011, 40, 102-113.
156. J. W. Tucker and C. R. J. Stephenson, *J. Org. Chem.*, 2012, 77, 1617-1622.
157. J. Xuan and W.-J. Xiao, *Angew. Chem. Int. Ed.*, 2012, 51, 6828-6838.
158. L. Shi and W. Xia, *Chem. Soc. Rev.*, 2012, 41, 7687-7697.
159. D. Ravelli and M. Fagnoni, *ChemCatChem*, 2012, 4, 169-171.
160. C. K. Prier, D. A. Rankic and D. W. C. MacMillan, *Chem. Rev.*, 2013, 113, 5322-5363.
161. T. P. Yoon, *ACS Catalysis*, 2013, 3, 895-902.
162. J. Hu, J. Wang, T. H. Nguyen and N. Zheng, *Beilstein J. Org. Chem.*, 2013, 9, 1977-2001.
163. M. Reckenthäler and A. G. Griesbeck, *Adv. Synth. Catal.*, 2013, 355, 2727-2744.
164. H. Liu, W. Feng, C. W. Kee, Y. Zhao, D. Leow, Y. Pan and C.-H. Tan, *Green Chem.*, 2010, 12, 953-956.
165. V. Nair and A. Deepthi, *Chem. Rev.*, 2007, 107, 1862-1891.
166. B. M. Trost, *Science*, 1991, 254, 1471-1477.
167. Z. Li, D. S. Bohle and C.-J. Li, *Proc. Natl. Acad. Sci. U. S. A.*, 2006, 103, 8928-8933.
168. A. G. Condie, J. C. González-Gómez and C. R. J. Stephenson, *J. Am. Chem. Soc.*, 2010, 132, 1464-1465.
169. Y. Pan, C. W. Kee, L. Chen and C.-H. Tan, *Green Chem.*, 2011, 13, 2682-2685.
170. Y. Pan, S. Wang, C. W. Kee, E. Dubuisson, Y. Yang, K. P. Loh and C.-H. Tan, *Green Chem.*, 2011, 13, 3341-3344.
171. K. Müller-Dethlefs and P. Hobza, *Chem. Rev.*, 2000, 100, 143-168.
172. P. Muller, *Pure Appl. Chem.*, 1994, 66, 1077-1184.
173. J.-M. Lehn, *Angew. Chem. Int. Ed.*, 1988, 27, 89-112.
174. J.-M. Lehn, *Angew. Chem. Int. Ed.*, 1990, 29, 1304-1319.
175. J. L. Atwood and J. M. Lehn, *Comprehensive supramolecular chemistry*, Pergamon, New York, 1st edn., 1996.
176. K. E. Uhrich, S. M. Cannizzaro, R. S. Langer and K. M. Shakesheff, *Chem. Rev.*, 1999, 99, 3181-3198.
177. R. Langer, *Science*, 2001, 293, 58-59.
178. D. E. Discher and A. Eisenberg, *Science*, 2002, 297, 967-973.
179. R. Duncan, *Nat. Rev. Drug Discov.*, 2003, 2, 347-360.
180. R. Haag, *Angew. Chem. Int. Ed.*, 2004, 43, 278-282.
181. Y. Chen and Y. Liu, *Chem. Soc. Rev.*, 2010, 39, 495-505.
182. X. Zhang and C. Wang, *Chem. Soc. Rev.*, 2011, 40, 94-101.
183. Z. Ma and B. Moulton, *Coord. Chem. Rev.*, 2011, 255, 1623-1641.
184. K. Miyata, N. Nishiyama and K. Kataoka, *Chem. Soc. Rev.*, 2012, 41, 2562-2574.
185. A. J. Kirby, *Angew. Chem. Int. Ed.*, 1994, 33, 551-553.
186. W. B. Motherwell, M. J. Bingham and Y. Six, *Tetrahedron*, 2001, 57, 4663-4686.
187. P. R. Schreiner, *Chem. Soc. Rev.*, 2003, 32, 289-296.
188. J. Meeuwissen and J. N. H. Reek, *Nature Chem*, 2010, 2, 615-621.
189. J. K. M. Sanders, *Chem. - Eur. J.*, 1998, 4, 1378-1383.
190. L. Kovbasyuk and R. Krämer, *Chem. Rev.*, 2004, 104, 3161-3188.
191. V. Balzani, A. Juris, M. Venturi, S. Campagna and S. Serroni, *Chem. Rev.*, 1996, 96, 759-834.
192. M. D. Ward, *Coord. Chem. Rev.*, 2007, 251, 1663-1677.

193. L. Fabbrizzi and A. Poggi, *Chem. Soc. Rev.*, 1995, 24, 197-202.
194. P. D. Beer and S. R. Bayly, *Top. Curr. Chem.*, 2005, 255, 125-162.
195. T. Gunnlaugsson, M. Glynn, G. M. Tocci, P. E. Kruger and F. M. Pfeffer, *Coord. Chem. Rev.*, 2006, 250, 3094-3117.
196. B. T. Nguyen and E. V. Anslyn, *Coord. Chem. Rev.*, 2006, 250, 3118-3127.
197. J. R. Pinzon, A. Villalta-Cerdas and L. Echegoyen, *Top. Curr. Chem.*, 2012, 312, 127-174.
198. M. C. Petty, *Molecular Electronics: From Principles to Practice*, John Wiley & Sons, Ltd, 2007.
199. U. Pischel, *Angew. Chem. Int. Ed.*, 2007, 46, 4026-4040.
200. G. R. Desiraju, P. S. Ho, L. Kloo, A. C. Legon, R. Marquardt, P. Metrangolo, P. Politzer, G. Resnati and K. Rissanen, *Pure Appl. Chem.*, 2013, 85, 1711-1713.
201. F. Guthrie, *J. Chem. Soc.*, 1863, 16, 239-244.
202. H. A. Benesi and J. H. Hildebrand, *J. Am. Chem. Soc.*, 1949, 71, 2703-2707.
203. O. Hassel, *Science*, 1970, 170, 497-502.
204. A. C. Legon, *Angew. Chem. Int. Ed.*, 1999, 38, 2686-2714.
205. T. Clark, M. Hennemann, J. Murray and P. Politzer, *J. Mol. Model.*, 2007, 13, 291-296.
206. M. Erdélyi, *Chem. Soc. Rev.*, 2012, 41, 3547-3557.
207. T. M. Beale, M. G. Chudzinski, M. G. Sarwar and M. S. Taylor, *Chem. Soc. Rev.*, 2013, 42, 1667-1680.
208. H. I. Bloemink, K. Hinds, A. C. Legon and J. C. Thorn, *Angew. Chem. Int. Ed.*, 1994, 33, 1512-1513.
209. R. Bianchini, D. Lenoir, R. Herges, J. Grunenberg, C. Chiappe and P. Lemmen, *Angew. Chem. Int. Ed.*, 1997, 36, 1284-1287.
210. M.-F. Ruasse, *Adv. Phys. Org. Chem.*, 1993, 28, 207-291.
211. M. D. Esrafili, G. Mahdavinia, M. Javaheri and H. R. Sobhi, *Mol. Phys.*, 2013, 1-7.
212. S. E. Denmark, W. E. Kuester and M. T. Burk, *Angew. Chem. Int. Ed.*, 2012, 51, 10938-10953.
213. D. Huang, H. Wang, F. Xue, H. Guan, L. Li, X. Peng and Y. Shi, *Org. Lett.*, 2011, 13, 6350-6353.
214. S. E. Denmark and M. T. Burk, *Org. Lett.*, 2011, 14, 256-259.
215. L. Zhou, C. K. Tan, X. Jiang, F. Chen and Y.-Y. Yeung, *J. Am. Chem. Soc.*, 2010, 132, 15474-15476.
216. A. Bruckmann, M. A. Pena and C. Bolm, *Synlett*, 2008, 2008, 900-902.
217. S. M. Walter, F. Kniep, E. Herdtweck and S. M. Huber, *Angew. Chem. Int. Ed.*, 2011, 50, 7187-7191.
218. F. Kniep, S. H. Jungbauer, Q. Zhang, S. M. Walter, S. Schindler, I. Schnapperelle, E. Herdtweck and S. M. Huber, *Angew. Chem. Int. Ed.*, 2013, 52, 7028-7032.
219. P. Hobza and R. Zahradnik, *Chem. Rev.*, 1988, 88, 871-897.
220. K. E. Riley, M. Pitoňák, P. Jurečka and P. Hobza, *Chem. Rev.*, 2010, 110, 5023-5063.
221. C. Allemann, R. Gordillo, F. R. Clemente, P. H.-Y. Cheong and K. N. Houk, *Acc. Chem. Res.*, 2004, 37, 558-569.
222. P. H.-Y. Cheong, C. Y. Legault, J. M. Um, N. Çelebi-Ölçüm and K. N. Houk, *Chem. Rev.*, 2011, 111, 5042-5137.
223. E. H. Krenske and K. N. Houk, *Acc. Chem. Res.*, 2013, 46, 979-989.
224. S. Shaik, D. Kumar, S. P. de Visser, A. Altun and W. Thiel, *Chem. Rev.*, 2005, 105, 2279-2328.
225. S. Shaik, S. Cohen, Y. Wang, H. Chen, D. Kumar and W. Thiel, *Chem. Rev.*, 2010, 110, 949-1017.
226. D. W. Robbins and J. F. Hartwig, *Angew. Chem. Int. Ed.*, 2013, 52, 933-937.

227. T. Hatakeyama, T. Hashimoto, Y. Kondo, Y. Fujiwara, H. Seike, H. Takaya, Y. Tamada, T. Ono and M. Nakamura, *J. Am. Chem. Soc.*, 2010, 132, 10674-10676.

228. Z. Lu and G. C. Fu, *Angew. Chem. Int. Ed.*, 2010, 49, 6676-6678.

229. C.-T. Yang, Z.-Q. Zhang, Y.-C. Liu and L. Liu, *Angew. Chem. Int. Ed.*, 2011, 50, 3904-3907.

230. J. Zhou and G. C. Fu, *J. Am. Chem. Soc.*, 2004, 126, 1340-1341.

231. H. Shaw, H. D. Perlmutter, C. Gu, S. D. Arco and T. O. Quibuyen, *J. Org. Chem.*, 1997, 62, 236-237.

232. R. Montoro and T. Wirth, *Synthesis*, 2005, 2005, 1473,1478.

233. T. Gan, R. Liu, P. Yu, S. Zhao and J. M. Cook, *J. Org. Chem.*, 1997, 62, 9298-9304.

234. M. Cossi, N. Rega, G. Scalmani and V. Barone, *J. Comput. Chem.*, 2003, 24, 669-681.

235. M. J. Frisch, G. W. Trucks, H. B. Schlegel, G. E. Scuseria, M. A. Robb, J. R. Cheeseman, G. Scalmani, V. Barone, B. Mennucci, G. A. Petersson, H. Nakatsuji, M. Caricato, X. Li, H. P. Hratchian, A. F. Izmaylov, J. Bloino, G. Zheng, J. L. Sonnenberg, M. Hada, M. Ehara, K. Toyota, R. Fukuda, J. Hasegawa, M. Ishida, T. Nakajima, Y. Honda, O. Kitao, H. Nakai, T. Vreven, J. A. Montgomery, J. E. Peralta, F. Ogliaro, M. Bearpark, J. J. Heyd, E. Brothers, K. N. Kudin, V. N. Staroverov, R. Kobayashi, J. Normand, K. Raghavachari, A. Rendell, J. C. Burant, S. S. Iyengar, J. Tomasi, M. Cossi, N. Rega, J. M. Millam, M. Klene, J. E. Knox, J. B. Cross, V. Bakken, C. Adamo, J. Jaramillo, R. Gomperts, R. E. Stratmann, O. Yazyev, A. J. Austin, R. Cammi, C. Pomelli, J. W. Ochterski, R. L. Martin, K. Morokuma, V. G. Zakrzewski, G. A. Voth, P. Salvador, J. J. Dannenberg, S. Dapprich, A. D. Daniels, Farkas, J. B. Foresman, J. V. Ortiz, J. Cioslowski and D. J. Fox, in *Gaussian 09, Revision A.02*, Wallingford CT, 2009.

236. Y. Zhao and D. Truhlar, *Theor. Chem. Acc.*, 2008, 120, 215-241.

237. C. E. Check, T. O. Faust, J. M. Bailey, B. J. Wright, T. M. Gilbert and L. S. Sunderlin, *J. Phys. Chem. A*, 2001, 105, 8111-8116.

238. L. Furst, B. S. Matsuura, J. M. R. Narayanam, J. W. Tucker and C. R. J. Stephenson, *Org. Lett.*, 2010, 12, 3104-3107.

239. C. Dai, J. M. R. Narayanam and C. R. J. Stephenson, *Nature Chem*, 2011, 3, 140-145.

240. Y. C. Teo, Y. Pan and C. H. Tan, *ChemCatChem*, 2013, 5, 235-240.

241. E. Rizzardo, A. K. Serelis and D. H. Solomon, *Aust. J. Chem.*, 1982, 35, 2013-2024.

242. E. Megiel, A. Kaim and M. K. Cyrański, *J. Phys. Org. Chem.*, 2010, 23, 1146-1154.

243. G. A. Russell, in *Free radicals*, ed. J. K. Kochi, New York, 1973, vol. 1, ch. 7, p. 275.

244. C. Walling and B. Miller, *J. Am. Chem. Soc.*, 1957, 79, 4181-4187.

245. G. A. Russell and R. C. Williamson, *J. Am. Chem. Soc.*, 1964, 86, 2357-2364.

246. R. E. Pearson and J. C. Martin, *J. Am. Chem. Soc.*, 1963, 85, 3142-3146.

247. E. D. Glendening, J. K. Badenhoop, A. E. Reed, J. E. Carpenter, J. A. Bohmann, C. M. Morales and F. Weinhold, in *NBO 5.0.*, Theoretical Chemistry Institute, University of Wisconsin, , Madison, 2001.

248. J. K. Badenhoop and F. Weinhold, *J. Chem. Phys.*, 1997, 107, 5406-5421.

249. J. K. Badenhoop and F. Weinhold, *Int. J. Quantum Chem*, 1999, 72, 269-280.

250. R. L. Dorta, C. G. Francisco and E. Suarez, *J. Chem. Soc., Chem. Commun.*, 1989, 0, 1168-1169.

251. P. Buchschacher, J. Kalvoda, D. Arigoni and O. Jeger, *J. Am. Chem. Soc.*, 1958, 80, 2905-2906.

252. E. J. Corey and W. R. Hertler, *J. Am. Chem. Soc.*, 1960, 82, 1657-1668.

253. D. H. R. Barton and J. M. Beaton, *J. Am. Chem. Soc.*, 1961, 83, 4083-4089.

254. G. van De Woude, M. Biesemans and L. van Hove, *Bull. Soc. Chim. Belg.*, 1980, 89, 993-1000.

255. C. Y. Legault, Université de Sherbrooke, 1.0.562 BETA edn., 2012.

256. P. G. M. Wuts and T. W. Greene, in *Greene's protective groups in organic synthesis*, Wiley-Interscience, Hoboken, NJ ; Chichester, 4th edn., 2007, ch. 3, p. 411.
257. F. H. Westheimer, *Chem. Rev.*, 1961, 61, 265-273.
258. R. P. Bell, *The tunnel effect in chemistry*, Chapman and Hall, London ; New York, 1980.
259. D. G. Truhlar, B. C. Garrett and S. J. Klippenstein, *J. Phys. Chem.*, 1996, 100, 12771-12800.
260. E. V. Anslyn and D. A. Dougherty, *Modern physical organic chemistry*, University Science, Sausalito, CA, 2006.
261. A.-P. Schaffner, V. Darmency and P. Renaud, *Angew. Chem. Int. Ed.*, 2006, 45, 5847-5849.
262. Y.-R. Luo, in *Handbook of Bond Dissociation Energies in Organic Compounds*, CRC Press, 2002, ch3, pp. 19-144.

263. B. C. Garrett and D. G. Truhlar, *J. Phys. Chem.*, 1979, 83, 2921-2926.
264. A. Miyoshi, rev. 2013.07.15 edn.
265. S. Hamasaki, M. Kamigaito and M. Sawamoto, *Macromolecules*, 2002, 35, 2934-2940.
266. T. Furuya, A. S. Kamlet and T. Ritter, *Nature*, 2011, 473, 470-477.
267. T. Liang, C. N. Neumann and T. Ritter, *Angew. Chem. Int. Ed.*, 2013, 52, 8214-8264.
268. D. A. Watson, M. Su, G. Teverovskiy, Y. Zhang, J. García-Fortanet, T. Kinzel and S. L. Buchwald, *Science*, 2009, 325, 1661-1664.
269. K. S. L. Chan, M. Wasa, X. Wang and J.-Q. Yu, *Angew. Chem. Int. Ed.*, 2011, 50, 9081-9084.
270. V. Rauniyar, A. D. Lackner, G. L. Hamilton and F. D. Toste, *Science*, 2011, 334, 1681-1684.
271. X.-G. Zhang, H.-X. Dai, M. Wasa and J.-Q. Yu, *J. Am. Chem. Soc.*, 2012, 134, 11948-11951.
272. M. Rueda-Becerril, C. Chatalova Sazepin, J. C. T. Leung, T. Okbinoglu, P. Kennepohl, J.-F. Paquin and G. M. Sammis, *J. Am. Chem. Soc.*, 2012, 134, 4026-4029.
273. Z. Gao, Y. H. Lim, M. Tredwell, L. Li, S. Verhoog, M. Hopkinson, W. Kaluza, T. L. Collier, J. Passchier, M. Huiban and V. Gouverneur, *Angew. Chem. Int. Ed.*, 2012, 51, 6733-6737.
274. J.-A. Ma and D. Cahard, *Chem. Rev.*, 2008, 108, PR1-PR43.
275. C. Hollingworth and V. Gouverneur, *Chem. Commun.*, 2012, 48, 2929-2942.
276. M. P. Sibi and Y. Landais, *Angew. Chem. Int. Ed.*, 2013, 52, 3570-3572.
277. F. Yin, Z. Wang, Z. Li and C. Li, *J. Am. Chem. Soc.*, 2012, 134, 10401-10404.
278. D. Leow, G. Li, T.-S. Mei and J.-Q. Yu, *Nature*, 2012, 486, 518-522.
279. P. T. Nyffeler, S. G. Durón, M. D. Burkart, S. P. Vincent and C.-H. Wong, *Angew. Chem. Int. Ed.*, 2005, 44, 192-212.
280. S. Stavber and M. Zupan, *Acta Chim. Slov.*, 2005, 52, 13-26.
281. H. P. Shunatona, N. Früh, Y.-M. Wang, V. Rauniyar and F. D. Toste, *Angew. Chem. Int. Ed.*, 2013, 52, 7724-7727.
282. J. R. Wolstenhulme, J. Rosenqvist, O. Lozano, J. Ilupeju, N. Wurz, K. M. Engle, G. W. Pidgeon, P. R. Moore, G. Sandford and V. Gouverneur, *Angew. Chem. Int. Ed.*, 2013, 52, 9796-9800.
283. E. W. Oliver and D. H. Evans, *J. Electroanal. Chem.*, 1999, 474, 1-8.
284. M. Wasa, K. M. Engle and J.-Q. Yu, *J. Am. Chem. Soc.*, 2009, 131, 9886-9887.
285. A. Renaudat, L. Jean-Gérard, R. Jazzar, C. E. Kefalidis, E. Clot and O. Baudoin, *Angew. Chem. Int. Ed.*, 2010, 49, 7261-7265.
286. Y. Ano, M. Tobisu and N. Chatani, *J. Am. Chem. Soc.*, 2011, 133, 12984-12986.
287. M. T. Pirnot, D. A. Rankic, D. B. C. Martin and D. W. C. MacMillan, *Science*, 2013, 339, 1593-1596.

288.   Z. Fu, J. Xu, T. Zhu, W. W. Y. Leong and Y. R. Chi, *Nature Chem*, 2013, 5, 835-839.
289.   J. He, M. Wasa, K. S. L. Chan and J.-Q. Yu, *J. Am. Chem. Soc.*, 2013, 135, 3387-3390.
290.   T. Newhouse and P. S. Baran, *Angew. Chem. Int. Ed.*, 2011, 50, 3362-3374.
291.   R. Atta ur, A. Farooq and M. I. Choudhary, *J. Nat. Prod.*, 1997, 60, 1038-1040.
292.   R. Dolin, R. C. Reichman, H. P. Madore, R. Maynard, P. N. Linton and J. Webber-Jones, *N. Engl. J. Med.*, 1982, 307, 580-584.
293.   S. Kempers, H. I. Katz, R. Wildnauer and B. Green, *Cutis; cutaneous medicine for the practitioner*, 1998, 61, 347-350.
294.   A. V. Marenich, C. J. Cramer and D. G. Truhlar, *J. Phys. Chem. B*, 2009, 113, 6378-6396.
295.   A. A. Lamola and G. S. Hammond, *J. Chem. Phys.*, 1965, 43, 2129-2135.
296.   T. Wolff and H. Görner, *Journal of Photochemistry and Photobiology A: Chemistry*, 2010, 209, 219-223.
297.   M. Ashraf and J. B. Headridge, *Talanta*, 1969, 16, 1439-1441.
298.   G. P. Girina, A. A. Fainzil'berg and L. G. Feoktistov, *Russ. J. Electrochem.*, 2000, 36, 162-163.
299.   F. Scholz, in *Electroanalytical Methods*, ed. F. Scholz, Springer Berlin Heidelberg, 2010, ch. 2, pp. 11-31.
300.   G. A. Zalesskaya, *J. Appl. Spectrosc.*, 2002, 69, 328-336.
301.   P. W. Atkins and J. De Paula, W.H. Freeman, New York, 9th edn., 2010, p. 503.
302.   G. Lauer, W. Schäfer and A. Schweig, *Chem. Phys. Lett.*, 1975, 33, 312-315.
303.   G. Centineo, I. Fragala, G. Bruno and S. Spampinato, *J. Mol. Struct.*, 1978, 44, 203-210.
304.   R. A. Marcus, *Annu. Rev. Phys. Chem.*, 1964, 15, 155-196.
305.   N. S. Hush, *Trans. Faraday Soc.*, 1961, 57, 557-580.
306.   G. L. Closs and J. R. Miller, *Science*, 1988, 240, 440-447.
307.   S. Das, J. S. D. Kumar, K. Shivaramayya and M. V. George, *J. Chem. Soc., Perkin Trans. 1*, 1995, 1797-1799.
308.   N. Tada, K. Hattori, T. Nobuta, T. Miura and A. Itoh, *Green Chem.*, 2011, 13, 1669-1671.
309.   S. Kamijo, T. Hoshikawa and M. Inoue, *Org. Lett.*, 2011, 13, 5928-5931.
310.   T. Akiyama, J. Itoh and K. Fuchibe, *Adv. Synth. Catal.*, 2006, 348, 999-1010.
311.   M. S. Taylor and E. N. Jacobsen, *Angew. Chem. Int. Ed.*, 2006, 45, 1520-1543.
312.   P. Metrangolo, H. Neukirch, T. Pilati and G. Resnati, *Acc. Chem. Res.*, 2005, 38, 386-395.
313.   Y. Zhang, C. W. Kee, R. Lee, X. Fu, J. Y.-T. Soh, E. M. F. Loh, K.-W. Huang and C.-H. Tan, *Chem. Commun.*, 2011, 47, 3897-3899.
314.   H. Liu, W. Feng, C. W. Kee, D. Leow, W.-T. Loh and C.-H. Tan, *Adv. Synth. Catal.*, 2010, 352, 3373-3379.
315.   H. Liu, D. Leow, K.-W. Huang and C.-H. Tan, *J. Am. Chem. Soc.*, 2009, 131, 7212-7213.
316.   H. D. Flack and G. Bernardinelli, *Chirality*, 2008, 20, 681-690.
317.   M. Kwit, M. D. Rozwadowska, J. Gawroński and A. Grajewska, *J. Org. Chem.*, 2009, 74, 8051-8063.
318.   J. I. Seeman, *Chem. Rev.*, 1983, 83, 83-134.
319.   J. I. Seeman and W. A. Farone, *J. Org. Chem.*, 1978, 43, 1854-1864.
320.   J. I. Seeman, *J. Chem. Educ.*, 1986, 63, 42.
321.   Y. Pan, C. W. Kee, Z. Jiang, T. Ma, Y. Zhao, Y. Yang, H. Xue and C.-H. Tan, *Chem. - Eur. J.*, 2011, 17, 8363-8370.
322.   N. Blaquiere, D. G. Shore, S. Rousseaux and K. Fagnou, *J. Org. Chem.*, 2009, 74, 6190-6198.
323.   K. C. Fortner and M. D. Shair, *J. Am. Chem. Soc.*, 2007, 129, 1032-1033.
324.   Z. Jiang, Y. Pan, Y. Zhao, T. Ma, R. Lee, Y. Yang, K.-W. Huang, M. W. Wong and C.-H. Tan, *Angew. Chem.*, 2009, 121, 3681-3685.
325.   J. Baudoux, P. Lefebvre, R. Legay, M.-C. Lasne and J. Rouden, *Green Chem.*, 2010, 12, 252-259.

326. J. Wang, J. Chen, C. W. Kee and C.-H. Tan, *Angew. Chem. Int. Ed.*, 2012, 51, 2382-2386.

327. S. Bertelsen, M. Marigo, S. Brandes, P. Dinér and K. A. Jørgensen, *J. Am. Chem. Soc.*, 2006, 128, 12973-12980.

328. P. Politzer, J. S. Murray and T. Clark, *PCCP*, 2010, 12, 7748-7757.

329. F. Bulat, A. Toro-Labbé, T. Brinck, J. Murray and P. Politzer, *J. Mol. Model.*, 2010, 16, 1679-1691.

330. K. E. Riley, J. S. Murray, P. Politzer, M. C. Concha and P. Hobza, *J. Chem. Theory Comput.*, 2009, 5, 155-163.

331. Z. P. Shields, J. S. Murray and P. Politzer, *Int. J. Quantum Chem*, 2010, 110, 2823-2832.

332. K. Riley, J. Murray, J. Fanfrlík, J. Řezáč, R. Solá, M. Concha, F. Ramos and P. Politzer, *J. Mol. Model.*, 2011, 17, 3309-3318.

333. A. Bundhun, P. Ramasami, J. Murray and P. Politzer, *J. Mol. Model.*, 2013, 19, 2739-2746.

334. S. M. Huber, E. Jimenez-Izal, J. M. Ugalde and I. Infante, *Chem. Commun.*, 2012, 48, 7708-7710.

335. T. H. Dunning, *J. Chem. Phys.*, 1989, 90, 1007-1023.

336. R. A. Kendall, T. H. Dunning and R. J. Harrison, *J. Chem. Phys.*, 1992, 96, 6796-6806.

337. D. E. Woon and T. H. Dunning, *J. Chem. Phys.*, 1993, 98, 1358-1371.

338. K. A. Peterson, D. E. Woon and T. H. Dunning, *J. Chem. Phys.*, 1994, 100, 7410-7415.

339. J. M. L. Martin and A. Sundermann, *J. Chem. Phys.*, 2001, 114, 3408-3420.

340. M. W. Schmidt, K. K. Baldridge, J. A. Boatz, S. T. Elbert, M. S. Gordon, J. H. Jensen, S. Koseki, N. Matsunaga, K. A. Nguyen, S. Su, T. L. Windus, M. Dupuis and J. A. Montgomery, *J. Comput. Chem.*, 1993, 14, 1347-1363.

341. M. S. Gordon and M. W. Schmidt, in *Theory and Applications of Computational Chemistry*, eds. C. E. Dykstra, G. Frenking, K. S. Kim and G. E. Scuseria, Elsevier, Amsterdam, 2005, pp. 1167-1189.

342. S. F. Boys and F. Bernardi, *Mol. Phys.*, 1970, 19, 553-566.

343. S. Grimme, *J. Comput. Chem.*, 2006, 27, 1787-1799.

344. P. Su and H. Li, *J. Chem. Phys.*, 2009, 131, 014102.

345. P. Politzer, K. E. Riley, F. A. Bulat and J. S. Murray, *Computational and Theoretical Chemistry*, 2012, 998, 2-8.

346. K. Morokuma, *Acc. Chem. Res.*, 1977, 10, 294-300.

347. U. Mayer, V. Gutmann and W. Gerger, *Monatshefte für Chemie / Chemical Monthly*, 1975, 106, 1235-1257.

348. M. A. Beckett, G. C. Strickland, J. R. Holland and K. Sukumar Varma, *Polymer*, 1996, 37, 4629-4631.

349. F. Kniep, S. M. Walter, E. Herdtweck and S. M. Huber, *Chem. - Eur. J.*, 2012, 18, 1306-1310.

350. F. Kniep, L. Rout, S. M. Walter, H. K. V. Bensch, S. H. Jungbauer, E. Herdtweck and S. M. Huber, *Chem. Commun.*, 2012, 48, 9299-9301.

351. T. Ma, X. A. Fu, C. W. Kee, L. L. Zong, Y. H. Pan, K. W. Huang and C. H. Tan, *J. Am. Chem. Soc.*, 2011, 133, 2828-2831.

352. Y. Y. Yang, F. Moinodeen, W. Chin, T. Ma, Z. Y. Jiang and C. H. Tan, *Org. Lett.*, 2012, 14, 4762-4765.

353. T. Kita, A. Georgieva, Y. Hashimoto, T. Nakata and K. Nagasawa, *Angew. Chem. Int. Ed.*, 2002, 41, 2832-2834.

354. P. R. Blakemore and C. Wang, *Abstr Pap Am Chem S*, 2008, 236.

355. K. Ohmatsu, M. Kiyokawa and T. Ooi, *J. Am. Chem. Soc.*, 2011, 133, 1307-1309.

356. A. E. Sheshenev, E. V. Boltukhina, A. J. P. White and K. K. Hii, *Angew. Chem. Int. Ed.*, 2013, 52, 6988-6991.

357. I. Fernandez and N. Khiar, *Chem. Rev.*, 2003, 103, 3651-3705.

358. J. Legros, J. R. Dehli and C. Bolm, *Adv. Synth. Catal.*, 2005, 347, 19-31.
359. H. B. Kagan, in *Organosulfur Chemistry in Asymmetric Synthesis*, ed. T. Toru, Bolm, C., WILEY-VCH, Weinheim, 2008, ch. 1, pp. 1-30.
360. E. Wojaczyńska and J. Wojaczyński, *Chem. Rev.*, 2010, 110, 4303-4356.
361. G. E. O'Mahony, P. Kelly, S. E. Lawrence and A. R. Maguire, *Arkivoc*, 2011, 1-110.
362. H. Cotton, T. Elebring, M. Larsson, L. Li, H. Sorensen and S. von Unge, *Tetrahedron-Asymmetr*, 2000, 11, 3819-3825.
363. F. Difuria, G. Modena and R. Seraglia, *Synthesis*, 1984, 325-326.
364. P. Pitchen, E. Dunach, M. N. Deshmukh and H. B. Kagan, *J. Am. Chem. Soc.*, 1984, 106, 8188-8193.
365. P. Pitchen and H. B. Kagan, *Tetrahedron Lett.*, 1984, 25, 1049-1052.
366. S. Liao, I. Coric, Q. Wang and B. List, *J. Am. Chem. Soc.*, 2012, 134, 10765-10768.
367. N. Kharasch, S. J. Potempa and H. L. Wehrmeister, *Chem. Rev.*, 1946, 39, 269-332.
368. J. S. O'Donnell and A. L. Schwan, *Journal of Sulfur Chemistry*, 2004, 25, 183-211.
369. C. Caupene, C. Boudou, S. Perrio and P. Metzner, *J. Org. Chem.*, 2005, 70, 2812-2815.
370. G. Maitro, G. Prestat, D. Madec and G. Poli, *Tetrahedron-Asymmetr*, 2010, 21, 1075-1084.
371. E. Bernoud, G. Le Duc, X. Bantreil, G. Prestat, D. Madec and G. Poli, *Org. Lett.*, 2010, 12, 320-323.
372. J. S. O'Donnell and A. L. Schwan, *Tetrahedron Lett.*, 2003, 44, 6293-6296.
373. G. Maitro, S. Vogel, G. Prestat, D. Madec and G. Poli, *Org. Lett.*, 2006, 8, 5951-5954.
374. F. Foucoin, C. Caupene, J. F. Lohier, J. S. D. O. Santos, S. Perrio and P. Metzner, *Synthesis*, 2007, 1315-1324.
375. F. Sandrinelli, S. Perrio and M. T. Averbuch-Pouchot, *Org. Lett.*, 2002, 4, 3619-3622.
376. N. Maezaki, S. Yagi, S. Ohsawa, H. Ohishi and T. Tanaka, *Tetrahedron*, 2003, 59, 9895-9906.
377. G. Maitro, G. Prestat, D. Madec and G. Poli, *J. Org. Chem.*, 2006, 71, 7449-7454.
378. J. F. Lohier, F. Foucoin, P. A. Jaffres, J. I. Garcia, J. S. D. O. Santos, S. Perrio and P. Metzner, *Org. Lett.*, 2008, 10, 1271-1274.
379. A. L. Schwan, M. J. Verdu, S. P. Singh, J. S. O'Donnell and A. N. Ahmadi, *J. Org. Chem.*, 2009, 74, 6851-6854.
380. S. C. Soderman and A. L. Schwan, *Org. Lett.*, 2011, 13, 4192-4195.
381. S. Vogel, X. Bantreil, G. Maitro, G. Prestat, D. Madec and G. Poli, *Tetrahedron Lett.*, 2010, 51, 1459-1461.
382. G. Maitro, S. Vogel, M. Sadaoul, G. Prestat, D. Madec and G. Poli, *Org. Lett.*, 2007, 9, 5493-5496.
383. F. Gelat, J. Jayashankaran, J. F. Lohier, A. C. Gaumont and S. Perrio, *Org. Lett.*, 2011, 13, 3170-3173.
384. F. Gelat, A.-C. Gaumont and S. Perrio, *Journal of Sulfur Chemistry*, 2013, 1-9.
385. F. C. Meotti, D. O. Silva, A. R. Dos Santos, G. Zeni, J. B. Rocha and C. W. Nogueira, *Environ. Toxicol. Pharmacol.*, 2003, 15, 37-44.
386. S. Nakamura, M. Kondo, K. Goto, M. Nakamura, Y. Tsuda and K. Shishido, *Heterocycles*, 1996, 43, 2747-2755.
387. E. Bey, S. Marchais-Oberwinkler, M. Negri, P. Kruchten, A. Oster, T. Klein, A. Spadaro, R. Werth, M. Frotscher, B. Birk and R. W. Hartmann, *J. Med. Chem.*, 2009, 52, 6724-6743.
388. K. E. Andersen, C. Braestrup, F. C. Gronwald, A. S. Jorgensen, E. B. Nielsen, U. Sonnewald, P. O. Sorensen, P. D. Suzdak and L. J. S. Knutsen, *J. Med. Chem.*, 1993, 36, 1716-1725.
389. L. A. McAllister, M. S. Hixon, J. P. Kennedy, T. J. Dickerson and K. D. Janda, *J. Am. Chem. Soc.*, 2006, 128, 4176-4177.

390. S. Dapprich, I. Komáromi, K. S. Byun, K. Morokuma and M. J. Frisch, *Journal of Molecular Structure: THEOCHEM*, 1999, 461–462, 1-21.
391. C. D. Anderson, T. Dudding, R. Gordillo and K. N. Houk, *Org. Lett.*, 2008, 10, 2749-2752.
392. L. Simón and J. M. Goodman, *J. Am. Chem. Soc.*, 2012, 134, 16869-16876.
393. J. J. P. Stewart, Stewart Computational Chemistry, Colorado Springs, CO, USA, 2012.
394. J. P. Stewart, *J. Mol. Model.*, 2013, 19, 1-32.
395. A. K. Rappe, C. J. Casewit, K. S. Colwell, W. A. Goddard and W. M. Skiff, *J. Am. Chem. Soc.*, 1992, 114, 10024-10035.

Publications

1. H. Liu, W. Feng, C. W. Kee, Y. Zhao, D. Leow, Y. Pan, C.-H. Tan, *Green Chem.* **2010**, *12*, 953-956.

2. H. Liu, W. Feng, C. W. Kee, D. Leow, W.-T. Loh, C.-H. Tan, *Adv. Synth. Catal.* **2010**, *352*, 3373-3379.

3. Y. Pan, C. W. Kee, L. Chen, C.-H. Tan, *Green Chem.* **2011**, *13*, 2682-2685.

4. Y. Pan, S. Wang, C. W. Kee, E. Dubuisson, Y. Yang, K. P. Loh, C.-H. Tan, *Green Chem.* **2011**, 13, 3341-3344.

5. Y. Pan, C. W. Kee, Z. Jiang, T. Ma, Y. Zhao, Y. Yang, H. Xue, C.-H. Tan, *Chem. - Eur. J.* **2011**, *17*, 8363-8370.

6. Y. Zhang, C. W. Kee, R. Lee, X. Fu, J. Y.-T. Soh, E. M. F. Loh, K.-W. Huang, C.-H. Tan, *Chem. Commun.* **2011**, *47*, 3897-3899.

7. T. Ma, X. Fu, C. W. Kee, L. Zong, Y. Pan, K.-W. Huang, C.-H. Tan, *J. Am. Chem. Soc.* **2011**, *133*, 2828-2831.

8. J. Wang*, J. Chen*, C. W. Kee*, C.-H. Tan, *Angew. Chem. Int. Ed.* **2012**, *51*, 2382-2386. *these authors contribute equally

9. C. W. Kee, K. M. Chan, M. W. Wong, C.-H. Tan, *Asian J. Org. Chem.* **2014**, *3*, 535-544.

10. C. W. Kee, K. F. Chin, M. W. Wong, C. –H. Tan, *Chem. Commun.* **2014**, *50*, 8211-8214.

11. L. Zong, X. Ban, C. W. Kee*, C.-H. Tan*, *Angew. Chem. Int. Ed.* **2014**, DOI: 10.1002/anie.201407512 *corresponding authors